Bioengineering New Therapeutics for Pulmonary Infections

Fang-Yi Su

A dissertation

submitted in partial fulfillment of the

requirements for the degree of

Doctor of Philosophy

University of Washington

2018

Reading Committee:

Patrick Stayton, Chair

Daniel Ratner

Shawn Skerrett

Wayne Gombotz

Program Authorized to Offer Degree:
Bioengineering

University of Washington

Abstract

Bioengineering New Therapeutics for Pulmonary Infections

Fang-Yi Su

Chair of the Supervisory Committee:
Professor Patrick Stayton
Bioengineering

Pulmonary intracellular infections including tuberculosis, legionellosis, tularemia, and melioidosis present serious global health threats. Those intracellular infections, localized to the lung alveolar macrophage (AM), remain one of the most challenging settings for antimicrobial therapy. Current systemic antibiotic treatment fails to deliver sustained doses to intracellular bacterial reservoirs, which necessitates prolonged treatment regimens. The goal of this thesis is to improve the suboptimal antibiotic treatments by developing targeted polymeric antibiotic therapeutics that can effectively improve the pharmacokinetics (PK) profiles of antibiotics in the lungs and AMs, where the bacteria reside in. This thesis investigated two different drug carrier systems: (1) polymer-augmented liposomes (PALs) to physically encapsulate antibiotics that are not chemically amenable to direct covalent conjugation and (2) polymeric antibiotic prodrugs with varying cleavable linker chemistries to spatially and timely control drug release. All the polymeric carriers used in this study were synthesized by Reversible-Addition Fragmentation chain-Transfer (RAFT) polymerization. Moreover, these carriers were functionalized with mannose residues to target and enhance AM uptake and intracellular delivery.

The first part of this thesis demonstrates that the streptomycin-loaded PALs significantly improved intracellular antibacterial activity in a Francisella-macrophage co-culture model, compared to free streptomycin or streptomycin delivered by control PEGylated liposomes.

However, PALs showed a typical burst release profile that was suboptimal to sustain drug release *in vivo*. To achieve better control over drug release kinetics, we engineered a polymeric antibiotic prodrug, termed drugamer, with either enzyme-cleavable dipeptides linker or hydrolytic ester linker. Following intratracheal administration, a single dose of drugamers sustained ciprofloxacin concentration in the lungs and AMs above the minimum inhibitory concentration (MIC) over at least a 48 h period. Notably, the enzyme-cleavable drugamer achieved greater than 10-fold increase in sustained ciprofloxacin dosing in AM, and maintained significantly higher pharmacokinetic properties in whole lungs as well.

Inhalation of drugamers achieved full survival (100%) in a highly lethal mouse model of pneumonic tularemia, contrasted with 0% survival using free ciprofloxacin. Impressively, the enzyme-cleavable drugamer also achieved full protection in a more challenging disease model of pneumonic melioidosis. This model requires a MIC of ciprofloxacin 100x higher than the tularemia model and ciprofloxacin is widely considered ineffective in treating melioidosis clinically. Collectively, these findings demonstrate that the targeted polymeric drugamer therapeutics are highly effective in treating pulmonary intracellular infections and also acts as a useful PK modifier for improving the dosing regimens (e.g., reduce dosage and frequency).

Keywords: Drug conjugate, liposome, macrophage targeting, enzyme-cleavable linker, tularemia, melioidosis

TABLE OF CONTENTS

LIST OF FIGURES

LIST OF TABLES

LIST OF ABBREVIATIONS

ABCVA	4,4′-azobis(4-cyanovaleric acid)
AM	Alveolar macrophage
AUC	Area-under-the curve
BAL	Bronchoalveolar lavage
BMA	Butyl methacrylate
Cat B	Cathepsin b
CD206	Mannose receptor
CFU	Colony-forming unit
Cipro	Ciprofloxacin
C_{max}	Maximum concentration
CPM	Ciprofloxacin monomer with phenol ester linkers
CTLD	c-type lectin-like domain
CTM	Ciprofloxacin monomer with phenol ester linkers linking through tyramine
CTP	4-cyano-4-(phenylcarbonothioylthio)pentanoic acid
DEAEMA	Dimethylaminoethyl methacrylate
Drugamer	Polymeric prodrug, coined by Prof. Patrick Stayton
ECT	4-cyano-4-(ethylsulfanylthiocarbonyl) sulfanylvpentanoic acid
ELISA	Enzyme-linked immunosorbent assay
ESI-MS	Electrospray ionization mass spectrometry
FBS	4-cyano-4-(thiobenzoylthio)pentanoic acid
FCP	Francisella-containing phagosome
HBC	Polymerizable ciprofloxacin with alkyl ester linkers
LC-MS/MS	Tandem liquif chromatography mass spectrometry
LTH	Lung tissue homogenate
CTA	Chain transfer agent
Man/ManEMA	Mannose ethyl methacrylate

MIC	Minimum inhibitory concentration
M_n	Number averaged molecular weight
O950	Poly(ethylene glycol) methacrylate
PAB	p-aminobenzyl alcohol
PAL	Polymer-augmented liposome
PD	Pharmacodynamics
PEG	Poly(ethylene glycol)
PK	Pharmacokinetics
RAFT	Reversible addition-fragmentation chain transfer
T>MIC	Duration that antibiotic concentrations are higher than minimum inhibitory concentration
TB	Tuberculosis
TNF-α	Tumor necrosis factor alpha
V40	1,1'-azobis(cyclohexane-1-carbonitrile)
VC	Valine-citrulline dipeptide linker
VCPAB-CIPRO	Polymerizable ciprofloxacin with valine-citrulline linker and p-aminobenzyl alcohol spacer

ACKNOWLEDGEMENTS

Looking back my adventure at UW BioE in the past 5 years, I am really grateful that I have met many people who helped me grow in professional and/or personal levels. I also appreciate the unconditional support from my family and friends. This thesis would have been impossible without any of them and I would have not become a better person.

I would like to express deep gratitude to my thesis advisor, Prof. Pat Stayton, for his guidance in the past 4.5 years. He has been pushing the boundary of my knowledge and challenging me with questions that motivated me to think deeply and thoroughly. Additionally, Pat has shown me the importance of communication and collaboration with experts in the same or complementary fields. As an international student with language barriers, I especially appreciate Pat guiding me with patience and giving me the time and environment to develop my research capability and independence.

I would like to give special thanks to Prof. Dan Ratner, my committee member and close collaborator, for his patience and support in overcoming numerous obstacles I have been facing through my research. His cheerful personality and approachable mentoring style make doing science with him like a fun adventure. Heartfelt thanks to Prof. Suzie Pun, my committee member, for her gracious mentorship on both professional and personal levels. Without her strong support, I would not have overcome several critical obstacles in my graduate study and stayed focused on my research. She has been a great role model for me as I pursue my academic career.

My sincere thanks to Profs. Shawn Skerrett and Eoin West, my committee members and collaborators, for their insightful clinical input and invaluable help with animal studies. I appreciate their guidance on how to carefully design animal studies and interpret the *in vivo* results. They have strengthened my knowledge in animal models and taught me the importance of paying attention to disease and physiological settings.

I would also like to thank the rest of my thesis committee: Prof. Elizabeth Nance, Dr. Wayne Gombotz and Prof. Andrew Boydston (prior GSR), for their valuable feedback on my research

projects and advice on my career goals. I appreciate they taking time to meet with me individually and to attend my exams.

My special thanks also goes to Dr. Selvi Srinivasan, who provided me with the continuous support throughout my Ph.D. study and taught me the beauty of chemistry. She has taught me more than I could ever give her credit for here. She has shown me, by her example, what a good scientist should be. Also thank Selvi for her encouragement and advice during difficult times.

I thank my fellow labmates in the Stayton and Ratner labs for the stimulating discussions, for the helps on conducting experiments, for editing my manuscripts, and for all the fun we have had in the last five years. Many thanks to research technicians from Dr. Shawn Skerrett's lab, Brian Lee and Frank Radella, and research technicians from Dr. Eoin West's lab, Lara Lovelace and Deirdre Ducken. Animal work would not have been possible without them, especially Brian, who played a key role in many of my animal studies. I would also like to thank Dale Whittington and Dr. Scott Edgar from UW Department of Medicinal Chemistry's Mass Spec center and Dr. Martin Sadilek from UW Department of Chemistry for teaching me all I know about LC-MS/MS. I would like to express my gratitude to the past and current members of Suzie's lab for all the help, support, and friendship that they have provided me with.

I would also like to acknowledge my friends for their support and encouragement that have pulled me through the tough days. Many thanks to my Taiwanese friends who I met in the US for all the happy memories and adventures we have had in the past five years. Also thanks my friends from BioE 2013 cohort for exploring tasty food together and providing me with constructive feedback when I prepared for my examinations. I would like to thank my friends from the Cosmos Toastmaster Club for helping me improve my public speaking skills and for their friendship and mentorship.

Last but not least, I would like to thank my family for their unconditional love and support throughout my graduate study. Despite being 6,138 miles away from Seattle, my family is undoubtedly the most important part of my support system. Additionally, I would also like to give special thanks to my host mother in Seattle, Dr. Liz Moore, for helping me along the way and giving me a home when I am away from home. Graduate school is challenging, but this experience made me believe that there are many angels on Earth.

Chapter 1. Introduction & Background information

1.1 RESPIRATORY INTRACELLULAR INFECTIONS REMAIN A GLOBAL HEALTH BURDEN

Lower respiratory infections remained the most deadly communicable disease, accounting for 3.0 million deaths worldwide in 2016 (www.who.int). Especially, intracellular infections based in the lung alveolar macrophages remain one of the most challenging anti-infective settings and unmet medical needs. For example, tuberculosis caused by *Mycobacterium tuberculosis* led to 1.3 million deaths worldwide in 2016. Moreover, most of the bacterial bioterrorism agents monitored by the U.S. Centers for Disease Control and Prevention (CDC) are intracellular pathogens, such as multidrug-resistant Mycobacterium (tuberculosis, TB), *Yersinia pestis* (plague), *Salmonella species* (salmonellosis), *Fancisella tularensis* (tularemia), *Brucella species* (brucellosis), and *Burkholderia pseudomallei* (melioidosis) (www.selectagents.gov).

F. tularensis and *B. pseudomallei*, CDC Tier 1 select agents, are the causative agents of highly infectious pulmonary tularemia and melioidosis, respectively[1-3]. The two pathogens are CDC Tier 1 select agents because of their high infectivity via inhalation, low infectious doses, and potential for misuse as biothreat agents, especially in the aerosolized form[2,4]. *F. tularensis* and *B. pseudomallei* therefore pose a severe threat to public health and safety [2,3]. No clinically approved prophylactic vaccines are currently available for either of these infections. The development of effective countermeasures is of outmost importance to combat the two pathogens, which are therefore the focuses of this research dissertation[5,6].

1.1.1 *Francisella tularensis*: Prevalence, etiology, and intracellular life cycle

F. tularensis is a highly infectious, facultative intracellular bacterium that caused tularemia, a serious and potentially fatal disease[2]. Tularemia has been reported in several parts of the northern hemisphere with high incidence, such as Regions of Scandinavia, Russia, and the United States (**Figure 1.1**)[2]. Inhalation of *F. tularensis* would lead to the most acute form of tularemia

(respiratory tularemia) with less than 10 colony-forming unit (CFU)[2]. Clinical manifestations of respiratory tularemia include dry cough, headache, fever, and chest pain[7]. Without prompt antibiotic treatment, a fatality rate of up to 30% has been observed. Additionally, relapses are common and often associated with delayed and/or insufficiently long treatment[8].

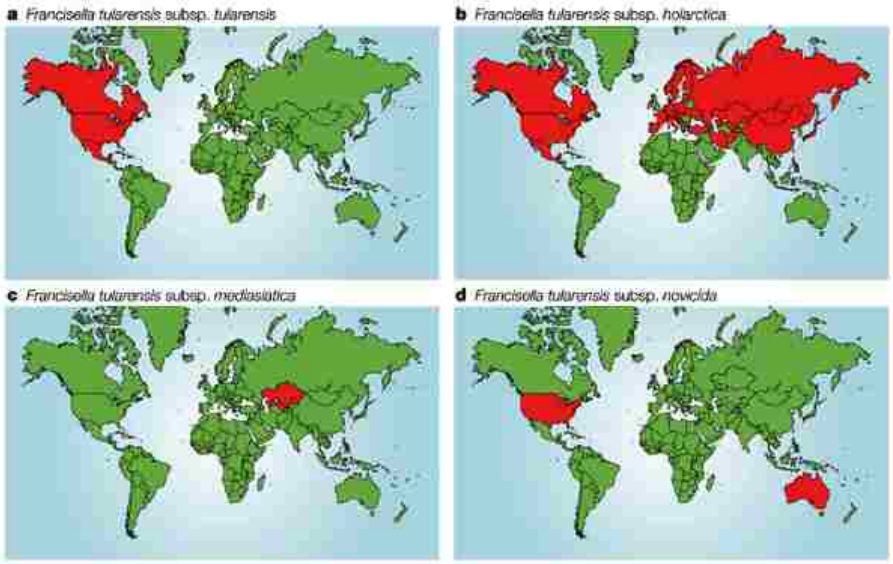

Figure 1.1. Worldwide incidence map of the four main Francisella subspecies. Regions where tularemia has been reported are shown in red[2].

The virulence of *F. tularensis* relies on its ability to invade, survive, and proliferate within mammalian cells, such as alveolar macrophages, neutrophils and epithelial cells [9]. Among them, alveolar macrophages (AMs) are considered to be the major target of this pathogen in the early stages of respiratory tularemia (**Figure 1.2**)[10]. Inhaled *F. tularensis* can be recognized by multiple macrophage receptors (e.g., FcγR, scavenger receptor A) and are engulfed by a unique pseudopod loop mechanism[11,12]. The bacteria are then trafficked to an early phagosome called the Francisella-containing phagosome (FCP), which contains an array of toxic antimicrobials aimed at degrading the bacteria. However, *F. tularensis* are able to evade these measures through multiple mechanisms. For example, *F. tularensis* block the NADPH oxidase and also detoxifies reactive oxygen species (ROS). They can also resist the action of antimicrobial peptides (AMPs). *F. tularensis* then escapes the FCP to avoid phagosomal antimicrobials and, importantly, reach the cytosol, where it replicates to high numbers before lysing the cell to initiate a new round of

infection. This intracellular compartmentalization of *F. tularensis* is a significant barrier to bacteria clearance and contributes to their associated morbidity and mortality.

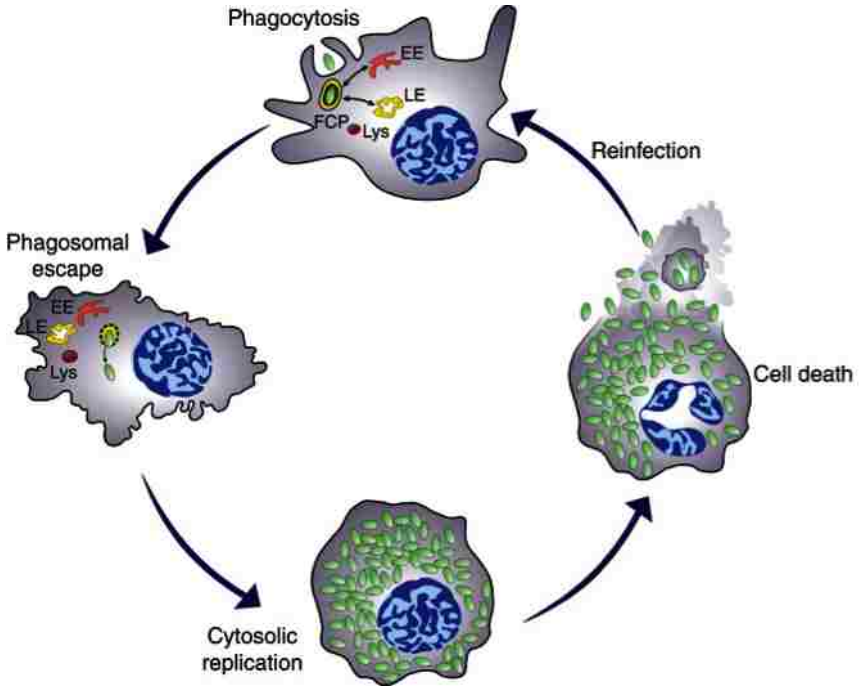

Figure 1.2. Intracellular life cycle of *Francisella tularensis*. Model of the Francisella intracellular cycle depicting stages that are common to murine and human phagocytes. Upon phagocytosis, bacteria reside in an early phagosome (FCP) that interacts with early (EE) and late (LE) endocytic compartments but not lysosomes (Lys). Bacteria rapidly disrupt the FCP membrane and reach the cytosol where they undergo extensive replication, a process followed by cell death, bacterial release, and subsequent infection[9].

1.1.2 *Burkholderia pseudomallei*: Prevalence, etiology, and intracellular life cycle

Burkholderia pseudomallei is a highly pathogenic bacterium that causes melioidosis, a severe disease that is endemic in areas of Southeast Asia and Northern Australia (**Figure 1.3**)[3,13]. Melioidosis can be difficult to diagnose due to its diverse clinical manifestations and the inadequacy of conventional bacterial identification methods. The most severe clinical manifestation is melioidosis septic shock, which is often associated with pneumonia and bacterial dissemination to distant sites. *B. pseudomallei* is intrinsically resistant to a wide range of antimicrobials, including penicillin, first- and second-generation cephalosporins, macrolides,

rifamycins, colistin and aminoglycosides[3]. Treatment with ineffective antimicrobials may result in case fatality rates (CFRs) exceeding 70%[13]. Furthermore, recurrence of infection is common despite adequate antimicrobial therapy[3].

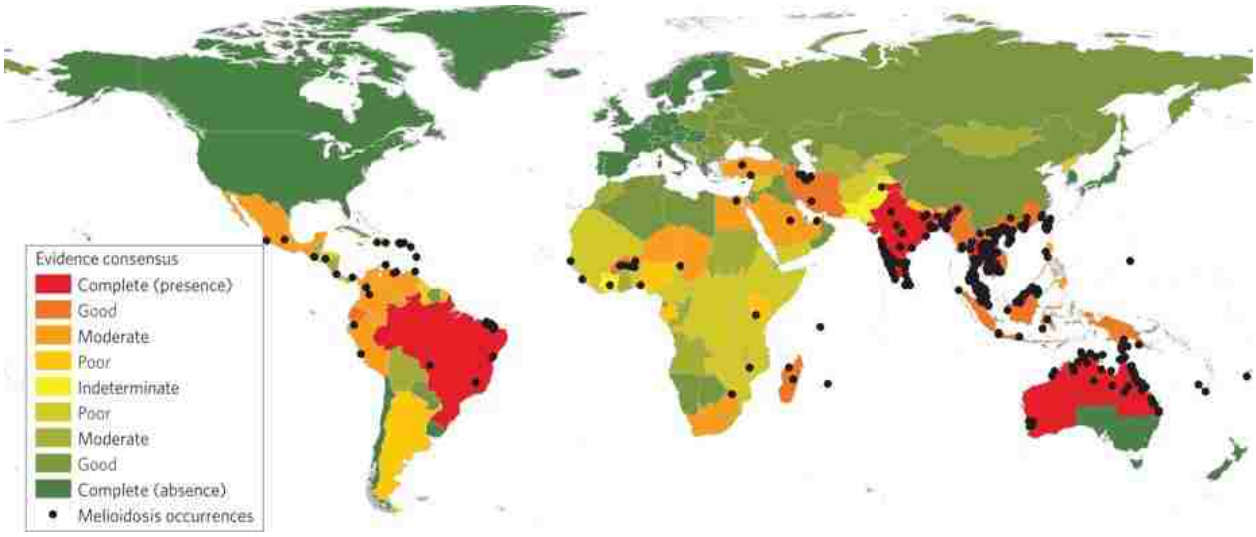

Figure 1.3. Global evidence consensus and geographic locations of occurrence data from 1910 to 2014. Country colouring is based on evidence-based consensus, with green representing a complete consensus on absence of *B. pseudomallei* and red a complete consensus on presence of *B. pseudomallei*. Black dots represent geo-located records of melioidosis cases or presence of *B. pseudomallei*[13].

Similar to *F. tularensis*, *B. pseudomallei* is capable of invading many cell types, and can survive and proliferate for prolonged periods within phagocytic cells[14,15]. AMs are one of the primary early target cells for Burkholderia infection in the lungs[14,16]. The Burkholderia secretion apparatus (BSA) system, type III secretion gene cluster encodes proteins, is required for bacterial invasion, escape from phagosomes and intercellular spread (**Figure 1.4a**)[3]. *B. pseudomallei* has evolved to resist several host antimicrobial peptides (e.g., protamine and certain defensins) and interfere with the synthesis of inducible nitric-oxide synthase (iNOS), which is known to have an important role in the killing of intracellular bacteria[15,17]. As early as 15 minutes after internalization, *B. pseudomallei* can escape from endocytic vacuoles into the cytoplasm of infected cells by lysing the endosome membrane thus avoiding degradation through the lysosomal system (**Figure 1.4b**)[15]. Once inside the cytoplasm, *B. pseudomallei* not only replicates rapidly, but induces the formation of actin-based membrane protrusions by continuous

nucleation of actin at one pole of the bacterial cell (**Figure 1.4c**)[18]. When a neighboring cell phagocytoses this protrusion, *B. pseudomallei* spreads to the new cell without exposure to antibodies or immunoactive molecules. In the new cell, *B. pseudomallei* will subsequently escape from the secondary vacuoles and multiply intracellularly[18,19].

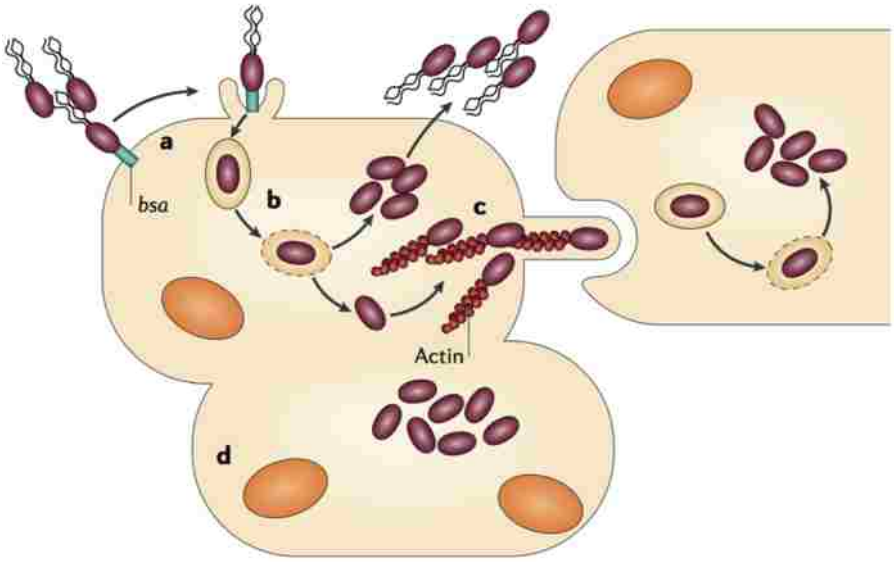

Figure 1.4. **The intracellular life cycle of *Burkholderia pseudomellei.*** (a) Invasion of phagocytic and non-phagocytic cells. (b) Endosome escape and intracellular proliferation. (c) Cell-to-cell spread. (d) Cell fusion[3]. bsa: Burkholderia secretion apparatus.

1.1.3 Current treatment regimens and limitations

Current clinical management for tularemia and melioidosis is antibiotic therapy through intravenous (IV) injection or oral administration with exhausted dose for prolonged periods of time (**Table 1.1 & 1.2**)[20,21]. This treatment is suboptimal in two perspectives. First, systemic delivery including IV and oral administration provides poor drug distribution and relatively unfavorable pharmacokinetics (PK) profiles in the lower respiratory tract and especially in the AMs, the primary site of early stage infection[22,23]. This unfavorable PK properties include a relatively short retention time and a low area under the concentration-time curve (i.e., total drug exposure)[22]. Second, clinically used antibiotics exhibits suboptimal cellular pharmacokinetic properties (**Table 1.3**)[1]. For example, aminoglycoside (e.g., streptomycin and gentamicin) shows

slow intracellular accumulation and takes several days to achieve an apparent cellular-to-extracellular ratio of 2 to 4[24,25]. While fluoroquinolones like ciprofloxacin rapidly accumulate in the cell, the fluoroquinolones efflux is greater than uptake, leading to poor intracellular retention[26,27]. The resulting off-target drug distribution induces side effects, including aminoglycoside-associated ototoxicity and fluoroquinolone-associated tendon rupture[28,29].

Table 1.1. Working group consensus recommendations for treatment of patients with tularemia under different scenarios[20].

Stage		Drug	Dose*	Duration
Pre-exposure prophylaxis		No vaccine is currently available		
Post-exposure prophylaxis		Doxycycline	100 mg	orally twice daily for 14 days
		Ciprofloxacin	500 mg	orally twice daily for 14 days
Treatment (symptoms are evident)	Contained casualty setting	Preferred: Streptomycin, Gentamicin	1 g, 5 mg/kg	IM twice day, IM/IV once daily for 10 days
		Alternative: Doxycycline, Chloramphenicol, Ciprofloxacin	100 mg, 15 mg/kg, 400 mg	IV twice daily for 14-21 days, IV 4 times daily for 14-21 days, IV twice daily for 10 days
	Mass casualty setting	Same as Post-exposure prophylaxis		

Favorable intracellular penetration, accumulation and disposition, in addition to lung distribution, are essential to antibacterial agents for the treatment for pulmonary intracellular infections[1]. Due to the suboptimal systemic and cellular pharmacokinetic properties of systemic drug delivery, high dose and prolonged antimicrobial therapy is usually prescribed for infected patients to reduce chance of relapse[20,30]. However, this dosing regimen may not only causes side effects as mentioned earlier, but also potentially result in emergence of antibiotic resistance, making treatments more problematic[31]. Moreover, no licensed vaccines are current available for

prophylaxis of tularemia and melioidosis[5,6]. For those reasons, new approaches to provide effective prophylactic and therapeutic therapy for *F. tularensis* and *B. pseudomallei* infections are urgently needed.

Table 1.2. Antibiotic therapy for culture confirmed melioidosis[21].

Severe, acute melioidosis including septicaemia, with or without pneumonia, central nervous system infection and other invasive forms of the disease:
EITHER Ceftazidime (adult) 2-3 g or 40 mg/kg/dose every eight hours intravenously for 2-4 weeks PLUS Co-trimoxazole (Trimethoprim-Sulphamethoxazole) 10/50 mg/kg (up to 320/1600 g) every 12 hours
OR Meropenem 1 g or 25 mg/kg every eight hours intravenously for ≥ 2 weeks
Eradication phase 1 Trimethoprim-Sulphamethoxazole 8/40 mg/kg every 12 hours for ≥ 12-20 weeks 2 Doxycycline 4 mg/kg/day plus Trimethoprim-Sulphamethoxazole 8/40 mg/kg every 12 hours for ≥ 12-20 weeks 3 Chloramphenicol 40 mg/kg/day plus Doxycycline 4 mg/kg/day, Trimethoprim-Sulphamethoxazole 8/40 mg/kg every 12 hours for ≥ 12-20 weeks

Table 1.3. Influx, accumulation levels (at equilibrium), efflux, and predominant subcellular localization of the main antibiotics (grouped by pharmacochemical classes)[1].

Pharmacochemical class	Antibiotic	Influx[a]	Efflux[a]	Accumulation level (at equilibtrum)[b]	Predominant subcellular localization
β-Lactams	All	Fast	Variable	<1	Cytosol
Macrolides	Erythromycin	Fast	Fast	4–10	Two third lysosomes/ one third cytosol
	Clarithromycin, roxithromycin	Fast	Fast	10–20	
	Azithromycin	Fast	Slow to very slow	40–300	
	Telithromycin	Fast	Fast to slow	15–50	
Fluoroquinolones	All	Fast to very fast	Very fast	4–10	Cytosol
Aminoglycosides	All	Very slow	Very slow	2–4 (after several days)	Lysosomes
Lincosaminides	Clindamycin	Fast	Fast	5–20	Unknown
	Lincomycin	Fast	Fast	1–4	
Tetracyclines	All (?)	Fast	?	1–4	Unknown
Ansamycins (rifamycins)	Rifampin	Fast	?	2–10	Unknown
	Rifapentin	Fast	?	60–80	
Glycopeptides	Vancomycin	Slow	?	8 (after 24 h)	Lysosomes (in kidney)
	Teicoplanin	Fast	?	60	Unknown
	Oritavancin	Slow	Slow	150–300 (after 24 h)	Probably lysosomal
Oxazolidinones	Linezolid	Fast	Fast	~1	Unknown

[a] very fast: less than 3 min to equilibrium; fast: 3 to 15 min to equilibrium; slow: 15 min to 3 h to equilibrium; very slow: more than 3 h to equilibrium.

[b] C_c/C_E: accumulation factor (ratio between the cellular concentration and the extracellular concentration).

1.2 PULMONARY ANTIBIOTIC DELIVERY

1.2.1 *Promises and challenges*

Pulmonary delivery is the most efficient way for the local administration of drugs to treat disease locally within the lung. The same anatomical and physiological characteristics that make airways susceptible to infection by external pathogens can be exploited for drug delivery (**Figure**

1.5)[32,33]. Pulmonary drug delivery provides several advantages for treating infections in the lungs. First, pulmonary administration can achieve higher local drug concentration at the infection site[34,35]. Second, the lung provides enormous absorptive surface area (100 m^2) and a highly permeable membrane (0.2–0.7 mm thickness) in the alveolar region[36]. Third, pulmonary drug administration avoids first-pass metabolism and decreases enzymatic drug degradation, since lower enzymatic activity is present in the lungs compared to other organs (e.g., liver and gastrointestinal tract)[32].

Currently, several inhaled antibiotic formulations are available on the market (**Table 1.4**)[37]. For example, Cayston® and TOBI®, have been approved for chronic pulmonary infection involving *Pseudomonas aeruginosa* in patients with cystic fibrosis. There is, however, no inhaled antibiotic formulation approved for tularemia and melioidosis. It is conceivable that inhaled antibiotic formulations would be convenient and feasible for prophylactic and therapeutic treatments against *F. tularensis* and *B. pseudomallei* in terrorist attack settings or battlefields.

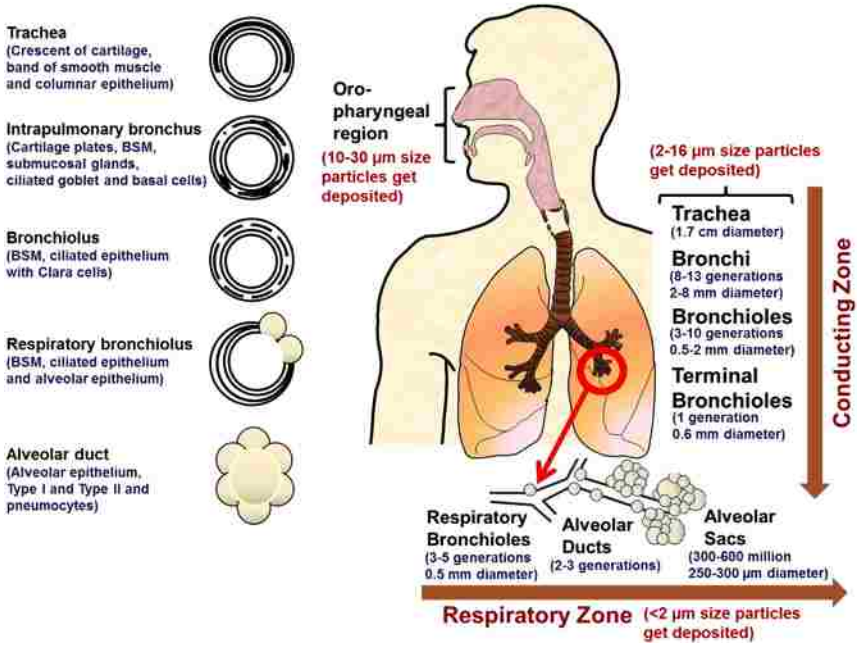

Figure 1.5. Lung physiology. The number and dimensions of the airways of the adult lung and structure of the airway wall.

Despite of the promises of inhaled antibiotic therapeutics, a major challenge lies in the short half-life of small-molecule drugs in the lung[38], which then necessitates frequent drug administration. For instance, inhaled ciprofloxacin were cleared out of the lung in about 30 min post-inhalation as shown in a murine model (**Figure 1.6**)[39]. Additionally, as mentioned earlier in Section 1.1.3, free drugs do not preferentially accumulate and retain in AMs, where intracellular bacteria reside in. Therefore, inhalable drug carriers that can sustain drug delivery in both the lung and AMs provide new opportunities to develop prophylactic and therapeutic treatments against *F. tularensis* and *B. pseudomallei* and potentially other pulmonary intracellular infections as well.

1.2.2 Alveolar macrophage as an important target cell for antibiotic delivery

AMs, the resident mononuclear phagocytes of the lung, provide the first line of defence against organisms or particles reaching the lower airways[40]. When *F. tularensis* and *B. pseudomallei* enter human bodies through inhalation, AMs are the major host cells at the early stage of infection, because those bacteria are facultative intracellular pathogens (i.e., can replicate extracellularly, but prefers the intracellular environment) (**Figure 1.2 & 1.4**) [2,14]. It is therefore important to deliver concentrated doses of antibiotics to the lower respiratory tract so that these agents can be killed before they spread systemically from the lungs. Aerosol inhalation of liposomal-encapsulated ciprofloxacin has shown to provide mice with complete protection against a lethal *F. tularensis* pulmonary infection, where the free ciprofloxacin was not active[39,41]. The enhanced therapeutic efficacy can be attributed to the increased retention of ciprofloxacin in the lungs and better intracellular delivery of ciprofloxacin by liposomes. As for Burkholderia infections, no report has shown if targeted antibiotic delivery to AMs would enhance antibacterial efficacy against Burkholderia infections. Based on the current understanding of *B. pseudomallei* and the lessons learned from drug carriers designed for *F. tularemia*, we hypothesize that drug carriers that enhance intracellular antibiotic delivery to AMs would be promising strategy to improve current treatments for Burkholderia infections.

Table 1.4. Characteristics of inhaled antibiotic formulations on the market[37].

Characteristics of inhaled antibiotic formulations.

Drug product (company)	Drug substance	Device	Drug product	Nominal dose	Osmolarity (mOsm/kg)	pH	Excipients	Ref
TOBI® (Novartis)	Tobramycin	Jet nebulizer	Solution	300 mg (5 ml)	158-183	6.0	2.25 mg/ml NaCl (Cl^- ~75 mM); pH adjusted with sulfuric acid	132
Bethkis® (Cornerstone)	Tobramycin	Jet nebulizer	Solution	300 mg (4 ml)	280-350	5.2	0.45% NaCl; pH adjusted with sulfuric acid	190
TOBI® Podhaler™ (Novartis)	Tobramycin	Podhaler™ DPI	Spray-dried powder	112 mg (4 caps)	–	–	15% w/w, 2:1 molar ratio of DSPC:$CaCl_2$	87
Arikace™ (Insmed)	Amikacin	eFlow®	Liposome	560 mg (8 ml)	~485		~30 mg/ml DPPC, 15 mg/ml cholesterol, 1.5% NaCl QS	194
Cayston® (Gilead)	Aztreonam	Altera® eFlow	Powder for reconstitution	75 mg (1 ml)	550	4.5-6.0	46.7 mg lysine monohydrate, 0.17% NaCl	195
Pulmaquin™ (Grifols)	Ciprofloxacin HCl	Jet nebulizer	Liposome encapsulated Free drug	150 mg (3 ml) 60 mg (3 ml)	255-345	6.0	65.9 mg/ml HSPC, 27 mg/ml cholesterol	29, 196
Aeroquin® (Aptalis)	Levofloxacin	eFlow®	Solution	240 mg (2.4 ml)	350-500	5-7	Complex with metal ion (e.g., Mg^{++}) to increase solubility	197, 198
Ciprofloxacin DPI (Bayer)	Ciprofloxacin betaine	Podhaler™ DPI	Spray-dried powder	32.5 mg (1 cap)	–	~7.0	30% w/w, 2:1 molar ratio of DSPC:$CaCl_2$	110, 111
Colomycin® (Pharmax)	Colistimethate	Jet nebulizer	Powder for reconstitution	80 mg (3.0 ml)	288-335	7.3-7.8	Normal saline	Pkg insert
Colobreathe® (Forest)	Colistimethate	Turbospin®	Neat micronized drug	125 mg (1 cap)	–	–	None	73
FTI (CURx)	Fosfomycin / Tobramycin	eFlow	Solution	160 mg/40 mg (4 ml)	837			124, 133
AeroVanc™ (Savara)	Vancomycin	RS01 DPI (Plastiape)	Spray-dried powder	≤64 mg (4 caps)	–	–		199
ABIP Novartis)	Amphotericin B	Podhaler™ DPI	Spray-dried powder	10 mg (1 cap) following loading dose	–	–	50% w/w, 2:1 molar ratio of DSPC:$CaCl_2$	–
FAI (Cardeas)	Fosfomycin / Amikacin	eFlow (CMV)	Solution	TBD 20 mg/ml 50 mg/ml				52,133
BAY 41-6551 (Bayer)	Amikacin	PDDS (CMV)	Solution	400 mg (3.2 ml)				51, 192

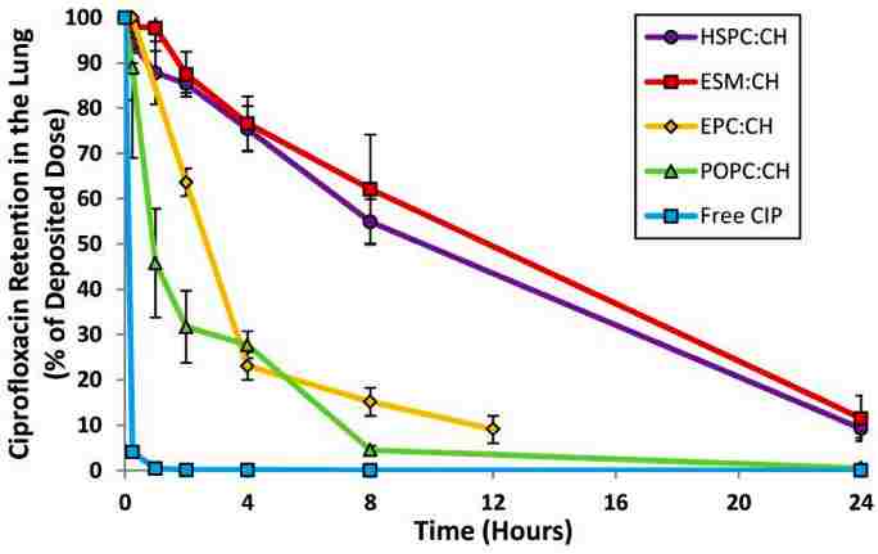

Figure 1.6. Retention of free form or liposomal ciprofloxacin in the lung following intranasal instillation in mice (or inhalation for EPC:CH formulation). * CIP = Ciprofloxacin. CH = cholesterol[39].

1.3 PHARMACOKINETIC/PHARMACODYNAMIC CONSIDERATIONS FOR OPTIMAL ANTIBIOTIC THERAPY

1.3.1 *Antibiotic classification: concentration-/time-dependent*

Antibiotics can be categorized into two types based on their antimicrobial patterns: concentration-dependent and time-dependent[42,43]. For drugs that have concentration-dependent bactericidal action, such as aminoglycosides and fluoroquinolones, the rate of bactericidal activity will be maximized at the peak concentration (C_{max}) in serum. Higher doses of the drug will increase not only the rate of reduction of bacteria but also the length of time of drug exposure to bactericidal concentrations[22,44]. Time-dependent killing refers to the time it takes for a pathogen to be killed by exposure to an antimicrobial agent. Time-dependent killing is characteristic of many antibiotic classes, such as β -lactams and macrolides, and seeks to optimize the duration of exposure of a pathogen to an antimicrobial[45,46]. Therefore, the killing patterns provide a rational basis for determination of optimal dosing regimens in terms of dose and the dosing intervals.

1.3.2 *Pharmacokinetics/pharmacodynamics parameters governing antibiotic efficacy*

Pharmacokinetics/pharmacodynamics (PK/PD) parameters have been developed as a new discipline to understand and predict outcomes of clinical antibiotic therapy[42]. PK/PD index presents the quantitative relationship between a pharmacokinetic parameter and a microbiological parameter. The three main PK/PD parameters are the time during which the concentration of the drug was over the MIC (T>MIC), the peak concentration and MIC ratio (C_{max}/MIC), and the ratio of the 24-h area under the concentration-time curve divided by the MIC (AUC/MIC) (**Figure 1.7**)[47,48]. For concentration-dependent antibiotics, such as fluoroquinolones or aminoglycosides, C_{max}/MIC and AUC/MIC are the main factors that establish efficacy. For instance, For gram-negative infections, a C_{max}/MIC of 10 or greater and an $AUC_{0–24}$/MIC of 125 or greater have been associated with an increased probability of a successful clinical outcomes[49]. Time-dependent antibiotics generally have their efficacy linked to T>MIC, and these include beta-lactams and macrolides. For beta-lactams, literature has shown

that serum concentrations above the MIC of at least 50 or 60% of the dosing interval seem to be required for optimal efficacy[45]. Notably, for intracellular infections, studying intracellular PK/PD indexes of antibiotics is of prime importance because it defines the access of drugs to the site of infections[50]. By applying these concepts to antibiotic agents, it is possible to optimize their dosages and dosing regimens, thus maximizing the therapeutic efficacy[51].

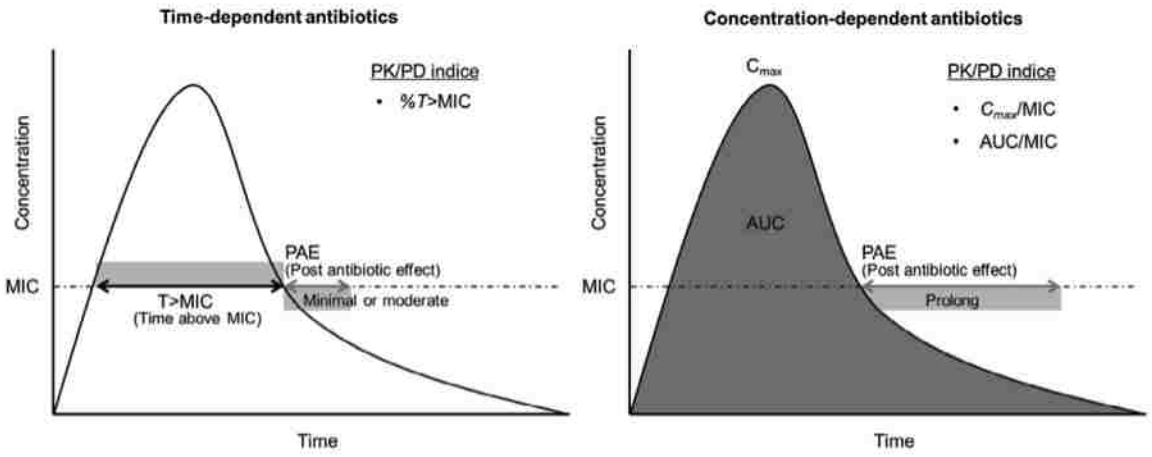

Figure 1.7. Principal PK/PD characteristics of antimicrobial drugs[48].

1.4 ENGINEERING NANOCARRIERS AS PK MODIFIERS IN ALVEOLAR MACROPHAGES

Use of nanocarriers (e.g., liposomes, micelles, polymeric prodrugs) in delivery of antimicrobial agents has been explored as a promising strategy to enhance therapeutic efficacy of the current suboptimal antibiotics-based therapies[52-54]. The advantages of this strategy include improved solubility of poorly water-soluble drugs, prolonged drug half-life and systemic circulation time, and sustained and stimuli-responsive drug release, which eventually lowers administration frequency and dose[31]. Moreover, nanocarriers can minimize systemic side effects by targeted delivery in three distinct levels[55]. First-level targeting refers to distribution restricted to the target organ or tissue; second-level targeting refers to selective direction to the target cells; third-level targeting refers to delivery to selected intracellular sites[56]. The first-level targeting to the lungs can theoretically be enhanced by inhalation delivery of nanocarriers with proper aerodynamic

size. Additional considerations on physicochemical properties of nanocarriers have to be met for efficient uptake by AMs, including aerodynamic size and surface properties[57]. Those were further discussed in the following sections.

1.4.1 Optimal size for alveolar deposition and macrophage uptake

Deposition in the alveolar sacs is essential for antibiotic-containing nanocarriers targeting AMs. After inhalation, external particles will be transported with the inhaled air through the respiratory tract until they are deposited or exhaled. Among the features that influence the behavior of inhaled particles in the airways, the mean aerodynamic diameter is a critical parameter that governs the particle deposition. Particles with aerodynamic diameter of 1-3 μm have been shown to deposit optimally in the alveolar region of the lungs[58]. Particles less than 100 nm in diameter are also able to deposit by diffusion in the alveolar region (**Figure 1.8**)[32,58]. Based on those empirical data, care must be taken to ensure the aerodiameter of aerosol droplets containing drug carriers allowing deep lung deposition.

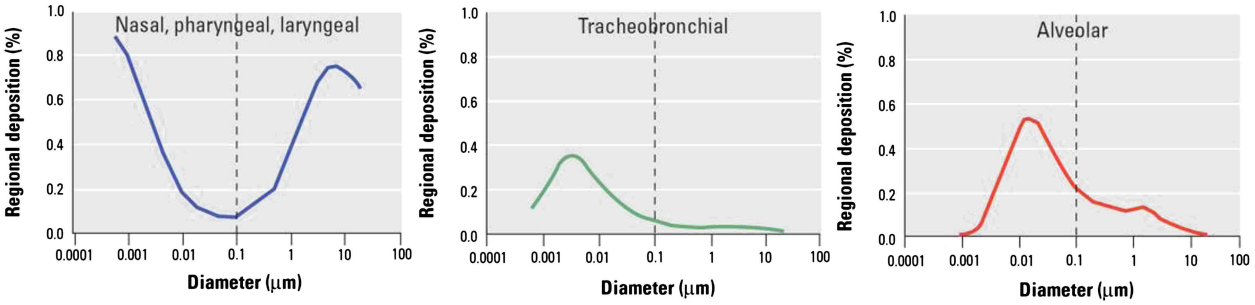

Figure 1.8. Regional deposition pattern of particles according to their aerodynamic[32].

Regarding the ideal size for AM uptake via phagocytosis, the general consensus is that, particles, ranging between 1-6 μm, are the most accessible to AMs, while particle larger than 10 μm or smaller than 0.2 μm are able to escape phagocytosis[57,59]. Although nanoparticles smaller than 0.2 μm can escape phagocytosis, AMs ingest nanoparticles through pinocytosis with optimal size range to be around 100-200 nm[59]. Considering the factors of lower respiratory deposition and AM uptake, the optimal size ranges of inhaled drug carriers for passive AM targeting are 1-3 μm and around 100 nm for passive AM targeting.

1.4.2 Ligand modification for alveolar macrophage targeting

Using ligand modifications to enhance AM–targeting of drug carriers has the potential advantage of increasing target specificity, in comparison to passive targeting achieved by tailoring physicochemical properties of drug carriers, such as size and surface charge[60]. A various types of targeting ligands for AMs have been assessed, including peptides, antibodies, proteins, and carbohydrates[60]. Compared with other ligands, carbohydrates can be easily synthesized in large scale[61], are stable to indefinite storage at ambient temperatures[62], and can leverage low-affinity binding interactions through multivalency[63]. Specifically, mannose has been shown to engage the carbohydrate-binding domains (i.e., C-type lectin-like domain or CTLD) of macrophage mannose receptors (i.e. CD206) on the AM surface (**Figure 1.9**)[64,65]. The binding affinity between mannose and mannose receptor can be significantly strengthened by the multivalent effect of clustered sugars (cluster glycoside effect) from micro-molar scale to nano-molar[63,66].

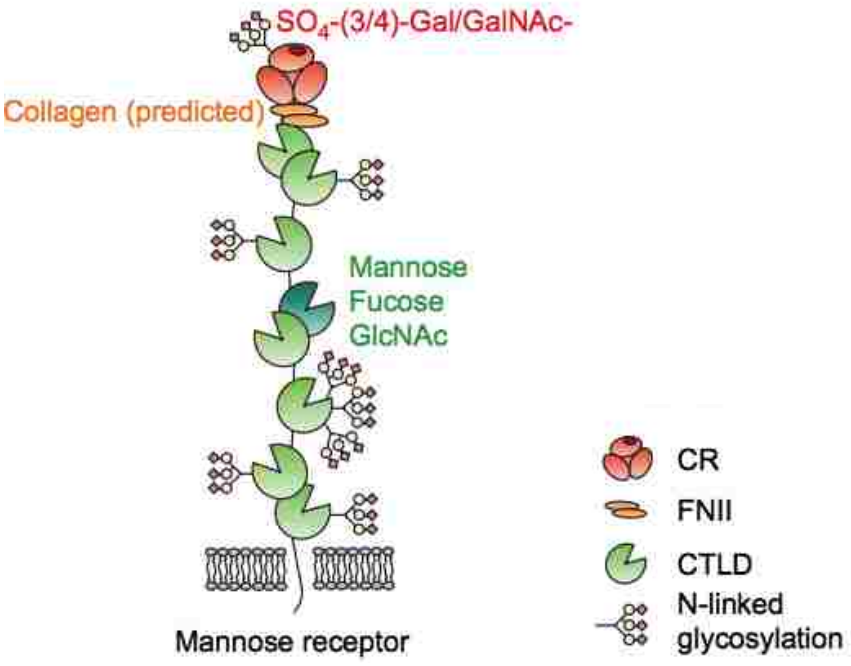

Figure 1.9. Structure of the mannose receptor. Domain structure of the mannose receptor showing the proposed extended conformation and predicted N-linked glycosylation (proposed sialylation indicated by red diamonds). The cysteine-rich (CR) domain (red), fibronectin type II (FNII) repeat (brown) and C-type lectin-like domain (CTLD, green) are shown. CTLD4, the

CTLD mostly responsible for sugar binding, is shown in dark green. Ligands for each of the binding regions have also been included (colors correspond to the binding domain where known)[65].

Our group has shown that multivalent mannose-functionalized polymer demonstrated 6-fold higher internalization by AMs, as compared with galactose, following intratracheal administration in mice[64]. Additionally, mannose modification has been shown to increase liposome uptake by AMs, and thereby significantly increased cellular pharmacokinetics properties of ciprofloxacin (1.5- and 2.4-fold higher in area under curve and maximum concentration than unmodified liposomes)[67]. Therefore, enhancing AM internalization by mannose targeting ligands could be a promising approach to achieve therapeutically relevant concentrations in target cells.

1.4.3 Inhalable liposomal antibiotics under clinical trials

Inhalable liposomal formulations have been developed to improve tolerability or to modify the pharmacokinetic and biodistribution profile of free antibiotics[68]. Liposomal formulations improve tolerability by reducing the incidences of respiratory side effects, such as free antibiotic-induced irritations on the respiratory tracks[68]. As mentioned earlier, most inhaled antibiotics have a short half-life in the lung due to rapid systemic absorption, thus requiring multiple administrations each day to ensure that drug concentrations in the lungs remain higher than the minimum inhibitory concentration (MIC)[69]. Thus, the use of a formulation agent to extend the residence time of the antibiotic in the lungs may allow for a reduction in the dosing frequency while still continuously maintaining adequately high drug concentrations in the lungs. Additionally, liposomes can also deliver antibiotics to macrophages by passive targeting (e.g., phagocytosis) and active targeting (e.g., mannose modification for receptor-mediated endocytosis).

Currently two inhalable liposomal formulations are in late stage development: amikacin (Insmed, Inc.) and ciprofloxacin (Aradigm®)[68,70]. Amikacin liposome inhalation suspension (ALIS), developed by Insmed, Inc., is a once-daily formulation of amikacin for the treatment of nontuberculous mycobacterial (NTM) lung infections. ALIS is composed of neutral,

biocompatible lipids (DPPC and cholesterol, 2:1 mole ratio), and aerosolized via eFlow® Nebulizer System manufactured by PARI Pharma GmbH (PARI). ALIS liposomes are readily taken up by AMs, which is important to achieve effective intracellular drug concentrations against NTM[71]. New drug application (NDA) for ALIS liposomes is currently under Priority Review by the FDA with an action date of September 28, 2018 under the Prescription Drug User Fee Act (PDUFA) (http://www.insmed.com/).

As for liposomal ciprofloxacin, Aradigm has developed two clinical-stage formulations– Lipoquin® and Linhaliq® (formerly known as Pulmaquin®) (**Figure 1.10**). Lipoquin® is a slow release liposomal formulation, composed of hydrogenated soy phosphatidylcholine and cholesterol in a 7:3 ratio (by weight)[72]. Linhaliq®, dual release ciprofloxacin for inhalation, is an equivolume mixture of Lipoquin (3 mL, 50 mg/mL ciprofloxacin HCl) and free ciprofloxacin dissolved in an aqueous medium (3 mL, 20 mg/mL ciprofloxacin HCl). The two formulations were aerosolized through a PARI LC Sprint powered by a PARI Turbo Boy-S compressor (PARI, Richmond, USA). These liposomal formulations have demonstrated up through human trials that the pharmacokinetics (PK) of antibiotics in the lung can be modulated by the carriers. Dispersal based formulation approaches, however, can also suffer from various drawbacks including instability in biological fluids and tissues, initial burst release profiles, challenges in drug loading and difficulties in combination drug formulations[73,74].

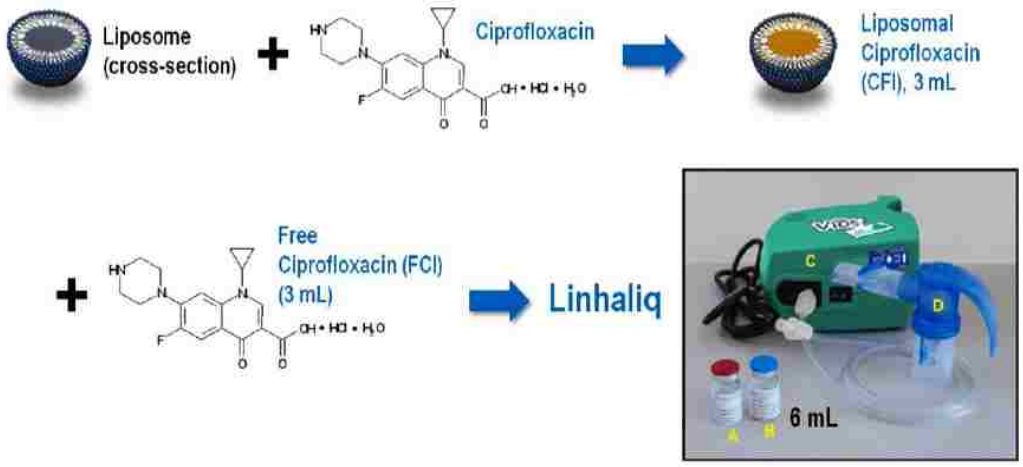

Figure 1.10. Aradigm® Linhaliq design and delivery.
(Source: AMDAC Briefing Document – Linhaliq)

1.4.4 Polymeric prodrug conjugates for better control of drug release

Chemical conjugation of drug molecules to polymers offers numerous advantages for small molecule delivery[75,76]. A key feature of a polymeric prodrug conjugate is that rather than containing a drug that is physically encapsulated within a polymeric structure, the drug is covalently conjugated to the polymeric carrier[77]. In this regard, problems associated with 'burst' and/or uncontrolled drug release can be largely overcome and the drug can be covalently linked to the polymer via varying linker chemistries (e.g., ester, amide, and urethane) that are specifically designed to liberate drug within certain structures, or at a predicted rate *in vivo*. Through simple chemical modifications, the bioactive release rate can potentially be fine-tuned from days to many months, depending on the desired application and need[75].

Polymeric prodrug conjugates are often synthesized by one of three strategies, including 1) conjugating the drug to an established polymer, 2) conjugating the drug to a monomer, followed by polymerization, and 3) using an existing drug containing two or more functional groups as a monomer for poly-drug polymerization[77]. The first strategy is used more often, but can lead to poor control over drug conjugation and limited drug loading, depending on the size and nature of the polymer structure. In contrast, polymerization of drug-monomer conjugates generally provides good control over drug loading and the final product, but it may require more steps of synthesis procedures[78,79].

As an example for the first strategy (antibiotic conjugation to preformed polymers), norfloxacin was conjugated to a poly(L-lysine citramide) carrier using an ethyl carbamate linker. The resulting polymer-drug conjugate released 25% and 8% of free drug after 30 days at pH 4.5 and 7.4 buffers, respectively[80]. Our group has recently developed a polymeric antibiotic prodrug platform that was built upon polymerizable prodrug monomers[81]. The tunable hydrolysis kinetics of this platform was mediated by drug linkage chemistry (slower-releasing alkyllic vs faster-releasing phenolic esters). Copolymers containing ciprofloxacin linked via phenolic esters showed faster hydrolysis rates with 50% drug released at 5 d, whereas copolymers with the corresponding aliphatic ester linkages showed the same drug release over 22 d. Together with other reported systems, those observations indicates that polymeric prodrug conjugates better sustain drug release compared with drug-encapsulated nanoparticle systems[82,83].

1.5 REVERSIBLE-ADDITION FRAGMENTATION CHAIN-TRANSFER (RAFT) POLYMERIZATION FOR DEVELOPING POLYMERIC ANTIBIOTIC CARRIERS

1.5.1 Mechanism behind RAFT

Polymeric nanocarriers designed for clinical applications must have well-defined architectures, controlled molecular weights, and high uniformity. Living radical polymerizations (LRPs) including reversible addition-fragmentation chain transfer (RAFT) and atom-transfer radical-polymerization (ATRP) have been used to minimize the heterogeneity of polymers[84]. RAFT polymerization is one of the most versatile LRPs, because of its compatibility with a wide range of functional monomers/reaction conditions, and the lack of any toxic metal catalysts[85-87].

A key feature of RAFT polymerization is the use of a RAFT or chain transfer agent (CTA) (typically thiocarbonylthio compounds) containing an R group that is a free radical leaving-group capable of reinitiating polymerization, and a Z group that (1) activates the thiocarbonyl bond towards radical addition and (2) stabilizes the resulting radical[88,89]. The mechanism of RAFT polymerization was shown in **Figure 1.11**. Polymerization is initiated when a free radical reacts with the CTA, followed by fragmentation of this intermediate into a polymeric thiocarbonylthio compound and a new radical. Reaction of the latter with monomer forms a further propagating radical. Rapid equilibrium between the active propagating species and dormant polymeric thiocarbonylthio compounds (macroCTAs) reduces concentrations of free radicals in solution, limiting termination and uncontrolled polymer propagation[86,90]. Consequently, RAFT provides unprecedented control over polymer molecular weight, size distribution, composition and architecture[85].

The “living” character retained by most macroCTAs allows subsequent polymerizations to create block copolymers, macromolecules that incorporate two or more monomer sequences. Also, the RAFT process can be combined with naturally occurring building blocks such as carbohydrates, cyclodextrins, proteins, and peptides for bioapplications[91,92]. A sophisticated tool for designing advanced polymeric materials, RAFT has much potential for the development of novel pharmaceutical carriers.

1.5.2 RAFT synthesis of antimicrobial polymers

Application of RAFT polymerization for the synthesis of antimicrobial polymers was mostly on polymers with intrinsic antimicrobial properties[93]. For example, synthesis of amphiphilic polymers having both hydrophilic cationic and hydrophobic segments is a suitable strategy to afford antimicrobial materials. Thoma et al. developed antimicrobial homopolymers composed of ammonium ethyl methacrylate homopolymers (AEMPs) via RAFT polymerization[94]. The homopolymers have shown antimicrobial activity against both MRSA and non-MR S. aureus and significant reduction in the number of viable S. aureus cells in cotton rat nasal infections. Additionally, polymer structures mimicking antimicrobial peptides have also been synthesized by RAFT[95]. In contrast, RAFT polymerization for polymeric prodrugs of small molecules was relatively less explored until recent studies reported by our group, as described in the section 1.3.4[81,96].

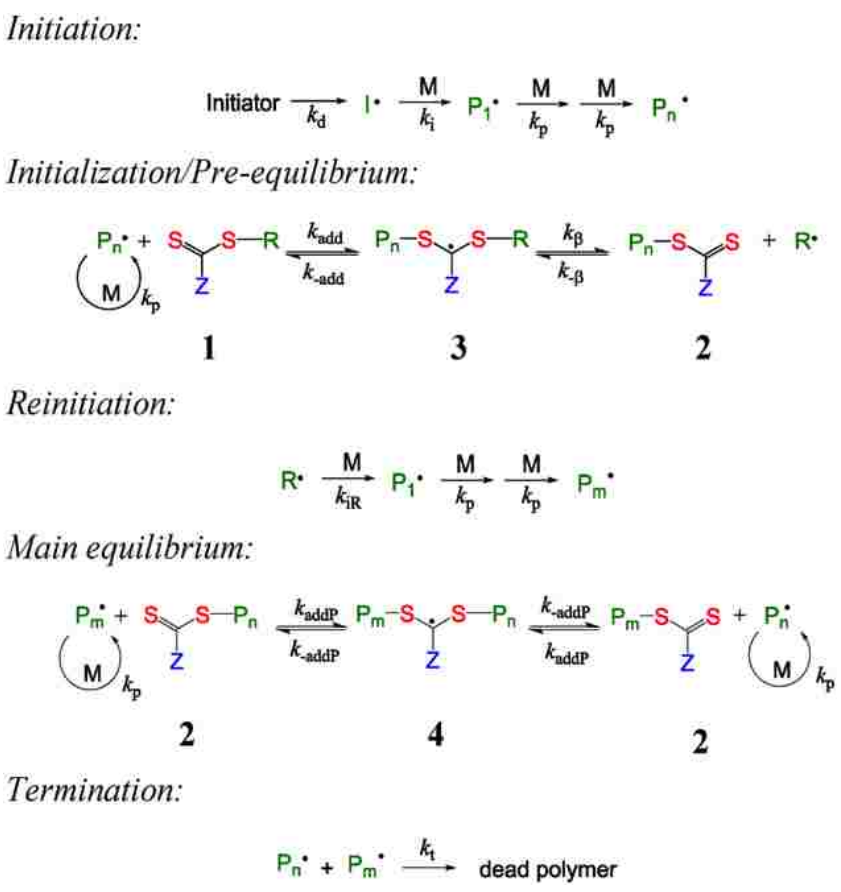

Figure 1.11. Equilibria of reversible-addition fragmentation chain transfer (RAFT) polymerization[88].

1.6 OVERALL OBJECTIVE

Building upon the literatures reviewed above, the criteria to engineer nanocarriers for targeted antibiotic delivery against respiratory tularemia and melioidosis are:

a) Well-defined materials with biocompatibility: first and the most important characteristic of any external materials used in human body.
b) Pulmonary administration: direct delivery of concentrated drugs to the infection site
c) Targeting ligand: facilitating cellular internalization into AMs through receptor-mediated endocytosis. This feature is particularly important for antibiotics with poor membrane permeability.
d) Bioresponsive release: releasing payload in response to intracellular signals to prevent premature release.
e) Controlled/sustained release: providing the lungs and AMs with therapeutic relevant concentration of antibiotics for longer duration than free drugs.

Those criteria were used to design and evaluate two types of antibiotic nanocarriers developed in this work: (1) pH-responsive polymeric nanocarriers for hydrophilic antibiotics [chapter 2], and (2) enzyme-cleavable polymeric antibiotic prodrugs [chapter 3-5]. The ultimate goal of this work is not only to develop successful strategies targeting tularemia and melioidosis, but also principles that can be applied to other bacterial pathogens that are highly lethal by the respiratory route, such as tuberculosis.

1.7 REFERENCE

1. Carryn, S. *et al.* Intracellular pharmacodynamics of antibiotics. *Infect Dis Clin North Am* **17,** 615–634 (2003).
2. Oyston, P. C. F., Sjostedt, A. & Titball, R. W. Tularaemia: bioterrorism defence renews interest in Francisella tularensis. *Nat. Rev. Microbiol.* **2,** 967–978 (2004).
3. Wiersinga, W. J., van der Poll, T., White, N. J., Day, N. P. & Peacock, S. J. Melioidosis: insights into the pathogenicity of Burkholderia pseudomallei. *Nat. Rev. Microbiol.* **4,** 272–282 (2006).

4. Lipsitz, R. *et al.* Workshop on treatment of and postexposure prophylaxis for Burkholderia pseudomallei and B. mallei Infection, 2010. *Emerg Infect Dis* **18,** e2 (2012).
5. Patel, N. *et al.* Development of vaccines against burkholderia pseudomallei. *Front Microbiol* **2,** 198 (2011).
6. Sunagar, R., Kumar, S., Franz, B. J. & Gosselin, E. J. Tularemia vaccine development: paralysis or progress? *Vaccine : development and therapy* **6,** 9–23 (2016).
7. Matyas, B. T., Nieder, H. S. & Telford, S. R. 3. Pneumonic tularemia on Martha's Vineyard: clinical, epidemiologic, and ecological characteristics. *Ann N Y Acad Sci* **1105,** 351–377 (2007).
8. Boisset, S., Caspar, Y., Sutera, V. & Maurin, M. New therapeutic approaches for treatment of tularaemia: a review. *Front Cell Infect Microbiol* **4,** 40 (2014).
9. Celli, J. & Zahrt, T. C. Mechanisms of Francisella tularensis Intracellular Pathogenesis. *Cold Spring Harbor Perspectives in Medicine* **3,** a010314 (2013).
10. Hall, J. D. *et al.* Infected-host-cell repertoire and cellular response in the lung following inhalation of Francisella tularensis Schu S4, LVS, or U112. *Infect Immun* **76,** 5843–5852 (2008).
11. Oyston, P. C. F. Francisella tularensis: unravelling the secrets of an intracellular pathogen. *J Med Microbiol* **57,** 921–930 (2008).
12. Jones, C. L. *et al.* Subversion of host recognition and defense systems by Francisella spp. *Microbiol Mol Biol Rev* **76,** 383–404 (2012).
13. Limmathurotsakul, D. *et al.* Predicted global distribution of Burkholderia pseudomallei and burden of melioidosis. *Nat Microbiol* **1,** (2016).
14. Jones, A. L., Beveridge, T. J. & Woods, D. E. Intracellular survival of Burkholderia pseudomallei. *Infect Immun* **64,** 782–790 (1996).
15. Harley, V. S., Dance, D. A., Drasar, B. S. & Tovey, G. Effects of Burkholderia pseudomallei and other Burkholderia species on eukaryotic cells in tissue culture. *Microbios* **96,** 71–93 (1998).
16. Goodyear, A. *et al.* Protection from pneumonic infection with burkholderia species by inhalational immunotherapy. *Infect Immun* **77,** 1579–1588 (2009).
17. Pruksachartvuthi, S., Aswapokee, N. & Thankerngpol, K. Survival of Pseudomonas pseudomallei in human phagocytes. *J Med Microbiol* **31,** 109–114 (1990).
18. Kespichayawattana, W., Rattanachetkul, S., Wanun, T., Utaisincharoen, P. & Sirisinha, S. Burkholderia pseudomallei induces cell fusion and actin-associated membrane protrusion: a possible mechanism for cell-to-cell spreading. *Infect Immun* **68,** 5377–5384 (2000).
19. Breitbach, K. *et al.* Actin-based motility of Burkholderia pseudomallei involves the Arp 2/3 complex, but not N-WASP and Ena/VASP proteins. *Cell Microbiol* **5,** 385–393 (2003).
20. Dennis, D. T. *et al.* Tularemia as a Biological Weapon. *JAMA* **285,** 2763 (2001).
21. Inglis, T. J. J., Rolim, D. B. & Rodriguez, J. L. N. Clinical guideline for diagnosis and management of melioidosis. *Rev Inst Med Trop Sao Paulo* **48,** 1–4 (2006).
22. Wise, R. & Honeybourne, D. Pharmacokinetics and pharmacodynamics of fluoroquinolones

in the respiratory tract. *Eur Respir J* **14,** 221–229 (1999).
23. Toso, C., Williams, D. M. & Noone, P. G. Inhaled antibiotics in cystic fibrosis: a review. *Ann Pharmacother* **30,** 840–850 (1996).
24. Bonventre, P. F. & Imhoff, J. G. Uptake of (3)H-Dihydrostreptomycin by Macrophages in Culture. *Infect Immun* **2,** 89–95 (1970).
25. Bonventre, P. F., Hayes, R. & Imhoff, J. Autoradiographic evidence for the impermeability of mouse peritoneal macrophages to tritiated streptomycin. *J Bacteriol* **93,** 445–450 (1967).
26. Cao, C. *et al.* Probenecid-resistant J774 cell expression of enhanced organic anion transport by a mechanism distinct from multidrug resistance. *Infect Agents Dis* **2,** 193–200 (1993).
27. Pinto-Alphandary, H., Andremont, A. & Couvreur, P. Targeted delivery of antibiotics using liposomes and nanoparticles: research and applications. *Int. J. Antimicrob. Agents* **13,** 155–168 (2000).
28. de Jager, P. & van Altena, R. Hearing loss and nephrotoxicity in long-term aminoglycoside treatment in patients with tuberculosis. *Int. J. Tuberc. Lung Dis.* **6,** 622–627 (2002).
29. Aschenbrenner, D. S. The FDA Revises Boxed Warning For Fluoroquinolones-Again. *Am J Nurs* **116,** 22–23 (2016).
30. Dance, D. Treatment and prophylaxis of melioidosis. *Int. J. Antimicrob. Agents* **43,** 310–318 (2014).
31. Huh, A. J. & Kwon, Y. J. 'Nanoantibiotics': A new paradigm for treating infectious diseases using nanomaterials in the antibiotics resistant era. *J Control Release* **156,** 128–145
32. Andrade, F. *et al.* Nanotechnology and pulmonary delivery to overcome resistance in infectious diseases. *Adv. Drug Deliv. Rev.* **65,** 1816–1827 (2013).
33. Mehanna, M. M., Mohyeldin, S. M. & Elgindy, N. A. Respirable nanocarriers as a promising strategy for antitubercular drug delivery. *J Control Release* **187,** 183–197 (2014).
34. W S Yapa, S. *et al.* Pulmonary and Systemic Pharmacokinetics of Inhaled and Intravenous Colistin Methanesulfonate in Cystic Fibrosis Patients: Targeting Advantage of Inhalational Administration. *Antimicrob. Agents Chemother.* **58,** 2570–2579 (2014).
35. Garcia-Contreras, L. *et al.* Pharmacokinetics of Sequential Doses of Capreomycin Powder for Inhalation in Guinea Pigs. *Antimicrob. Agents Chemother.* **56,** 2612–2618 (2012).
36. Labiris, N. R. & Dolovich, M. B. Pulmonary drug delivery. Part I: physiological factors affecting therapeutic effectiveness of aerosolized medications. *Br J Clin Pharmacol* **56,** 588–599 (2003).
37. Weers, J. Inhaled antimicrobial therapy – Barriers to effective treatment. *Adv. Drug Deliv. Rev.* **85,** 24–43 (2015).
38. Patton, J. S., Fishburn, C. S. & Weers, J. G. The lungs as a portal of entry for systemic drug delivery. *Proceedings of the American Thoracic Society* **1,** 338–344 (2004).
39. Cipolla, D., Blanchard, J. & Gonda, I. Development of Liposomal Ciprofloxacin to Treat Lung Infections. *Pharmaceutics* **8,** (2016).
40. Nicod, L. P. Lung defences: an overview. *European Respiratory Review* **14,** 45–50 (2005).
41. Wong, J. P. *et al.* Liposome delivery of ciprofloxacin against intracellular Francisella

tularensis infection. *J Control Release* **92,** 265–273 (2003).
42. Jacobs, M. R. Optimisation of antimicrobial therapy using pharmacokinetic and pharmacodynamic parameters. *Clinical Microbiology and Infection* **7,** 589–596
43. Levison, M. E. & Levison, J. H. Pharmacokinetics and Pharmacodynamics of Antibacterial Agents. *Infect Dis Clin North Am* **23,** 791–vii (2009).
44. Lacy, M. K., Nicolau, D. P., Nightingale, C. H. & Quintiliani, R. The pharmacodynamics of aminoglycosides. *Clin Infect Dis* **27,** 23–27 (1998).
45. Cars, O. Efficacy of beta-lactam antibiotics: integration of pharmacokinetics and pharmacodynamics. *Diagn Microbiol Infect Dis* **27,** 29–33 (1997).
46. Van Bambeke, F. & Tulkens, P. M. Macrolides: pharmacokinetics and pharmacodynamics. *Int. J. Antimicrob. Agents* **18,** 17–23 (2001).
47. Asín-Prieto, E., Rodríguez-Gascón, A. & Isla, A. Applications of the pharmacokinetic/pharmacodynamic (PK/PD) analysis of antimicrobial agents. *Journal of Infection and Chemotherapy* **21,** 319–329 (2015).
48. Zhao, M., Lepak, A. J. & Andes, D. R. Animal models in the pharmacokinetic/pharmacodynamic evaluation of antimicrobial agents. *Bioorg. Med. Chem.* **24,** 6390–6400 (2016).
49. Forrest, A. *et al.* Pharmacodynamics of intravenous ciprofloxacin in seriously ill patients. *Antimicrob. Agents Chemother.* **37,** 1073–1081 (1993).
50. Van Bambeke, F., Barcia-Macay, M., Lemaire, S. & Tulkens, P. M. Cellular pharmacodynamics and pharmacokinetics of antibiotics: current views and perspectives. *Curr Opin Drug Discov Devel* **9,** 218–230 (2006).
51. Toutain, P. L., del Castillo, J. R. E. & Bousquet-Mélou, A. The pharmacokinetic–pharmacodynamic approach to a rational dosage regimen for antibiotics. *Research in Veterinary Science* **73,** 105–114
52. Briones, E., Colino, C. I. & Lanao, J. M. Delivery systems to increase the selectivity of antibiotics in phagocytic cells. *J Control Release* **125,** 210–227 (2008).
53. Imbuluzqueta, E. *et al.* Novel bioactive hydrophobic gentamicin carriers for the treatment of intracellular bacterial infections. *Acta Biomaterialia* **7,** 1599–1608
54. Zhu, C. *et al.* A traceless reversible polymeric colistin prodrug to combat multidrug-resistant (MDR) gram-negative bacteria. *J Control Release* **259,** 83–91 (2017).
55. Zhang, L., Pornpattananangku, D., Hu, C.-M. J. & Huang, C.-M. Development of nanoparticles for antimicrobial drug delivery. *Curr Med Chem* **17,** 585–594 (2010).
56. Takakura, Y. & Hashida, M. Macromolecular carrier systems for targeted drug delivery: pharmacokinetic considerations on biodistribution. *Pharm Res* **13,** 820–831 (1996).
57. Lee, W.-H., Loo, C.-Y., Traini, D. & Young, P. M. Nano- and micro-based inhaled drug delivery systems for targeting alveolar macrophages. *Expert Opin. Drug Deliv.* **12,** 1009–1026 (2015).
58. Sung, J. C., Pulliam, B. L. & Edwards, D. A. Nanoparticles for drug delivery to the lungs. *Trends in biotechnology* **25,** 563–570

59. Patel, B., Gupta, N. & Ahsan, F. Particle engineering to enhance or lessen particle uptake by alveolar macrophages and to influence the therapeutic outcome. *Eur J Pharm Biopharm* **89,** 163–174 (2015).
60. Kelly, C., Jefferies, C. & Cryan, S.-A. Targeted liposomal drug delivery to monocytes and macrophages. *J Drug Deliv* **2011,** 727241 (2011).
61. Zhang, J. B. *et al.* Large-scale synthesis of carbohydrates for pharmaceutical development. *Current Organic Chemistry* **5,** 1169–1176 (2001).
62. KALLIN, E., LONN, H. & NORBERG, T. New Derivatization and Separation Procedures for Reducing Oligosaccharides. *Glycoconj. J.* **3,** 311–319 (1986).
63. Biessen, E. A. *et al.* Lysine-based cluster mannosides that inhibit ligand binding to the human mannose receptor at nanomolar concentration. *J Biol Chem* **271,** 28024–28030 (1996).
64. Song, E.-H. *et al.* In vivo targeting of alveolar macrophages via RAFT-based glycopolymers. *Biomaterials* **33,** 6889–6897 (2012).
65. TAYLOR, P., Gordon, S. & MARTINEZPOMARES, L. The mannose receptor: linking homeostasis and immunity through sugar recognition. *Trends in Immunology* **26,** 104–110 (2005).
66. Munoz, E. M., Correa, J., Fernandez-Megia, E. & Riguera, R. Probing the Relevance of Lectin Clustering for the Reliable Evaluation of Multivalent Carbohydrate Recognition. *J. Am. Chem. Soc.* **131,** 17765–17767 (2009).
67. Chono, S., Tanino, T., Seki, T. & Morimoto, K. Efficient drug targeting to rat alveolar macrophages by pulmonary administration of ciprofloxacin incorporated into mannosylated liposomes for treatment of respiratory intracellular parasitic infections. *J Control Release* **127,** 50–58 (2008).
68. Serisier, D. J. *et al.* Inhaled, dual release liposomal ciprofloxacin in non-cystic fibrosis bronchiectasis (ORBIT-2): a randomised, double-blind, placebo-controlled trial. *Thorax* **68,** 812–817 (2013).
69. Cipolla, D. & Chan, H.-K. Inhaled antibiotics to treat lung infection. *Pharm Pat Anal* **2,** 647–663 (2013).
70. Rose, S. J., Neville, M. E., Gupta, R. & Bermudez, L. E. Delivery of aerosolized liposomal amikacin as a novel approach for the treatment of nontuberculous mycobacteria in an experimental model of pulmonary infection. *PLoS ONE* **9,** e108703 (2014).
71. Zhang, J. *et al.* Amikacin Liposome Inhalation Suspension (ALIS) Penetrates Non-tuberculous Mycobacterial Biofilms and Enhances Amikacin Uptake Into Macrophages. *Front Microbiol* **9,** 915 (2018).
72. Cipolla, D. *et al.* Development and Characterization of an In Vitro Release Assay for Liposomal Ciprofloxacin for Inhalation. *J Pharm Sci* **103,** 314–327 (2014).
73. Kashi, T. S. J. *et al.* Improved drug loading and antibacterial activity of minocycline-loaded PLGA nanoparticles prepared by solid/oil/water ion pairing method. *Int J Nanomedicine* **7,** 221–234 (2012).

74. Thote, A. J. & Gupta, R. B. Formation of nanoparticles of a hydrophilic drug using supercritical carbon dioxide and microencapsulation for sustained release. *Nanomedicine* **1,** 85–90 (2005).
75. Stebbins, N. D., Ouimet, M. A. & Uhrich, K. E. Antibiotic-containing polymers for localized, sustained drug delivery. *Adv. Drug Deliv. Rev.* **78 IS ,** 77–87 (2014).
76. Seidi, F., Jenjob, R. & Crespy, D. Designing Smart Polymer Conjugates for Controlled Release of Payloads. *Chem. Rev.* **118,** 3965–4036 (2018).
77. Marasini, N., Haque, S. & Kaminskas, L. M. Polymer-drug conjugates as inhalable drug delivery systems: A review. *Current Opinion in Colloid & Interface Science* **31,** 18–29 (2017).
78. Feng, Q. & Tong, R. Anticancer nanoparticulate polymer-drug conjugate. *Bioengineering & Translational Medicine* **1,** 277–296 (2016).
79. Delplace, V., Couvreur, P. & Nicolas, J. Recent trends in the design of anticancer polymer prodrug nanocarriers. *Polym. Chem.* **5,** 1529–1544 (2014).
80. Gac-Breton, S., Coudane, J., Boustta, M. & Vert, M. Norfloxacin-poly(L-lysine citramide imide) conjugates and structure-dependence of the drug release. *J Drug Target* **12,** 297–307 (2004).
81. Das, D. *et al.* RAFT polymerization of ciprofloxacin prodrug monomers for the controlled intracellular delivery of antibiotics. *Polym. Chem.* **7,** 826–837 (2016).
82. D'Souza, A. J. M. & Topp, E. M. Release from polymeric prodrugs: linkages and their degradation. *J Pharm Sci* **93,** 1962–1979 (2004).
83. Kamaly, N., Yameen, B., Wu, J. & Farokhzad, O. C. Degradable Controlled-Release Polymers and Polymeric Nanoparticles: Mechanisms of Controlling Drug Release. *Chem. Rev.* **116,** 2602–2663 (2016).
84. Moad, G., Rizzardo, E. & Thang, S. H. Toward living radical polymerization. *Acc. Chem. Res.* **41,** 1133–1142 (2008).
85. Moad, G., Chong, Y. K., Postma, A., Rizzardo, E. & Thang, S. H. Advances in RAFT polymerization: the synthesis of polymers with defined end-groups. *Polymer* **46,** 8458–8468 (2005).
86. Moad, G., Rizzardo, E. & Thang, S. H. Living Radical Polymerization by the RAFT Process A Second Update. *Aust. J. Chem.* **62,** 1402–1472 KW – (2009).
87. Moad, G., Rizzardo, E. & Thang, S. H. Living Radical Polymerization by the RAFT Process. *Aust. J. Chem.* **58,** 379–410 (2005).
88. Keddie, D. J. A guide to the synthesis of block copolymers using reversible-addition fragmentation chain transfer (RAFT) polymerization. *Chem Soc Rev* **43,** 496–505 (2014).
89. Moad, G. *et al.* Living free radical polymerization with reversible addition-fragmentation chain transfer (the life of RAFT). *Polymer International* **49,** 993–1001 (2000).
90. Moad, G., Rizzardo, E. & Thang, S. H. Living Radical Polymerization by the RAFT ProcessA First Update. *Aust. J. Chem.* **59,** 669–692 KW – (2006).
91. Boyer, C. *et al.* Bioapplications of RAFT polymerization. *Chem. Rev.* **109,** 5402–5436

(2009).
92. Gregory, A. & Stenzel, M. H. Complex polymer architectures via RAFT polymerization: From fundamental process to extending the scope using click chemistry and nature's building blocks. *Topical Issue on Biorelevant Polymers* **37,** 38–105
93. Santos, M. R. E. *et al.* Recent Developments in Antimicrobial Polymers: A Review. *Materials* **9,** 599 (2016).
94. Thoma, L. M., Boles, B. R. & Kuroda, K. Cationic methacrylate polymers as topical antimicrobial agents against Staphylococcus aureus nasal colonization. *Biomacromolecules* **15,** 2933–2943 (2014).
95. Locock, K. E. S. *et al.* Guanylated polymethacrylates: a class of potent antimicrobial polymers with low hemolytic activity. *Biomacromolecules* **14,** 4021–4031 (2013).
96. Das, D. *et al.* Synthetic Macromolecular Antibiotic Platform for Inhalable Therapy against Aerosolized Intracellular Alveolar Infections. *Mol. Pharmaceutics* **14,** 1988–1997 (2017).

Chapter 2. Polymer-augmented liposomes enhancing antibiotic delivery against intracellular infections

Abstract

Pulmonary intracellular infections, such as tuberculosis, anthrax, and tularemia, remain a significant challenge to conventional antibiotic therapy. Ineffective antibiotic treatment of these infections can lead not only to undesired side effects, but also the emergence of antibiotic resistance. Aminoglycosides (e.g., streptomycin) have long been part of the therapeutic regiment for many pulmonary intracellular infections. Their bioavailability for intracellular bacterial pools, however, is limited by poor membrane permeability and rapid elimination. To address this challenge, polymer-augmented liposomes (PALs) were developed to provide improved cytosolic delivery of streptomycin to alveolar macrophages, an important host cell for intracellular pathogens. A multifunctional diblock copolymer was engineered to functionalize PALs with carbohydrate-mediated targeting, pH-responsive drug release, and endosomal release activity with a single functional polymer that replaces the pegylated lipid component to simplify the liposome formulation. The pH-sensing functionality enabled PALs to provide enhanced release of streptomycin under endosomal pH condition (70% release in 6 hours) with limited release at physiological pH 7.4 (16%). The membrane-destabilizing activity connected to endosomal release was characterized in a hemolysis assay and PALs displayed a sharp pH profile across the endosomal pH development target range. The direct connection of this membrane-destalizing pH profile to model drug release was demonstrated in an established pyranine / p-xylene bispyridinium dibromide (DPX) fluorescent dequenching assay. PALs displayed similar sharply pH-responsive release, whereas PEGylated control liposomes did not, and similar profiles were then shown for streptomycin release. The mannose-targeting capability of the PALs was also demonstrated with 2.5 times higher internalization compared to non-targeted PEGylated liposomes. Finally, the streptomycin-loaded PALs were shown with a significantly improved intracellular antibacterial activity in a Francisella-macrophage co-culture model, compared with free streptomycin or streptomycin delivered by control PEGylated liposomes (13x and 16x, respectively). This study suggests the potential of PALs as a useful platform to deliver antibiotics for the treatment of intracellular macrophage infections.

2.1 INTRODUCTION

Respiratory infections caused by intracellular bacteria, such as *Mycobacterium tuberculosis*, *Bacillus anthracis*, *Francisella tularensis* and *Burkholderia pseudomallei*, remain a major global health and biological threat[1-4]. For instance, inhaled *Francisella tularensis* can result in the most severe form of tularemia at even low infectious dose (estimated LD_{50} < 10 CFU)[3,5]. Without immediate antibiotic treatment, pulmonary tularemia can be fatal in 30% of cases[3,5]. The pathogenicity of intracellular bacteria is highly associated with their ability to seclude themselves and multiply within phagocytic cells, such as alveolar macrophages (AMs) in respiratory infections[6-8]. This intracellular localization protects the bacteria from the humoral and cellular immune responses, and limits the efficacy of conventional antibiotic treatments[9-11].

Current treatment for *F. tularensis* infections relies on rigorous oral and IV antibiotic therapy with aminoglycoside, tetracycline, and/or fluoroquinolone drugs[12]. Aminoglycosides, including streptomycin and gentamicin, have been recommended as the agents of choice for the treatment of tularemia, due to their improved outcomes and lower relapse rates[12]. However, aminoglycosides suffer from suboptimal pharmacokinetics because of their rapid elimination rate (plasma half-life 2-3 hours)[13]. Additionally, owing to their hydrophilic nature, the efficacy of aminoglycosides is limited by their poor membrane permeability and slow cytosolic accumulation[14]. Due to those limitations, multiple daily high-dose injections are required for a prolonged period of time to achieve therapeutic efficacy, and this treatment regimen can have undesired side effects (e.g., nephrotoxicity and ototoxicity) and potentially induce drug resistance[15,16]. Consequently, drug delivery systems that can enhance cytosolic accumulation of aminoglycosides in the intracellular space might potentiate activity.

Liposomes have been previously utilized to improve antibiotic efficacy by enhancing cellular delivery and improving pharmacokinetics (PK) at the site of infections[17-19]. A liposomal ciprofloxacin (Lipoquin®, Aradigm Corp.) has shown improved antibacterial activity compared to free drug in *F. tularensis* Schu S4-infected mice[20,21]. Liposomal surfaces have also been modified with mannose to increase uptake by AMs through receptor-mediated endocytosis mediated by the macrophage mannose receptor[22]. This enhanced uptake improved PK properties

in AMs compared to unmodified liposomes[23]. However, drugs released from those liposome formulations still rely on passive diffusion through vesicular or cellular membranes to reach cytosolic bacteria. This could limit the efficacy of aminoglycosides, as they preferentially accumulate in lysosomes following endocytosis[10].

To achieve endosomal release, various approaches have been taken to provide drug carriers with membrane destabilizing and/or membrane fusion activities, such as fusogenic peptides and synthetic polymers[24-26]. Synthetic polymers with endosomal-destabilizing activity, particularly at a weakly acidic pH, are especially useful for cytoplasmic delivery[27-29]. When liposomes modified with these pH-sensitive polymers are taken up by cells through endocytosis, they can introduce entrapped cargos to the cytosol by destabilizing endo-lysosomal membranes. For example, a pH-sensitive fusogenic polymer, 3-methylglutarylated hyperbranched poly(glycidol), formulated with liposomes effectively introduced ovalbumin to the cytosol of dendritic cells[30].

In this study, a multifunctional, diblock copolymer was developed to augment liposomes with macrophage-targeting and endosomal release functionality for the cytosolic delivery of hydrophilic aminoglycoside antibiotics against *Francisella* infection (**Figure 2.1A**). This diblock copolymer was employed to functionalize liposomes to create the polymer-augmented liposome (PAL) system with the following advantageous properties: (1) surface mannose modification for targeted association and enhanced internalization by AMs; (2) pH-responsive streptomycin release from PALs; (3) membrane-destabilizing activity for enhancing streptomycin bioavailability to cytosolic bacteria; and (4) a simplified liposomal formulation where the polymer replaces the typical hydrophilic lipid (**Figure 2.1B**). The efficacy against intracellular infections was characterized in an intracellular Francisella-macrophage co-culture model. The enhanced antibacterial activity of streptomycin delivered by PALs suggests that this carrier design could provide important benefits for intracellular delivery of drugs with poor membrane permeability.

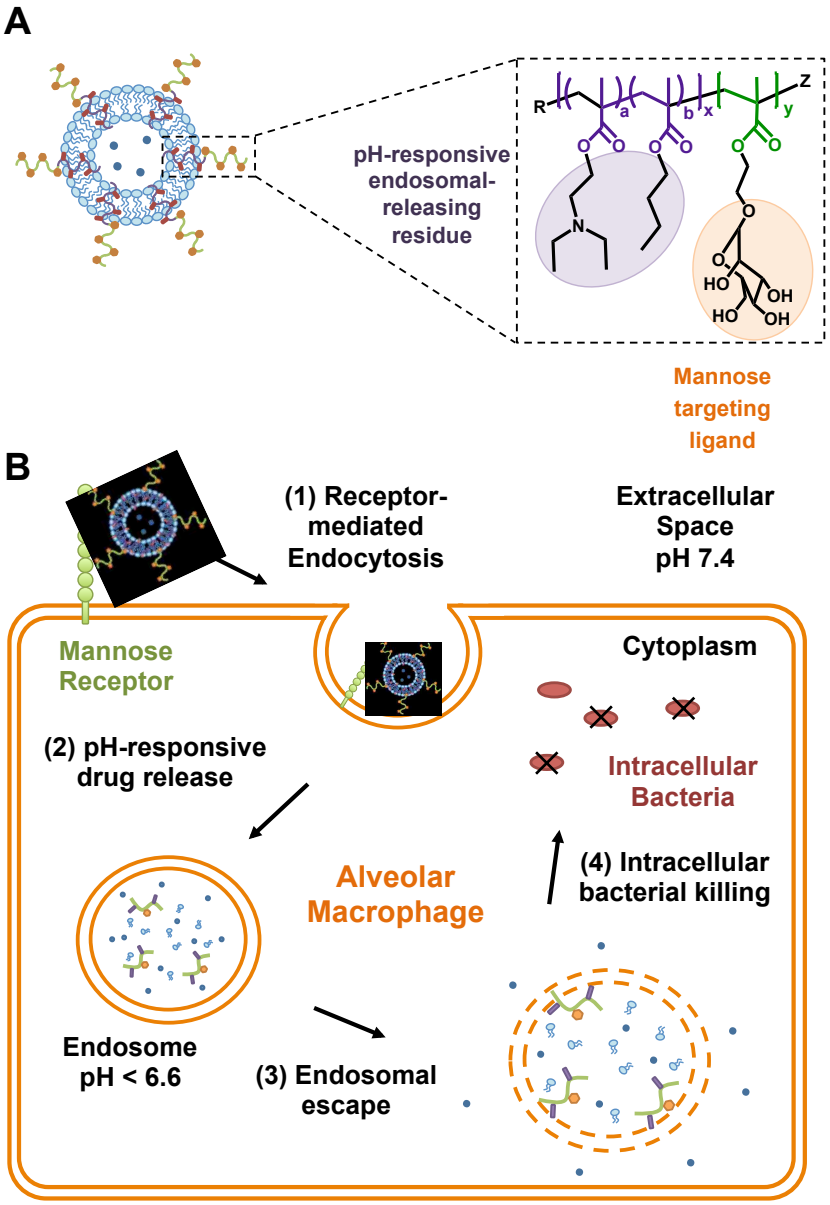

Figure 2.1. (A) **Schematic of the formulation and functionalities of polymer-augmented liposomes (PALs).** PAL was formulated through the hydrophobic effect between the lipid bilayer and hydrophobic block (purple) of the amphiphilic diblock copolymer; (B) **Envisioned pathway for the cellular uptake of PALs and subsequent intracellular release of the cargo in alveolar macrophages.** (Note: illustrations are not to scale.)

2.2 MATERIALS AND METHOD

2.2.1 *Materials*

Materials were purchased from Sigma Aldrich (St Louis, MO) unless otherwise specified. 1,2-distearoyl-sn-glycero-3-phosphocholine (DSPC) and 1,2-distearoyl-sn-glycero-3-phosphoethanolamine-N-[methoxy(polyethylene glycol)-2000] (DSPE-PEG) were purchased from Avanti Polar Lipids (Alabaster, AL). Rhodamine B-labeled dihexadecanoyl-sn-glycero-3-phosphoethanolamine (DHPE-Rhodamine) was acquired from Thermo-Fisher Scientific (Pittsburgh, PA). Diethylaminoethyl methacrylate (DEAEMA) and butyl methacrylate (BMA) were distilled prior to use. 4-Cyano-4-(ethylsulfanylthiocarbonyl) sulfanylpentanoic acid (ECT) and mannose functionalized with ethyl methacrylate (ManEMA) were synthesized and fully characterized as described previously[31,32]. Spectra/Por regenerated cellulose dialysis membranes were purchased from Spectrum Laboratories (Houston, TX). Sephadex G-25 prepacked PD10 columns were obtained from GE Healthcare Life Sciences (Pittsburg, PA).

2.2.2 *Reversible addition−fragmentation chain-transfer (RAFT) polymerization and characterization of poly[(DEAEMA-co-BMA)-b-ManEMA]*

Please see supplementary information.

2.2.3 *Formulation and characterization of streptomycin-loaded PALs*

PALs were prepared using an ethanol injection method described previously with some modifications[33]. Briefly, DSPC (23.7 mg), cholesterol (7.8 mg), and poly[(DEAEMA-*co*-BMA)-*b*-ManEMA] (7.9 mg) were dissolved in ethanol (0.25 mL) to uniformly mix the lipids with polymer in a single phase. The lipid/polymer mixture was added into phosphate buffer saline (PBS, 3.15 mL, 10 mM, pH 7.4) containing streptomycin (100 mg/mL) under magnetic stirring to form streptomycin-loaded PALs. The PAL suspension was then sonicated for 15 min and extruded at 60 °C through the following polycarbonate filters: 800, 400, 200, and 100 nm (Whatman, GE Healthcare, Pittsburgh, PA USA) to obtain uniform PALs suspension. Ethanol

and unencapsulated streptomycin were removed by dialysis against PBS using Spectra/Por dialysis tubing (MWCO 3kDa). Non-pH-responsive PEGylated control liposomes with similar formulation as Lipo-Dox® (DSPC: cholesterol: DSPC-PEG= 6:4:0.5 molar ratio) were also prepared to serve as a control[34]. For fluorescence labeled liposomes, fluorescent lipids, rhodamine DHPE, were incorporated in PALs and PEGylated liposomes at 0.5 mol% total lipids via the same preparation procedures. Co-formulation of the diblock copolymer with liposomes was characterized using high performance size exclusion chromatography (HPSEC); procedures were described in detail in Supplementary Information.

The hydrodynamic diameter of PALs and PEGylated liposomes were determined using a Malvern Instruments Zetasizer Nano series instrument equipped with a 22 mW He-Ne laser operating at 632.8 nm. To compare the hydrodynamic diameters of PALs and PEGylated liposomes in the pH range of the endosomal pathway (7.4, 7.0, 6.6, 6.2, and 5.8), both liposome formulations were dispersed in sodium phosphate buffer (100 mM, pH 7.4-6.2, supplemented with 150 mM NaCl) or sodium acetate buffer (100 mM, pH 5.8, supplemented with 150 mM NaCl). Mean diameters were reported as the intensity-average ± standard deviation from three or more independently prepared formulations.

2.2.4 *Quantification of streptomycin encapsulation*

Encapsulated streptomycin concentration in PALs was determined using a fluorescamine assay, which has been used to quantify the concentration of peptides, proteins, and aminoglycosides[35,36]. Fluorescamine is a non-fluorescent reagent that reacts readily under mild conditions with amines to form stable, highly fluorescent compounds[37]. The encapsulated streptomycin was first released from PALs by lysing the PAL suspension (0.015 mL, 5.6 mg/mL lipids) with 1% Triton X-100 (0.135 mL). The released streptomycin was then reacted with fluorescamine (3 mg/mL in dimethyl sulfoxide, 0.05 mL) for 15 min at room temperature. Fluorescence (λ_{ex}=390 nm, λ_{em}=470 nm) was measured using a plate reader (Tecan M1000). Known concentrations of streptomycin solution were also reacted with fluorescamine solution to obtain a calibration curve.

2.2.5 *Red blood cell hemolysis assay*

The membrane destabilizing activity of the diblock copolymer and the streptomycin-loaded PALs was measured using a red blood cell hemolysis assay as previously described[38,39]. Polymer/PAL suspensions were incubated in triplicate wells of a 96-well plate (V-shaped bottom) for 1 h at 37 °C in the presence of human red blood cells at various polymer concentrations (10, 20, 40, 80 μg/mL) in 100 mM sodium phosphate buffers (pH 7.4, 7.0, 6.6, and 6.2, supplemented with 150 mM NaCl) or 100 mM sodium acetate buffer (pH 5.8, supplemented with 150 mM NaCl) intended to mimic the acidifying pH gradient in the lysosomal pathway. Polymer concentrations in PALs were estimated based on the amount of polymer added during PAL preparation procedures. To remove the unlysed cells, the plate was centrifuged at 1500 rpm for 5 min, and the supernatant was transferred to another 96-well plate (flat-bottom) for absorbance measurement. The percent hemolysis was determined by measuring the amount of released hemoglobin in the supernatant (λ_{abs}=541 nm) and normalized to a 100% hemolysis control (1% Triton X-100).

2.2.6 *pH-dependent fluorescence dequenching assay*

To study the pH-dependent release characteristics of PALs, a fluorescent dye-quencher pair, pyranine (35 mM) and p-xylene bispyridinium dibromide (DPX, 50 mM), was encapsulated in the aqueous compartment of PALs using the method described above. Untrapped dye was removed by gel filtration using PD-10 column twice. Subsequently, the PALs encapsulating pyranine and DPX were diluted 20 times in sodium phosphate buffers (pH 7.4, 7.0, 6.6, and 6.2) or sodium acetate buffer (pH 5.8 and 5.4) same as used for the hemolysis assay. Following a 3-h incubation in buffers at varying pH at 37 °C, the extent of contents release was quantified by measuring the fluorescence of pyranine (λ_{ex}=413 nm, λ_{em}=512 nm) via a microplate reader (Tecan M1000). 100% release was achieved by adding 1% Triton X-100 to PAL suspension at pH 7.4 (final concentration 0.1%). Pyranine/DPX loaded PEGylated control liposomes were prepared similarly.

2.2.7 *In vitro streptomycin release kinetics*

The release kinetics of streptomycin from PALs was investigated in two pH conditions, pH 5.8 (endosomal) and pH 7.4 (physiologic), using acetate and phosphate buffered saline, respectively. The prepared streptomycin-loaded PALs were divided into two 2.5 ml aliquots and transferred to two dialysis tubes with a MWCO of 3.5 kDa. The two dialysis tubes were immersed into 30 mL of pH 5.8 and 7.4 buffer at 37 °C, respectively. At desired time intervals, 1 mL of release media was taken out and replenished with an equal volume of fresh media. The amount of streptomycin released was determined using fluorescamine assay as described above. Calibration curves were obtained with streptomycin in corresponding buffer solutions at pH 5.8 and 7.4. 100% streptomycin release was measured by lysing PALs with 1% Triton X-100 in PBS.

2.2.8 *Cell uptake study*

Cellular uptake of rhodamine-labeled PALs was investigated using flow cytometry and visualized via fluorescence microscopy. To induce higher expression of mannose receptors, RAW 264.7 cells were treated with 20 ng/mL IL-4 for 24 h[40]. RAW 264.7 cells with and without IL-4 pretreatment were suspended at a density of 1 X 10^6 cells/ml and blocked with growth media containing 10% FBS for 30 min at 37°C. Cells were subsequently treated with rhodamine-labeled PALs or PEGylated control liposomes at a total lipid concentration of 400 μg/ml for 20 min, 1 hr, and 3 hr at 37°C. The cells were then washed and resuspended in cold PBS containing 0.01% FBS to remove extracellular liposomes. The uptake level was presented as the intensity of rhodamine measured via a PE filter on a BD LSRII flow cytometer (BD Biosciences, San Jose, CA), and analyzed using FlowJo software (Tree Star, Inc.). For microscopy, cells were treated as above for 1 hr but instead fixed with 10% formaldehyde solution, and nuclei were counterstained with DAPI (Molecular probe). Random fields were observed at 600x or 100x magnification using a Nikon Ti-E live-cell fluorescence microscope.

2.2.9 *Bacteria-macrophage co-culture therapeutic study*

RAW 264.7 cells were seeded (500,000 cells/mL, 250 µL/well) into a 48 well plate with antibiotic free DMEM with 10% FBS, and incubated at 37°C with 5% CO_2. After 18 hours, cells were infected with *F. novicida* U112 at early log phase of growth (OD600=0.2) at a multiplicity of infection of 50, and then incubated for 1 hour. Subsequently, growth media was replaced with fresh DMEM containing 10% FBS and 250 µg/mL kanamycin to eliminate extracellular bacteria not internalized by the cells; cells were then incubated for another hour. Growth media was then replaced with fresh, unsupplemented media containing varying concentrations of free streptomycin (0-115 µg/mL), streptomycin-loaded PEGylated control liposomes (equivalent to 0-115 µg/mL streptomycin), or streptomycin-loaded PALs (equivalent to 0-115 µg/mL streptomycin). Cells were incubated for another 22 hours (24 hours post-infection). After incubation, cells were washed three times with 1x PBS and lysed with 100 µL of PBS containing 0.1% (v/v) Triton X-100. Lysates were serially diluted and plated onto triplicate TSB agar plates and incubated for 24 hours and individual bacterial colonies were counted. Data represented as CFU/well vs. streptomycin dose.

2.2.10 *Statistics*

Numerical data were represented as mean ± SD. Statistical analysis was performed by Student's paired t test. (**) denotes a P-value of < 0.005. All samples were performed in triplicate.

2.3 RESULTS AND DISCUSSION

Macrophages are key regulators of the inflammatory process and represent an attractive therapeutic target due to their many important roles in combating infection and maintaining homeostasis in the body[41]. Uncontrolled inflammatory response of macrophages becomes pathogenic resulting in significant levels of non-specific tissue damage, resulting in inflammatory and autoimmune disease[42]. Additionally, facultative or obligate intracellular parasites often use macrophages as a safe reservoir to protect them from host immune response and antibiotic treatment[43]. For example, prior research has shown that AMs are major reservoirs

of *F. tularensis* during early-stage infection[44], and that nanoparticles enhancing antibiotic delivery to macrophages led to better efficacy then free drug[45]. To eliminate intracellular pathogens within AMs, the intracellular antibiotic concentration must be higher than the minimum inhibitory concentration (MIC)[11]. Especially for concentration-dependent antibiotics, including aminoglycosides and fluoroquinolones, the rate and extent of their bactericidal activity has been shown to associate with the ratio of the maximum concentration to MIC (C_{max}/MIC ≥ 10) in serum or target tissues[46]. Consequently, efficient cytosolic delivery of concentrated antibiotics to AMs is required to eradicate intracellular *F. tularensis*, and therefore may potentially minimize therapeutic failure as well as relapse rate. Due to its clinical use and poor membrane permeability, streptomycin was used as a model aminoglycoside in the present study to demonstrate the PAL system.

2.3.1 *Synthesis of multifunctional diblock copolymer*

The diblock copolymer, poly[(DEAEMA-*co*-BMA)-*b*-ManEMA], was prepared via RAFT polymerization according to **Figure 2.2**[47]. RAFT allows the three desired functionalities (targeting, pH-sensitivity, endosome releasing activity) to be integrated into this simple, well-defined diblock copolymer construct. poly(DEAEMA-*co*-BMA) was first prepared by copolymerizing DEAEMA and BMA with a comonomer feed ratio of 60 mol% DEAEMA and 40 mol% BMA, which has been shown to exhibit sharp pH-dependent response at pH 6.6 and strong endosomal-releasing properties[48]. The resultant polymer was used as a macro chain transfer agent (macroCTA) to prepare the poly[(DEAEMA-*co*-BMA)-*b*-ManEMA] diblock copolymer. The diblock copolymer was successfully synthesized under controlled conditions with consistent size and composition as determined by GPC and ^{1}H-NMR spectroscopy. The obtained diblock copolymer has narrow and symmetric molecular weight distributions that cleanly move to lower elution volumes (**Figure 2.3A**). Copolymer composition was confirmed by analysis of resonances associated with each of the comonomers (**Figure 2.3B**). The feed ratios, monomer compositions, molecular weight (M_n), and dispersity (Đ) for macroCTA and the diblock copolymer are given in **Figure 2.3C**.

2.3.2 *Preparation and characterization of polymer-augmented liposomes (PALs)*

Two design principles were exploited to avoid potential side effects associated with the PALs. First, the PAL formulation was based upon lipid components (i.e., DSPC and cholesterol) that were previously approved by the US FDA for liposomal doxorubicin (Lipo-Dox®)[34]. Second, regarding the polymer clearance and safety properties, the molecular weight of the diblock copolymer was designed to be smaller than the renal clearance threshold (~ 50 kDa, ~ 6 nm)[49], and all monomers were designed with ester junctions at the carbon backbone to degrade down to the minimal backbone segment (< 10 kDa).

Prior studies have shown that a variety of hydrophilic polymers with hydrophobic anchoring moieties can be co-formulated with liposomes[50,51]. The PAL was designed to incorporate poly[(DEAEMA-*co*-BMA)-*b*-ManEMA] with DSPC/cholesterol liposomes through the hydrophobic effect between the lipid bilayer and the hydrophobic polymer block, poly(DEAEMA-*co*-BMA). The incorporation of the diblock copolymer with the liposomal membrane was examined using high performance size exclusion chromatography (HPSEC)[52]. Thiocarbonyl RAFT agents exhibit absorption at 300-310 nm, which was used to assess co-formulation (**Figure S1a†**). A rhodamine DHPE detectable at 580 nm was used to follow the lipid components. As shown in Fig. S1b†, co-elution of fluorescent lipids (fluorescence signal, 580 nm) and polymers (absorption signal, 310 nm) after injecting fluorescently-labeled PALs indicates that poly[(DEAEMA-*co*-BMA)-*b*-ManEMA] was associated with the liposomes, rather than forming micelles. This lack of micelle formation was confirmed by the monomodal size distribution of the PALs (**Figure 2.4A**).

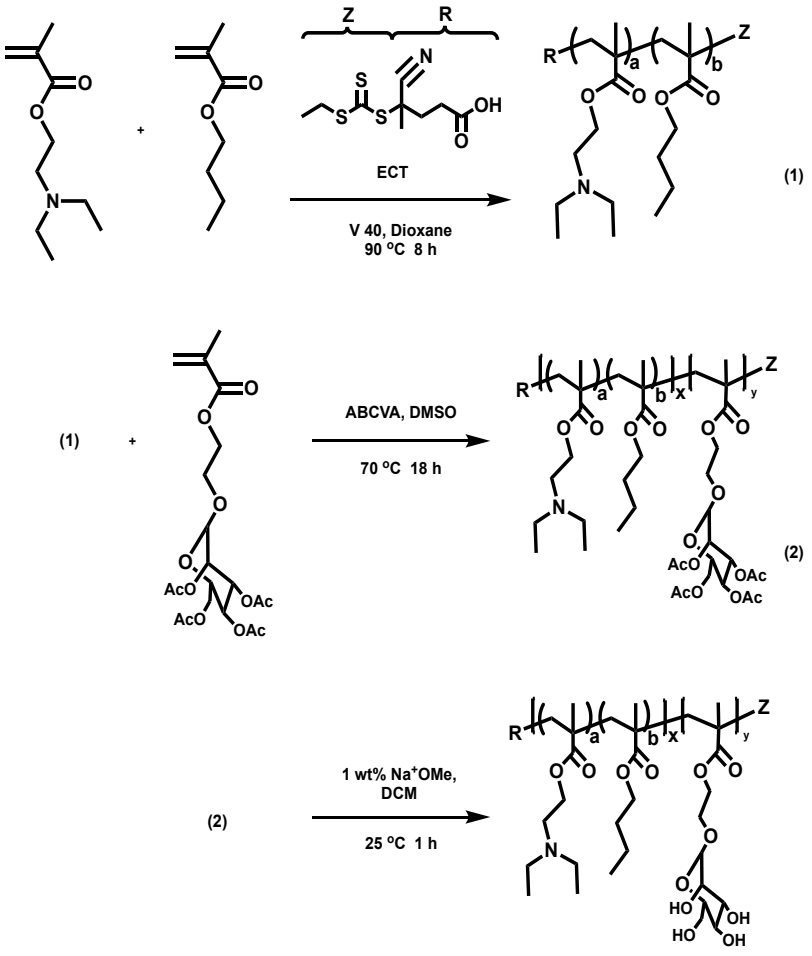

Figure 2.2. RAFT polymerization of poly([DEAEMA-*co*-BMA]-*b*-ManEMA). DEAEMA, diethylaminoethyl methacrylate; BMA, butyl methacrylate; ManEMA, mannose functionalized with ethyl methacrylate.

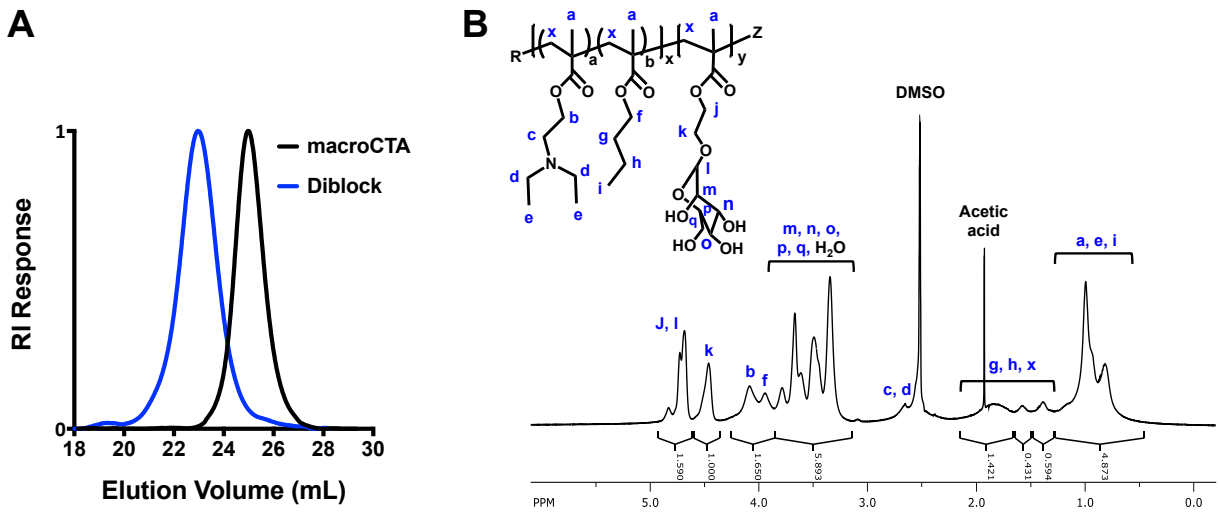

C

macroCTA					Diblock Copolymer				
DP	% feed/comp		M_n (kD)	Đ	DP of 2nd block	M_n (kD)	M_n (kD) Deprotected	Đ	Block Ratio
	DEAEMA	BMA							
50	60/55	40/45	8.6	1.07	25	22.8	17.5	1.12	1:1.03

Figure 2.3. SEC-GPC and ^{1}H-NMR characterization of macroCTA and diblock copolymer. (a) Representative SEC chromatogram showing the narrow and symmetric molecular weight distribution of poly(DEAEMA-*co*-BMA) macroCTA and of poly[(DEAEMA-*co*-BMA)-*b*-mannose ethyl methacrylate] (diblock); (b) ^{1}H-NMR of the diblock copolymer in d-DMSO with assignment of the resonances associated with the respective comonomer residues; (c) Chemical composition and molecular weight of the diblock copolymer employed to formulate the polymer-augmented liposomes. Experimental M_n, Đ, and block ratios were determined by GPC analysis. The block ratios were determined as the ratio of the M_n of the second block to the first block. RI, refractive index; DP, degree of polymerization; DEAEMA, diethylaminoethyl methacrylate; BMA, butyl methacrylate; macroCTA, macro chain transfer agent; Đ, dispersity.

To study the pH-responsive properties of the PALs, the hydrodynamic sizes were evaluated by dynamic light scattering (DLS). Non-pH-responsive PEGylated liposomes were prepared as a control. PALs with and without streptomycin loading show similar hydrodynamic size transitions in response to the pH gradient (**Figure 2.4B**). The hydrodynamic size of PALs gradually decreased with decreasing pH, in contrast to the control PEGylated liposomes maintained a constant size independent of pH. The destabilization of the PALs results from the protonation of DEAEMA at acidic pH, which increases the charge density of the hydrophobic segment, thus destabilizing the liposomal membranes[48]. It is postulated that with the higher charge density on DEAEMA, the poly(DEAEMA-co-BMA) block was no longer well embedded in the liposomal membrane at low pH, and that lipids were released from the disrupted bilayer structure, forming random aggregates with the polymer. Therefore, we speculate that the smaller hydrodynamic diameters measured by DLS at lower pH reflect the formation of the random aggregates driven by the hydrophobic effects between the lipid tails and the hydrophobic BMA in the diblock copolymer.

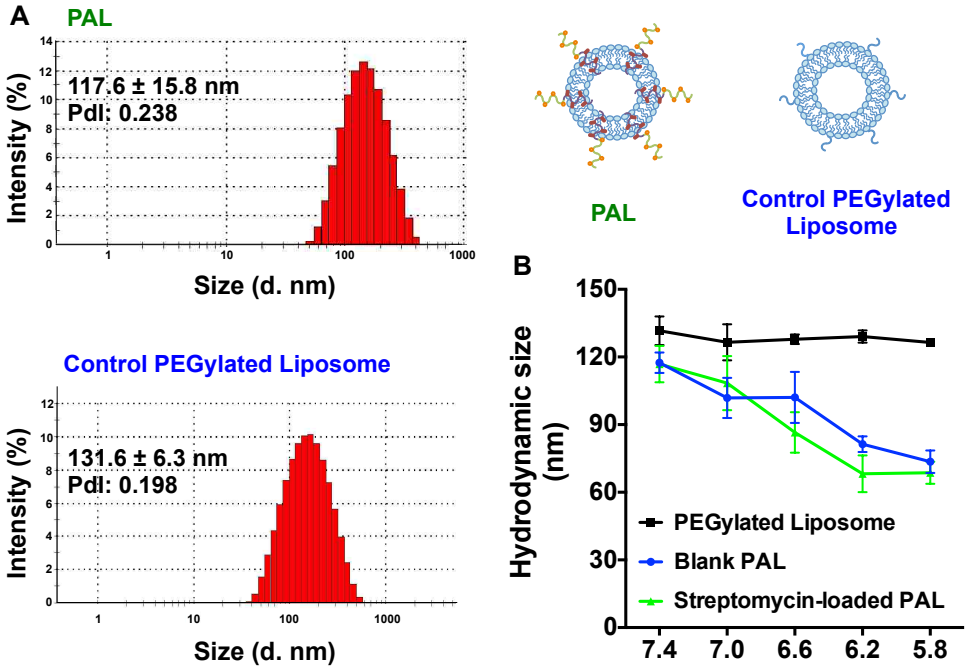

Figure 2.4. Hydrodynamic size measurement as a function of pH. (A) The hydrodynamic distribution of streptomycin-loaded polymer-augmented liposomes (PAL) and control PEGylated liposomes in pH 7.4 phosphate buffer; (B) Blank or streptomycin-loaded PALs and non-pH-

responsive PEGylated control liposomes (streptomycin-loaded) incubated in buffers ranging from pH 7.4 to 5.8. PdI: Polydispersity (Mean ± SD, n=3).

The capability of PALs to encapsulate streptomycin was evaluated by reacting amines on streptomycin with fluorescamine to form a fluorescent streptomycin analogue (**Figure S2a†**), and quantified using a calibration curve (**Figure S2b†**)[37]. The streptomycin loading concentrations in PALs and PEGylated liposomes were 0.77 ± 0.04 mg/mL and 0.65 ± 0.01 mg/mL. The loading of streptomycin was 12.06 ± 0.36% and 10.44 ± 0.12%, respectively (weight of encapsulated streptomycin/weight of loaded PALs or PEGylated liposomes).

2.3.3 *In vitro pH-dependent release*

The pH-dependent release from PALs was examined using a pyranine/p-xylene bispyridinium dibromide (DPX) fluorescent dequenching assay, widely used to investigate the stability or pH-dependent release properties of liposomes[53,54]. PALs co-loaded with both pyranine and DPX were diluted with buffers mimicking the endosomal acidification profile. The degree of release was normalized relative to a positive control, pyranine/DPX-loaded PALs lysed with 1% v/v Triton X-100 (**Figure 2.5A**). As expected, no significant pyranine release was detected from PEGylated liposomes throughout the test pH range. In contrast, the release from PALs was nearly complete at pH 5.4 within three hours of incubation. Above pH 6.2, only background pyranine fluorescence was observed. This pH-dependent response correlates well with the pH gradient found in endosomal-lysosomal trafficking[55], facilitating the preferential release of therapeutic cargo in the endosomal compartment.

Streptomycin release kinetics were then evaluated in pH 5.8 and pH 7.4 buffers via a dynamic dialysis technique. Notably, the release profiles of PALs at pH 5.8 contained two phases, which included a relatively large burst effect in the initial stage (**Figure 2.5B**, about 60% within 1 hour) followed by a slower release phase. We postulated that the burst release at pH 5.8 was due to the rapid transition of DEAEMA from hydrophobic to hydrophilic, thus disturbing the integrity of the lipid bilayer. The slower release phase may be attributed to the gradual detachment of streptomycin that attached to lipids or polymers. In contrast, at pH 7.4, streptomycin released

from PALs was much slower but not negligible, which is postulated to result from a small fraction of surface bound drug in the liposome formulation. This controlled release nature of PALs has potential to deliver concentrated streptomycin to the intracellular infection site, and therefore to provide improved therapeutic efficacy.

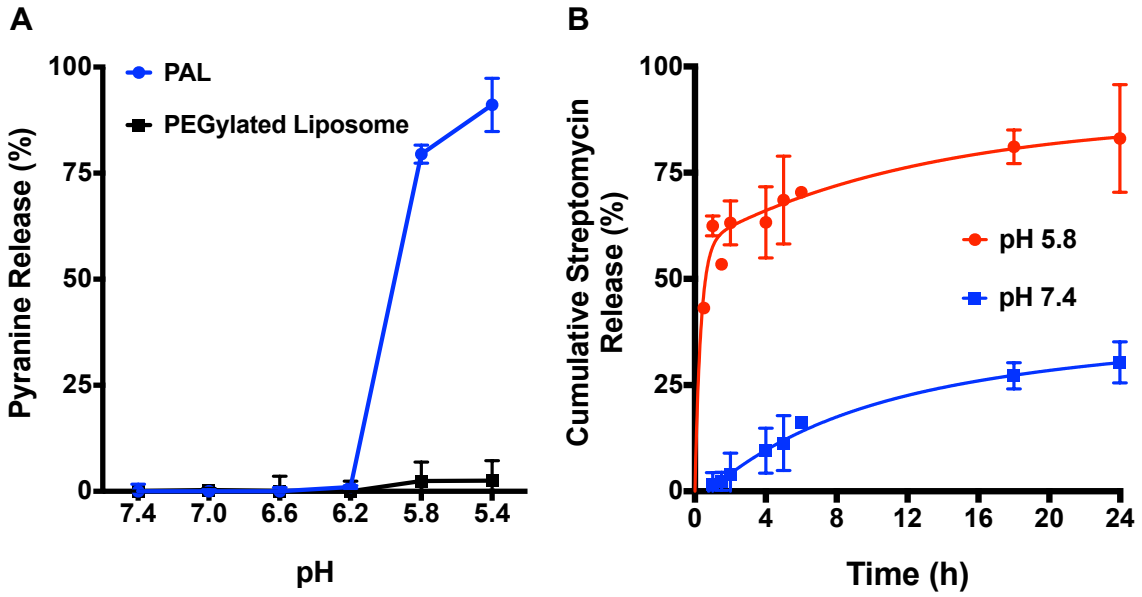

Figure 2.5. pH-dependent release characteristics. (A) Fluorescent dequenching assay. A fluorescent dye-quencher pair, pyranine and p-xylene bispyridinium dibromide, were encapsulated in polymer-augmented liposomes (PALs) and non-pH-responsive PEGylated liposomes. Pyranine release was evaluated in the pH range of the endosomal processing pathway (λ_{ex}=413 nm, λ_{em}=512 nm); (B) Streptomycin release kinetics of PALs at pH 5.8 and 7.4. The release studies were carried out by exposing streptomycin-loaded PALs to physiological (pH 7.4) and acidic (pH 5.8) conditions at 37 °C. Percentage release was normalized relative to a positive control, 1% w/v Triton X-100 (Mean ± SD, n=3).

2.3.4 *pH-dependent membrane-destabilizing activity*

The endosomal-releasing potential of synthetic polymers is frequently assessed using a red blood cell hemolysis assay due to a proven correlation between hemolytic efficiency and endosomal release[56]. The pH-responsive, membrane destabilizing activity of the free diblock copolymer and corresponding PALs were evaluated at several different pH values to mimic the endosomal acidification profile. No significant hemolytic activity was observed at pH 7.4 for polymer alone

(**Figure 2.6A**) or the PALs (**Figure 2.6B**) at any of the concentrations evaluated. A significant increase in red blood cell hemolysis was observed upon reduction of the pH to 6.6. Also, as expected, hemolysis increased in a dose-dependent manner with increasing polymer concentration. Indeed the hemolysis profiles as a function of pH were very similar for both the polymer and PALs. In contrast, no significant hemolytic activity was present in the group treated with control PEGylated liposomes across pH range studied.

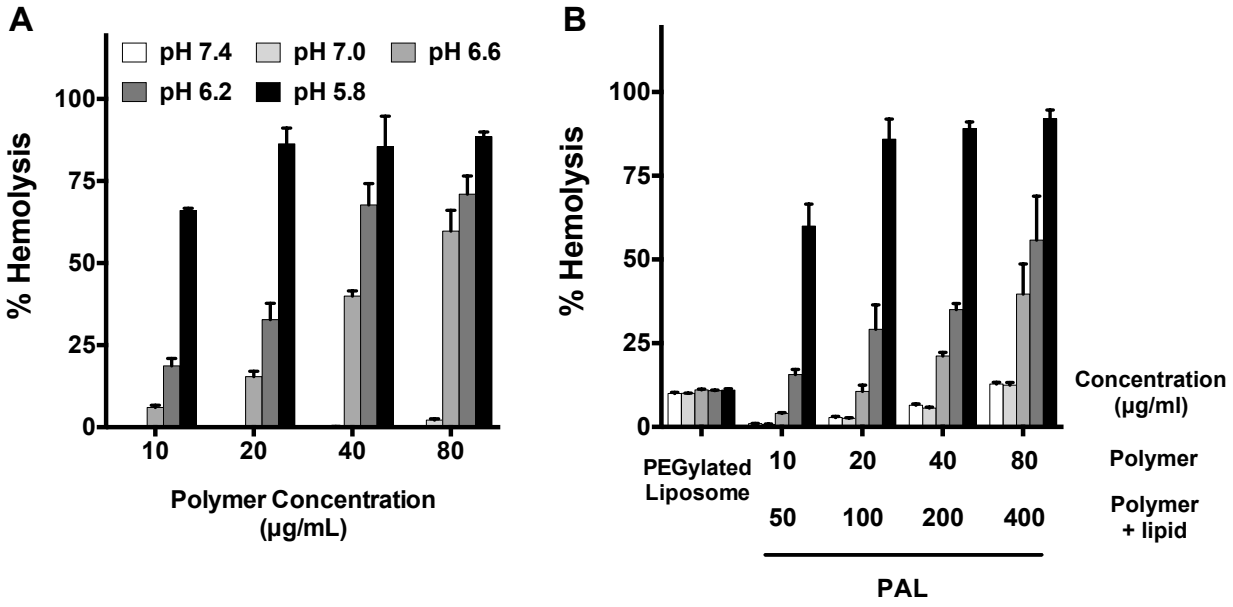

Figure 2.6. Hemolytic assay demonstrating pH-dependent membrane-destabilizing activity of (A) diblock copolymer alone as a function of pH at concentrations of 10, 20, 40, and 80 µg/mL and (B) polymer-augmented liposomes with same polymer concentration range in (A). Non-pH-responsive PEGylated liposomes were used as a negative control. Hemolytic activity was normalized relative to a positive control, 1% v/v Triton X-100, and the data represent a single experiment conducted in triplicate ± SD.

The observed pH-responsive hemolytic effects of PALs near pH 6.6 could be attributed to the composition of the hydrophobic block, poly(DEAEMA-*co*-BMA). Our group has shown that the transition pH could be tuned by varying the hydrophobic content (i.e. BMA) in a relevant diblock copolymer composed of poly(DEAEMA-*co*-BMA)[48]. With 40% BMA and 60% DEAEMA, at pH 6.6, the diblock copolymer has a sharp transition from micelles to unimers and from nonhemolytic to hemolytic activity[48]. Poly[(DEAEMA-*co*-BMA)-*b*-ManEMA] developed in this study has similar BMA to DEAEMA ratio, which could account for the observed pH-

responsive transition at ~pH 6.6. To evaluate if the endosomal-releasing activity of the PALs lead to cytoxicity, RAW 264.7 cells were incubated with the polymer alone and PALs separately for 24 h. The viability of RAW cells was evaluated using a MTS assay (**Figure S3†**). Although the polymer alone shows notable toxicity (~75% viability at 0.05 mg/mL), formulating the polymer with liposomes significantly reduced the toxicity (~92% viability, at 0.05 mg/mL).

Taken together, those results indicate that poly[(DEAEMA-*co*-BMA)-*b*-ManEMA] augmented the liposomes with pH-responsive endosomal-releasing activity and the incorporation of the hydrophobic block into the liposomal membrane did not reduce the pH-selective, membrane destabilizing properties of the polymer. Additionally, the endosomal-releasing activity of PALs did not lead to notable toxicity. These results together with *in vitro* release results suggest that poly[(DEAEMA-*co*-BMA)-*b*-ManEMA] can enhance endosomal release to provide concentrated antibiotics to the cytoplasm where intracellular bacteria accumulate.

2.3.5 *Mannose ligands enhance macrophage uptake of PALs*

AMs highly express internalizing mannose-binding receptors (CD206)[57,58] for recognizing carbohydrates on infectious agents such as bacteria, fungi, and viruses[59]. Carbohydrate-based ligands therefore represent a promising approach for targeting therapeutic agents to macrophages[22,23]. The pH-responsive polymer was thus designed to display multivalent mannose ligands by incorporating poly[(DEAEMA-*co*-BMA)-*b*-ManEMA] into liposomes. RAW 264.7 murine macrophage cells, expressing moderate levels of the CD206 mannose receptor[31], were used to study the cellular uptake of rhodamine-labeled PALs. Rhodamine-labeled PEGylated liposomes without mannose modification were used as a negative control. Cells were respectively incubated with either rhodamine-labeled PALs or PEGylated liposomes (400 μg/mL) with similar fluorescent intensities (**Figure S4†**). Uptake levels were evaluated using flow cytometry and fluorescence microscopy. The observed fluorescent intensity in the group treated with the PEGylated control liposomes was limited, which was likely due to the surface PEGylation (**Figure 2.7A**), as PEG is well-known to inhibit uptake by phagocytic cells of the mononuclear phagocyte system[54]. Conversely, the PAL treatment group produced an increased fluorescent intensity as incubation progressed and revealed considerably greater cellular uptake,

an essential feature to enhance the delivery of intracellular drug. The enhanced uptake in RAW 264.7 cells of PALs was also visualized by fluorescence microscopy (**Figure 2.7B**& **Figure S5**†).

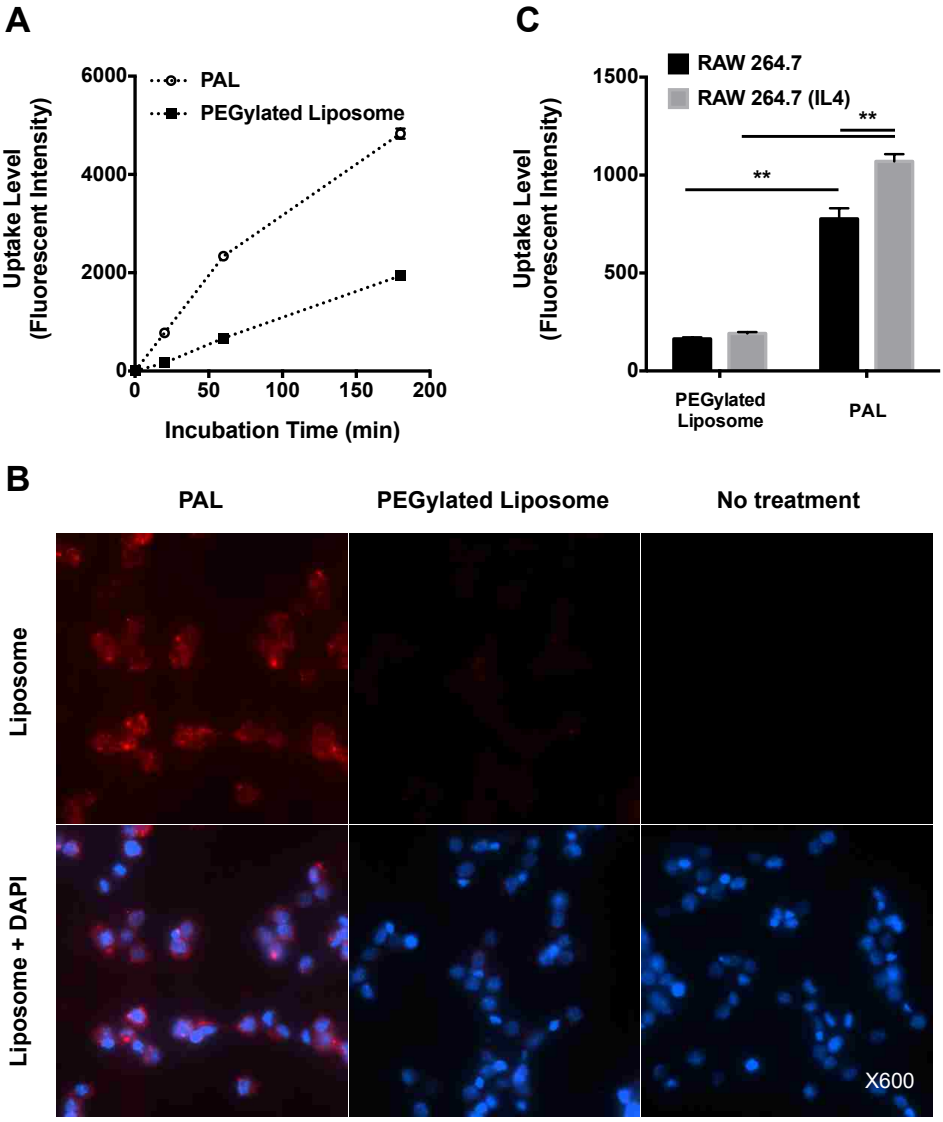

Figure 2.7. Mannose-receptor mediated uptake of rhodamine-labeled polymer-augmented liposomes by RAW 264.7 cells. (A) Time course of RAW 264.7 cell uptake of mannose-functionalized polymer-augmented liposomes (PAL) and non-targeted PEGylated liposomes; (B) Representative fluorescence microscopy images of RAW 264.7 incubated with rhodamine-labeled PALs or PEGylated liposomes (400 μg/mL) for 1 h; (C) Liposome uptake level of RAW 264.7 cells with and without IL-4 stimulation (mannose receptor upregulation). Data were reported as mean fluorescence intensity ± SD (n=3, $^{**}p < 0.005$).

To further demonstrate mannose receptor-mediated interactions between the PALs and RAW 264.7 cells, cells were treated with IL-4 to upregulate their expression of the mannose receptor[40]. Following 20 min incubation, the uptake of PALs was significantly higher in IL-4 treated cells than in non-treated cells ($P < 0.005$), indicating the involvement of mannose receptors in the effective PAL uptake by macrophages (**Figure 2.7C**). As expected, PEGylated control liposomes show significantly lower uptake levels in RAW 264.7 cells than that of PALs, regardless of IL-4 pretreatment. Those results were in agreement with a prior study showing that the uptake mechanism of mannosylated liposomes was mannose-receptor mediated endocytosis in NR8383, a cell line expressing mannose receptors[23]. Additionally, our lab has previously demonstrated that mannose functionalized polymers show specific mannose receptor-mediated uptake by IL-4 treated RAW 264.7 macrophages[31]. Taken together, the uptake study results demonstrate that mannose modification significantly increased the internalization of PALs, likely via the mannose receptor-mediated endocytosis.

2.3.6 *Bactericidal effect of streptomycin-loaded PALs*

The intracellular bactericidal efficacy of streptomycin-loaded PALs was evaluated using a co-culture challenge assay with *F. novicida* infected RAW 264.7 cells. *F. novicida* is commonly used as a laboratory surrogate for *F. tularensis*, due to its low virulence for humans and high degree of genetic similarities with *F. tularensis* (~95%)[55]. Additionally, *F. novicida* exhibits the same evasion of phagolysosome fusion and phagosome escape within infected human-derived macrophages as *F. tularensis*[56]. Bactericidal activity was quantified by enumerating the colony forming units (CFU) of surviving intracellular bacteria after incubating streptomycin-loaded PAL, streptomycin-loaded PEGylated control liposomes or free streptomycin with infected RAW 264.7 cells for 22 hours. Non-drug containing blank PALs or PEGylated liposomes showed no inhibitory effect (**Figure 2.8A**), similar to the no treatment control.

Streptomycin-loaded PALs showed concentration-dependent intracellular bacterial growth inhibition, and exhibited better inhibitory capability against intracellular bacteria than streptomycin-loaded PEGylated liposomes and free streptomycin (**Figure 2.8B**). At ~15 μg/mL dosing, the PAL system demonstrated a 13-16 fold increased efficacy, compared to free

streptomycin and PEGylated liposomes. The better efficacy of PALs than PEGylated liposomes may result from the fact that endosomal-releasing activity of PALs facilitates the cytosolic delivery of streptomycin, which would otherwise be mainly entrapped in acidic lysosomes due to the polycationic nature of streptomycin[10]. This observation was in accordance with a previous study showing that gentamicin-loaded fusogenic liposomes had better efficacy against intracellular bacteria than non-fusogenic liposomes[18]. It is worth noting that PALs did not show significant cytotoxicity in RAW 264.7 cells within the dose range (**Figure. S3b**†). Those findings revealed the superior inhibition of intracellular bacterial growth by streptomycin-loaded PALs, which can account for its efficient intracellular drug release in infected RAW 264.7 cells. Additional studies are needed to elucidate the individual contribution of the targeting and pH-responsive functionalities to the superior activity of PALs.

Building upon the findings of the current study, future design criteria for antibiotic carriers against intracellular infections may include differential release mechanisms that respond to the microenvironemnt of the intracellular infection setting (e.g., bacterial enzymes[60]), or respond to physical stimuli (e.g, ultrasound) to minimize off-target release[61]. Additionally, antibiotic carriers that can provide sustained release at the site of infection are postulated to improve drug retention, and therefore potentially reduce dosing frequency[62].

2.4 CONCLUSION

This study demonstrates a utility of a multifunctional diblock copolymer, poly[(DEAEMA-*co*-BMA)-*b*-ManEMA], to functionalize liposomes for intracellular antibiotic delivery. Liposomes formulated with this polymer (PALs) enhanced the cellular uptake level through mannose receptor-mediated endocytosis, as confirmed in macrophage uptake study. Additionally, the PALs show endosomal pH-induced enhanced drug release and endosomal-releasing activity. Streptomycin loaded in PALs shows better bactericidal efficacy than free drug and non-pH responsive and non-targeted PEGylated control liposomes in a representative bacteria-macrophage co-culture model. Taken together, the PAL system developed here provides a new delivery platform for effective cytosolic antibiotic delivery against Francisella and potentially other intracellular bacterial infections.

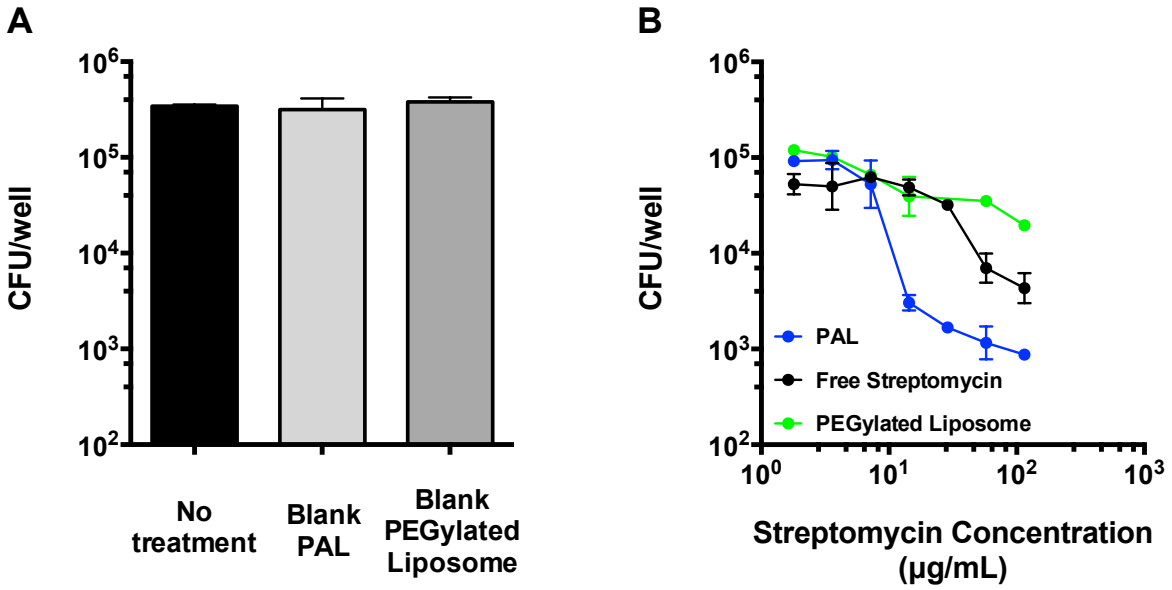

Figure 2.8. Antibacterial activity of streptomycin-loaded polymer-augmented liposomes. (A) RAW 264.7 cells were treated with blank polymer-augmented liposomes (PAL) or control PEGylated liposomes following an infection with *F. novicida*. Concentrations used here equaled to the maximum liposome concentration (highest streptomycin dose) used in Fig. 5b. (B) RAW 264.7 cells were treated with varying streptomycin concentrations (115 µg/mL to 1.8 µg/mL) of different formulations following an infection with *F. novicida* to determine the efficacy against intracellular bacteria. CFU: colony-forming unit. (Mean ± SD, n=3).

2.5 Acknowledgements

This work was funded by the Defense Threat Reduction Agency (Grant #HDTRA1-13-1-0047). F.Y.S. is an international student research fellow of the Howard Hughes Medical Institute. J.C. and A.M.K. were graduate research fellows of the National Science Foundation.

2.6 References

1. K. Zaman, *Journal of Health, Population, and Nutrition*, 2010, **28**, 111–113.
2. A. K. Goel, *World Journal of Clinical Cases: WJCC*, 2015, **3**, 20–33.
3. J. Ellis, P. C. F. Oyston, M. Green and R. W. Titball, *Clin. Microbiol. Rev.*, 2002, **15**, 631–646.
4. R. Perumal Samy, B. G. Stiles, G. Sethi and L. H. K. Lim, *PLoS Neglected Trop. Di.s*,

2017, **11**, e0004738.
5. P. C. F. Oyston, A. Sjostedt and R. W. Titball, *Nat. Rev. Microbiol.*, 2004, **2**, 967–978.
6. K. Ray, B. Marteyn, P. J. Sansonetti and C. M. Tang, *Nat. Rev. Microbiol.*, 2009, **7**, 333–340.
7. R. S. Flannagan, G. Cosio and S. Grinstein, *Nat. Rev. Microbiol.*, 2009, **7**, 355–366.
8. A. Fink, M. A. Hassan, N. A. Okan, M. Sheffer, A. Camejo, J. P. J. Saeij and D. L. Kasper, *mBio*, 2016, **7**, e02243–15.
9. S. H. Kaufmann, *Annu. Rev. Immunol.*, 1993, **11**, 129–163.
10. S. Carryn, H. Chanteux, C. Seral, M.-P. Mingeot-Leclercq, F. Van Bambeke and P. M. Tulkens, *Infectious Disease Clinics of North America*, 2003, **17**, 615–634.
11. F. Van Bambeke, M. Barcia-Macay, S. Lemaire and P. M. Tulkens, *Curr. Opin. Drug Discovery Dev.*, 2006, **9**, 218–230.
12. D. T. Dennis, T. V. Inglesby, D. A. Henderson, J. G. Bartlett, M. S. Ascher, E. Eitzen, A. D. Fine, A. M. Friedlander, J. Hauer, M. Layton, S. R. Lillibridge, J. E. McDade, M. T. Osterholm, T. O'Toole, G. Parker, T. M. Perl, P. K. Russell, K. Tonat and for the Working Group on Civilian Biodefense, *JAMA*, 2001, **285**, 2763–2773.
13. J.-C. Pechere and R. Dugal, *Clin. Pharmacokinet.*, 1979, **4**, 170–199.
14. P. M. Tulkens, *Scandinavian Journal of Infectious Diseases. Supplementum*, 1990, **74**, 209–217.
15. P. de Jager and R. van Altena, *Int. J. Tuberc. Lung Dis.*, 2002, **6**, 622–627.
16. C. Jernberg, S. Lofmark, C. Edlund and J. K. Jansson, *Microbiology*, 2010, **156**, 3216–3223.
17. J. P. Wong, H. Yang, K. L. Blasetti, G. Schnell, J. Conley and L. N. Schofield, *J. Controlled Release*, 2003, **92**, 265–273.
18. P. Lutwyche, C. Cordeiro, D. J. Wiseman, M. St-Louis, M. Uh, M. J. Hope, M. S. Webb and B. B. Finlay, *Antimicrob. Agents Chemother.,* 1998, **42**, 2511–2520.
19. S. P. Vyas, M. E. Kannan, S. Jain, V. Mishra and P. Singh, *Int. J. Pharm.*, 2004, **269**, 37–49.
20. D. Cipolla, J. Blanchard and I. Gonda, *Pharmaceutics*, 2016, **8**, 1–31.
21. K. A. Hamblin, S. J. Armstrong, K. B. Barnes, C. Davies, J. P. Wong, J. D. Blanchard, S. V. Harding, A. J. H. Simpson and H. S. Atkins, *Antimicrob. Agents Chemother.,* 2014, **58**, 3053–3059.
22. W. Wijagkanalan, S. Kawakami, M. Takenaga, R. Igarashi, F. Yamashita and M. Hashida, *J. Controlled Release*, 2008, **125**, 121–130.
23. S. Chono, T. Tanino, T. Seki and K. Morimoto, *J. Controlled Release*, 2008, **127**, 50–58.
24. S. Kobayashi, I. Nakase, N. Kawabata, H.-H. Yu, S. Pujals, M. Imanishi, E. Giralt and S. Futaki, *Bioconjugate Chem.*, 2009, **20**, 953–959.
25. J. Yen, Y. Zhang, N. P. Gabrielson, L. Yin, L. Guan, I. Chaudhury, H. Lu, F. Wang and J. Cheng, *Biomater. Sci.*, 2013, **1**, 719–727.
26. W.-J. Song, J.-Z. Du, T.-M. Sun, P.-Z. Zhang and J. Wang, *Small*, 2010, **6**, 239–246.

27. D. D. Lane, F. Y. Su, D. Y. Chiu, S. Srinivasan, J. T. Wilson, D. M. Ratner, P. S. Stayton and A. J. Convertine, *Polym. Chem.*, 2015, **6**, 1255–1266.
28. S. Raisin, M. Morille, C. Bony, D. Noel, J.-M. Devoisselle and E. Belamie, *Biomater. Sci*, 2017, **5**, 1910–1921.
29. S. Keller, J. T. Wilson, G. I. Patilea, H. B. Kern, A. J. Convertine and P. S. Stayton, *J. Controlled Release*, 2014, **30**, 24–33.
30. Y. Yoshizaki, E. Yuba, N. Sakaguchi, K. Koiwai, A. Harada and K. Kono, *Biomaterials*, 2014, **35**, 8186–8196.
31. J. Chen, H.-N. Son, J. J. Hill, S. Srinivasan, F.-Y. Su, P. S. Stayton, A. J. Convertine and D. M. Ratner, *Nanomedicine*, 2016, **12**, 2031–2041.
32. A. J. Convertine, D. S. W. Benoit, C. L. Duvall, A. S. Hoffman and P. S. Stayton, *J. Controlled Release*, 2009, **133**, 221–229.
33. P. Stano, S. Bufali, C. Pisano, F. Bucci, M. Barbarino, M. Santaniello, P. Carminati and P. L. Luisi, *J. Liposome Res.*, 2004, **14**, 87–109.
34. H.-I. Chang and M.-K. Yeh, *Int. J. Nanomed.*, 2012, **7**, 49–60.
35. A. C. Chen and R. T. Mayer, *Journal of Chromatography A*, 1981, **207**, 445–448.
36. S. E. K. Tekkeli, A. Onal and A. O. Sagirli, *Luminescence*, 2014, **29**, 87–91.
37. S. Udenfriend, S. Stein, P. Böhlen, W. Dairman, W. Leimgruber and M. Weigele, *Science*, 1972, **178**, 871–872.
38. C. Chen, P. Zheng, Z. Cao, Y. Ma, J. Li, H. Qian, W. Tao and X. Yang, *Biomater. Sci.*, 2016, **4**, 412–417.
39. N. Murthy, J. R. Robichaud, D. A. Tirrell, P. S. Stayton and A. S. Hoffman, *J. Controlled Release*, 1999, **61**, 137–143.
40. M. Stein, S. Keshav, N. Harris and S. Gordon, *J. Exp. Med.*, 1992, **176**, 287–292.
41. A. Singh, M. Talekar, A. Raikar and M. Amiji, *J. Controlled Release*, 2014, **190**, 515–530.
42. D. L. Laskin, V. R. Sunil, C. R. Gardner and J. D. Laskin, *Annual review of pharmacology and toxicology*, 2011, **51**, 267–288.
43. G. R. Donowitz, *Clin. Infect. Dis.*, 1994, **19**, 926–930.
44. L. M. Roberts, S. Tuladhar, S. P. Steele, K. J. Riebe, C.-J. Chen, R. I. Cumming, S. Seay, R. Frothingham, G. D. Sempowski, T. H. Kawula and J. A. Frelinger, *Infect. Immun.*, 2014, **82**, 2504–2510.
45. Z. Li, D. L. Clemens, B.-Y. Lee, B. J. Dillon, M. A. Horwitz and J. I. Zink, *ACS Nano*, 2015, **9**, 10778–10789.
46. K. A. Rodvold, *Pharmacotherapy*, 2001, **21**, 319S–330S.
47. G. Moad, E. Rizzardo and S. H. Thang, *Aust. J. Chem.*, 2005, **58**, 379–410.
48. M. J. Manganiello, C. Cheng, A. J. Convertine, J. D. Bryers and P. S. Stayton, *Biomaterials*, 2012, **33**, 2301–2309.
49. M. Longmire, P. L. Choyke and H. Kobayashi, *Nanomedicine*, 2008, **3**, 703–717.
50. H. Ringsdorf, J. Venzmer and F. M. Winnik, *Angew. Chem. Int. Ed. Engl.*, 1991, **30**, 315–318.

51. H. Kitano, Y. Akatsuka and N. Ise, *Macromolecules*, 1991, **24**, 42–46.
52. C. Grabielle-Madelmont, S. Lesieur and M. Ollivon, *Size-Exclusion Chromatography*, 2003, **56**, 189–217.
53. N. Bertrand, P. Simard and J.-C. Leroux, *Methods Mol. Biol.*, 2010, **605**, 545–558.
54. L. Di Marzio, S. Esposito, F. Rinaldi, C. Marianecci and M. Carafa, *Colloids Surf., B*, 2014, **104**, 200–206.
55. S. Ohkuma and B. Poole, *Proc. Natl. Acad. Sci. U.S.A.*, 1978, **75**, 3327–3331.
56. C. Plank, B. Oberhauser, K. Mechtler, C. Koch and E. Wagner, *J. Biol. Chem.*, 1994, **269**, 12918–12924.
57. R. A. B. Ezekowitz, D. J. Williams, H. Koziel, M. Y. K. Armstrong, A. Warner, F. F. Richards and R. M. Rose, *Nature*, 1991, **351**, 155–158.
58. T. Hussell and T. J. Bell, *Nat. Rev. Immunol.*, 2014, **14**, 81–93.
59. A. K. Azad, M. V. S. Rajaram and L. S. Schlesinger, *Journal of cytology & molecular biology*, 2014, **1**, 1000003.
60. V. V. Komnatnyy, W.-C. Chiang, T. Tolker-Nielsen, M. Givskov and T. E. Nielsen, *Angew. Chem. Int. Ed. Engl.*, 2014, **53**, 439–441.
61. M. L. Noble, P. D. Mourad and B. D. Ratner, *Biomater. Sci.*, 2014, **2**, 839–902.
62. P. M. Mountziaris, S. R. Shah, J. Lam, G. N. Bennett and A. G. Mikos, *Biomater. Sci.*, 2016, **4**, 121–129.

2.7 SUPPLEMENTARY INFORMATION

S1. Supplementary method

1. RAFT synthesis of poly[(DEAEMA-*co*-BMA)-*b*-ManEMA]

A macro chain transfer agent (macroCTA) is the initial polymer block of a diblock copolymer that functions as the CTA for subsequent polymerizations. Here macroCTA was synthesized *via* RAFT using 2,2'-Azobis(4-methoxy-2.4-dimethyl valeronitrile) (V 40) as the initiator, ECT as the CTA, with 50 wt% monomer in dioxane. The initial monomer ($[M]_o$) to CTA ($[CTA]_o$) to initiator ($[I]_o$) ratios for the macroCTA synthesis was 25:1:0.1. Feed ratios of diethylaminoethyl methacrylate (DEAEMA) and butyl methacrylate (BMA) can be found in Fig. 1. Polymerization solutions were vortexed, transferred to septa-sealed round bottom flasks, purged under N_2 for 30 min and incubated in a 90 °C water bath for 8 h. The resultant polymers were purified by dialysis against acetone for two days and then isolated by further dialysis against water in Spectra/Por dialysis tubing (MWCO 6-8 kDa). The final polymers were then lyophilized for further use.

To synthesize the mannose-containing block, mannose functionalized with ethyl methacrylate (ManEMA) was synthesized and fully characterized as described previously[1]. The synthesized ManEMA monomers with acetyl protecting groups (1g, 480 mM) were added to the macroCTA (1.1g, 38.4 mM) and dissolved in dioxane. 4,4-azobis(4-cyanovaleric acid) (ABCVA) was used as the radical initiator. The initial monomer to macroCTA molar ratio ($[M]_0$:$[macroCTA]_0$) was 12.5:1, and the initial macroCTA to initiator molar ratio ($[macroCTA]_0$:$[I]_0$) was 5:1. A stock solution of ABCVA (9.79 mg, 7.68 mM) dissolved in dioxane was added to the reaction solution. Following the addition of ABCVA the solution was purged with nitrogen for 30 min and allowed to polymerize at 70 °C for 18 h. The resulting diblock copolymer was obtained via precipitation in diethyl ether (6x) and placed in vacuum overnight. To deprotect acetyl groups on ManEMA monomers, the obtained diblock copolymer was added to a solution of 1 wt% sodium methoxide in methanol at a copolymer concentration of 50 mg/mL. After 1 h incubation at room temperature, the solution was quenched and neutralized with acetic acid to a pH 7 and dialyzed against deionized water. The solution was then lyophilized to obtain the final deprotected glycopolymer, poly[(DEAEMA-*co*-BMA)-*b*-ManEMA].

Characterization of diblock copolymer by SEC-GPC and NMR

The compositions of the macroCTA and the diblock copolymer were determined by ^{1}H-NMR (Bruker DRX499) in deuterated dimethylsulfoxide (DMSO-d_6) at 25 °C. The number average molecular weight (M_n) and dispersity (Đ) were measured by GPC using Tosoh SEC TSK GEL α-3000 and α-4000 columns (Tosoh Bioscience, Montgomeryville, PA) connected in series to a 1200 Series liquid chromatography system (Agilent, Santa Clara, CA) and a miniDAWN TREOS three-angle light scattering instrument with an Optilab TrEX refractive index detector (Wyatt Technology, Santa Barbara, CA).

2. High-performance size exclusion chromatography (HPSEC)

Incorporation of poly[(DEAEMA-*co*-BMA)-*b*-ManEMA] with liposomes was examined using HPSEC[2]. This analysis was performed with a HPLC (Agilent 1260 series HPLC, USA) equipped with an Acclaim™ SEC-1000 LC Column (7.8 mm × 150 mm, 7 μm ThermoFisher). The eluent was PBS and the flow rate was 1 mL/min. Diluted polymer solution or rhodamine-labeled PALs in 10-μL aliquots were injected. The elution was followed by absorbance (λ= 310 nm) and

fluorescence measurement (Ex. 560 nm, Em. 580 nm) to detect the polymer and rhodamine-labeled liposomes, respectively.

3. MTS assay

Cell viability of the polymer alone or PALs with streptomycin encapsulation was evaluated by MTS assay in a murine macrophage cell line, RAW 264.7. Culture condition of RAW 264.7 cells was DMEM supplemented with 10% FBS, 100 U/mL penicillin and 100 μg/mL streptomycin in a 37°C, 5% CO_2 incubator. The RAW 264.7 cells were seeded into 96-well plates at a density of 50,000 cells per well in 100 μL DMEM supplemented with 10% fetal bovine serum (FBS) in 5% CO_2 incubator at 37 °C. After 16-18 h, cells were incubated with the polymer or PALs (100 μL per well) at a series of PAL concentrations (polymer + lipid). After continued incubation for 24 h, the effect of different treatments on cell viability was assessed by the MTS assay. The absorbance at 490 nm in each well was determined by a microplate reader (Tecan Safire2). Untreated cells were used as a control with 100% viability. The relative cell viability (%) compared to control cells was calculated by $(A_{sample}/A_{control}) \times 100$. All treatments were done in triplicates.

S2. Supplementary data

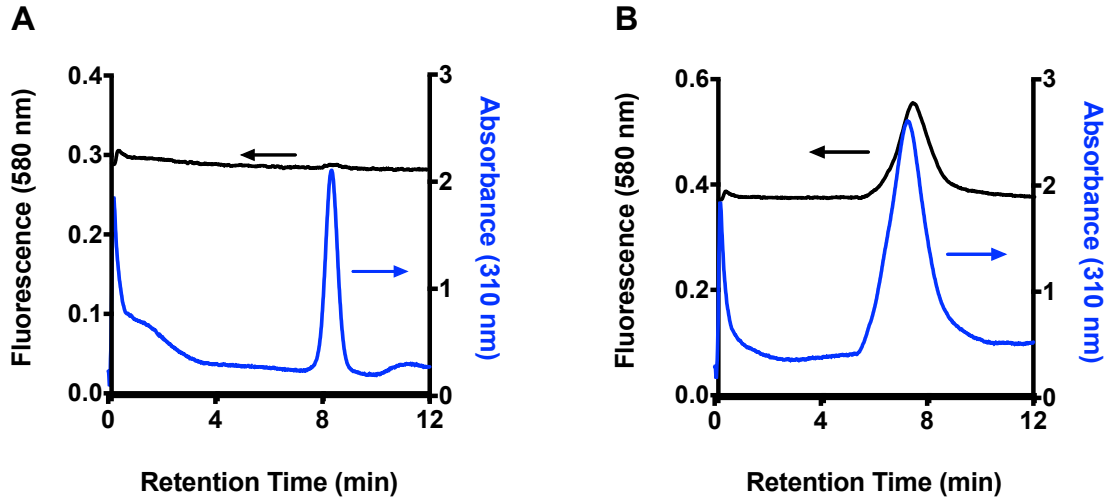

[redacted]

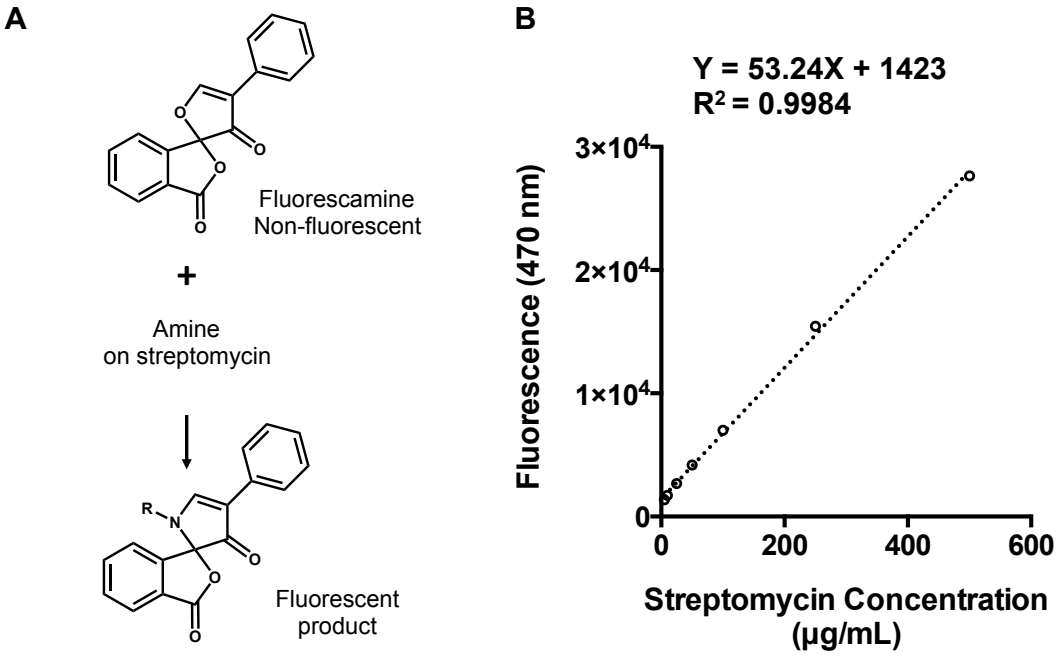
A
Fluorescamine
Non-fluorescent
+
Amine
on streptomycin
R
N
Fluorescent
product
B
Y = 53.24X + 1423
R2 = 0.9984
3×10^4
2×10^4
1×10^4
0
Fluorescence (470 nm)
0
200
400
600
Streptomycin Concentration
(µg/mL)

[redacted]

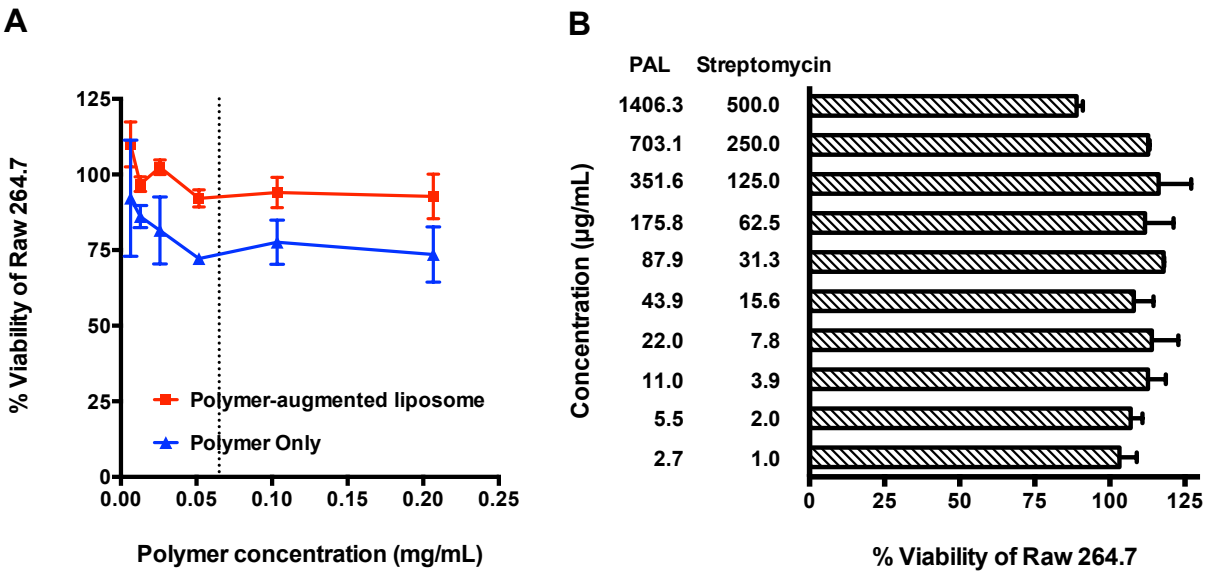
A
% Viability of Raw 264.7
125
100
75
50
25
0
0.00
0.05
0.10
0.15
0.20
0.25
Polymer concentration (mg/mL)
Polymer-augmented liposome
Polymer Only
B
PAL
Streptomycin
Concentration (µg/mL)
1406.3
500.0
703.1
250.0
351.6
125.0
175.8
62.5
87.9
31.3
43.9
15.6
22.0
7.8
11.0
3.9
5.5
2.0
2.7
1.0
0
25
50
75
100
125
% Viability of Raw 264.7

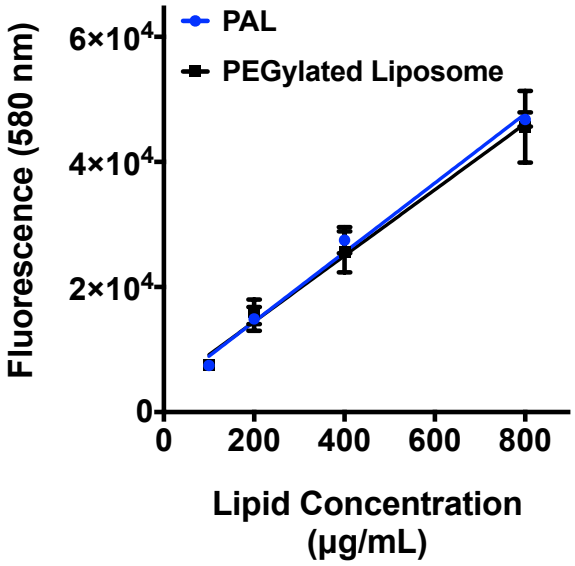

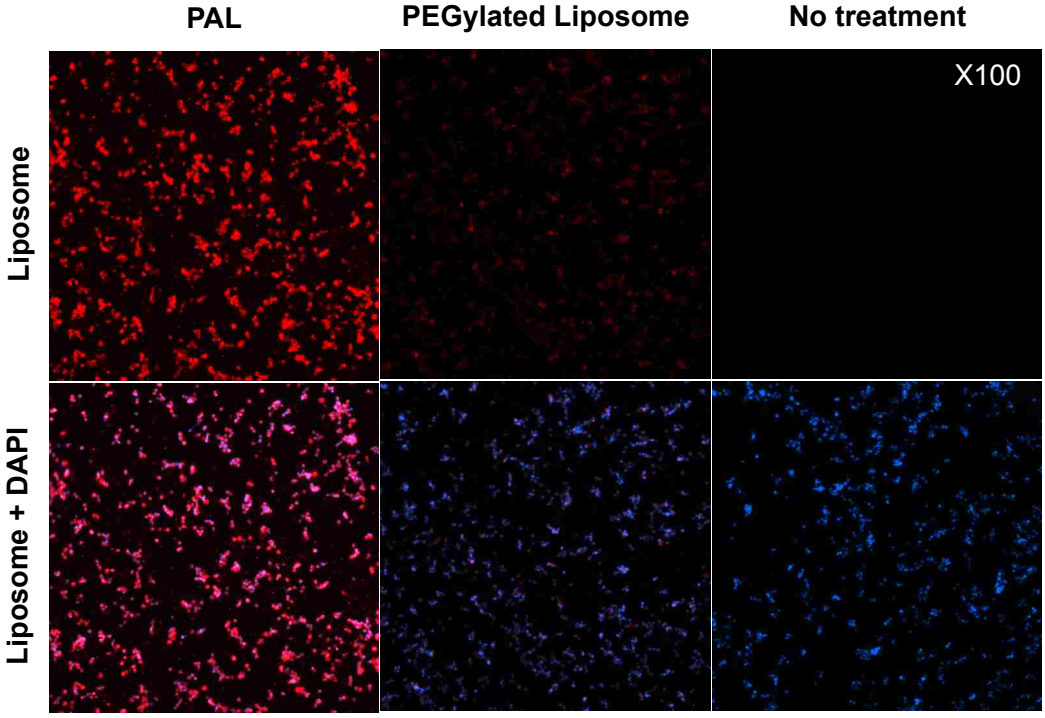

Fig. S5 Representative fluorescence microscopy images of RAW 264.7 incubated with rhodamine-labeled polymer-augmented liposomes (PALs) or non-targeted PEGylated liposomes (400 μg/mL) for 1 h (100X magnification).

S3. Reference

1. J. Chen, H.-N. Son, J. J. Hill, S. Srinivasan, F.-Y. Su, P. S. Stayton, A. J. Convertine and D. M. Ratner, *Nanomedicine*, 2016, 12, 2031–2041.
2. C. Grabielle-Madelmont, S. Lesieur and M. Ollivon, *Journal of Biochemical and Biophysical Methods*, 2003, 56, 189–217.

Chapter 3. Synthesis and optimization of enzyme-labile polymeric prodrug for intracellular antibiotic delivery

Abstract

This chapter attempted to exploit an enzyme-labile dipeptide linker to endow polymeric antibiotic prodrugs, termed drugamer, with specific intracellular drug release in alveolar macrophages (AMs), where *Francisella tularensis* and *Burkholderia pseudomallei* reside at the early stage of infections. As a peptide bond is a covalent chemical bond, which could theoretically prevent premature and burst drug release as observed in the previous chapter. A polymerizable ciprofloxacin drugamer was developed with an enzyme-cleavable dipeptide linking ciprofloxacin prodrug to a polymerizable methacrylate. This ciprofloxacin drugamer was copolymerized with mannose ethyl methacrylate (mannose monomer) to provide hydrophilicity and AM-targeting. The composition of the initial enzyme-cleavable drugamer was determined to be 82% mannose monomer and 18% ciprofloxacin prodrug monomer (14.5 wt% drug) via ^{1}H-NMR. Similar wt% of ciprofloxacin (14.0 %) was obtained in the non-enzyme cleavable control polyme (without dipeptide linker), PAB drugamer. Active ciprofloxacin released from VC drugamer was found to be rapid and cathepsin B-dependent, especially in lysosomal pH (92.94% release in 4 hours at pH 5.0; 12.32% at pH 7.4). Whereas no detectable drug release was observed from PAB drugamer, regardless of the presence of cathepsin B. Additionally, VC drugamer was significantly more stable in human serum than PAB drugamer–the projected half-life for VC drugamer was 21 day in human plasma, in contrast to 8 days for PAB drugamer. Despite of the fact that the VC drugamer with 14.5 wt% drug shows desired *in vitro* release properties and stability, the composition of VC drugamer was further optimized to achieve sufficient PBS solubility and avoid *in vivo* lung toxicity.

Keywords: Enzyme responsive, polymeric prodrug, intracellular delivery, pulmonary infection

3.1 INTRODUCTION

Drug delivery systems aiming at eliminating intracellular infections (e.g., *Francisella tularensis* and *Burkholderia thailandensis*) would be desirable to escort drugs during transportation, and specifically release drugs inside target cells in a controlled release manner. Although liposomal formulations have been intensively investigated for treating infectious diseases[1-3], their systemic stability and burst release kinetics in physiological condition are often contested[4-6]. For instance, Lipoquin™ and Pulmaquin™ are two liposomal ciprofloxacin formulations undergoing clinical trial for the treatment of lung infections[7]. More than 90% of the encapsulated ciprofloxacin was released in 2 h in the presence of 50% bovine serum[8]. Drug leakage in physiological condition was also observed in the polymer-augmented liposomes described in Chapter 2 (25% release in PBS over 24 hours). Those release kinetics studies were performed in 50% serum or PBS condition, and thus the premature drug release is likely more significantly *in vivo*. In the circumstances of intracellular infections, better therapeutic efficacy could be potentially achieved by drug deliver systems that can release the payload mainly in target tissues/cells with a sustained release manner.

To achieve better stability and control over intracellular release rate, chemical conjugation of drug molecules to polymer matrixes, so-called polymeric prodrugs, presents a promising alternative for physical drug encapsulation, the drug loading approach used in liposomes[9,10]. Covalent bonds (e.g., ester, amide) are relatively more stable in physiological condition and provide more tunable drug release rates than physical encapsulation[9,11]. For instance, norfloxacin conjugated to a poly(L-lysine citramide) carrier through a carbamate ester spacer demonstrates 25% release at pH 4.5 and 8% release at pH 7.4 after 30 days[12]. With the controlled and sustained release profiles, those polymeric antibiotic prodrugs offer a window of opportunity for providing target cells with a therapeutic relevant antibiotic concentration for a extended period of time.

Our group has recently developed a polymerizable "drugamer" technology that conjugates drug to a methacrylate monomer through various cleavable linkages to control the drug release rate of polymeric prodrugs (**Figure 3.1**)[13]. For example, aliphatic ester and phenolic ester linkers were

utilized to conjugate ciprofloxacin, a potent broad spectrum antibiotic, to a methacrylate monomer for copolymerization with poly(ethylene glycol) methacrylate (O950) (**Figure 3.2**)[13]. The polymer functionalized with phenolic ester linkage, poly(O950-*co*-CPM), demonstrated significantly faster hydrolysis rate in serum (nearly 50% drug release at 120 h) than aliphatic ester linker [poly(O950-*co*-HBC), about 21 day]. This faster release kinetic of poly(O950-*co*-CPM) resulted in better therapeutic efficacy than poly(O950-*co*-HBC) in an in *vivo Francisella* challenge model (**Figure 3.1**). Additionally, the "drugamer" approach can avoid post-conjugation of drugs to pre-made polymers, and can potentially achieve higher drug loading[14]. Together with the versatile reversible addition-fragmentation chain-transfer (RAFT) polymerization, this drugamer technology allows the preparation of polymeric prodrugs with tunable release profiles for different disease settings.

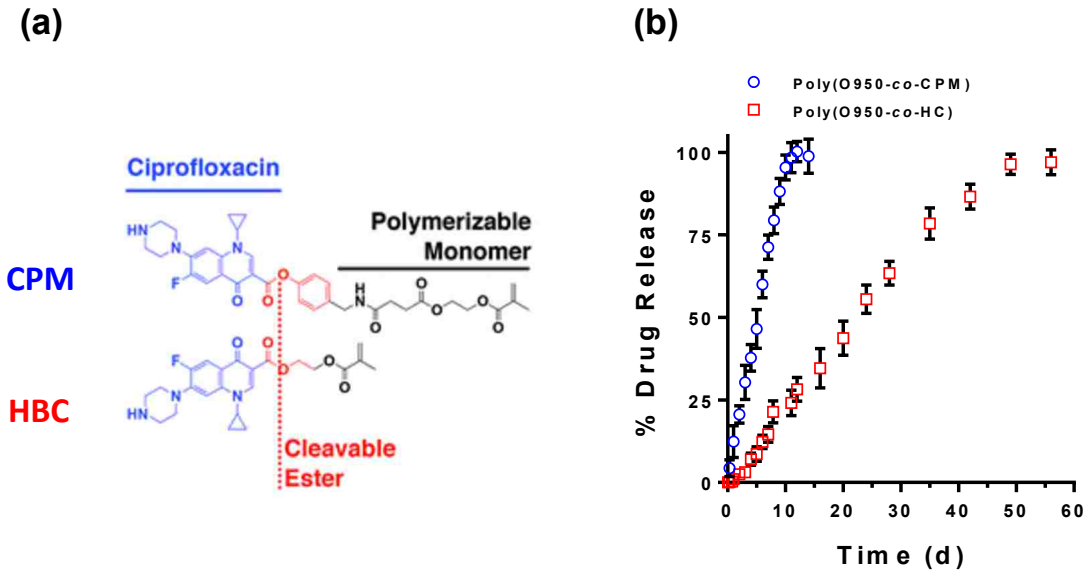

Figure 3.1. (a) Ciprofloxacin drugmers contain phenyl (CPM) and aliphatic (HBC) esters linking the Cipro prodrugs to the polymerizable methacrylate; (b) ciprofloxacin release kinetics of copolymers composed of CPM/HBC and polyethylene glycol methacrylate (O950).

To develop efficient polymeric prodrugs against intracellular infections in alveolar macrophages (AMs), delivering the majority of payload in AMs is crucial to reduce the required dose and prevent systemic toxicity. Although poly(O950-*co*-CPM) mentioned earlier indeed demonstrates therapeutic efficacy against pulmonary tularemia, its suboptimal balance between the drug

release rate ($T_{1/2}$: 2.5 days) and the polymer clearance from the lungs ($T_{1/2}$: 24 h) might potentially reduce the drug bioavailability in AMs (**Figure 3.1 & 3.2**). Additionally, phenol ester linker is susceptible to esterases in lungs and serum, thus might leading to nonspecific drug release outside alveolar macrophages [15,16]. To further optimize the polymeric prodrug system, instead of PEG comonomer (O950), mannose methacrylate monomer (Man) was copolymerized with ciprofloxacin phenol ester monomer (CTM) to facilitate internalization by AMs. This copolymer, poly(Man-*co*-CTM), shows significantly higher drug concentration in the lungs at all time points post administration compared to other organs and blood (**Figure 3.2**), leading to better efficacy than free ciprofloxacin and a non-targeting galactose control polymer in a mice model of *Francisella* infection [87.5% survival rate than 0% of free ciprofloxacin and 25% galactose control polymer]. This suggests that targeting polymeric antibiotic prodrugs to intracellular pool of pathogens is key for clinical success in the treatment of Francisella infection.

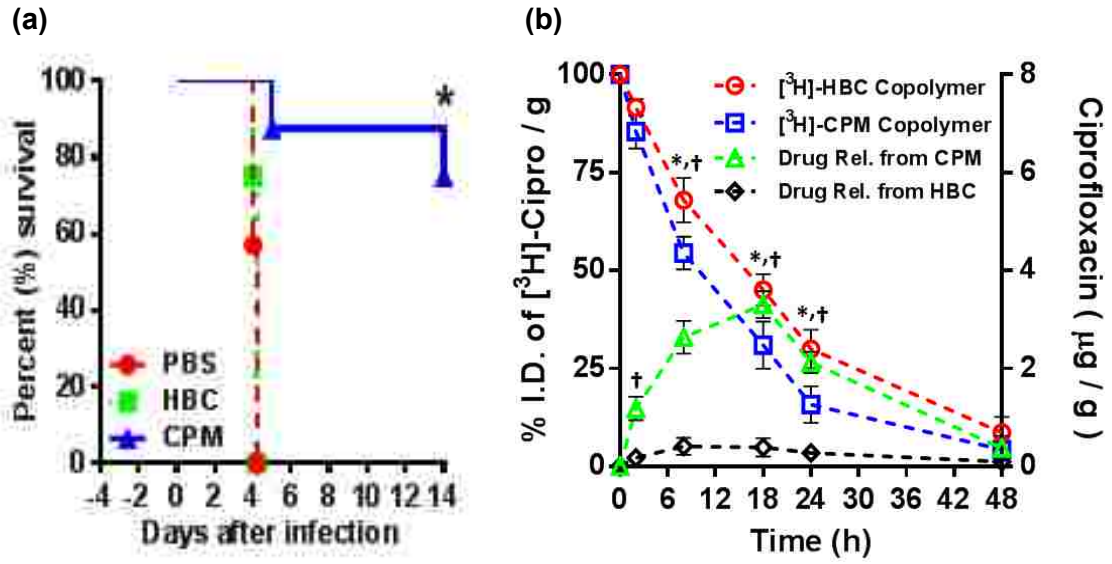

Figure 3.2. (a) *In vivo* antimicrobial efficacy of ciprofloxacin polymeric prodrugs using aerosolized, highly-virulent *Franciscella novicida*; (b) lung and blood pharmacokinetics and biodistribution properties of aerosolized poly(O950-co-HBC) and poly(O950-co-CPM). [^{3}H]-radiolabeled polymers were synthesized to track polymer biodistribution in mice, and the concentration of the liberated ciprofloxacin was quantified using LC-MS.

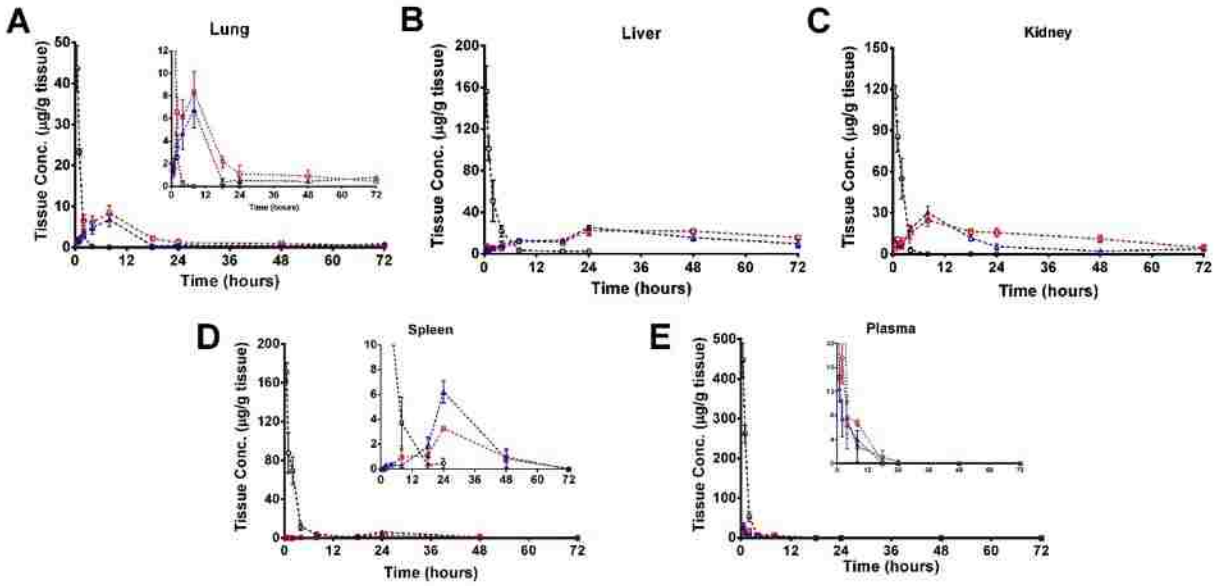

Figure 3.3. Pharmacokinetics of ciprofloxacin Poly(Man-*co*-Cipro) and controls, free ciprofloxacin and poly(Gal-co-Cipro), were administered via intratracheal aerosolization at a dose of 40mg kg^{-1} of ciprofloxacin in mice. Animals were euthanized at various time points to determine ciprofloxacin biodistribution and pharmacokinetics in the **(A)** lungs, **(B)** liver, **(C)** kidneys, **(D)** spleen, and **(E)** plasma. Data represent mean values ± s.d. (*n*=3).

Building upon those promising findings, this study attempts to incorporate an enzyme-cleavable dipeptide linkage to polymeric prodrugs for providing rapid, specific intracellular antibiotic delivery, while keeps prodrugs inactive during transportation to target cells. Peptide bonds are generally more resistant to hydrolysis in physiological condition than other chemistry linkers (e.g., disulfide, ester, hydrazone), but rapidly hydrolyze in the presence of specific enzymes[9,17]. Inspired by the lysosomal enzyme-cleavable dipeptide linker used by Seattle Genetics for antibody drug conjugates (ADCETRIS®), this study used a similar linker design in the drugamer prodrug system to provide rapid, specific intracellular drug delivery to AMs (**Figure 3.4**). This Val-Cit dipeptide linker is known to be extracellularly stable (half-life in monkeys: 9.6 days), but is cleaved upon internalization by proteases such as cathepsin B (half-life: 60 min)[17,18]. A self-immolative spacer, p-aminobenzyl (PAB), is necessary to situate the drug from the enzymatic cleavage site[19]. Combining this dipeptide-PAB linker with our drugamer technology, we have

developed a polymerizable, protease-labile ciprofloxacin drugamer to copolymerize with mannose monomer through RAFT polymerization. Ciprofloxacin weight percent in the copolymer was optimized for PBS solubility and *in vivo* safety by adjusting the monomer feed ratio, and quantified by H-NMR and HPLC. Ciprofloxacin release kinetics of the copolymer was evaluated in the presence/absence of cathepsin B under various conditions. Systemic stability of the copolymer was evaluated in human serum. A control ciprofloxacin monomer without the dipeptide linker (with self-immolative PAB spacer only, **Figure 3.4**) was synthesized to prepare a control polymer, PAB drugamer, for comparison.

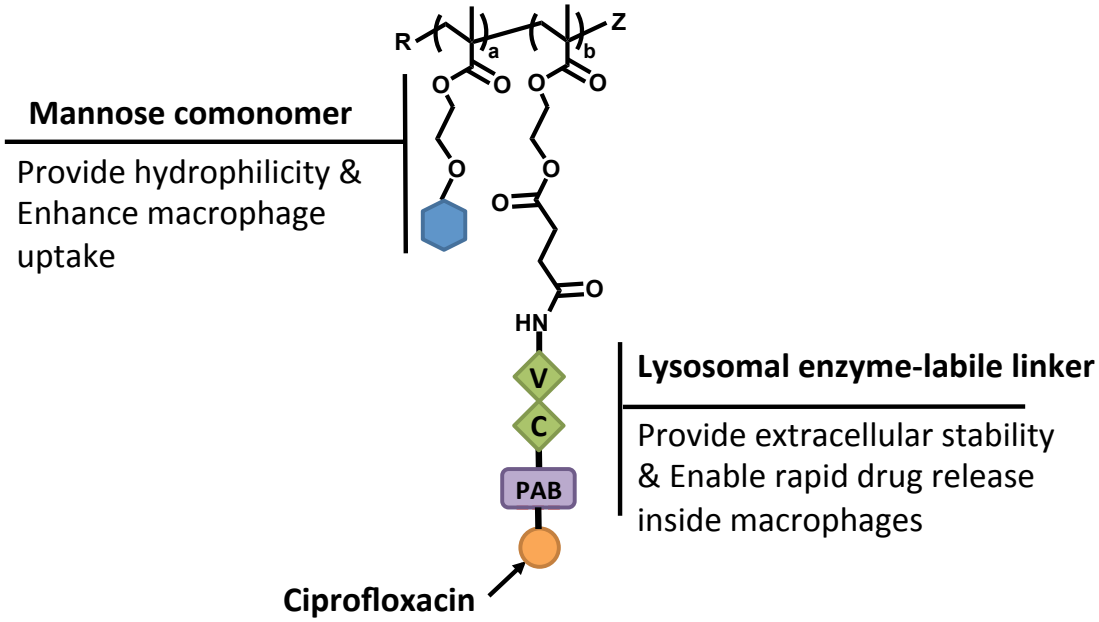

Figure 3.4. A schematic illustration of the enzyme-labile copolymer drug delivery system. This copolymer integrates a Valine-Citrulline dipeptide linker with a self-immolative spacer (p-aminobenzylalcohol, PAB) to provide serum stability and facile intracellular drug release. Mannose comonomer enhances the hydrophilicity of the copolymer construct, and facilitates the cellular internalization by target cells.

3.2 EXPERIMENTAL METHOD

3.2.1 *Materials*

Materials were supplied by Sigma Aldrich (St Louis, MO) unless otherwise specified. 4-Cyano-4-(ethylsulfanylthiocarbonyl) sulfanylpentanoic acid (ECT) was synthesized as described previously[20]. Spectra/Por regenerated cellulose dialysis membranes were purchased from Spectrum Laboratories (Houston, TX). Sephadex G-25 prepacked PD10 columns were obtained from GE Healthcare Life Sciences.

3.2.2 *Cipro monomer synthesis [Thanks Dr. Selvi Srinivasan for develoingd synthesis procedures and synthesizing monomers]*

Ciprofloxacin methacrylate monomer containing cathepsin B sensitive Val-Cit-PAB linker was synthesized as shown in **Figure 3.5**. Fmoc-Valine (**1**) was first activated by DCC/NHS coupling to form NHS ester (**2**) which was subsequently reacted with L-Citruline to give Fmoc-Val-Cit (**3**). This dipeptide was connected to p-aminobenzyl alcohol (PABA) via an amide bond using EEDQ mediated coupling to provide Fmoc-Val-Cit-PAB (**4**). Deprotection of **4** with diethylamine in NMP afforded free base **5** which was further reacted with a methacrylate activated ester SMA-NHS (**7**), obtained by activation of SMA (**6**) with DCC/NHS, to give SMA-Val-Cit-PAB monomer (**8**). HBTU assisted coupling reaction between Boc-ciprofloxacin and monomer **8** in the presence of DMAP as the catalyst and diisopropylethylamine as the base provided Boc-protected monomer (**10**) in moderate yield. Final deprotection in 20 % TFA/dichloromethane gave the desired cathepsin B sensitive monomer (**11**) in good yield.

A control monomer not sensitive to cathepsin B was synthesized as shown in **Figure 3.6**. Monomer SMA-PAB (**12**) was obtained by reacting SMA with PABA using EEDQ. Compound **12** was conjugated with Boc-ciprofloxacin via HBTU coupling, and the resulting monomer (**13**) was subsequently subjected to Boc deprotection in 20 % TFA/dichloromethane to obtain the control monomer (**14**). This Boc-deprotection step caused some Cipro cleavage, resulting in a mixture of monomer **14** and free Cipro 3:1 ratio.

Thin layer chromatography was used to monitor the progress of the reaction in each step. Synthesized monomers **8**, **10**, **12** and **13** were purified by flash column chromatography while compounds **3**, **4**, **5**, **11** and **14** were purified by precipitation techniques. Purity of all the materials was validated by ^{1}H NMR spectroscopy (Bruker Avance spectrometers 300 MHz or 500 MHz) and electron spray ionization mass spectrometry (ESI-MS, Bruker Esquire ion trap mass spectrometer integrated with liquid chromatography).

Figure 3.5. Synthesis of polymerizable Cipro methacrylate monomer with Val-Cit-PAB linker (11)

Figure 3.6. Synthesis of control Cipro methacrylate monomer without Val-Cit dipeptide linker (14).

3.2.3 *Synthesis of mannose monomer*

The synthetic strategy for α-D-mannose pentaacetate was synthesized as per a reported method[21]. D-mannose pentaacetate (5 g, 12.8 mmol) and 2-(hydroxyethyl)methacrylate (HEMA, 8.34 g, 64 mmol, 7.77 mL, 5 equivalent) were dissolved in anhydrous dichloromethane (30 mL) in a round bottom flask containing molecular sieves (10 g, 4 Å, activated at 180-200 °C under high vaccum for 5 hrs). The mixture was stirred at 0°C and a solution of boron trifluoride diethyl etherate ($BF_3.Et_2O$, 18.18g, 16.16 ml, 0.13 mol, 10 equivalent) in anhydrous dichloromethane (5 ml) was added dropwise with stirring. After addition of the $BF_3.Et_2O$, the solution was stirred for a further 10 minutes at 0°C, and then stirred at room temperature with a balloon containing air. After 2 hrs, butylhydroxytoulene (BHT, 15 mg) was added to the reaction mixture, and the solution was stirred for another 37 hrs at room temperature. After molecular sieve was filtered out, the resulting mixture was diluted with dichloromethane (150 mL) and poured into ice-water. The organic solution was washed with sat. NaHCO3 (aq.) (150 mL x 2), ice-water (150 mL x 2), and 10% sodium chloride (aq.) (150 mL x 1), dried over anhydrous $MgSO_4$, and evaporated under reduced pressure to give a yellow oil (5.82 g). The reaction was about 60% complete based on NMR. The obtained crude product was used for the next step without purification.

Crude 2-(2',3',4',6'-tetra-O-acetyl-α-D-mannosyloxy)ethyl methacrylate (5.82 g, about 60% product) was dissolved in damp methanol (46 ml). To the solution was added K_2CO_3 (2.3 g, 16.56 mmol). After 30 min, the solution was neutralized by filtering into a flask containing DOWEX 50WX4-200 (Sigma-Aldrich) cation exchange resin, and the mixture was stirred for 10 min. After removal of the resin, the solvent was evaporated under reduced pressure to give a yellow oil. The resulting oil was then purified by a 12.5 % MeOH in $CHCl_3$ using column chromatography to yield a colorless oil, which was further precipitated in 50% ether-hexane and dried under vacuum. Yield 0.55 g (1.83 mmol, 23.8%). MS (ESI, m/z): calc. for $C_{12}H_{20}NaO_8$ (M): 315.1, found: 315.3 $[M + Na]^+$ and 606.7 $[2M + Na]^+$. (**Figure 3.14 & 3.15**)

3.2.4 *RAFT polymerization*

Synthesis of poly(Man-*co*-VCPABCip)

Polymerizations of ManEMA and SMAVCPABCip to obtain poly(Man-*co*-VCPABCip) were conducted in dimethyl sulfoxide (DMSO) under a nitrogen atmosphere for 4 h using ECT (4-cyano-4-[(ethylsulfanylthiocarbonyl)sulfanyl]pentanoic acid) as the chain-transfer agent (CTA) and 4,4'-Azobis(4-cyanovaleric acid) (ABCVA) as the radical initiator (**Figure 3.7**). The reaction temperature was 70 °C. The initial monomer/CTA ratio ($[M]_0/[CTA]_0$) was 50:1; CTA/initiator ratio ($[CTA]_0/[I]_0$) was 10:1. The resultant polymers were isolated by precipitation in diethyl ether to remove DMSO. The precipitated polymers were then redissolved in distilled water (dH_2O) and purified by dialysis against dH_2O using dialysis tubing (MWCO = 3500 Da) to remove unreacted monomer and solvent. Purified polymers were then lyophilized and stored in -20°C freezer for further use.

Synthesis of poly(ManEMA-co-SMAPABCip)

Radical addition-fragmentation chain transfer (RAFT) polymerization of Man and control cipro monomer (SMAPABCip) was conducted in dimethyl sulfoxide (DMSO) under a nitrogen atmosphere at 70°C for 24 h using CTP as the chain-transfer agent (CTA) and 4,4'-Azobis(4-cyanovaleric acid) (ABCVA) as the radical initiator (**Figure 3.8**). The initial monomer/CTA and CTA/initiator ratios for the polymerization were $[M]_0/[CTA]_0$ = 20:1 and $[CTA]_0/[I]_0$ = 10:1, respectively. The resultant polymers were isolated by precipitation in diethyl ether to remove

DMSO. The precipitated polymers were then redissolved in dH_2O and purified by dialysis against dH_2O using dialysis tubing (MWCO = 3500 Da) to remove unreacted monomer and solvent. Purified polymers were then lyophilized and stored in -20°C freezer for further use.

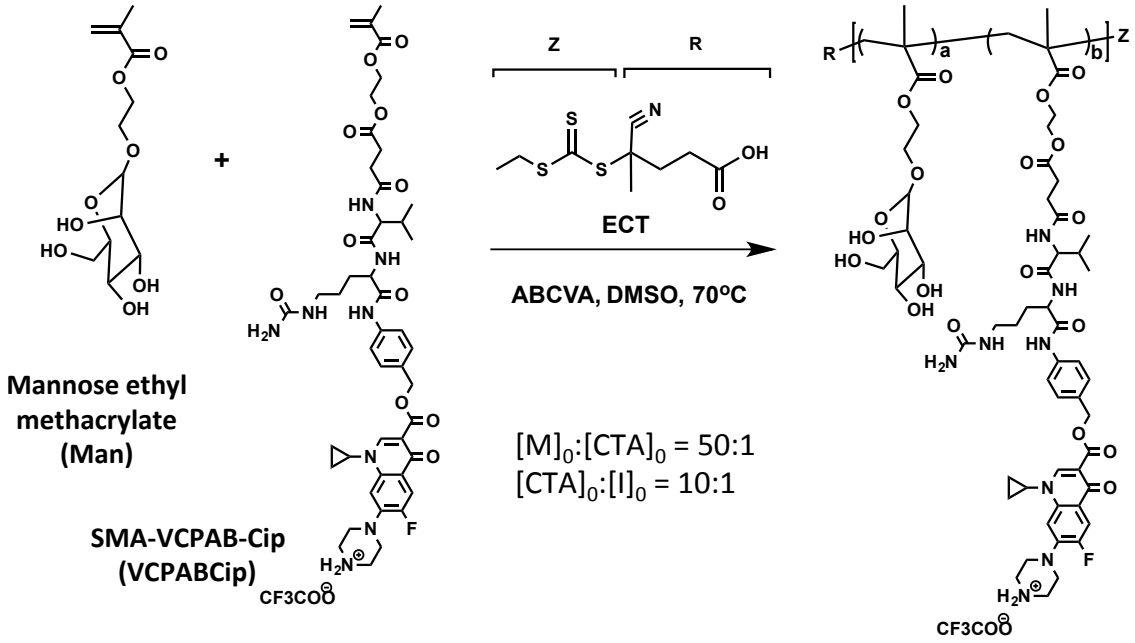

Figure 3.7. RAFT polymerization of poly(Man-co-VCPABCip) using ECT as the chain transfer agent and ABCVA as the initiator. ECT (4-cyano-4-[(ethylsulfanylthiocarbonyl)sulfanyl]pentanoic acid). ABCVA: 4,4'-Azobis(4-cyanovaleric acid).

3.2.5 *Polymer characterization*

^{1}H-NMR spectra were recorded on a Bruker AV 300 (Bruker Corporation, Billerica, MA) nuclear magnetic resonance (NMR) instrument in deuterated dimethyl sulfoxide (d-DMSO). The monomer composition and ciprofloxacin wt% was determined using 1H NMR with boc-protected ciprofloxacin as an internal standard. Ciprofloxacin wt% in polymers was also quantified using high performance liquid chromatography (HPLC). The molecular weight and molecular weight distribution (PDI) of the polymers were determined by size exclusion chromatography. To prepare materials for analysis, the purified polymer was dissolved at 5 mg/mL in running buffer (0.15 M sodium acetate buffered to pH 4.4 with acetic acid) for

analysis by SEC. Samples were then applied to an OHpak SB-804 HQ column (Shodex) in line with a miniDAWN TREOS light scattering detector (Wyatt) and a OptiLab rEX refractive index detector (Wyatt). Absolute molecular weight averages (Mw and Mn) was calculated using ASTRA software (Wyatt).

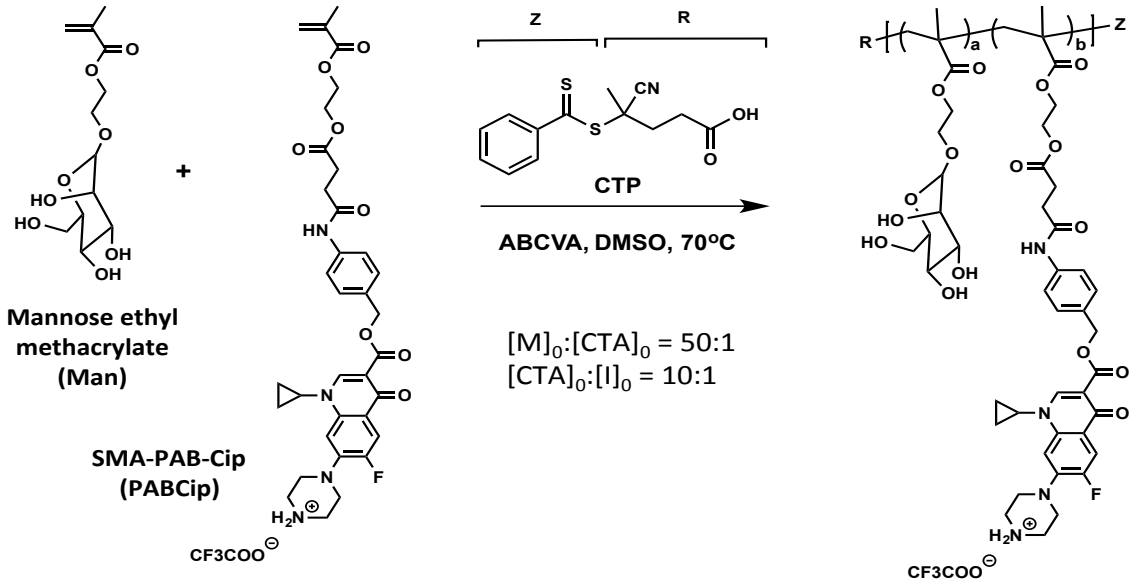

Figure 3.8. RAFT polymerization of poly(Man-co-PABCip) using CTP as the chain transfer agent and ABCVA as the initiator. CTP: 4-cyano-4-(phenylcarbonothioylthio)-pentanoic acid. ABCVA: 4,4'-Azobis(4-cyanovaleric acid).

3.2.6 *Cathepsin B-mediated ciprofloxacin release*

Enzymatic release rate of ciprofloxacin from monomers and polymers were conducted at conditions approximating the lyosomal medium as a model for intracellular drug release[19]. Human liver cathepsin B (Enzo Life Sciences) was activated for 15 minutes in a solution of 0.151 mg/mL cathepsin B, 30 mM DTT, and 15 mM EDTA at 37 °C. Monomer or polymer was then solubilized in reaction buffer (25 mM sodium acetate, 1 mM EDTA, pH 5, or phosphate buffered saline, 1 mM EDTA pH 7.4, 37 °C) and added to the enzyme solution for a final concentration of 2.1 μg/mL cathepsin B and 100 μM peptide/polymer. At various time points, enzymatic activity was halted by addition of a thioprotease inhibitor (E-64 (Thermo Scientific), 1 mg/mL, 10 μL). The amount of the released ciprofloxacin was quantified by LC-MS (C18 reversed-phase column, Agilent zorbax SB-C18, narrow bore RP 2.1 X 100 mm, 3.5 μM,

acetonitrile-water gradient 10-90%, at 0.2 mL/min, λ=276 nm). 100% cipro release was defined by incubating monomers/polymers in 0.1 N NaOH for 24 hours at room temperature to hydrolyze all ester bonds between PAB and cipro. Quantification of total ciprofloxacin in the monomers or polymer conjugates was measured by incubating monomers/polymers in 0.1 N NaOH for 24 h at room temperature, denoted by Peak(NaOH). Percent (%) drug released was subsequently quantified using the formula:

% Drug released = [peak(t_x)-peak(t_0)]/[peak(NaOH)],

where t_x and t_0 are the ciprofloxacin peaks resolved by the HPLC at time x and zero, respectively.

3.2.7 *Serum stability of polymers*

The stability of the ciprofloxacin monomers and polymers in the presence of serum proteases and esterases was evaluated by incubating the monomers and polymers in human serum and analyzing the released ciprofloxacin over time. Polymer [2.28 mg/mL for poly(Man-*co*-VCPABCip), 2.36 mg/mL for poly(Man-*co*-PABCip) in H_2O, in equivalent to 1 mM ciprofloxacin) was added to human serum to a final ciprofloxacin concentration of 100 μM and incubated at 37 °C. At various time points, samples were diluted with acetonitrile 5 times to precipitate serum proteins and halt the reaction. Precipitated solutions were centrifuged at 13,000 rpm for 4 min to separate supernatants. Supernatants were concentrated 4 times by speedvac and analyzed by LC-MS (C18 reversed-phase column, Agilent zorbax SB-C18, narrow bore RP 2.1 X 100 mm, 3.5 μM, acetonitrile-water gradient 5-90%, at 0.2 mL/min, λ=276 nm). The method to calculate % release was described earlier in section 3.2.5.

3.2.8 *In vivo lung safety study*

C57Bl/6 mice (Female, 6-8 weeks old, n=5) were anesthetized with 5% isoflurane for 5 min before administration of 50 μL of PBS (negative control) or drugamer solution in PBS (0.2 μm filtered, equivalent to 20 mg/kg ciprofloxacin dose) via intratracheal aerosolization using a

MicroSprayer® Aerosolizer–Model IA-1C (Penn-Century. Wyndmoor Inc., PA, USA). Mice received one daily dose for three consecutive days and their body weight changes were monitored each day before dosing. Twenty-four h after the last dose, the mice were weighed and then euthanized by CO2 asphyxiation. Bronchoalveolar lavage (BAL) was conducted with 1 mL of PBS flush followed by three 0.8 mL flushes. Lungs were harvested and placed into 1 mL PBS on ice.

Lung tissue in 1 mL of PBS was subsequently mixed with 1 mL of PBS containing protease inhibitor cocktail (Pierce™ Protease Inhibitor, Thermo Fisher Scientific) before mechanical homogenization using a TissueRuptor (Qiagen, Valencia, CA, USA). Lung tissue homogenates (LTH) were then stored at 4°C for 30 min followed by centrifuge at 5000xg for 15 minutes to collect the supernatant for TNF-α quantification. BAL fluid was spun at 400 g for 15 min to pellet lavage cells. Cell-free BAL fluid was retained and stored at -80°C. BAL cells were resuspended into 0.5 mL RPMI 1640 supplemented with 10% FBS. BAL cells were mounted onto microscopy slides with a Cytospin centrifuge at 500 rpm for 5 min, and then stained with Hemacolor (EMD Millipore, Billerica, MA, USA) prior to cytology analysis. Stained slides were analyzed for macrophage to neutrophil ratio with a minimum of 200 cells per slide counted. TNF-α concentrations in the supernatant of LTH and cell free BAL fluid were assayed using mouse TNF-α ELISA MAXTM Standard kit (BioLegend, San Diego, CA, USA) as per manufacturer's instructions.

3.3 RESULTS AND DISCUSSION

3.3.1 *Ciprofloxacin monomer synthesis and characterization [Thanks Dr. Selvi Srinivasan for developing synthesis procedures and synthesizing monomers]*

In the design of cathepsin B-responsive ciprofloxacin monomer, Val-Cit dipeptide linker was chosen, because it's serum stability and enzyme sensitivity have led to clinical success in the case of antibody-drug conjugates[17]. **Figure 3.5** presents the synthetic route and structure of cathepsin B sensitive ciprofloxacin methacrylate monomer, SMA-VCPAB-Cip. The structure of SMA-VCPAB-Cip was confirmed by ^{1}H-NMR with all characteristic peaks observed and ESI-

MS (**Figure 3.9 & 3.10**). This design was hypothesized to undergo enzymatic hydrolysis, and release PAB-Cip, which is unstable and can quickly releases free ciprofloxacin through spontaneous 1, 6-benzyl elimination based on the chemical point of view (**Figure 3.6**). [Note: detailed step-by-step synthesis and 1H-NMR spectrum are available in the supplementary information of chapter 4]

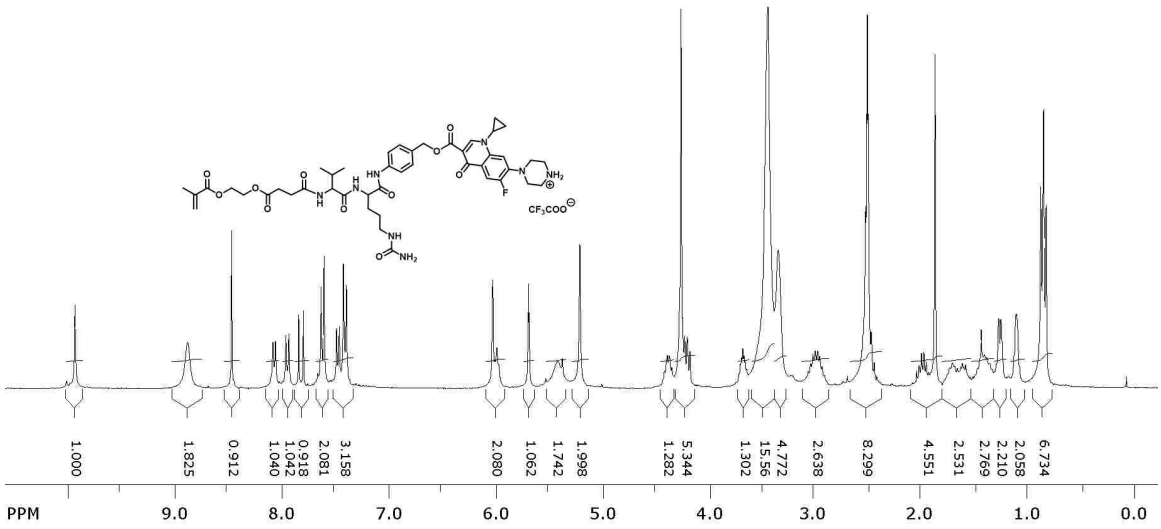

Figure 3.9. [1]H-NMR spectrum of cathepsin B sensitive Cipro monomer (SMA-VCPAB-Cip) **11**

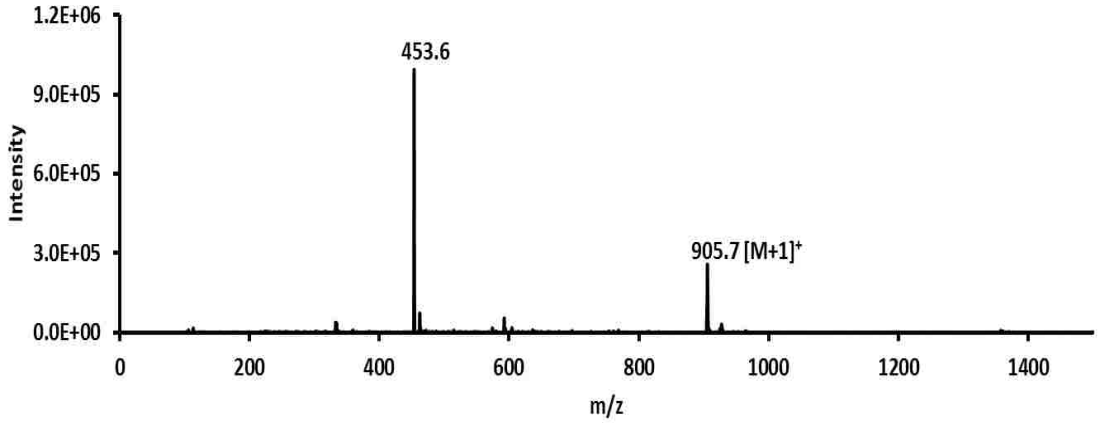

Figure 3.10. ESI-MS spectrum of cathepsin B sensitive Cipro monomer (SMA-VCPAB-Cip) **11**

Additionally, ciprofloxacin monomer lacking in Val-Cit dipeptide linker (SMA-PAB-Cip) was synthesized to serve as a control monomer (**Figure 3.6**). The successful preparation of SMA-PAB-Cip was also proved by both ^{1}H NMR and ESI-MS (**Figure 3.12 & 3.13**).

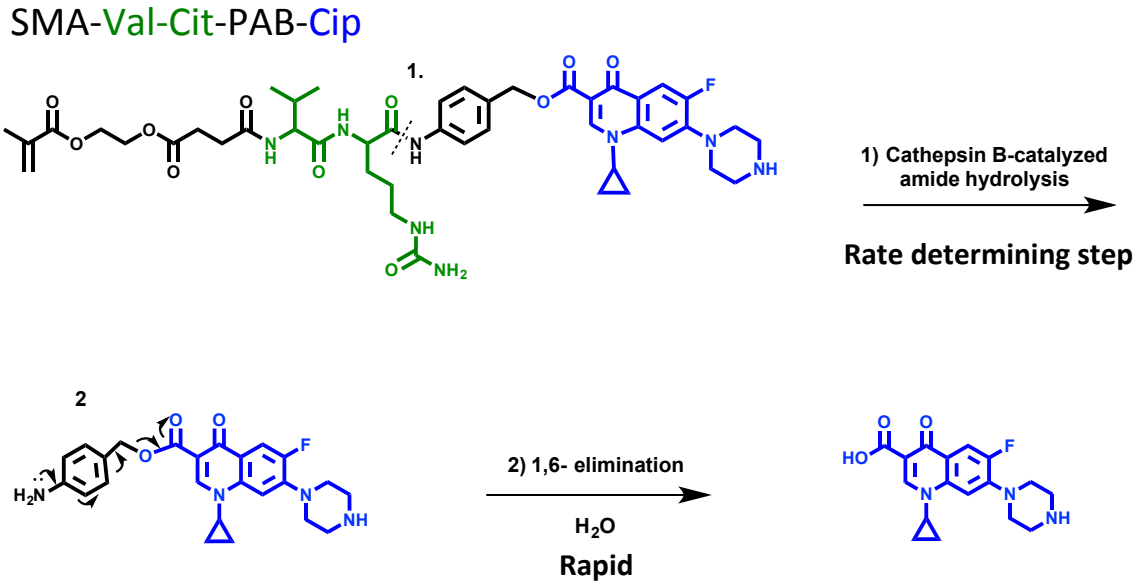

Figure 3.11. Proposed mechanism of ciprofloxacin release from cathepsin B sensitive Cipro monomer (SMA-VCPAB-Cip) by a two-step process: rate determining enzyme-catalyzed amide hydrolysis followed by fast 1, 6-elimination.

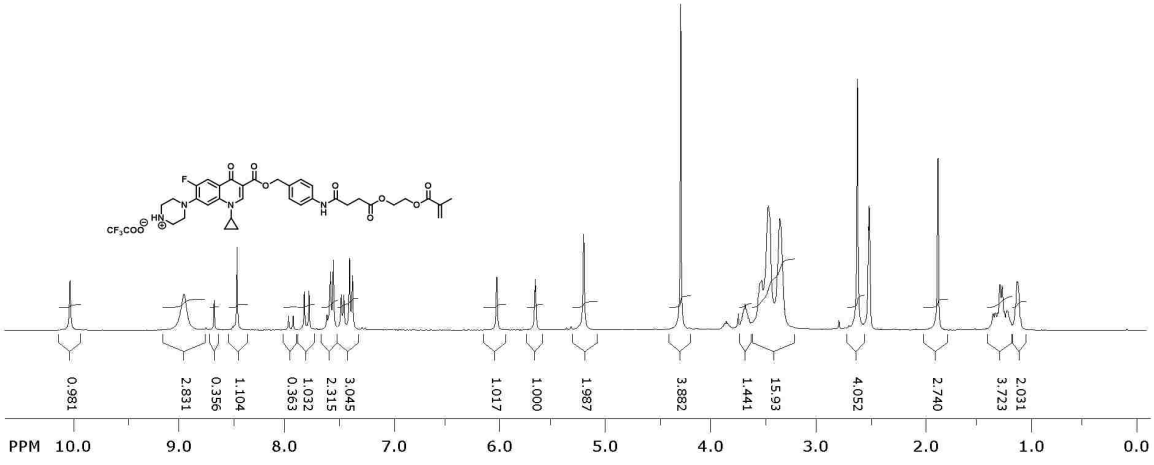

Figure 3.12. ^{1}H-NMR spectrum of control Cipro monomer **14**

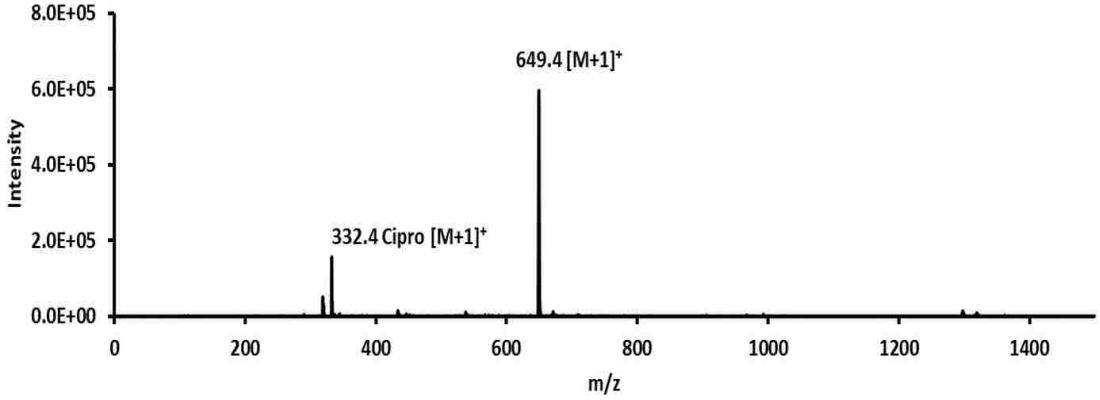

Figure 3.13. ESI-MS spectrum of control Cipro monomer **14**

3.3.2 *Mannose monomer synthesis and characterization*

Mannose was chosen as the targeting motif of the polymeric prodrug, because mannose receptor (CD206) has been shown to highly express on alveolar macrophages[22]. Mannose-functionalized methacrylate monomers was synthesized and purified using a flash column. The purified mannose monomer was confirmed by ^{1}H-NMR, and all the characteristic peaks corresponding to protons on the monomer were identified (**Figure 3.14**). The NMR spectrum helped to confirm the purity of the obtained mannose monomer, as impurities often leads to retardation or even inhibition in RAFT polymerization[23]. The successful preparation of the mannose monomer was also confirmed by ESI-MS (**Figure 3.15**).

3.3.3 *Cathepsin B-mediated ciprofloxacin release of ciprofloxacin monomer*

The bond linking ciprofloxacin to PAB on SMA-VCPAB-Cip is an ester rather than carbamate in Seattle Genetics' antibody-drug conjugates and most literature that used PAB as a self-immolative spacer[17,19]. To investigate if the linkage difference would hinder 1, 6-β elimination, SMA-VCPAB-Cip was incubated with or without cathepsin B (CatB) in acetate buffer (pH 5.0)

at 37°C; samples were taken at pre-determined time points and analyzed the released products using LC-MS.

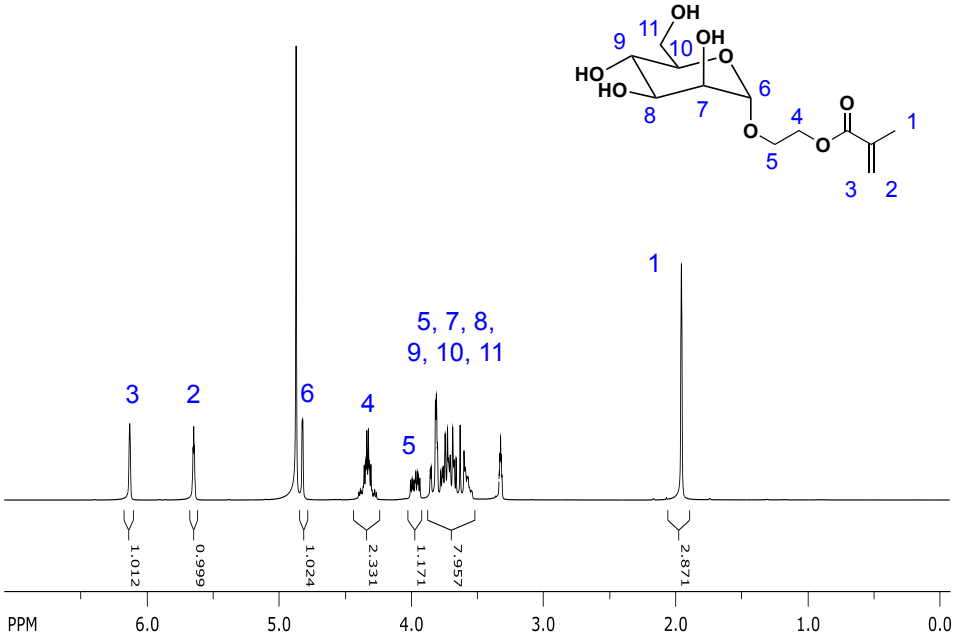

Figure 3.14. 1H NMR spectrum of 2-O-(α-D-mannosyl)hydroxyethyl methacrylate. Proton NMR scans were conducted in MeOD-d4 at 300 MHz. Successful preparation of the indicated chemical structure was confirmed by the appearance of resonances associated with 2-hydroxyethyl methacrylate (1-5) and mannose (6-11).

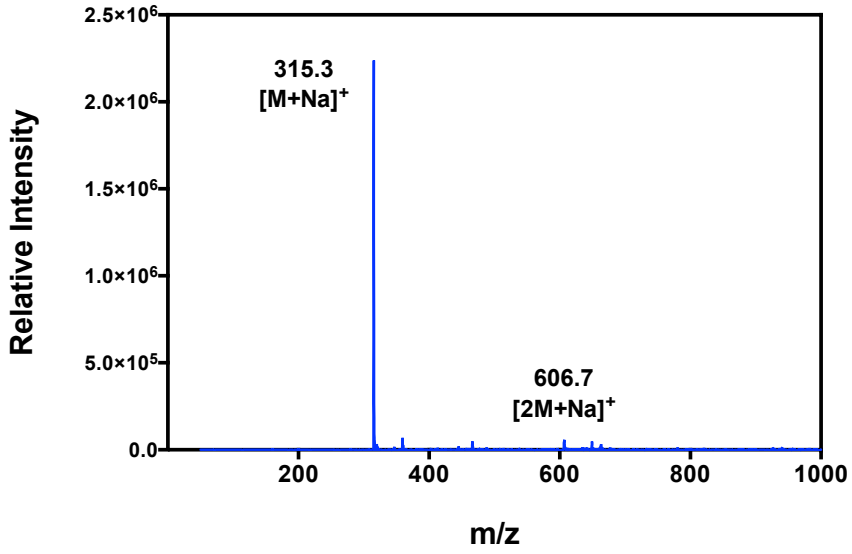

Figure 3.15. ESI-MS spectrum of 2-O-(α-D-mannosyl)hydroxyethyl methacrylate.

After 24 h incubation with CatB, only single peak with m/z 332.2 was observed in the HPLC profile (**Figure 3.16a**), which corresponding to the theoretical m/z value of ciprofloxacin (MW: 331.3 g, m/z 332.1). In contrast, no ciprofloxacin release from SMA-VCPAB-Cip was detectable over 24 h in the absence of CatB (**Figure 3.16b**). These observations suggest that CatB-induced proteolytic cleavage of Val-Cit dipeptide triggers the 1, 6-elimination to liberate active ciprofloxacin. In other words, without 1, 6- β elimination, PAB-Cip would be the expected product in this experiment setting (pH 5.0, 24 h), as non-enzymatic ester hydrolysis is relatively slow[13].

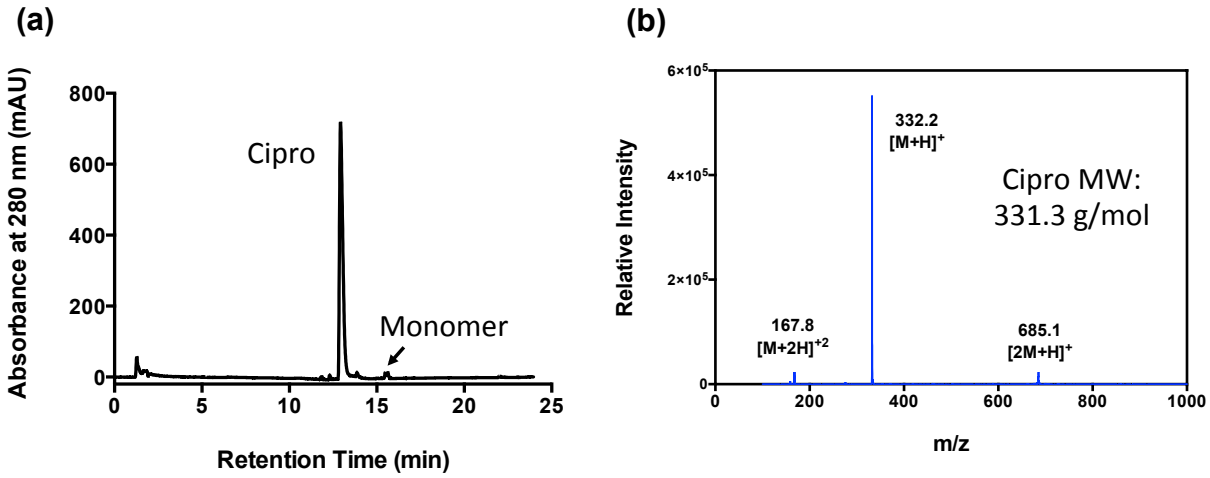

Figure 3.16. ESI-MS spectrum of 2-O-(α-D-mannosyl)hydroxyethyl methacrylate. LC-MS results confirming the occurrence of 1, 6-elimination following the cathepsin B-catalyzed hydrolysis of SMA-VCPAB-Cip monomer. SMA-VCPAB-Cip monomer was treated with cathepsin B for 24 h at pH 5.0. (a) HPLC trace showing a dominant peak and (b) the mass spectrum of the dominant peak, which corresponding well to the molecular weight of free ciprofloxacin (cipro).

The enzyme-dependent ciprofloxacin release of SMA-VCPAB-Cip was rapid, with 85% release achieved in 2 h (**Figure 3.17**). However, SMA-PAB-Cip, ciprofloxacin monomer without Val-Cit dipeptide linker, shows less than 5% ciprofloxacin release after 24 h incubation in pH 5.0 acetate buffer, regardless of the presence of CatB. This result suggests that SMA-PAB-Ciprofloxacin is not enzyme-responsive, and could be an adequate control for studying the efficacy of the enzyme-responsive Val-Cit-PAB linker in polymeric antibiotic prodrug.

Therefore, the ciprofloxacin monomers with and without dipeptide linker were used for the following polymer synthesis.

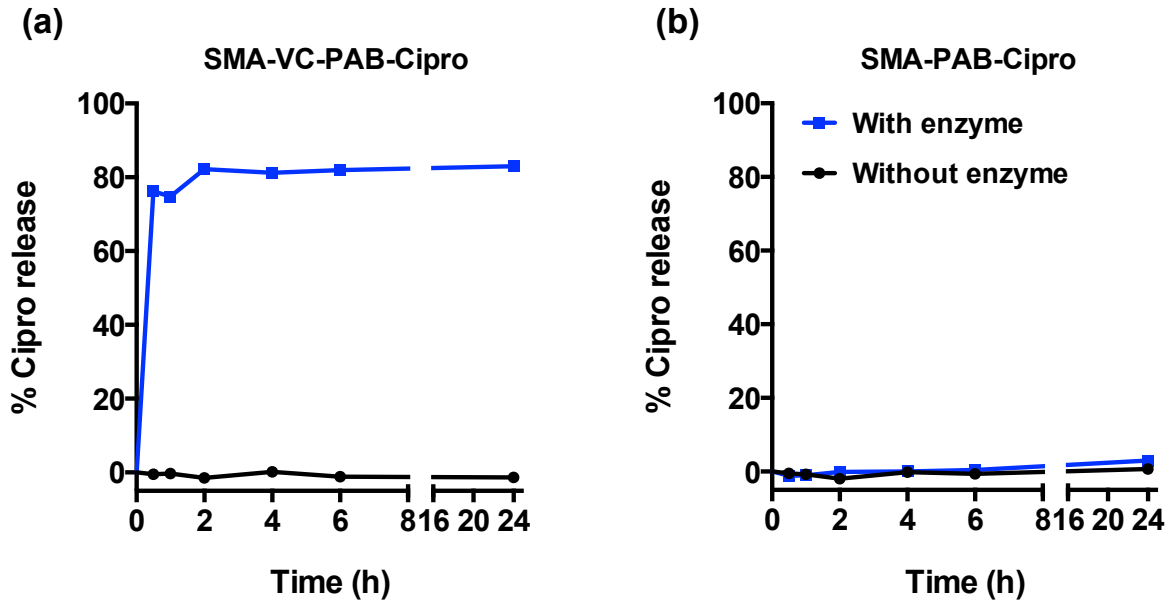

Figure 3.17. Cathepsin B-mediated ciprofloxacin (cipro) release kinetics of (a) cathepsin B-responsive cipro monomer, SMA-VC-PAB-Cip and (b) control monomer, SMA-VC-PAB-Cip. Ciprofloxacin release kinetics of both monomers was conducted in the presence or absence of cathepsin B in acetate buffer at pH 5.0. At various time points, the reactions were stopped by addition of E-64 thioprotease inhibitor, and the liberated ciprofloxacin was quantified using LC-MS.

3.3.4 *Synthesis of poly(Man-co-VCPABCip)*

RAFT polymer synthesis was exploited to copolymerize mannose monomer (Man) with SMA-VCPAB-Cip to make the CatB cleavable copolymer, poly(Man-*co*-VCPABCip). RAFT polymerization is chosen, because it is compatible with wide range of functional monomers/solvents, and provides unprecedented control over polymer molecular weight, size distribution, composition and architecture[24,25]. The first condition used for polymer synthesis was using CTP and ABCVA as RAFT agent and initiator, respectively. However, low monomer conversion (<5%) was observed based on 1H-NMR. We then investigated the monomer

conversion in different synthesis conditions (RAFT agent, initiator, solvent) with trial monomers. Finally the synthesis condition using ECT as RAFT agent (**Figure 3.7**) provides good monomer conversion (~ 75%) and was therefore selected for synthesizing poly(Man-*co*-VCPABCip). It is reasoned that the initial low conversion might due to the CTA degradation during polymerization, as the color change (pink to orange) in the reaction mixture was observed, indicating the degradation of the dithiobenzoate group on CTP[26]. Also trithiocarbonate RAFT agents, like ECT, are known to greater hydrolytic stability and are also known give less retardation than dithioester RAFT agent (e.g., CTP)[24,27].

Ciprofloxacin wt% in poly(Man-*co*-VCPABCip) was subsequently optimized by varying the monomer feed ratio between mannose monomer and SMA-VCPAB-Cip (**Table 3.1**), without compromising the monomer conversion and water solubility. We found that monomer conversion decreased when the feed of SMA-VCPAB-Cip increased, which might be attributed to the lower monomer reactivity of SMA-VCPAB-Cip compared to mannose monomer. The optimized feed ratio is 2.6 to 1 of mannose monomer to SMA-VCPAB-Cip, which gives 72.37% monomer conversion and 14.47% ciprofloxacin wt%, based on ^{1}H-NMR with boc-protected ciprofloxacin as an internal standard (**Figure 3.18**). **Table 3.2** shows the characterization of poly(Man-*co*-VCPABCip).

3.3.5 *Synthesis of poly(Man-co-PABCip)*

Figure 3.8 demonstrates RAFT polymerization of the non-enzyme responsive control copolymer, poly(Man-*co*-PABCip). The monomer feed ratio, monomer compositions, and ciprofloxacin wt% are given in **Table 3.2**. The monomer feed ratio was tuned to provide similar ciprofloxacin wt% as poly(Man-*co*-VCPABCip). ^{1}H-NMR spectroscopy was employed to confirm copolymer composition by analysis of resonances associated with each of the comonomers (**Figure 3.19**), and boc-protected ciprofloxacin was used as an internal standard.

Table 3.1. Optimization of ciprofloxacin (cipro) wt% and monomer conversion of poly(Man-co-VCPABCip) by varying the molar feed ratio of mannose ethyl methacrylate (Man) and SMA-VCPAB-Cip monomer

Monomer feed ratio (molar)		Monomer conversion[a] (%)	Cipro wt%[b]	Water solubility[c]
Man	SMA-VCPAB-Cip			
3	1	69.61	11.24	✓
2.6	1	72.37	14.47	✓
2	1	52.43	14.52	✓
1	1	37.39	17.40	✗

[a] Monomer conversion was evaluated via H-NMR in d-DMSO.
[b] Cipro wt% were determined by treating polymers with 0.1 N NaOH and quantifying free cipro using HPLC.
[c] Solubility of polymers were determined by dissolving 5 mg/mL of copolymer in deionized water at 25°C.

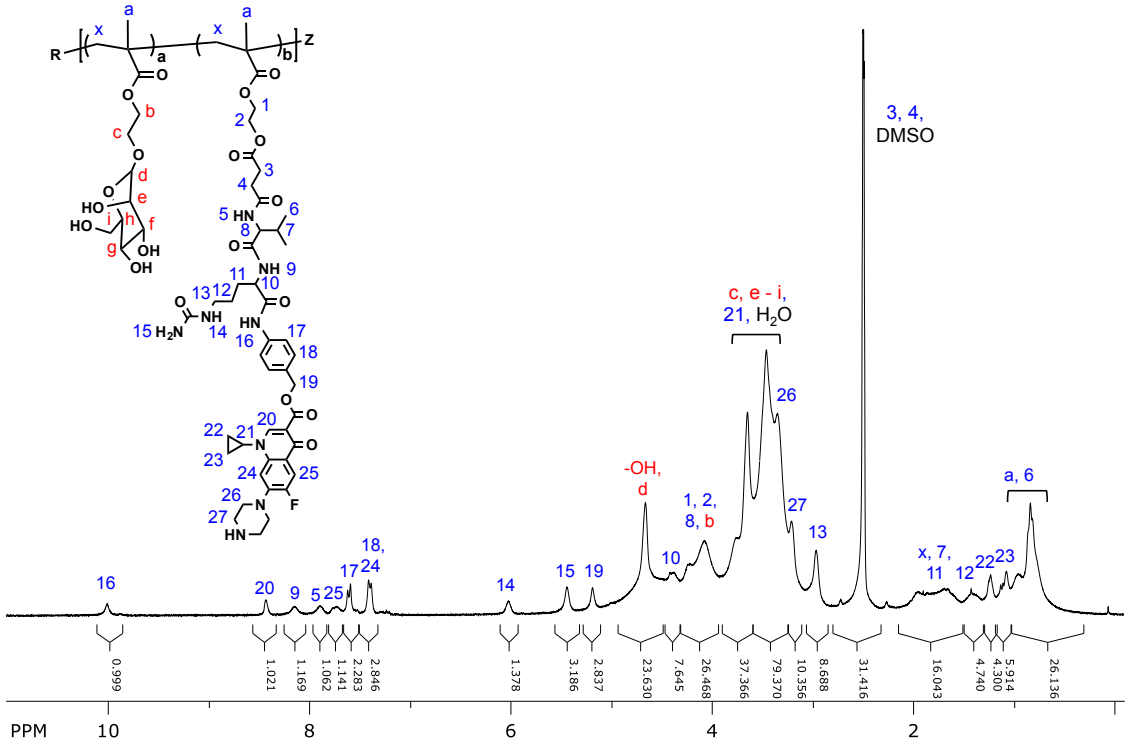

Figure 3.18. Representative ^{1}H-NMR spectra of poly(Man-*co*-VCPABCip) in DMSO-d6 with assignment of the characteristic resonances associated with the comonomers.

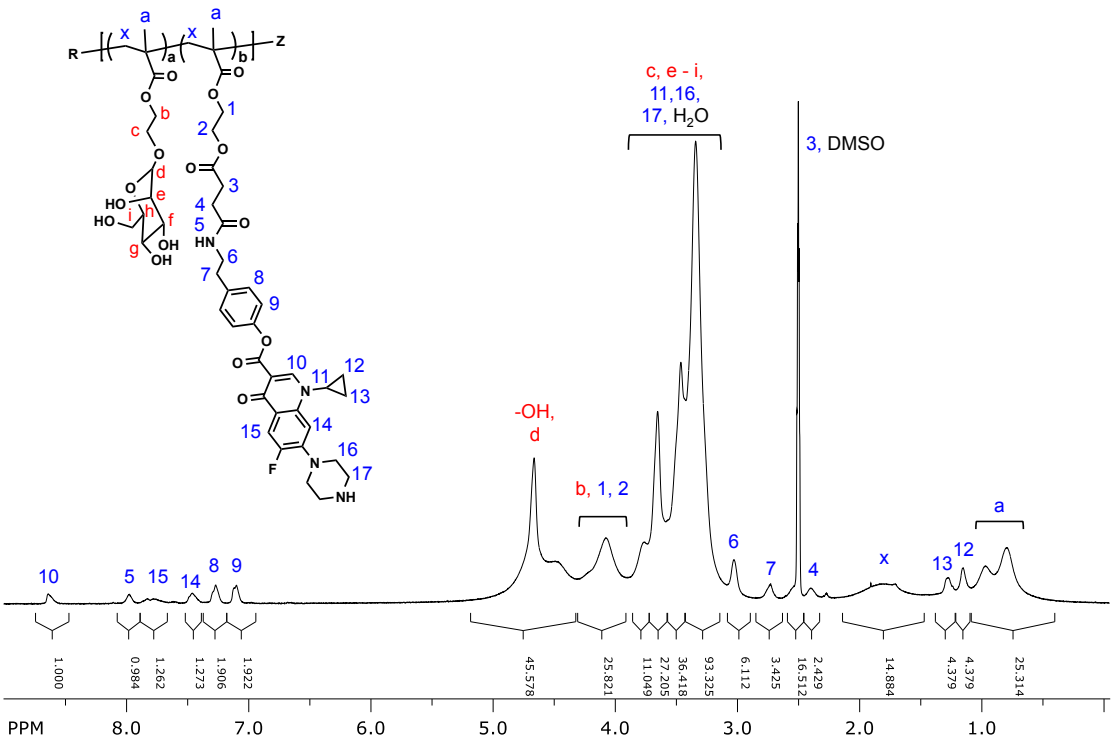

Figure 3.19. Representative ^{1}H-NMR spectra of poly(Man-*co*-PABCip) in DMSO-d6 with assignment of the characteristic resonances associated with the comonomers.

3.3.6 *Cathepsin B-mediated ciprofloxacin release from polymeric prodrugs*

Figure 3.20 shows the CatB-mediated ciprofloxacin release kinetics of poly(Man-*co*-VCPABCip) in lysosomal pH condition (pH 5.0). In contrast to the non-CatB responsive control polymer, incubation with CatB resulted in the rapid ciprofloxacin release from poly(Man-*co*-VCPABCip) with half-life about 30 min and 92% drug release was achieved in 4 h, suggesting the Val-Cit dipeptide linker attaching to the polymer backbone was still accessible to CatB. Additionally, ciprofloxacin release from poly(Man-*co*-VCPABCip) with time was cleared shown in the HPLC traces (**Figure 3.20b**). To investigate if the CatB-dependent release is specific in lysosomes, the same study was conducted at pH 7.4 to mimic extracellular condition. As shown in **Figure 3.21**, CatB-catalyzed ciprofloxacin release at pH 7.4 was slower than pH 5.0 (12.3% vs. 92.5% release in 4 h), which was consistent with previous finding showing that CatB exhibits limited stability and irreversible activity loss at neutral pH[28,29].

Table 3.2. Summary of monomer feed ratio, composition, and molecular weights for copolymers of VCPAB-Cip (enzyme responsive) and PAB-Cip (non-enzyme responsive) with mannose methacrylate (Man).

	Man (feed)	Man[a] (exp)	VCPAB-Cip (feed)	VCPAB-Cip[a] (exp)	PAB-Cip (feed)	PAB-Cip[a] (exp)	Mn[b] (kDa)	Cipro[a] wt% (^{1}H-NMR)	Cipro[c] wt% (HPLC)
1	72	82	28	18	-	-	28.4	14.8	14.5
2	80	85	-	-	20	15	26.6	14.3	14.0

[a]As determined by ^{1}H NMR in DMSO-d6 using boc-protected ciprofloxacin (cipro) as an internal standard. [b]As determined by size exclusion chromatography using OHpak SB-804 HQ column (Shodex) in line with a miniDAWN TREOS light scattering detector (Wyatt) and a OptiLab rEX refractive index detector (Wyatt). Absolute molecular weight averages (Mw and Mn) was calculated using ASTRA software (Wyatt). Sodium acetate buffer (0.15 M, pH 4.4) was used as the mobile phase at a flow rate of 1 mL min−1. [c]As determined by high performance liquid chromatography (HPLC). Polymers were treated with 0.1 N NaOH to hydrolyze all esters bonds and thus release cipro.

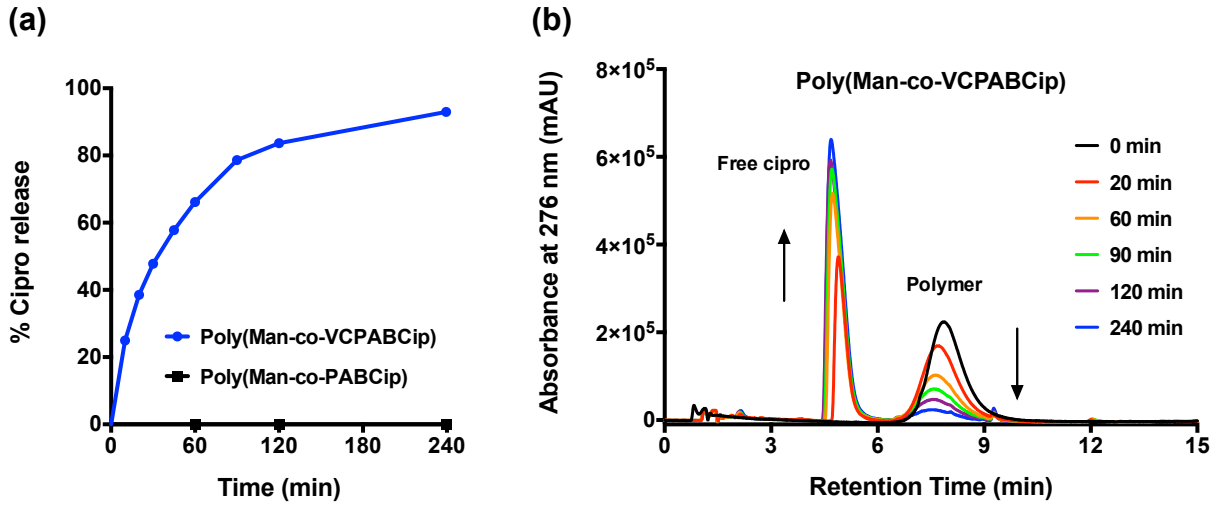

Figure 3.20. (a) Cathepsin B-mediated ciprofloxacin (cipro) release kinetics of polymers. (b) HPLC traces showing the free ciprofloxacin release and polymer hydrolysis with time. Ciprofloxacin release kinetics of both monomers was conducted in the presence or absence of cathepsin B in acetate buffer at pH 5.0. At various time points, the reactions were stopped by addition of E-64 thioprotease inhibitor, and the liberated ciprofloxacin was quantified using LC-MS.

To prove that the poly(Man-*co*-VCPABCip) is active mainly upon the cleavage by CatB, and not by spontaneous hydrolysis or cleavage by other enzymes, ciprofloxacin release kinetics was further monitored in pH 5.0 acetate buffer (without CatB) and human serum (**Figure 3.21**). Ciprofloxacin release was not detectable over the course of 4 h, indicating that poly(Man-*co*-VCPABCip) might not be susceptible to spontaneous hydrolysis, as well as serum esterases and proteases.

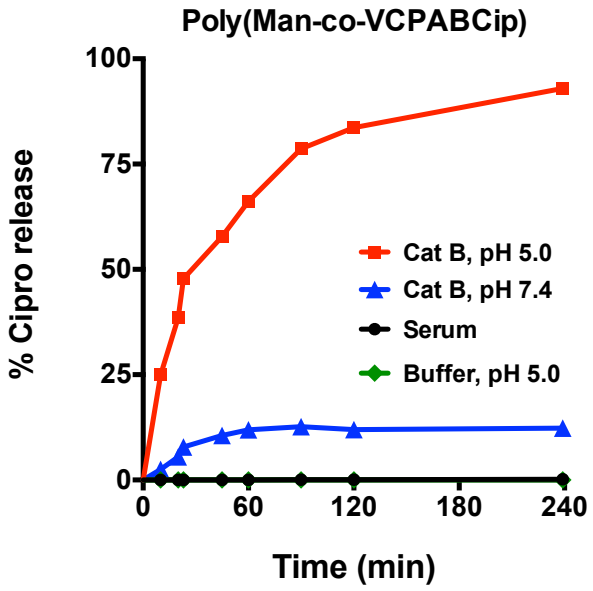

Figure 3.21. Ciprofloxacin (cipro) release kinetics of enzyme-sensitive polymer, poly(Man-co-VCPABCip), at various condition. The liberated cipro was quantified using LC-MS.

3.3.7 *Polymeric prodrug stability in human serum*

Although poly(Man-*co*-VCPABCip) was designed for aerosol administration to deliver higher local concentration at the site of drug action, its serum stability was evaluated for two reasons. First, esterases and albumin (one of the major proteins in epithelial lung fluids) are founds in human lungs[30,31]. Their esterase activities might potentially lead to premature drug release outside AMs, as the linkage between the self-immolative spacer PAB and ciprofloxacin is an ester bond. The other reason is that after lung administration, poly(Man-*co*-VCPABCip) might be cleared from lungs into systemic circulation, where the nonspecific drug release might result

in systemic side effects associated with the drug[32,33]. Therefore, it's critical to evaluate the polymer stability in human serum, which is rich in human serum albumin and esterases[34,35].

The stability of the both polymers in human serum was investigated over the course of 14 days at 37 °C and ciprofloxacin release as a function of time was quantified using LC-MS (**Figure 3.22a**). Consistent with previous findings with the Val-Cit dipeptide derivatives of doxorubicin and MMAE, poly(Man-*co*-VCPABCip) was quite stable in human serum, as no ciprofloxacin release was found in the first 2 days, and the projected half-life was 21 d. Conversely, control polymer lacking in the Val-Cit dipeptide linker was much less stable ($t_{1/2}$ 8 d). This finding may contribute to the steric hindrance associated with the dipeptide linker blocks the access of serum enzymes, as the rate of enzymatic ester hydrolysis has been observed to be a function of steric crowding[9,36].

To examine the hypothesis, both polymers were incubated with human butyrylchloinesterase (BChE), a human serum esterase involved in detoxification and metabolism of ester-containing drugs[37,38]. In the presence of BChE (5 μg/mL, mimic concentration in human serum), poly(Man-*co*-PABCip) shows 64.5% ciprofloxacin release in 4 d, whereas less than 6.3% ciprofloxacin release was detected from poly(Man-*co*-VCPABCip) (**Figure 3.22b**). This observation was accordance with the serum stability results, and also confirmed that the bulky nature of dipeptide linker blocks the ester bond accessibility to serum esterases. Together with the CatB-mediated ciprofloxacin release data, those results suggest that poly(Man-*co*-VCPABCip) undergoes rapid hydrolysis in the presence of the target enzyme, CatB, but has limited sensitivity to esterases.

3.3.8 *Optimization of drugamer compositions for in vivo lung safety*

Following the encouraging results from the *in vitro* release and serum stability tudies, the antibacterial efficacy of VC and PAB drugamers were tested using a mouse challenge model of pulmonary tularemia infections. Mice were treated with either VC/PAB drugamer (equivalent to 40 m/kg ciprofloxacin, 5% dextrose in water) or free ciprofloxacin solution (40 m/kg ciprofloxacin, 5% dextrose in water); one daily dose for three days. Notably, drugmaers were dissolved in 5% dextrose in water instead of PBS due to the limited PBS solubility of VC

drugamer. Infection of aerosolized *F. novicida* was conducted in a whole body chamber 2 h after the first dose. Acute toxicity was observed immediately after dosing the drugamer solution-either VC or PAB durgamer (**Figure 3.23**). The toxicity could be attributed to tow reasons. First, the trifluroacetate salt (counter ion of ciprofloxacin) remained on the drugamers is known to be toxic[39]. The other possible reason is the limited PBS solubility of VC drugamer. Such that VC drugamer may crash out in the tracheal and alveolar surface and therefore irritates the lungs.

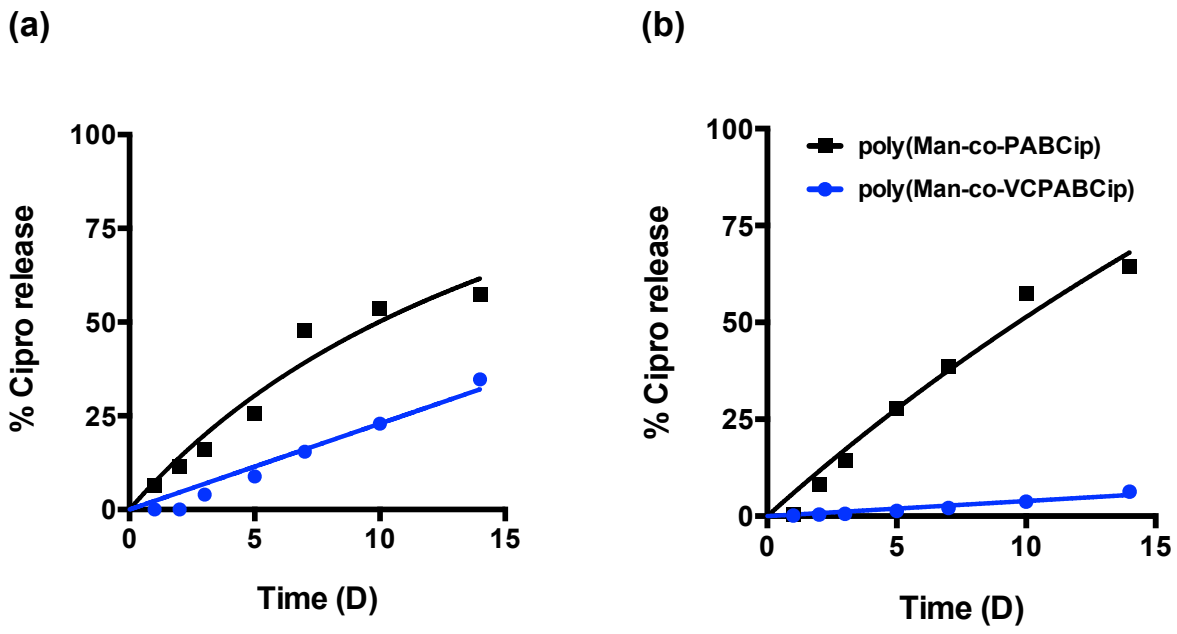

Figure 3.22. Ciprofloxacin (cipro) release kinetics of polymers in (a) human serum (90%) and (b) human butyrylcholinesterase (5 μg/mL, mimic concentration in human serum).

We first focused on troubleshooting the toxicity of VC drugamer. VC drugamer TFA salt was exchanged by biocompatible phosphate salt using a three-day dialysis against phosphate buffer (0.1 M K_2PO_4, pH 7.2-7.4) followed by three-day H_2O dialysis at 4°C. The complete removal of TFA salt wad confirmed using F^{19}-NMR. To evaluate if the purified VC drugamer is compatible to the lungs, VC drugamer solution or PBS was intratracheally delivered using microsprayer. Lung safety was evaluated based on the body weight change, neutrophil percentage, and TNF-α in lung tissues and bronchoalveolar space (**Figure 3.24**). At 40 mg/kg, one dose of VC drugamer led to14% body weight loss in two out of three mice and the averaged neutrophil percentage was

about 30%, which was significantly higher then that of PBS treated mice (ca. 3%). In an attempt to avoid the acute toxicity, we further reduced the dose to 20 mg/kg ciprofloxacin. All of the three mice lost 8-15% body weight after two doses of VC drugamer. This observation indicates that removing TFA salt did improve the toxicity level (no mice died immediately after dosing), but VC drugamer still induced severe toxicity as shown in the body weight change and neutrophil percentage.

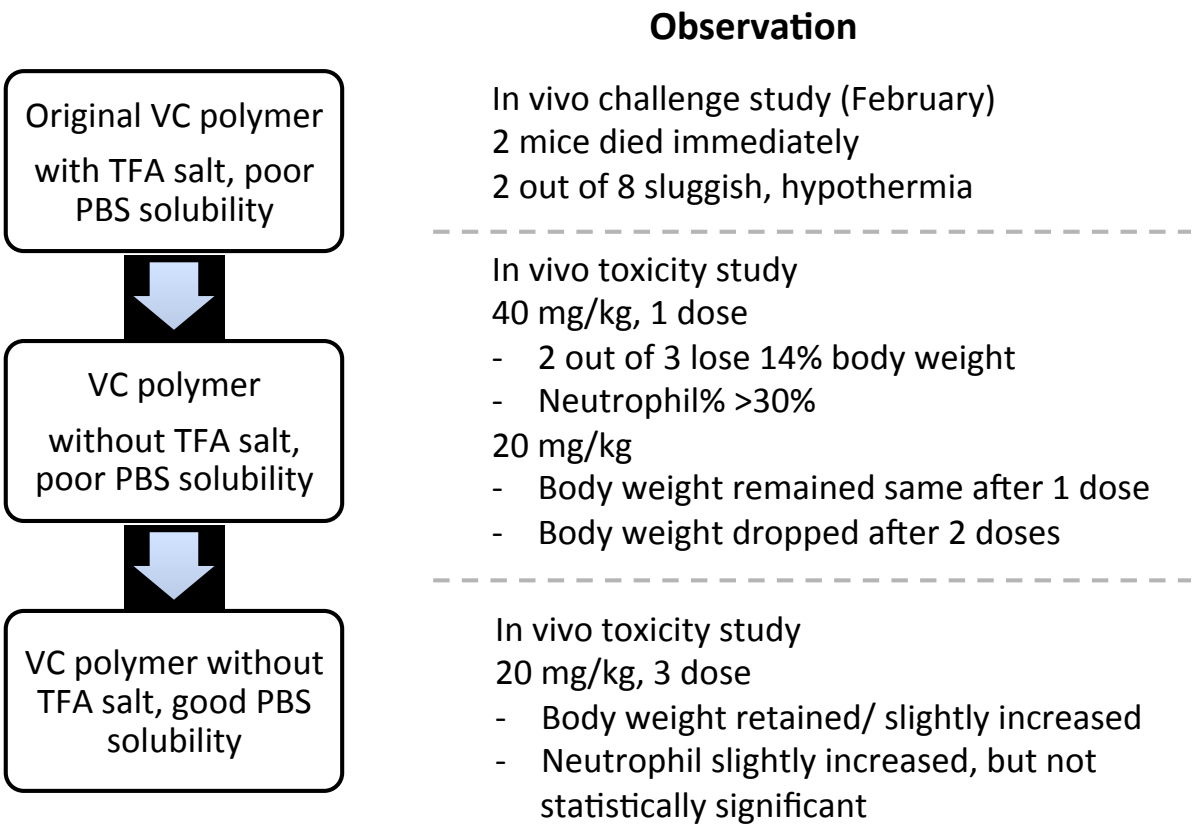

Figure 3.23. Process flow for trouble-shooting *in vivo* toxicity problem of poly(Man-*co*-VCPABCip) (VC drugamer).

To further reduce the toxicity associated with VC drugamer, we addressed the second possible reason for toxicity- limited PBS solubility. Knowing the limited solubility issue was resulting from the hydrophobicity of Val-Cit dipeptide linker and ciprofloxacin, we further reduced the feed ratio of mannose monomer to VC monomer (**Table 3.3**). We found that reducing mannose monomer to VC monomer ratio from 2.5:1 to 5.5:1 afforded enough PBS solubility (c.a. 80 mg/ml) to achieve 20 mg/kg dose for *in vivo* study, although the ciprofloxacin wt% was

decreased to around 10%. This VC drugamer with sufficient PBS solubility but without TFA salt was then tested in the *in vivo* safety study with 20 mg/kg ciprofloxacin dose–one daily dose for three consecutive days. This VC durgamer shows similar biocompatibility as PBS and the CTM drugamer, which was previously proven to be biocompatible at 40 mg/kg ciprofloxacin dose by our group (**Figure 3.25**). As PAB drugamer was still toxic even after TFA removal and with sufficient PBS solubility, we decided to use CTM drugamer as the non-enzyme cleavable control to replace PAB drugamer for the following PK and challenge studies shown in the next chapter.

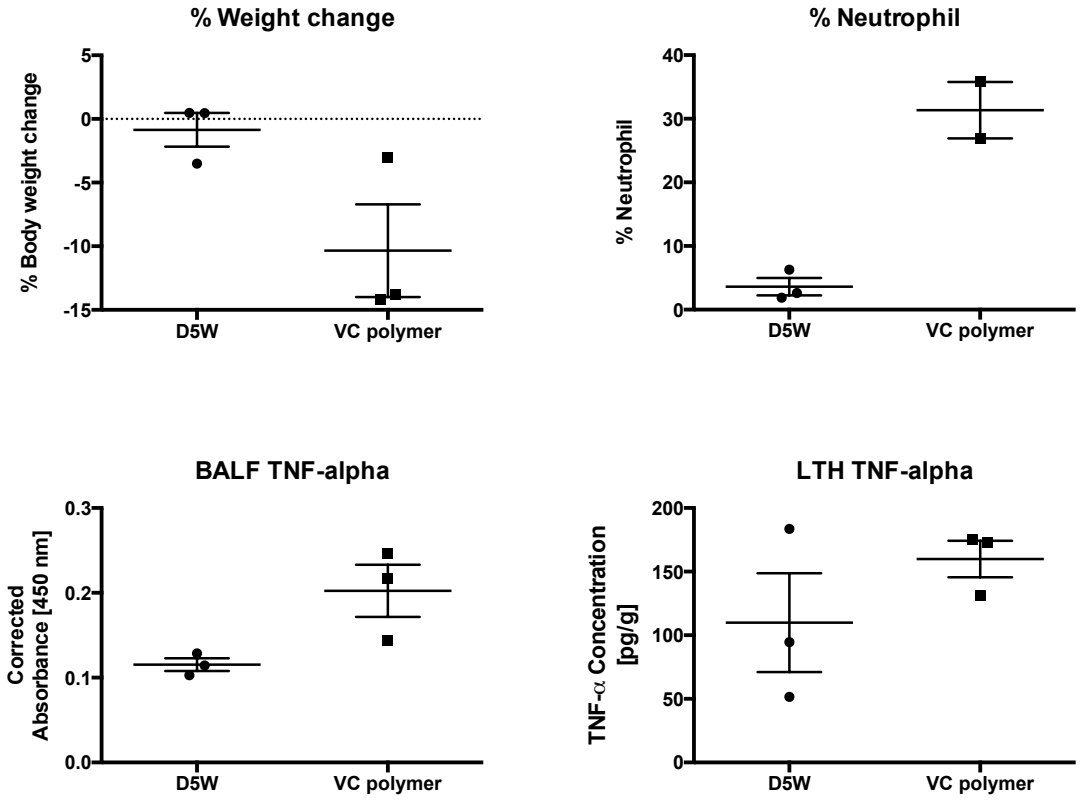

Figure 3.24. *In vivo* lung safety study of VC drugamer (no TFA salt but with poor PBS solubility). Mice were intratracheally delivered VC drugamer solution at 40 mg/kg ciprofloxacin dose (one dose). Notably, VC drugamer tested here was dissolved in 5% dextrose in water, due to the limited solubility in PBS. Data were present as mean ± SEM (n=3).

Table 3.3. Optimization of polymeric ciprofloxacin prodrug with Val-Cit dipeptide linker. Molar ratio of mannose monomer and VC monomer was adjusted to afford the polymer with sufficient PBS solubility for *in vivo* dosing.

Feed molar ratio		Monomer conversion[a] (%)	Ciprofloxacin wt%[b]	Solubility in PBS[c]
Mannose	VC			
5.5	1	78	9.70	✓
3	1	72	11.24	✗
2.5	1	70	14.47	✗
2	1	52	14.52	✗
1	1	37	17.40	✗

[a]Total monomer conversions were determined using ^{1}H NMR spectroscopy (DMSO-d_6) by comparing the area of the vinyl proton resonances before and after polymerization.
[b]As determined by ^{1}H NMR in DMSO-d_6 using a Boc-protected ciprofloxacin as an internal standard.
[c]Solubility of polymers were determined by dissolving polymers in PBS to achieve 20 mg/kg ciprofloxacin dose for *in vivo* studies (ca. 80 mg/mL polymer).

3.4 Conclusion

Herein a polymerizable ciprofloxacin prodrug monomer with enzyme-cleavable dipeptide linker was developed and copolymerized with mannose methacrylate *via* RAFT polymerization. The resulting drugamer, VC drugamer, provides a rapid, enzyme-dependent drug release in the

presence of cathepsin B. In addition, VC drugamer was more stable in human serum and more resistant to serum esterases, compared with the non-enzyme sensitive control drugamer (without the dipeptide linker). Although the VC drugamer was initially found to be toxic due to the remaining trifluoroacetate salt and poor PBS solubility, the biocompatibility of VC drugamer was established after phosphate salt exchange and optimization of VC drugamer composition to resolve the TFA salt and solubility issues. This biocompatible VC drugamer was further characterized using *in vitro* and *in vivo* assays in the following chapter.

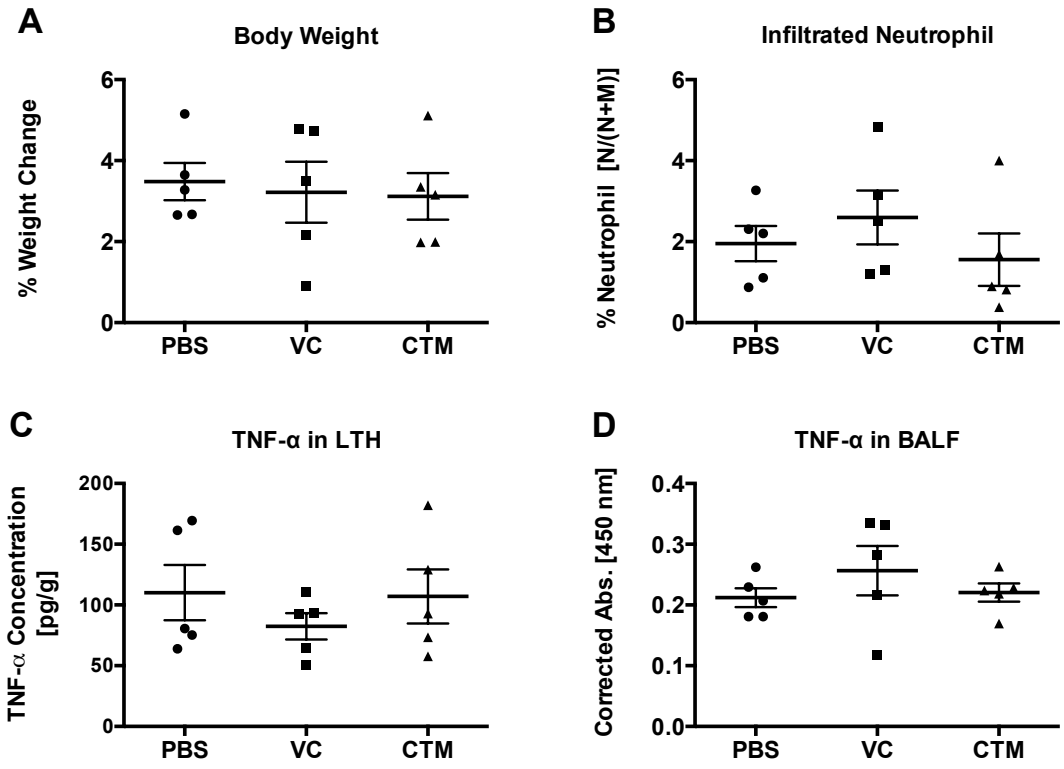

Figure 3.25. *In vivo* lung safety study of optimized VC drugamer. Drugamer solutions in PBS were intratracheally administered to uninfected C57BL/6 mice once a day for 3 days, and tissues were harvested 24 h after the last dose. (A) Animal weights measured prior to treatment and 24 h after the final dose were ratioed to calculate percent weight change per mouse. (B) Percentage of neutrophils was determined by differential cell counting of cells from bronchoalveolar lavage fluid (BALF). Values were calculated as [neutrophil / (neutrophil + macrophage)] × 100%. Tumor necrosis factor alpha (TNF-α) levels were measured by ELISA from (C) lung tissue homogenates (LTH) and (D) BALF. No statistically significant differences were observed using one-way ANOVA and a Dunnett *post hoc* test between polymer treated and PBS treated mice

(n = 5). Error bars represent means ± SEM. VC: polymer with protease-cleavable peptide linker. CTM: polymer with hydrolytic ester linker.

3.5 ACKNOWLEDGEMENTS

This work was funded by the Defense Threat Reduction Agency (Grant #HDTRA1-13-1-0047). F.Y.S. is an international student research fellow of the Howard Hughes Medical Institute.

3.6 REFERENCE

1. Schiffelers, R., Storm, G. & Bakker-Woudenberg, I. Liposome-encapsulated aminoglycosides in pre-clinical and clinical studies. *Journal of Antimicrobial Chemotherapy* **48,** 333–344 (2001).
2. Toti, U. S. *et al.* Targeted delivery of antibiotics to intracellular chlamydial infections using PLGA nanoparticles. *Biomaterials* **32,** 6606–6613
3. Drulis-Kawa, Z. & Dorotkiewicz-Jach, A. Liposomes as delivery systems for antibiotics. *Int J Pharm* **387,** 187–198
4. Ramana, L. N., Sharma, S., Sethuraman, S., Ranga, U. & Krishnan, U. M. Investigation on the stability of saquinavir loaded liposomes: Implication on stealth, release characteristics and cytotoxicity. *Int J Pharm* **431,** 120–129
5. Liu, J. *et al.* Liposomes for systematic delivery of vancomycin hydrochloride to decrease nephrotoxicity: Characterization and evaluation. *Asian Journal of Pharmaceutical Sciences* **10,** 212–222
6. Cipolla, D., Froehlich, J. & Gonda, I. Emerging Opportunities for Inhaled Antibiotic Therapy. *J Antimicro* (2015).
7. Cipolla, D., Blanchard, J. & Gonda, I. Development of Liposomal Ciprofloxacin to Treat Lung Infections. *Pharmaceutics* **8,** (2016).
8. Cipolla, D. *et al.* Modifying the release properties of liposomes toward personalized medicine. *J Pharm Sci* **103,** 1851–1862 (2014).
9. D'Souza, A. J. M. & Topp, E. M. Release from polymeric prodrugs: linkages and their degradation. *J Pharm Sci* **93,** 1962–1979 (2004).
10. Kaminskas, L. M., McLeod, V. M., Porter, C. J. H. & Boyd, B. J. Association of Chemotherapeutic Drugs with Dendrimer Nanocarriers: An Assessment of the Merits of Covalent Conjugation Compared to Noncovalent Encapsulation. *Mol. Pharmaceutics* **9,** 355–373 (2012).

11. Wei, H., Zhuo, R.-X. & Zhang, X.-Z. Design and development of polymeric micelles with cleavable links for intracellular drug delivery. *Topical Issue on Biorelevant Polymers* **38,** 503–535 (2013).
12. Gac-Breton, S., Coudane, J., Boustta, M. & Vert, M. Norfloxacin-poly(L-lysine citramide imide) conjugates and structure-dependence of the drug release. *J Drug Target* **12,** 297–307 (2004).
13. Das, D. *et al.* RAFT polymerization of ciprofloxacin prodrug monomers for the controlled intracellular delivery of antibiotics. *Polym. Chem.* **7,** 826–837 (2016).
14. Stebbins, N. D., Ouimet, M. A. & Uhrich, K. E. Antibiotic-containing polymers for localized, sustained drug delivery. *Adv. Drug Deliv. Rev.* **78 IS ,** 77–87 (2014).
15. Seligman, A. M. & Nachlas, M. M. THE COLORIMETRIC DETERMINATION OF LIPASE AND ESTERASE IN HUMAN SERUM 1. *J Clin Invest* **29,** 31–36
16. Leng, H. M. J. & Syce, J. A. Characterization of Pulmonary Alveolar Esterases of the Primate Cercopithecus pygerythrus. *Pharm Res* **14,** 203–207 (1997).
17. Doronina, S. O. *et al.* Development of potent monoclonal antibody auristatin conjugates for cancer therapy. *Nat Biotech* **21,** 778–784 (2003).
18. Ducry, L. & Stump, B. Antibody-drug conjugates: linking cytotoxic payloads to monoclonal antibodies. *Bioconjug Chem* **21,** 5–13 (2010).
19. Dubowchik, G. M. *et al.* Cathepsin B-Labile Dipeptide Linkers for Lysosomal Release of Doxorubicin from Internalizing Immunoconjugates: Model Studies of Enzymatic Drug Release and Antigen-Specific In Vitro Anticancer Activity. *Bioconjug Chem* **13,** 855–869 (2002).
20. Convertine, A. J., Benoit, D. S. W., Duvall, C. L., Hoffman, A. S. & Stayton, P. S. Development of a novel endosomolytic diblock copolymer for siRNA delivery. *J Control Release* **133,** 221–229 (2009).
21. Beignet, J., Tiernan, J., Woo, C. H., Kariuki, B. M. & Cox, L. R. Stereoselective synthesis of allyl-C-mannosyl compounds: use of a temporary silicon connection in intramolecular allylation strategies with allylsilanes. *J. Org. Chem.* **69,** 6341–6356 (2004).
22. Ezekowitz, R. A. B. *et al.* Uptake of Pneumocystis carinii mediated by the macrophage mannose receptor. *Nature* **351,** 155–158 (1991).
23. Moad, G., Rizzardo, E. & Thang, S. H. Living Radical Polymerization by the RAFT Process - A Third Update. *Australian Journal of Chemistry* **65,** 985–1076 (2012).
24. Moad, G., Chong, Y. K., Postma, A., Rizzardo, E. & Thang, S. H. Advances in RAFT polymerization: the synthesis of polymers with defined end-groups. *Polymer* **46,** 8458–8468 (2005).
25. Moad, G., Rizzardo, E. & Thang, S. H. Radical addition–fragmentation chemistry in polymer synthesis. *Polymer* **49,** 1079–1131
26. Gregory, A. & Stenzel, M. H. Complex polymer architectures via RAFT polymerization: From fundamental process to extending the scope using click chemistry and nature's building blocks. *Topical Issue on Biorelevant Polymers* **37,** 38–105

27. Rizzardo, E., Moad, G. & Thang, S. H. in *Handbook of RAFT Polymerization* 189–234 (Wiley-VCH Verlag GmbH & Co. KGaA, 2008). doi:10.1002/9783527622757.ch6
28. Jordans, S. *et al.* Monitoring compartment-specific substrate cleavage by cathepsins B, K, L, and S at physiological pH and redox conditions. *BMC Biochem* **10,** 23 (2009).
29. Turk, V. *et al.* Cysteine cathepsins: from structure, function and regulation to new frontiers. *Biochim. Biophys. Acta* **1824,** 68–88 (2012).
30. Bredberg, A. *et al.* Exhaled endogenous particles contain lung proteins. *Clin. Chem.* **58,** 431–440 (2012).
31. Olsson, B. *et al.* in *Controlled Pulmonary Drug Delivery* (eds. Smyth, H. D. C. & Hickey, A. J.) 21–50 (Springer New York, 2011). doi:10.1007/978-1-4419-9745-6_2
32. Patmore, L., Fraser, S., Mair, D. & Templeton, A. Effects of sparfloxacin, grepafloxacin, moxifloxacin, and ciprofloxacin on cardiac action potential duration. *Eur J Pharmacol* **406,** 449–452 (2000).
33. Tattevin, P., Messiaen, T., Pras, V., Ronco, P. & Biour, M. Confusion and general seizures following ciprofloxacin administration. *Nephrol Dial Transplant* **13,** 2712–2713 (1998).
34. Tsujita, T., Nagai, K. & Okuda, H. Purification and properties of human serum esterase. *Biochimica et Biophysica Acta (BBA) - Enzymology* **570,** 88–95
35. Anderson, N. L. & Anderson, N. G. The Human Plasma Proteome: History, Character, and Diagnostic Prospects. *Molecular & Cellular Proteomics* **1,** 845–867 (2002).
36. Greenwald, R. B. *et al.* Drug Delivery Systems Based on Trimethyl Lock Lactonization: Poly(ethylene glycol) Prodrugs of Amino-Containing Compounds. *J. Med. Chem.* **43,** 475–487 (2000).
37. Huang, Y.-J. *et al.* Recombinant human butyrylcholinesterase from milk of transgenic animals to protect against organophosphate poisoning. *Proceedings of the National Academy of Sciences* **104,** 13603–13608 (2007).
38. Lockridge, O. Review of human butyrylcholinesterase structure, function, genetic variants, history of use in the clinic, and potential therapeutic uses. *Pharmacol Ther* **148,** 34–46 (2015).
39. Pini, A. *et al.* Efficacy and toxicity of the antimicrobial peptide M33 produced with different counter-ions. *Amino Acids* **43,** 467–473 (2012).

Chapter 4. Macrophage-targeted drugamers with enzyme-cleavable linkers deliver high intracellular drug dosing and sustained drug pharmacokinetics against alveolar pulmonary infections

Abstract

Intracellular bacterial infections localized to the lung alveolar macrophage (AM) remain one of the most challenging settings for antimicrobial therapy. Current systemic antibiotic treatment fails to deliver sustained doses to intracellular bacterial reservoirs, which necessitates prolonged treatment regimens. Herein, we demonstrate a new intracellular enzyme-cleavable polymeric prodrug with tailored ciprofloxacin release profiles in the lungs and AM. The targeted polymeric prodrug, termed "drugamers", incorporates (1) hydrophilic mannose residues to solubilize the antibiotic cargo and to target and enhance AM uptake and intracellular delivery, and (2) enzyme-cleavable linkage chemistry to provide high and sustained intracellular AM drug dosing. Prodrug monomers, derived from the antibiotic ciprofloxacin, were synthesized with either an intracellular protease cleavable dipeptide linker or a hydrolytic phenyl ester linker. RAFT polymerization was used to copolymerize the prodrug monomers and mannose monomer to synthesize well-defined drugamers without requiring a post-polymerization conjugation step. In addition to favorable *in vivo* safety profiles following intratracheal administration, a single dose of the drugamers sustained ciprofloxacin dosing in lungs and AMs above the minimum inhibitory concentration (MIC) over at least a 48 h period. The enzyme-cleavable therapeutic achieved a greater than 10-fold increase in sustained ciprofloxacin in AM, and maintained a significantly higher whole lung PK as well. Ciprofloxacin dosed in identical fashion displayed rapid clearance with a half-life of approximately 30 min. Notably, inhalation of the mannose-targeted ciprofloxacin drugamers achieved full survival (100%) in a highly lethal mouse model of pneumonic tularemia, contrasted with 0% survival using free ciprofloxacin. These findings demonstrate the versatility of the drugamer platform for engineering the intracellular pharmacokinetic profiles and its strong therapeutic activity in treating pulmonary intracellular infections.

Keywords: prodrug, ciprofloxacin, drug conjugate, enzyme-cleavable linker, Francisella, tularemia

4.1 INTRODUCTION

Pulmonary infections are major contributors to the global burden of disease. Non-tuberculous pulmonary infections killed 2.74 million people in 2015, and as a consequence they constitute the leading infectious cause of death and the fifth leading cause of death overall[1]. *Mycobacterium tuberculosis* latently infected 1.7 billion of the world's population in 2014[2] and caused the disease tuberculosis (TB) in 10 million people in 2015; of these, 1.3 million died[3]. TB is therefore the ninth leading cause of death worldwide [4]. Combined, over 4 million people die annually from pulmonary infections. Intracellular infections including TB, legionellosis, tularemia, and melioidosis present therapeutic challenges. The causative bacteria for those diseases have evolved to inhabit mammalian cells, especially phagocytic alveolar macrophages (AMs), an important host cell for intracellular bacteria invading the lung[5-8]. This intracellular localization provides a protective niche for those bacteria in the presence of humoral immunity and antibiotic therapy, thus reducing the antibacterial efficacy of pulmonary host defenses.

Current antibiotic therapy for pulmonary intracellular infections usually relies on rigorous oral and IV administration for a prolonged period to ensure therapeutic success and reduce relapse rate (e.g., 26 weeks for TB, 2-3 weeks for pulmonary tularemia, 3-6 months for melioidosis)[9-11]. However, systemic delivery of antibiotics results in limited biodistribution and short retention in AMs, and the prolonged dosing regimen potentially promotes the emergence of drug resistance. In addition to the challenges associated with the delivery methods, the intrinsic properties of antibiotics also affects their efficacy against intracellular bacteria[12,13]. For example, aminoglycosides fail to penetrate efficiently into eukaryotic cells, while fluoroquinolones exhibit poor retention inside the cells. The resulting off-target drug distribution induces side effects, including aminoglycoside-associated ototoxicity and fluoroquinolone-associated tendon rupture[14,15].

Delivery vehicles, such as liposomes, have been used as "drug pharmacokinetic modifiers" for achieving spatially and/or temporally pre-defined drug delivery goals [16]. A prominent clinical-stage example is inhalable liposomal ciprofloxacin (Lipoquin®, Aradigm Corp.) that reports a lung clearance half-life of ~7.4 h (compared with ~1 h for free ciprofloxacin) in mice, leading to superior efficacy to free ciprofloxacin in a murine model of lethal pulmonary *Francisella tularensis* infection[17,18]. These important studies have demonstrated up through human trials that the pharmacokinetics (PK) of antibiotics in the lung can be modulated by the carrier. These dispersal based formulation approaches can also suffer from various drawbacks including instability in biological fluids and tissues, initial burst release profiles, challenges in drug loading and difficulties in combination drug formulations[19].

As an alternative approach to the classical dispersal based particle formulations, our group recently developed an inhalable macromolecular prodrug platform, termed "drugamers," that provides sustained lung delivery of ciprofloxacin with controlled dosing profiles[20,21]. This macromolecular prodrug platform has tunable hydrolysis kinetics mediated by drug linkage chemistry (slower-releasing alkyllic vs. faster-releasing phenolic esters). In highly lethal *F. novicida* mouse challenge models where the mice are inoculated via bacterial aerosolization, a faster-releasing ciprofloxacin macromolecular prodrug (with phenolic ester linker) provided higher cure efficiencies (75% survival rate) than a similar but slower-releasing prodrug system (0% survival with alkyl ester linker). Further PK analysis demonstrated that this efficacy resulted from the sustained and higher level of ciprofloxacin maintained in the lung with a higher drug concentration achieved over minimum inhibitory concentration (MIC).

These results motivated us to further improve the drugamer system in an attempt to provide more specific and higher dosing in the AM intracellular environment. To this end, we herein integrated two new strategies into a new drugamer therapeutic design (**Figure 4.1**): (1) a protease cleavable valine-citrulline (VC) linker to facilitate intracellular release while maintaining extracellular stability in the lung, and (2) multivalent mannose ligands to target and enhance internalization by AMs[22]. The VC dipeptide linker with a self-immolative spacer has been used in a commercialized antibody-drug conjugate (e.g., ADCETRIS®) to provide serum stability and efficient intracellular drug release [23]. Genentech Inc. has also recently reported an antibody–

antibiotic conjugate (THIOMAB™ DSTA4637S) with this protease-cleavable valine-citrulline dipeptide linker for systemic infection therapy[5,24]. The original polymer-drug conjugates with protease cleavable linkers were pioneered by Duncan and Kopeček and progressed to phase II oncology clinical trials[25,26].

Here, the *in vitro* conditional release characteristics, *in vivo* pharmacokinetics (PK) drug releasing profiles and therapeutic efficacy of the mannose-targeted, VC drugamer were compared to a drugamer linked through hydrolytic phenol esters. We found that the VC drugamer led to significantly higher maximum intracellular ciprofloxacin concentration (C_{max}) and area under curve (AUC) of the PK drug release profiles in the whole lung and in the AM compartment, compared to the drugamers with the hydrolytic ester linker. Both drugamers demonstrate markedly improved survival (100%) compared to free ciprofloxacin (0%) in a lethal mouse model of pneumonic tularemia, indicating the therapeutic potential of this drugamer platform in treating pulmonary intracellular infections.

4.2 MATERIALS AND METHODS

4.2.1 *Materials*

Materials were purchased from Sigma Aldrich (St Louis, MO, USA) unless otherwise specified. 4-Cyano-4-(ethylsulfanylthiocarbonyl) sulfanylpentanoic acid (ECT) was synthesized and fully characterized as described previously[27]. Spectra/Por regenerated cellulose dialysis membranes were purchased from Spectrum Laboratories (Houston, TX, USA). Sephadex G-25 prepacked PD-10 columns were obtained from GE Healthcare Life Sciences (Pittsburg, PA, USA). Acetonitrile (ACN) and ultrapure H_2O were HPLC grade and purchased from Thermo Fisher Scientific (Waltham, MA, USA).

4.2.2 *Synthesis of ciprofloxacin prodrug monomers*

Synthetic procedures illustrated in supplementary information (**Schemes S1-S3**) were followed to obtain ciprofloxacin prodrug monomers carrying enzyme sensitive VC or phenyl ester linker

and mannose ethylmethacrylate for AM targeting. All the synthesized monomers as well as intermediates were purified by precipitation and/or silica gel column chromatography techniques. The successful synthesis and purity of the monomers were confirmed and characterized by ^{1}H NMR spectroscopy (Bruker Avance spectrometers 300 MHz or 500 MHz) and Electrospray Ionization-Mass spectrometry (Bruker Esquire ion trap mass spectrometer).

4.2.3 *Reversible addition−fragmentation chain-transfer (RAFT) synthesis of VC drugamer*

RAFT polymerization of mannose monomer and VC monomer was conducted in dimethyl sulfoxide (DMSO) under a nitrogen atmosphere using 4-cyano-4-[(ethylsulfanylthiocarbonyl)sulfanyl]pentanoic acid (ECT) as the chain-transfer agent (CTA) and 4,4'-Azobis(4-cyanovaleric acid) (ABCVA) as the radical initiator (**Figure 4.1**). The reaction was conducted with monomer feed ratios shown in **Table 4.1**. The initial monomer/CTA ratio ($[M]_0/[CTA]_0$) was 40:1 with a CTA/initiator ratio ($[CTA]_0/[I]_0$) of 10:1. Initial monomer wt% was about 27%. To a 5 mL round bottom flask was added mannose monomer (0.20 g, 0.67 mmol), VC monomer trifluoroacetate (TFA) salt (0.12 g, 0.12 mmol), ECT (5.17 mg, 0.020 mmol), ABCVA (0.55 mg, 0.002 mmol), and DMSO (0.787 mL/0.869 g). The round bottom flask was then sealed with a rubber septa and purged with nitrogen for 0.5 h. After this time the polymerization solution was transferred to a preheated oil bath at 70 ^{o}C and allowed to react for 4 h. The resultant drugamer was isolated by precipitation in diethyl ether to remove DMSO. The precipitated polymer was dialyzed against phosphate buffer (100 mM Na_2HPO_4, pH 7.2, 3 days) and distilled water (dH_2O, 3 days) using dialysis tubing (MWCO = 3500 Da) to remove unreacted monomers and exchange TFA salt with phosphate salt. The drugamers were then frozen and lyophilized before further purification using PD-10 desalting column followed by lyophilization for an additional 48 h. Purified polymers were characterized using ^{1}H-NMR spectroscopy and size exclusion chromatography (supplementary information).

4.2.4 *RAFT synthesis of CTM drugamer*

RAFT polymerization of mannose monomer and CTM monomer was conducted in DMSO under a nitrogen atmosphere using 4-cyano-4-(phenylcarbonothioylthio)pentanoic acid (CTP) as the CTA and ABCVA as the radical initiator (**Figure 4.1**). The reaction was conducted with

monomer feed ratios shown in **Table 4.1**. The initial monomer/CTA ratio ($[M]_0/[CTA]_0$) was 50:1 with a CTA/initiator ratio ($[CTA]_0/[I]_0$) of 5:1. Initial monomer wt% was about 24 wt%. To a 5 mL round bottom flask was added mannose monomer (0.362 g, 1.24 mmol), CTM monomer TFA salt (0.120 g, 0.154 mmol), CTP (7.78 mg, 0.028 mmol), ABCVA (1.56 mg, 0.0056 mmol), and DMSO (1.39 mL/1.53 g). The round bottom flask was then sealed with a rubber septa and purged with nitrogen for 0.5 h. After this time the polymerization solution was transferred to a preheated oil bath at 70 ^{o}C and allowed to react for 3 h. The resultant drugamers were then purified and characterized using the same methods as for VC drugamer.

4.2.5 *Enzyme-mediated ciprofloxacin release*

Lysosomal protease induced ciprofloxacin release from the drugamers were conducted at conditions mimicking the lysosomal medium[28]. Human liver cathepsin B (Enzo Life Sciences, Farmingdale, USA) was activated for 15 minutes in a solution of 0.151 mg/mL cathepsin B, 30 mM DTT, and 15 mM EDTA at 37 °C. Monomers or drugamers were then solubilized in reaction buffer [25 mM sodium acetate, 1 mM EDTA, pH 5.0, or phosphate buffered saline (10 mM, 1x PBS), 1 mM EDTA pH 7.4, 37 °C] and added to the enzyme solution for a final concentration of 2.1 μg/mL cathepsin B and 0.3 mg/mL drugamer (equivalent to 0.1 mM ciprofloxacin/peptide). At various timepoints, enzymatic activity was halted by addition of a thioprotease inhibitor [E-64 (Thermo Scientific), 1 mg/mL, 10 μL]. 100% ciprofloxacin release was defined by incubating monomers/drugamers in 0.1 N NaOH for 24 h at room temperature to hydrolyze all ester bonds, thus releasing all ciprofloxacin from polymer backbone. The released ciprofloxacin concentration was quantified by liquid chromatography-electrospray ionization mass spectrometry (LC-ESI MS) as shown in the supplementary information.

To evaluate the drugamer stability in the presence of esterases, recombinant human butyrylcholine esterase (BChE, Novoprotein, Summit, NJ, USA) was used as a model esterase. Drugamer solution (concentration ~ 3 mg/mL, equivalent to 1 mM ciprofloxacin, 10 μL) was added to 1x PBS (90 μL, containing 0.5 μg BChE) to a final ciprofloxacin concentration of 100 μM and incubated at 37 °C. At various time points, samples were diluted with ACN 5 times to denature BChE and halt the reaction. The samples were centrifuged at 13,000 rpm for 4 min to collect supernatants. The supernatants were subsequently concentrated 4 times by speedvac and

analyzed by LC-ESI MS. 100% ciprofloxacin release was defined by incubating drugamers (concentration ~ 3 mg/mL, equivalent to 1 mM ciprofloxacin, 20 μL) in 0.1 N NaOH (90 μL) for 24 h at room temperature to hydrolyze all ester bonds, thus releasing all ciprofloxacin from the polymer backbone.

4.2.6 *Quantification of released ciprofloxacin inside macrophages.*

RAW 264.7 cells were seeded in a 48-well plate with antibiotic-free DMEM supplemented with 10% FBS and allowed to adhere overnight. The cells were washed with PBS and drugamers (equivalent to 250 μg/mL ciprofloxacin) or free ciprofloxacin (250 μg/mL) diluted in DMEM were added to each well (0.25 mL). After 2 h incubation, the cells were washed three times with PBS, and 0.25 mL of DMEM with 10% FBS was added to each well. The cells were then incubated for the indicated time points. At each time point, cells were trypsinized and lysed by acetonitrile (ACN) addition (3x dilution). The obtained cell lysates were centrifuged at 14,000×g for 15 min at 4°C to collect supernatants. Concentrations of the released ciprofloxacin were quantified using LC-MS/MS. The LC-MS/MS method was described in the supplementary information.

4.2.7 *Cell viability assay*

Viability of RAW 264.7 cells treated with VC or CTM drugamer was evaluated using MTS assay as per manufacturer's instructions. Cells were seeded into a 96-well plate (5×10^4 cells/well) and incubated for 18 h at 37°C with 5% CO_2. Subsequently, drugamers at predetermined concentration (2.5 – 0.039 mg/mL) were added to each well and incubated for 22 h, same as the incubation time used in the subsequent co-culture assay. After incubation, cell media was aspirated and cells were washed with 1x PBS prior to addition of Cell Titer 96®A_{queous} One Solution Reagent (Promega). Cells were incubated for 2 h in MTS reagent before absorbance was read at 490 nm. Cell viability was calculated by $(Abs_{sample} - Abs_{blank})/(Abs_{control} - Abs_{blank}) \times 100\%$.

4.2.8 *Bacterial preparation*

F. novicida was used as a laboratory surrogate for *F. tularensis*, due to its low virulence for humans and high degree of genetic similarities with *F. tularensis* (~95%)[29]. *F. novicida* U112 was originally obtained from Francis Nano (University of Victoria, Victoria, Canada). A stock was prepared from overnight growth in trypticase soy broth with 0.1% L- cysteine at 37 °C with aeration. Bacteria were harvested in stationary phase, diluted in 20% glycerol, aliquoted, flash-frozen, and stored at −80 °C, yielding a post-thaw titer of 10^9 CFU/mL.

4.2.9 *Francisella-macrophage co-culture assay*

RAW 264.7 cells were seeded (700,000 cells/mL, 250 µL/well) into a 48 well plate with antibiotic free DMEM containing 10% FBS, and incubated at 37°C with 5% CO_2. After 18 h, cells were infected with *F. novicida* U112 at early log phase of growth (OD600=0.2) at a multiplicity of infection of 50, and then incubated for 1 h. Subsequently, growth media was replaced with fresh DMEM containing 10% FBS and 250 µg/mL kanamycin to eliminate extracellular bacteria not internalized by the cells; cells were then incubated for another hour. After 1 h, cells were washed with 1x PBS and incubated with fresh media containing free ciprofloxacin or drugamers (equivalent to 250 µg/mL ciprofloxacin) for 2 h. Following incubation, cells were washed with 1x PBS and growth media was replaced with fresh DMEM containing 10% FBS. Cells were then incubated for another 22 h (24 h post-infection). After incubation, cells were washed three times with 1x PBS and lysed with 100 µL of PBS containing 0.1% [v/v] Triton X-100. Lysates were serially diluted and plated onto triplicate TSB agar plates, and incubated at 37°C for 24 h. CFUs were counted when individual bacterial colonies were distinguishable.

4.2.10 *Animals and ethics statement*

Female C57Bl/6 mice, 6 to 8 weeks old, were purchased from The Jackson Laboratory (Bar Harbor, ME), maintained at the University of Washington under specific pathogen-free conditions. All animal procedures and handling were conducted under protocols (4047-02 and

2671-10) approved by the Institutional Animal Care and Use Committee at the University of Washington.

4.2.11 *In vivo lung safety study*

C57Bl/6 mice (Female, 6-8 weeks old, n=5) were anesthetized with 5% isoflurane for 5 min before administration of 50 µL of PBS (negative control) or drugamer solution in PBS (0.2 µm filtered, equivalent to 20 mg/kg ciprofloxacin dose) via intratracheal aerosolization using a MicroSprayer® Aerosolizer–Model IA-1C (Penn-Century. Wyndmoor Inc., PA, USA). Mice received one daily dose for three consecutive days and their body weight changes were monitored each day before dosing. Twenty-four h after the last dose, the mice were weighed and then euthanized by CO_2 asphyxiation. Bronchoalveolar lavage (BAL) was conducted with 1 mL of PBS flush followed by three 0.8 mL flushes. Lungs were harvested and placed into 1 mL PBS on ice. Lung tissue in 1 mL of PBS was subsequently mixed with 1 mL of PBS containing protease inhibitor cocktail (Pierce™ Protease Inhibitor, Thermo Fisher Scientific) before mechanical homogenization using a TissueRuptor (Qiagen, Valencia, CA, USA). Lung tissue homogenates (LTH) were then stored at 4°C for 30 min followed by centrifuge at 5000xg for 15 minutes to collect the supernatant for TNF-α quantification.

BAL fluid was spun at 400 g for 15 min to pellet lavage cells. Cell-free BAL fluid was retained and stored at -80°C. BAL cells were resuspended into 0.5 mL RPMI 1640 supplemented with 10% FBS. BAL cells were mounted onto microscopy slides with a Cytospin centrifuge at 500 rpm for 5 min, and then stained with Hemacolor (EMD Millipore, Billerica, MA, USA) prior to cytology analysis. Stained slides were analyzed for macrophage to neutrophil ratio with a minimum of 200 cells per slide counted. TNF-α concentrations in the supernatant of LTH and cell free BAL fluid were assayed using mouse TNF-α ELISA MAXTM Standard kit (BioLegend, San Diego, CA, USA) as per manufacturer's instructions.

4.2.12 *In vivo pharmacokinetics (PK) and biodistribution studies of drugamer-released ciprofloxacin*

In vivo PK and biodistribution properties of free-form ciprofloxacin and drugamer-released ciprofloxacin were compared using C57BL/6 mice (female, 6-8 weeks old, n=4). Mice were treated with free ciprofloxacin solution (5% dextrose in water, 20 mg/kg) or drugamer solution (PBS, equivalent to 20 mg/kg ciprofloxacin) via intratracheal aerosolization using the MicroSprayer® Aerosolizer. Specifically, mice were anesthetized with 5% isoflurane with O_2 at 1 L/min exposure after filling the chamber for one min. Using a mouse laryngoscope (Penn-Century LS-2, LS-2M, PA, USA), and an intratracheal MicroSprayer®, 50 µL of free ciprofloxacin, VC drugamer, or CTM drugamer was administered. At various time points post drug administration (0.5, 1, 2, 4, 8, 18, 24 and 48 h), mice were euthanized and the blood was then collected by cardiac puncture. The left mainstem bronchus was tied off and the right lung was lavaged with 0.6 mL followed by three 0.5 mL flushes of 0.85% NaCl with 0.6 mM EDTA. The left lung, liver, spleen and kidney were then surgically removed and weighed fresh. To determine the actual deposited dose, mice were euthanized to collect tissue samples right after dosing. Details of the tissue process and ciprofloxacin quantification methods were described in the supplementary information.

4.2.13 *In vivo antibiotic activity studies using a lethal pulmonary Francisella infection model*

The antibiotic activity of drugamers was tested in C57Bl/6 mice (female, 8 weeks old, n=8) challenged with aerosolized *F. novicida* U112. Mice were given three consecutive doses of free ciprofloxacin or VC/CTM drugamers using MicroSprayer®, with 24 h interval between each dose (**Figure. 4.6A**). Two challenge studies were conducted with ciprofloxacin dosing at either 20 or 10 mg/kg. Lethal bacterial infection was conducted 1 h after the first dose using a method described previously by our lab [21]. Briefly, a bacterial aerosol was generated from 6 mL of bacteria suspension ($2x10^7$ CFU/mL) using a Heart Mini-hi-flow nebulizer (Westmed, Arizona, USA). Mice from all three treatment groups were simultaneously exposed to aerosolized bacteria using a Biaera whole-body exposure chamber (Biaera Technologies, Maryland, USA), with total airflow through the chamber maintained at 19.5 L/min during a 20 min exposure.

To determine bacterial deposition in the lungs, four mice were euthanized immediately post-exposure with pentobarbital (300 mg/kg intraperitoneally) followed by exsanguination. The left lungs were harvested, homogenized in PBS, and quantitatively cultured on trypticase soy agar supplemented with 0.1% L-cysteine. The bacteria titers in the two challenge studies were about 10-15x higher than LD50 (105 ± 9 CFU/lung for 20 mg/kg dose; 130 ± 5 CFU/lung for 10 mg/kg dose, Mean ± SEM) [29]. The infected animals were monitored daily for mobility and for deaths from the infection. At day 14 after infection, the number of mice that survived the otherwise lethal infection was recorded. Lungs were harvested from mice that survived 14 days after infection and plated to determine viable bacteria surviving after treatment.

4.2.14 *Statistical analysis*

Student's two-tailed t-tests were performed to compare two groups and analysis of variance (ANOVA) was performed for comparisons of multiple groups, through GraphPad Prism (version 5.0, GraphPad Software Inc.). Unless otherwise stated, data reported denote the means ± SD. Survival analyses were performed using a log-rank test in GraphPad Prism. No specific methods of randomization were applied to group or animal allocation. Investigators were not blinded to group allocation. $P < 0.05$ was considered statistically significant.

4.3 RESULTS

4.3.1 *Synthesis and characterization of ciprofloxacin prodrug monomers*

The Valine-Citruline (VC) dipeptide sequence was coupled with the self-immolative spacer *para*-aminobenzyl alcohol (PABOH) to construct the cathepsin B sensitive ciprofloxacin prodrug monomer (**Scheme S1**, supplementary information). Succinimidyl activated methacrylate monomer was first coupled with VC-PABOH to get SMA-VC-PABOH (**6**), which was then conjugated to Boc-ciprofloxacin using uronium-based coupling agent HBTU, the base diisopropylethylamine and the catalyst DMAP. Vinyl signals at 5.69 and 6.02 ppm, and aromatic signals of ciprofloxacin at 7.79 and 8.46 ppm in ^{1}H-NMR spectrum confirmed the successful conjugation. Finally, Boc group was deprotected in 20 % trifluoroacetic acid to get the enzyme

cleavable monomer (**11**). To evaluate linker effects on intracellular drug release kinetics, a control monomer CTM (**14**) containing phenyl ester linker susceptible for nonspecific drug hydrolysis was also synthesized following similar HBTU coupling and deprotection chemistry described above for VC-ciprofloxacin monomer (**Scheme S2**, supplementary information). ^{1}H-NMR spectrum and ESI-MS spectral characterizations, and protease-mediated ciprofloxacin release kinetics are available in Supplementary Information.

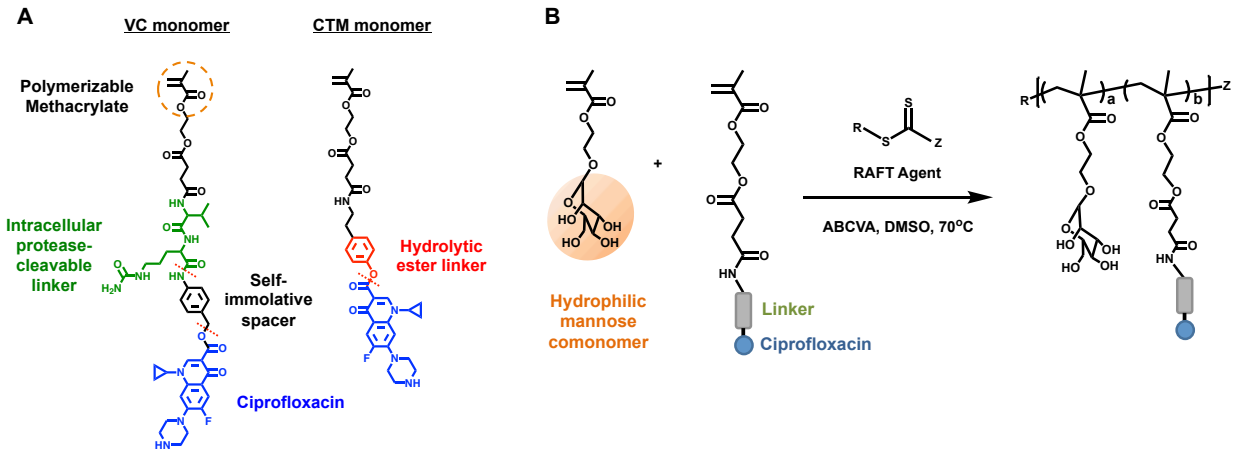

Figure 4.1. (A) Ciprofloxacin-derived polymerizable prodrug monomers with cleavable linkers. VC monomer: methacrylate-based monomer linking ciprofloxacin through intracellular protease-cleavable valine-citrulline dipeptide linker. A self-immolative spacer situates ciprofloxacin from the enzymatic cleavage site (top red dash line). CTM monomer: methacrylate-based monomer linking ciprofloxacin through hydrolytic ester linker. (B) Synthetic strategy for the preparation of polymeric ciprofloxacin prodrugs using reversible addition-fragmentation transfer (RAFT) polymerization. Mannosylated methacrylate was used as a biocompatible hydrophilic comonomer. Ciprofloxacin prodrug monomers were in the form of trifluoroacetate (TFA) salt.

4.3.2 *Optimizing compositions of protease-cleavable drugamer*

Ciprofloxacin prodrug monomers were copolymerized with mannose monomers by RAFT polymerization (**Figure 4.1**)[20,30]. Due to the hydrophobic nature of the dipeptide VC linker and ciprofloxacin, the feed mole ratio of VC monomer and mannose monomer was optimized such that resulting polymers would be sufficiently soluble in PBS to achieve the ciprofloxacin dosing for the subsequent *in vivo* studies (20 mg/kg ciprofloxacin dose, ~80 mg/mL polymer solution)

(**Table S1**). The optimized drugamer compositions were characterized using size exclusion chromatography (SEC) and ^{1}H-NMR spectrum, and are summarized in **Table 4.1** and **Figure S10-S12**. Monomer feed ratio and degree of polymerization for drugamers containing the phenol ester linker (CTM) were adjusted to yield a similar ciprofloxacin wt% and molecular weight (MW) as the VC drugamer for proper comparison. For example, the MW of VC and CTM drugamers was found to be 25.8 and 26.7 kDa with ciprofloxacin wt% around 9-10%. Additionally, both drugamers have narrow MW distributions (Đ) with dispersity of 1.10 and 1.02, for VC and CTM, respectively.

Table 4.1. Summary of compositions, molecular weights (M_n), and molar mass dispersity (Đ) for the polymeric ciprofloxacin prodrugs with either a protease cleavable linker (Man-*co*-VC) or a hydrolytic ester linker (Man-*co*-CTM). Mannose monomer: mannosylated ethyl methacrylate. Drug monomer: ciprofloxacin prodrug monomer with Val-Cit linker or phenol ester linker.

Polymer	**Mannose monomer (feed)** mol.%	**Mannose monomer[a] (exp)** mol.%	**Drug monomer (feed)** mol.%	**Drug monomer[a] (exp)** mol.%	**M_n[b] (kDa)**	**Đ[b]**	**Drug[a]** wt%
Man-co-VC	85	90.2 ± 0.8	15	9.8 ± 0.8	25.8 ± 1.2	1.10 ± 0.08	9.3 ± 0.7
Man-co-CTM	89	90.2 ± 0.6	11	9.8 ± 0.6	26.7 ± 6.8	1.02 ± 0.02	9.8 ± 0.5

[a]As determined by ^{1}H-NMR spectrum in DMSO-d_6 using a Boc-protected ciprofloxacin as an internal standard.
[b]As determined by size exclusion chromatography.

4.3.3 *Cathepsin B mediated ciprofloxacin release kinetics*

To verify the linker accessibility and enzyme-specific cleavage of ciprofloxacin from the VC linker, drugamers were incubated with human liver cathepsin B enzyme. The released ciprofloxacin was quantified as a function of time using LC-ESI MS. Incubation of VC drugamer with cathepsin B resulted in the rapid release of ciprofloxacin with a $t_{1/2}$ of ~30 min (**Figure**

4.2A). By contrast, drug release from a control drugamer containing a non-cleavable peptide linker (CTM drugamer) was not observed over 4 h in the presence of cathepsin B. Time-dependent ciprofloxacin release from VC drugamer was clearly observed in the LC chromatograms (**Figure 4.2B**). The aminobenzyl alcohol side product (**Scheme S4**) was detectable by LC-MS analysis with similar release rate as ciprofloxacin (**Figure S13**).

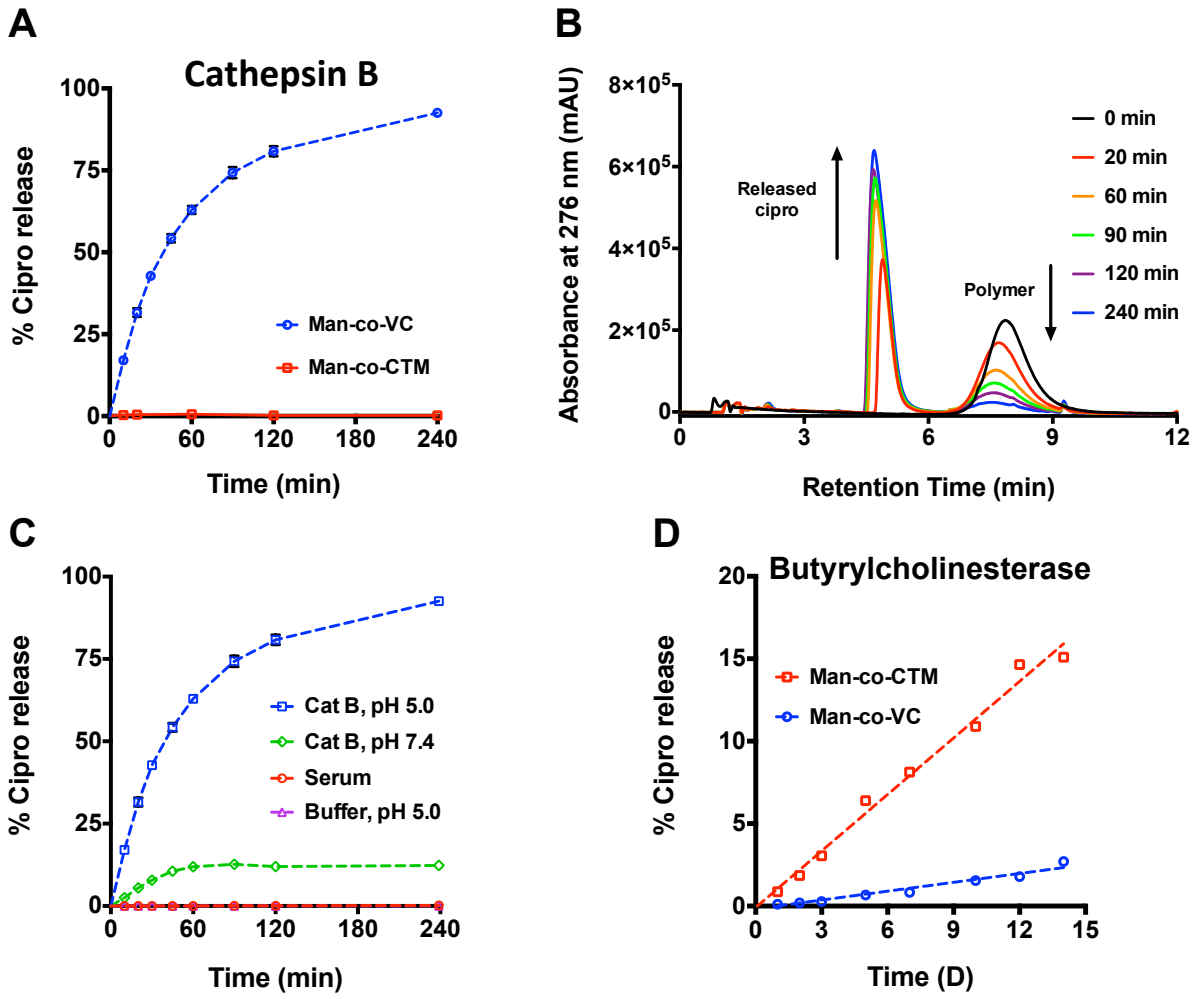

Figure 4.2. Lysosomal protease-mediated drug release from polymeric ciprofloxacin prodrug. (A) Ciprofloxacin release kinetics of polymeric ciprofloxacin prodrugs with either a protease-cleavable dipeptide linker (Man-co-VC) or a hydrolytic ester linker (Man-co-CTM) in the presence of a human lysosomal protease, cathepsin B (CatB). (B) Liquid chromatograms showing the time-dependent ciprofloxacin released from Man-co-VC incubated with CatB. (C) Ciprofloxacin release kinetics of Man-co-VC in the presence of CatB (pH 5.0 or 7.4), and in human serum or acetate buffer (pH 5.0). (D) Ciprofloxacin release kinetics of polymeric

ciprofloxacin prodrugs incubated with a model esterase, human butyrylcholinesterase. Error bars represent means ± SD from triplicate samples. Cipro: Ciprofloxacin.

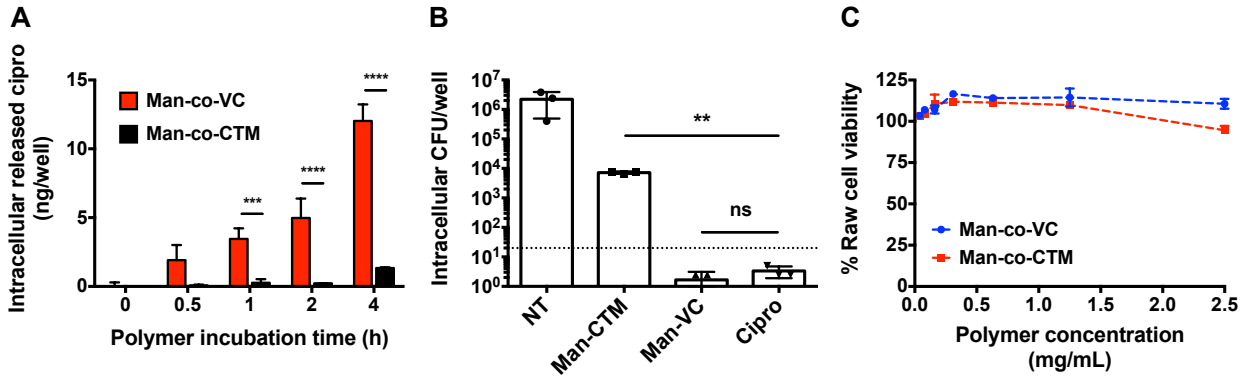

Figure 4.3. *In vitro* properties of polymeric ciprofloxacin prodrugs. (A) Mass spectrometric quantification of released antibiotic inside macrophages incubated with polymeric ciprofloxacin prodrugs made with Val-Cit dipeptide linker (protease cleavable, Man-co-VC) or ester linker (Man-co-CTM). (B) Intracellular antibacterial activity of polymeric prodrugs in RAW 264.7 macrophages infected with *Francisella novicida*. Surviving bacteria were enumerated 24 h after infection. NT: untreated control. (C) Cell viability of RAW 264.7 cells incubated with Man-co-VC or Man-co-CTM for 22 h. Cell viability numbers were relative to untreated controls as determined by MTS. Error bars represent means ± SD from triplicate wells. One-way ANOVA analysis with a Dunnett test was utilized to establish statistical significance (**$p < 0.01$, ***$p < 0.001$, ****$p < 0.0001$). Cipro: ciprofloxacin.

As cathepsin B could be translocated to the cell surface or secreted into the extracellular space under certain physiological and pathological conditions (e.g., inflammation)[31], we also evaluated cathepsin B-mediated release at neutral pH, which demonstrated minimal ciprofloxacin release (~10%) after 4 h incubation (**Figure 4.2C**). To investigate if ciprofloxacin release from VC drugamer is primarily attributed to the cleavage by cathepsin B, and not spontaneous hydrolysis, the release profile was evaluated in various aqueous conditions, including in an acetate buffer mimicking the lysosomal pH (pH 5.0) and human serum. No detectable ciprofloxacin release from VC drugamer was observed in 4 h under those aqueous conditions tested. To examine whether the ester bond in both drugamers is susceptible to non-specific esterase cleavage, we probed ciprofloxacin release from drugamers in the presence of butyrylcholinesterase (BChE), a

human serum esterase involved in detoxification and metabolism of ester-containing drugs[32]. Accumulation of the released ciprofloxacin was monitored for up to 14 days; only ~2.7% and ~15.1% of the active ciprofloxacin was released from VC and CTM drugamers, respectively (**Figure 4.2D**).

4.3.4 *In vitro intracellular ciprofloxacin release and efficacy against intracellular infections*

To compare the intracellular ciprofloxacin release kinetics of VC and CTM drugamers, tandem LC-MS (LC-MS/MS) was used to quantify ciprofloxacin concentrations in RAW 264.7 macrophages incubated with drugamers (0.25 mg/mL equivalent ciprofloxacin, ~2.5 mg/mL durgamer) over 4 h. At predetermined time points, drugamer treatment solutions were removed, and cells were washed several times with DPBS in order to remove all extracellular (non-bound or internalized) drugamers. Cells were then lysed to extract the intracellular ciprofloxacin and subjected to LC-MS/MS analysis to quantify drug concentrations. Notably, VC drugamer demonstrates a time-dependent intracellular release profile with significantly higher intracellular ciprofloxacin concentrations than CTM drugamer after 1-4 h incubations (**Figure 4.3A**). With the knowledge of the intracellular ciprofloxacin release profiles of the drugamers, we further investigated the ability of the drugamers to clear intracellular bacterial infections. Using an *in vitro* macrophage-bacteria co-culture assay, RAW 264.7 cells were infected with *F novicida*, a laboratory surrogate for *F. tularensis*[29](**Figure 4.3B**). The two drugamers were compared for their effectiveness in decreasing intracellular bacterial levels. Whereas CTM drugamer demonstrated modest reduction in the intracellular bacteria, VC drugamer displayed antimicrobial activity indistinguishable from free ciprofloxacin. This significant difference in antibacterial potency between VC drugamer and CTM drugamer corresponds with the faster intracellular release profile of VC drugamer shown in **Figure 4.3A**. Notably, drugamers displayed limited cytotoxicity to RAW 264.7 at concentration used in *in vitro* assays (~2.5 mg/mL, **Figure 4.3C**).

4.3.5 *In vivo lung safety of polymeric ciprofloxacin prodrugs*

To examine the *in vivo* utility of the drugamer system, intratracheal aerosolization of drugamer solutions (50 μL) or PBS as a control were delivered to mouse lungs at a ciprofloxacin dose of

20 mg/kg once daily for three-consecutive days. Respiratory rate and effort were not noted to differ among mice treated with drugamers compared to PBS control mice. Lung, bronchoalveolar lavage fluid (BALF), and alveolar cells were then collected 24 h after the last dose. Acute lung inflammation was evaluated using the metrics of animal weight change, infiltrating neutrophil in the bronchoalveolar space, and tumor necrosis factor alpha (TNF-α) concentration in lung tissue homogenate (LTH) and BALF (**Figure 4.4**). These metrics were selected based on the understanding that neutrophils are the earliest immune cells to be recruited to the site of lung injury or inflammation[33] and TNF-α is an early response cytokine in acute lung injury and inflammation[34,35]. As shown in **Figure 4.4**, all observed toxicity markers for the VC and CTM drugamers are indistinguishable from the PBS control ($P > 0.1$). The body weight of mice gradually increased with time to match typical growth curves and the neutrophil percentages were comparable to the reported values of healthy mice (~3%)[33].

4.3.6 *In vivo pharmacokinetics and biodistribution of polymeric ciprofloxacin*

In vivo PK and biodistribution of ciprofloxacin from drugamer-dosed or free-drug dosed animals were evaluated using an analytical LC−MS/MS technique after a single intratracheal administration at 20 mg/kg ciprofloxacin dose. All data were normalized to mass of tissue, volume of blood, or intracellular volume. To ensure proper comparisons across the three treatment groups, the actual deposited ciprofloxacin dose was determined from the ciprofloxacin concentration in the lung at about 10 min post-administration (minimal time required for animal euthanasia and tissue collection) (**Figure S14**). Similar deposited doses in right and left lungs were observed with VC and CTM drugamers. The single dose of free ciprofloxacin resulted in a relatively high initial concentration and rapid elimination from the lungs over 2 h, consistent with the reported PK profiles of free ciprofloxacin[18] (**Figure 4.5A & 4.5B**). In contrast, the concentration of ciprofloxacin in whole lung released from both drugamers remained detectable and higher than MIC (0.065 μg/g, see **Table 4.2**) over a 48 h period. Additionally, the measurement of total drug exposure in the whole lung (i.e. the area-under-the-curve, AUC) and maximum concentration (C_{max}) following single administration of VC drugamer were 1.8- and 2.3-fold higher, respectively, than those of CTM drugamer (**Table 4.2**).

Both the mannose-targeted VC and CTM parent drugamers were internalized and remained concentrated in AMs at similar levels throughout the 48 h time frame of the experiment (**Figure 4.5C**). The most striking effect of the VC linker was the order of magnitude increase in intracellular AM ciprofloxacin concentrations and their maintenance over the observed 48 h time period (**Figure 4.5D**). The time of maximum concentration observed (T_{max}) also appeared earlier in mice treated with VC drugamer compared to the T_{max} for the CTM drugamer (**Table 4.2**). Quantitatively, the VC drugamer in the AM compartment achieved a higher C_{max} compared to free ciprofloxacin (6.5x) and CTM drugamer (34.4x).

The sustained delivery of ciprofloxacin from the VC drugamer resulted in intracellular ciprofloxacin concentrations more than 3 magnitudes higher than the MIC over the entire 48 h period. This unique intracellular PK profile of the VC drugamer led to superior AUC compared to free ciprofloxacin (74.8x) and CTM drugamer (25.6x). Although the VC drugamer provided higher intracellular ciprofloxacin dosing, the released ciprofloxacin concentration from the VC drugamer in plasma and other organs (liver, spleen and kidney) was minimal compared to free ciprofloxacin (**Figure 4.5E, 4.5F & S15, Table S2**). In comparison to the CTM drugamer, the VC drugamer resulted in higher released ciprofloxacin concentrations in all the tested organs (see supplementary information), but similar ciprofloxacin concentrations in plasma.

4.3.7 *Therapeutic efficacy of polymeric ciprofloxacin prodrug against lethal pneumonic tularemia.*

With significant improvement in the PK profiles of the drugamer-released ciprofloxacin, we next investigated the antibacterial efficacy of drugamers in a lethal mouse model of airborne *F. novicida* infection. Drugamers were administered using an intratracheal microsprayer with a ciprofloxacin dose of 20 mg/kg or 10 mg/kg at 0 (1 h prior to infection), +1, and +2 days (**Figure 4.6A**). Animal health condition and survival were monitored until mice qualified for euthanasia or reached the experimental end-point (14 days post-infection). In the first challenge study where mice were dosed at 20 mg/kg ciprofloxacin, none of the mice receiving free ciprofloxacin survived to the experimental end-point. In contrast, VC and CTM drugamers provided full protection against the lethal infection of aerosolized *F. nocivida* (**Figure 4.6B**).

In an attempt to distinguish the efficacies of VC and CTM drugamers, we further reduced the ciprofloxacin dose to 10 mg/kg with the assumption that the high AUC and C_{max} of PK profiles in AM would allow the VC drugamer to lower the effective dose. The transition from 20 to 10 mg/kg dose led to the survival rate of mice treated with VC or CTM drugamer decreased from 100% to 62.5% (n= 5/8) and 50% (n= 4/8), respectively (**Figure 4.6C**). The body weight change and the number of bacteria in the lung of survived mice reflected the better health conditions of mice treated with the VC drugamer. For example, body weights of mice treated with the VC drugamer started recovering at 3 days post infection with maximum ~13% body weight loss, whereas, mice treated with free ciprofloxacin or CTM drugamer kept dropping to a minimum of 30% and 20%, respectively (**Figure S16**). Additionally, the bacteria titers in the surviving mice treated with VC and CTM drugamers were 7.6 ± 3.2 CFU/lung and 253.5 ± 243.2 CFU/lung, respectively.

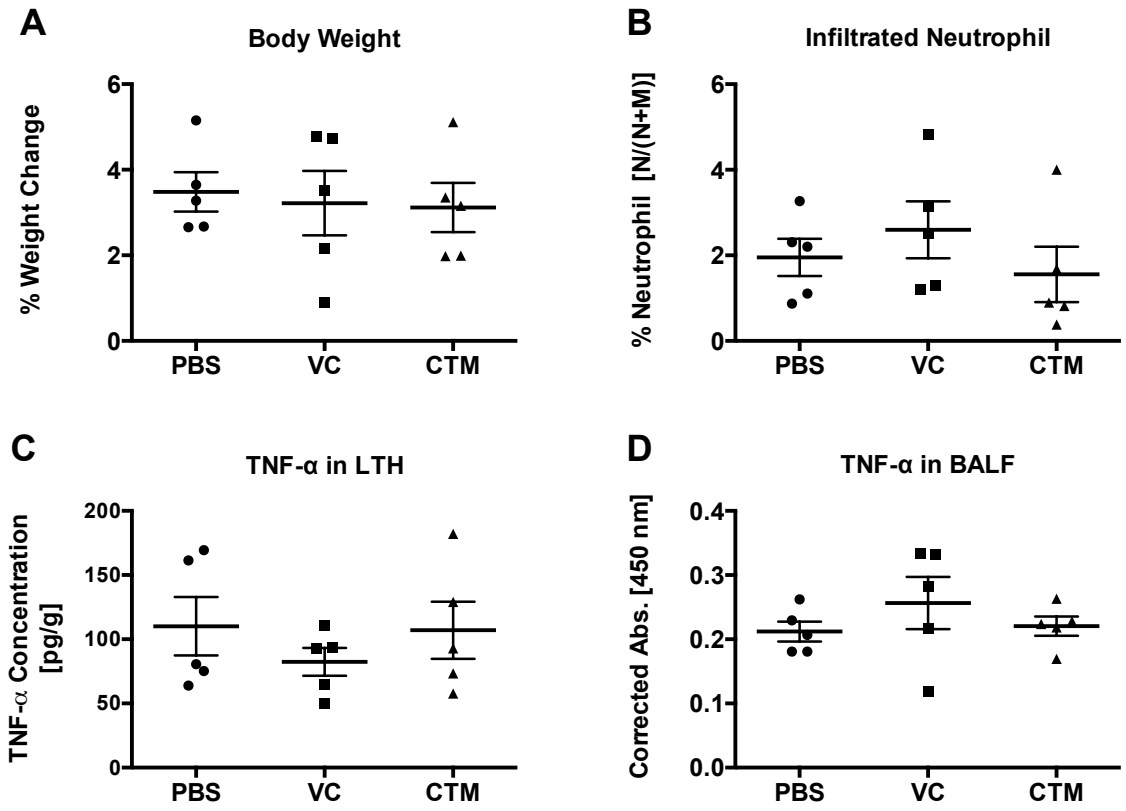

Figure 4.4. Pulmonary safety evaluation of polymeric prodrugs dosed at 20 mg/kg ciprofloxacin. Polymeric antibiotic prodrugs were intratracheally administered to uninfected C57BL/6 mice once a day for 3 days, and tissues were harvested 24 h after the last dose. (A) Animal weights measured prior to treatment and 24 h after the final dose were ratioed to calculate percent weight change per mouse. (B) Percentage of neutrophils was determined by differential cell counting of cells from bronchoalveolar lavage fluid (BALF). Values were calculated as [neutrophil/(neutrophil + macrophage)] × 100%. Tumor necrosis factor alpha (TNF-α) levels were measured by ELISA from (C) lung tissue homogenates (LTH) and (D) BALF. Concentration values of TNF-α from LTH were adjusted to mass of the harvested lungs, while BALF TNF-α levels are presented as absorbance values corrected to total volume of harvested fluid. No statistically significant differences were observed using one-way ANOVA and a Dunnett post hoc test between polymer treated and PBS treated mice (n = 5). Error bars represent means ± SEM. VC: polymer with protease-cleavable peptide linker. CTM: polymer with hydrolytic ester linker.

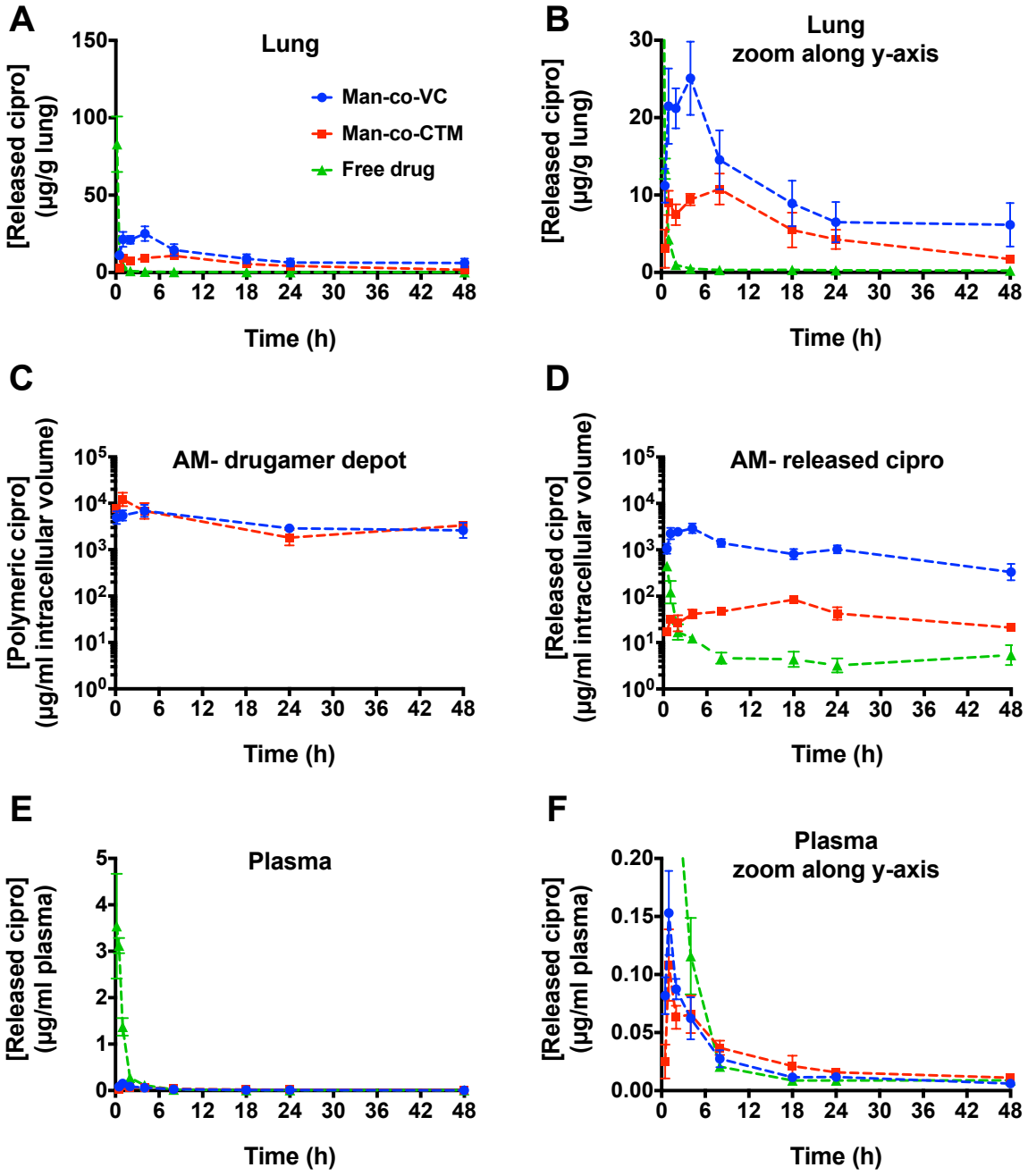

Figure 4.5. ***In vivo*** **pharmacokinetics analysis of polymer-released ciprofloxacin.** Time-course of ciprofloxacin concentration was evaluated in lung (A & B), alveolar macrophage (AM) (C & D) and plasma (E & F). All figures, except for Figure 5C, present the free/released ciprofloxacin concentrations; Figure 5C shows concentrations of the drugamer depot in AMs. Figure 5A and E were expanded along y-axis to yield Figure 5B & F. After intratracheal administration of each drugamer or free ciprofloxacin solution to mice, at predetermined time points, single bronchoalveolar lavage was conducted to collect AMs from the right lung and the left lung was collected intact. Ciprofloxacin concentration was determined using LC-MS/MS

with deuterated ciprofloxacin as an internal standard. In all cases, released drug was quantified by comparison to an authentic drug standard curve prepared in the same matrix. Each value represents the mean ± SEM (n=3-4). Cipro: ciprofloxacin.

Table 4.2. Pharmacokinetic parameters of ciprofloxacin in lung, alveolar macrophage (AM), and plasma after intratracheal administration of polymeric prodrugs to mice. Parameters were obtained from data shown in **Figure 4.5**.

Treatment	Tissue	T_{max}[a] (h)	C_{max}[b] (μg/g or μg/mL)	AUC_{0-24}[c] (μg*h/g or μg*h/mL)	C_{max}/MIC[d]	AUC_{0-24}/MIC[d] (h)
VC		4	25 ± 5	321	386	4945
CTM	Lung	8	11 ± 2	180	165	2766
Free		0.17	83 ± 18	38	1275	585
VC		4	2914 ± 772	33971	97149	1132351
CTM	AM	18	85 ± 19	1326	2821	44213
Free		0.5	447 ± 48	454	14885	15141
VC		1	0.15 ± 0.04	0.79	5.10	26.43
CTM	Plasma	1	0.11 ± 0.03	0.88	3.60	29.47
Free		0.17	3.54 ± 1.13	4.21	117.99	140.34

[a]The time to reach maximum concentration (C_{max}) after administration.
[b]C_{max} are represented as mean ± SEM. Values are normalized to lung mass (g) or intracellular/plasma volume (mL).
[c]Area under the curve are presented as mean value from 0 to 24 h (AUC_{0-24}) and determined by GraphPad Prism 5.
[d]MIC: 0.03 μg/mL; 0.065 μg/g. The volume distribution of ciprofloxacin (2.16 L/kg, for mice treated with 20 mg/kg ciprofloxacin) was used to convert MIC to a more tissue-relatable value (0.065 μg/g) [29,36].

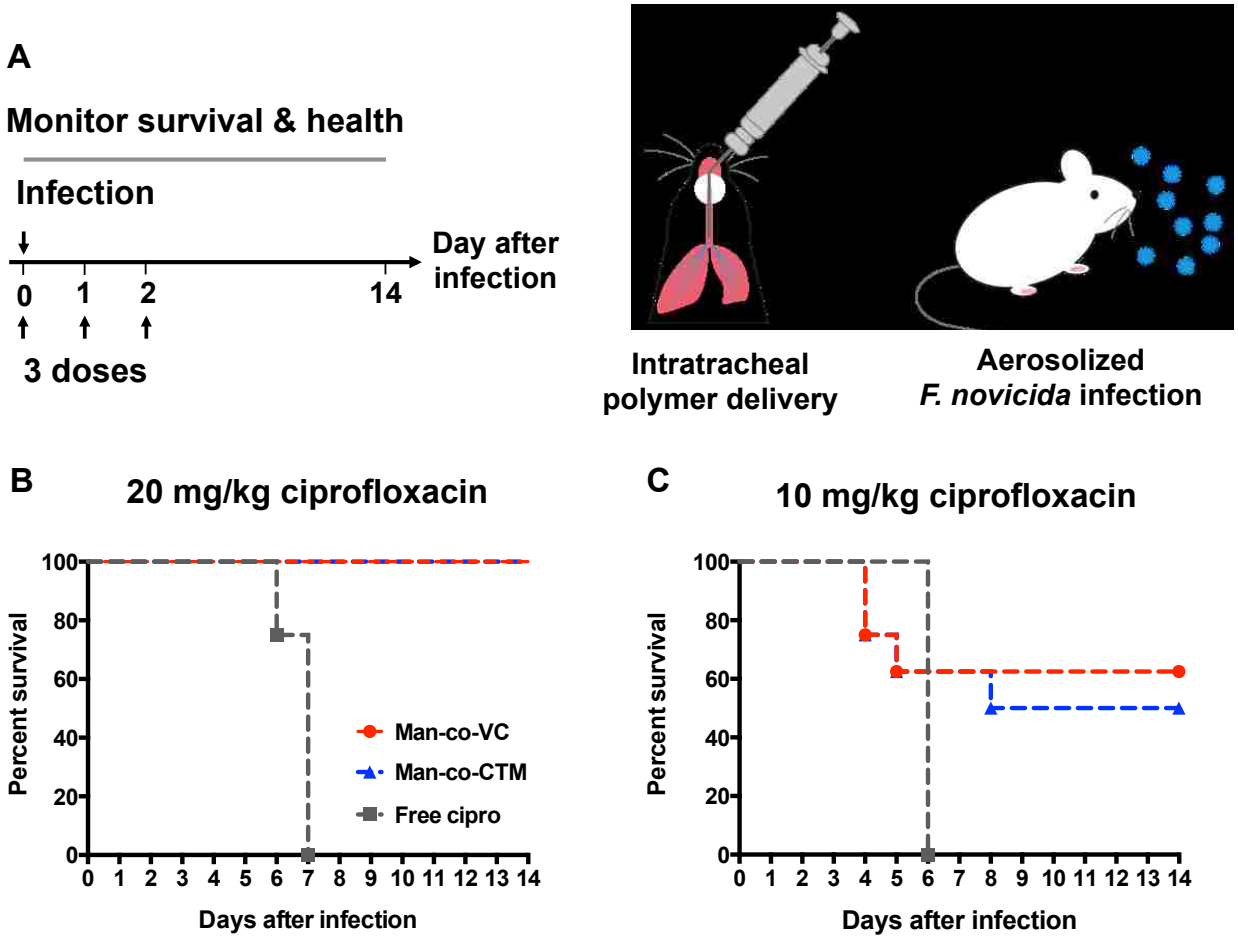

Figure 4.6. *In vivo* therapeutic efficacy of polymeric ciprofloxacin prodrugs against lethal pulmonary infections of *Francisella novicida* in mice. (a) Workflow schematic. Free ciprofloxacin or polymeric ciprofloxacin prodrugs with protease-cleavable linker (Man-co-VC) or hydrolytic ester linker (Man-co-CTM) were intratracheally administered (50 μL aerosolization) at 0, 1, and 2 days using a MicroSprayer® (n = 8 for each treatment group). All bacterial inoculation occurred 1 h after treatment on day 0. Survival rate and health condition of mice were monitored for 14 days. (B) and (C) survival rate of infected mice treated with 20 or 10 mg/kg ciprofloxacin dose.

4.4 Discussion

This study demonstrates the versatility of this polymeric antibiotic prodrug platform by adding mannose-targeting and an intracellular enzyme-cleavable linker to dramatically increase the alveolar macrophage drug PK and corresponding antibacterial efficacy. This prodrug strategy is needed to address significant limitations associated with conventional ciprofloxacin therapy.

Free ciprofloxacin is rapidly cleared from the site of infection, and its clinical significance can be compromised due to adverse reactions, including tendon rupture and irreversible nerve damage[37-39].

The new mannose-targeted ciprofloxacin drugamers reported here provide two advantageous features compared to prior pegylated ciprofloxacin drugamers. First, mannose-targeting affords increased alveolar macrophage uptake and internalization. Second, the drugamer with a protease-cleavable peptide linker (VC drugamer) displays a sustained 10-fold higher intracellular dosing of ciprofloxacin compared to the hydrolytic phenolyic ester drugamer. Both the mannose-targeted hydrolytic ester drugamer and the VC drugamer achieved full cohort survival in the aerosolized pulmonary intracellular Francisella infections, and at lower ciprofloxacin doses compared to prior pegylated phenyl ester linked drugamers[21]. The unique PK profile with the intracellular enzyme-cleavable linker may yield therapeutic advantages over current antibiotic therapy, especially in disease settings where bacteria are resident in AM, such as pneumonic tularemia and tuberculosis[6,40]. Additionally, the drug release mechanism and kinetics can be encoded into the polymer by choosing various linkers, such as the peptide linker and phenyl ester linker in the present study (**Figure 4.1**). The synthetic approach also allows facile design of multivalent mannose ligands that have been shown to actively target AMs[22,41,42]. The resulting targeted drugamers with a peptide linker (VC drugamer) or a hydrolytic ester (CTM drugamer) have a high degree of uniformity and reproducibility of molecular weight and compositions (**Table 4.1 & Figure S10**), which are important for future drug development.

The Val-Cit dipeptide linker with a self-immolative spacer has been preciously shown to be cleavable by lysosomal proteases in mice and human[5,23,43]. Consistent with previous findings of antibody-drug conjugates, the VC drugamer were stable under physiological conditions but was rapidly hydrolyzed by lysosomal protease cathepsin B particularly at lysosomal pH (**Figure 2**). This demonstrates that the dipeptide portion of the full linker is accessible within the context of the mannose monomer surrounding environment. Notably, no detectable cathepsin B-mediated drug release was identified from CTM drugamer and only limited release resulting from the model extracellular esterase BChE over 14 days. The faster intracellular release of VC drugamers than CTM drugamer was also demonstrated using *in vitro* RAW cells without and

with the *F. novicida* infection (**Figure 4.3A&B**). The VC drugamer showed similar antibacterial potency as free ciprofloxacin in a representative macrophage-bacteria assay, whereas CTM drugamer do not. This observation confirms the rapid intracellular drug release of VC drugamer in cells infected with *F. novicida*.

This inhalable drugamer platform shows high activity and favorable toxicity profiles. The prodrug-based drugamer therapeutic avoids burst release and its favorable safety profile could result from minimizing the dosing burst of active antibiotics compared to free drug formulations. The release profiles of prodrugs combined with active AM targeting could result in lowered drug contact with the airway during inhalation, a major reason for the respiratory adverse events (e.g, cough and dyspnea) associated with an inhalable antibiotic product[44]. Although the mannosylated drugamer systems did not cause any acute lung toxicity/injury, future studies are needed to characterize potential issues of the mannose-targeted ciprofloxacin in distributed organs and the reticuloendothelial system (RES) such as Kupffer cells in the liver. The ability to control the PK profile allows the design of dosing profiles to match antibiotic dosing requirements, e.g. by maximizing C_{max} and AUC for concentration-dependent antibiotics (e.g., fluoroquinolones and aminoglycoside) and extending T > MIC for time-dependent antibiotics (e.g., β-lactam and macrolides)[45,46]. The lung and alveolar macrophage PK profiles of both VC and CTM drugamers show greater AUC and extended T > MIC than free drug (**Figure 4.5 & Table 4.2**).

Though in this disease model the CTM was good enough to effect full cohort survival, the PK profiles of the VC drugamers were highly superior to the CTM drugamer and free drug in all the three PK parameters- $C_{max,}$ AUC, and T > MIC. This prominent difference between the cellular PK profiles of VC and CTM drugamers further demonstrates the modularity of the drugamer platform in targeting and enhancing intracellular release and dosing profiles. It is notable for future therapeutic and prophylactic studies that the dosing provided by the VC drugamer was sustained at the longest timepoint monitored of 48 h with intracellular ciprofloxacin concentration three magnitudes higher than MIC (0.03 μg/mL)[36,47]. While the intracellular C_{max} level of VC drugamer was found to be comparable to that of a liposomal ciprofloxacin formulation reported previously[41], the VC drugamer demonstrated markedly longer retention of

the released ciprofloxacin in the AMs (24 h for liposomal ciprofloxacin, > 48 h for VC drugamer), highlighting the sustained release characteristics of the drugamer platform. Future studies with a further optimized quantitative method will be conducted to evaluate the time frame that drugamers keep the released drug concentrations higher than MIC and also the subsequent duration when the concentrations is below MIC.

The superior antibiotic efficacy of the mannose-targeted drugamers was demonstrated in a highly lethal murine model of pulmonary *F. novicida* infection (**Figure 6)**. The full protection provided by both mannose-targeted drugamers (VC and CTM) compared to past pegylated drugamers in this model can be attributed to their increased internalization and sustained intracellular dosing achieved for both linkers[21]. The mannose-targeted CTM drugamer exhibits an excellent dosing profile that is sufficient to achieve full cohort survival in this *Francisella* challenge model and treatment regime. Thus it is not possible for the VC drugamer to show improvement in survival but the PK analysis clearly shows the strong improvement in dosing profile and extended intracellular dosing levels. We anticipate that these increases in the PK properties ($C_{max,}$ AUC, and T > MIC) of the VC drugamer will provide future opportunities for prophylactic therapy or for treatment of more advanced disease presentations. Additionally, the PK profiles of the VC drugamer could potentially fulfill the dosing requirements of both concentration- and time-dependent antibiotic classes. Taken together, the unique PK profiles and high activity may allow the mannose-targeted prodrug system (especially the VC drugamer) to be a useful PK modifier for improving the dosing regimens (e.g., reduce dosage and frequency) and for prophylactic application of different classes of antibiotics against pulmonary intracellular infections.

4.5 CONCLUSION

Pulmonary intracellular infections, such as *F. tularensis* and other CDC-classified Tier 1 pathogens (e.g. *Burkholderia pseudomallei*, the causative agent of melioidosis), require immediate medical intervention with localized and sustained intracellular delivery of concentrated drugs. We have demonstrated that a polymeric antibiotic prodrug platform can be engineered to dramatically enhance intracellular PK drug release profiles by incorporating mannose-targeting ligands and enzymatic drug release. Both targeted drugamers (VC & CTM)

provided higher AUC and persistent ciprofloxacin dosing above the minimum inhibitory concentration over a 48 h period in the lung and alveolar macrophages, resulting in full protection in a lethal *Francisella* murine challenge model. The overall enhancement of the intracellular PK properties ($C_{max,}$ AUC, and T > MIC) of the protease-responsive drugamer suggests the potential utility of this platform for prophylaxis or for treatment of more advanced disease presentations. Collectively, this drugamer platform creates new opportunities to construct effective antimicrobial systems with modular control of intracellular PK properties that match the dosing requirements of specific drug classes.

4.6 Acknowledgements

The authors thank LC-MS/MS support provided by School of Pharmacy's Mass Spectrometry Center at University of Washington. This work was supported by the Defense Threat Reduction Agency (Grant #HDTRA1-13-1-0047) and by the NIH (R01AI134729). F.Y.S. is an international student research fellow of the Howard Hughes Medical Institute and J.C. was a graduate research fellow of the National Science Foundation.

4.7 Competing financial interests

The authors declare no competing financial interests.

4.8 Appendix A. Supplementary information

4.9 Reference

1. Estimates of the global, regional, and national morbidity, mortality, and aetiologies of lower respiratory tract infections in 195 countries: a systematic analysis for the Global Burden of Disease Study 2015. *Lancet Infect Dis* **17,** 1133–1161 (2017).
2. Houben, R. M. G. J. & Dodd, P. J. The Global Burden of Latent Tuberculosis Infection: A Re-estimation Using Mathematical Modelling. *PLoS Med* **13,** e1002152 (2016).

3. The global burden of tuberculosis: results from the Global Burden of Disease Study 2015. *Lancet Infect Dis* **18,** 261–284 (2018).
4. World Health Organization. *Global Tuberculosis Report 2017*. (2017).
5. Lehar, S. M. *et al.* Novel antibody-antibiotic conjugate eliminates intracellular S. aureus. *Nature* **advance online publication SP - EP ,** 323–328 (2015).
6. Russell, D. G. Mycobacterium tuberculosis: here today, and here tomorrow. *Nat Rev Mol Cell Biol* **2,** 569–577 (2001).
7. Hall, J. D. *et al.* Infected-host-cell repertoire and cellular response in the lung following inhalation of Francisella tularensis Schu S4, LVS, or U112. *Infect Immun* **76,** 5843–5852 (2008).
8. Kubica, M. *et al.* A potential new pathway for Staphylococcus aureus dissemination: the silent survival of S. aureus phagocytosed by human monocyte-derived macrophages. *PLoS ONE* **3,** e1409 (2008).
9. World Health Organization. *Treatment of Tuberculosis*. (World Health Organization, 2010).
10. Dennis, D. T. *et al.* Tularemia as a Biological Weapon. *JAMA* **285,** 2763 (2001).
11. Dance, D. Treatment and prophylaxis of melioidosis. *Int. J. Antimicrob. Agents* **43,** 310–318 (2014).
12. Carryn, S. *et al.* Intracellular pharmacodynamics of antibiotics. *Infect Dis Clin North Am* **17,** 615–634 (2003).
13. Van Bambeke, F., Barcia-Macay, M., Lemaire, S. & Tulkens, P. M. Cellular pharmacodynamics and pharmacokinetics of antibiotics: current views and perspectives. *Curr Opin Drug Discov Devel* **9,** 218–230 (2006).
14. de Jager, P. & van Altena, R. Hearing loss and nephrotoxicity in long-term aminoglycoside treatment in patients with tuberculosis. *Int. J. Tuberc. Lung Dis.* **6,** 622–627 (2002).
15. Aschenbrenner, D. S. The FDA Revises Boxed Warning For Fluoroquinolones-Again. *Am J Nurs* **116,** 22–23 (2016).
16. Hamidi, M., Azadi, A., Rafiei, P. & Ashrafi, H. A pharmacokinetic overview of nanotechnology-based drug delivery systems: an ADME-oriented approach. *Crit Rev Ther Drug Carrier Syst* **30,** 435–467 (2013).
17. Hamblin, K. A. *et al.* Liposome Encapsulation of Ciprofloxacin Improves Protection against Highly Virulent Francisella tularensis Strain Schu S4. **58,** 3053–3059 (2014).
18. Cipolla, D., Blanchard, J. & Gonda, I. Development of Liposomal Ciprofloxacin to Treat Lung Infections. *Pharmaceutics* **8,** (2016).
19. Chang, M. *et al.* Smart linkers in polymer–drug conjugates for tumor-targeted delivery. *J Drug Target* **24,** 475–491 (2015).
20. Das, D. *et al.* RAFT polymerization of ciprofloxacin prodrug monomers for the controlled intracellular delivery of antibiotics. *Polym. Chem.* **7,** 826–837 (2016).
21. Das, D. *et al.* Synthetic Macromolecular Antibiotic Platform for Inhalable Therapy against Aerosolized Intracellular Alveolar Infections. *Mol. Pharmaceutics* **14,** 1988–1997 (2017).

22. Chen, J. *et al.* Nanostructured glycopolymer augmented liposomes to elucidate carbohydrate-mediated targeting. *Nanomedicine* **12,** 2031–2041 (2016).
23. Doronina, S. O. *et al.* Development of potent monoclonal antibody auristatin conjugates for cancer therapy. *Nat Biotech* **21,** 778–784 (2003).
24. Zhou, C. *et al.* Pharmacokinetics and pharmacodynamics of DSTA4637A: A novel THIOMAB antibody antibiotic conjugate against Staphylococcus aureus in mice. *MAbs* **8,** 1612–1619 (2016).
25. Synthetic polymeric drugs.
26. Kopecek, J. & Duncan, R. Targetable polymeric prodrugs. *J Control Release* **6,** 315–327 (1987).
27. Convertine, A. J., Benoit, D. S. W., Duvall, C. L., Hoffman, A. S. & Stayton, P. S. Development of a novel endosomolytic diblock copolymer for siRNA delivery. *J Control Release* **133,** 221–229 (2009).
28. Dubowchik, G. M. *et al.* Cathepsin B-Labile Dipeptide Linkers for Lysosomal Release of Doxorubicin from Internalizing Immunoconjugates: Model Studies of Enzymatic Drug Release and Antigen-Specific In Vitro Anticancer Activity. *Bioconjug Chem* **13,** 855–869 (2002).
29. Kingry, L. C. & Petersen, J. M. Comparative review of Francisella tularensis and Francisella novicida. *Front Cell Infect Microbiol* **4,** 35
30. Moad, G. *et al.* Living free radical polymerization with reversible addition-fragmentation chain transfer (the life of RAFT). *Polymer International* **49,** 993–1001 (2000).
31. Fonović, M. & Turk, B. Cysteine cathepsins and extracellular matrix degradation. *Matrix-mediated cell behaviour and properties* **1840,** 2560–2570 (2014).
32. Lockridge, O. Review of human butyrylcholinesterase structure, function, genetic variants, history of use in the clinic, and potential therapeutic uses. *Pharmacol Ther* **148,** 34–46 (2015).
33. Liu, W. *et al.* Antiflammin-1 attenuates bleomycin-induced pulmonary fibrosis in mice. *Respir Res* **14,** 101 (2013).
34. Malaviya, R., Laskin, J. D. & Laskin, D. L. Anti-TNFalpha therapy in inflammatory lung diseases. *Pharmacol Ther* **180,** 90–98 (2017).
35. Mazzon, E. & Cuzzocrea, S. Role of TNF-α in lung tight junction alteration in mouse model of acute lung inflammation. *Respir Res* **8,** 75–75 (2007).
36. Johansson, A., Berglund, L., Gothefors, L., Sjostedt, A. & Tarnvik, A. Ciprofloxacin for treatment of tularemia in children. *Pediatr Infect Dis J* **19,** 449–453 (2000).
37. Cohen, J. S. Peripheral neuropathy associated with fluoroquinolones. *Ann Pharmacother* **35,** 1540–1547 (2001).
38. Tennyson, L. E. & Averch, T. D. An Update on Fluoroquinolones: The Emergence of a Multisystem Toxicity Syndrome. *Urology Practice* **4,** 383–387 (2017).
39. Lowes, D. A., Wallace, C., Murphy, M. P., Webster, N. R. & Galley, H. F. The mitochondria targeted antioxidant MitoQ protects against fluoroquinolone-induced oxidative stress and

mitochondrial membrane damage in human Achilles tendon cells. *Free Radic. Res.* **43,** 323–328 (2009).
40. Oyston, P. C. F., Sjostedt, A. & Titball, R. W. Tularaemia: bioterrorism defence renews interest in Francisella tularensis. *Nat. Rev. Microbiol.* **2,** 967–978 (2004).
41. Chono, S., Tanino, T., Seki, T. & Morimoto, K. Efficient drug targeting to rat alveolar macrophages by pulmonary administration of ciprofloxacin incorporated into mannosylated liposomes for treatment of respiratory intracellular parasitic infections. *J Control Release* **127,** 50–58 (2008).
42. Su, F.-Y. *et al.* Polymer-augmented liposomes enhancing antibiotic delivery against intracellular infections. *Biomater Sci* **6,** 1976–1985 (2018).
43. Senter, P. D. & Sievers, E. L. The discovery and development of brentuximab vedotin for use in relapsed Hodgkin lymphoma and systemic anaplastic large cell lymphoma. *Nat Biotechnol* **30,** 631–637 (2012).
44. Barker, A. F. *et al.* Tobramycin solution for inhalation reduces sputum Pseudomonas aeruginosa density in bronchiectasis. *Am J Respir Crit Care Med* **162,** 481–485 (2000).
45. Jacobs, M. R. Optimisation of antimicrobial therapy using pharmacokinetic and pharmacodynamic parameters. *Clinical Microbiology and Infection* **7,** 589–596
46. Leekha, S., Terrell, C. L. & Edson, R. S. General principles of antimicrobial therapy. *Mayo Clin Proc* **86,** 156–167 (2011).
47. Urich, S. K. & Petersen, J. M. In Vitro Susceptibility of Isolates of Francisella tularensis Types A and B from North America. *Antimicrob. Agents Chemother.* **52,** 2276–2278 (2008).

4.10 SUPPLEMENTARY INFORMATION

A. Supplementary method

1. Synthesis of ciprofloxacin methacrylate monomer with Valine-Citrulline dipeptide linker (VC monomer)

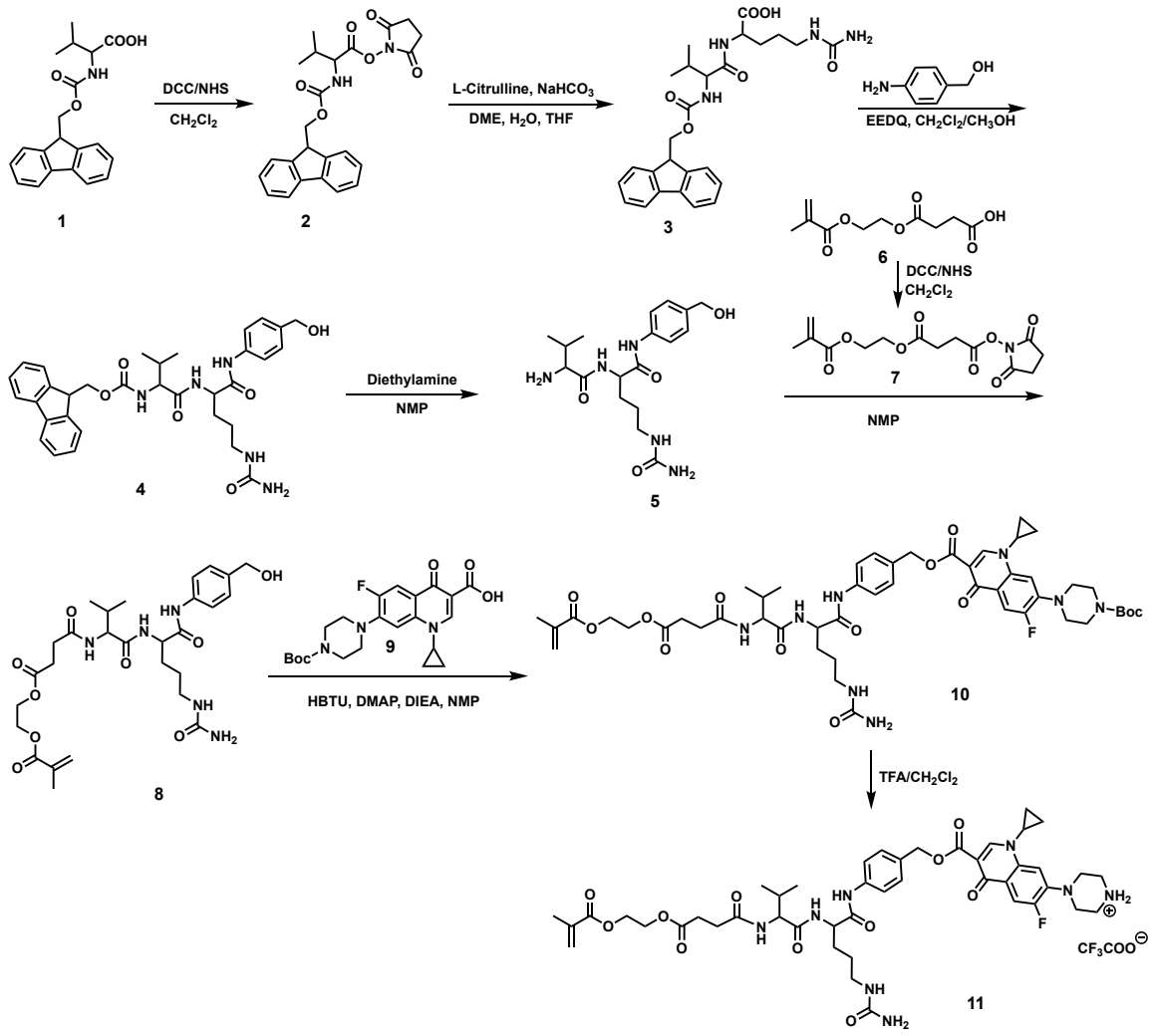

Scheme S1. Synthesis of ciprofloxacin methacrylate monomer with Val-Cit dipeptide linker (VC monomer, 11). A self-immolative spacer, *p*-aminobenzyl alcohol (PABOH), was used to situate the enzymatic cleavage site from the drugamer matrix.

SMA hydroxysuccinimide ester (7, SMA-OSu):

To an ice cold solution of mono-2-(methacryloyloxy)ethyl succinate (SMA, **6**) 11.5 g (50 mmol) in 140 mL CH_2Cl_2, were added *N*-hydroxysuccinimide 5.75 g (50 mmol) and *N*-*N*′-

dicyclohexylcarbodimide 10.29 g (53 mmol). After 15 min, the ice bath was removed, and the reaction mixture was stirred at room temperature for 16 h. The byproduct dicyclohexylurea was filtered off, and the filtrate was concentrated on the rotavap to obtain SMA-OSu (**7**). This product was used without purification for the next steps. Yield: 16.32 g (99.7 %). ^{1}H NMR (300 MHz, $CDCl_3$) δ 1.96 (s, 3H), 2.79 (t, J = 6.9 Hz, 2H), 2.85 (s, 4H), 2.97 (t, J = 6.9 Hz, 2H), 4.38 (m, 4H), 5.61 (s, 1H), 6.13 (s, 1H). MS (ESI, m/z): calculated for $C_{14}H_{17}NO_8$ (M): 327.3, found: 350.4 $[M+Na]^+$ and 677.7 $[2M+Na]^+$.

SMA-Val-Cit-PABOH (8):

Intermediates **2 - 5** were prepared according to published literature procedures[1].

To Val-Cit-PABOH (**5**) 1.75 g (4.61 mmol) in 15 mL N-methyl-2-pyrrolidone (NMP) was added SMA-OSu (**7**) 1.81 g (5.53 mmol) and the resulting solution was stirred at room temperature for 16 h. The reaction mixture was precipitated into 3:1 ether/hexane (160 mL), vortexed and centrifuged in 50 mL conical tubes. The sticky precipitate obtained was carefully separated by decanting the supernatant and washed repeatedly with ether by vortexing and centrifuging. Yield = 2.35 g (86.08 %). ^{1}H NMR (300 MHz, DMSO-d_6) δ 0.85 (t, J = 7.5 Hz, 6H), 1.41 (m, 2H), 1.51 – 1.81 (m, 2H), 1.87 (s, 3H), 1.99 (m, 1H), 2.41 – 2.59 (m, 4H, merged with solvent peak), 2.99 (m, 2H), 4.15 – 4.40 (m, 6H), 4.43 (d, J = 5.6 Hz, 2H), 5.10 (t, J = 5.7 Hz, 1H), 5.41 (s, 2H), 5.70 (s, 1H), 5.98 (t, J = 5.7 Hz, 1H), 6.04 (s, 1H), 7.23 (d, J = 8.5, 2H), 7.55 (d, J = 8.5, 2H), 7.96 (d, J = 8.5, 1H), 8.06 (d, J = 7.6 Hz, 1H), 9.85 (s, 1H). MS (ESI, m/z): calculated for $C_{28}H_{41}N_5O_9$ (M): 591.7, found: 614.5 $[M+Na]^+$.

7-(4-(*tert*-Butoxycarbonyl)piperazin-1-yl)-1-cyclopropyl-6-fluoro-4-oxo-1,4-dihydroquionoline-3-carboxylic acid (9, Boc ciprofloxacin):

Boc ciprofloxacin was synthesized as described previously[2]. To 20 g (60 mmol) of ciprofloxacin in 350 mL of dioxane:water (1:1) was added 90 mL 1N NaOH, followed by 20 g (91.6 mmol) of di-tert-butyl dicarbonate. The reaction mixture was stirred at room temperature for 17 h. The white precipitate obtained was filtered, washed with water and then with acetone. The product was dried under high vacuum overnight. Yield = 25.14 g (96.5 %). ^{1}H NMR (300 MHz, $CDCl_3$) δ 1.20 (m, 2H), 1.40 (m, 2H), 1.49 (s, 9H), 3.29 (t, J = 5.0 Hz, 4H), 3.54 (m, 1H), 3.67 (t, J = 5.0 Hz, 4H), 7.37 (d, J = 7.1 Hz, 1H), 7.99 (d, J = 12.9 Hz, 1H), 8.73 (s, 1H). MS (ESI, m/z): calculated for $C_{22}H_{26}FN_3O_5$ (M): 431.5, found: 432.6 $[M+H]^+$, 454.4 $[M+Na]^+$ and 885.6 $[2M+Na]^+$.

SMA-Val-Cit-PAB-Boc ciprofloxacin (10):

A mixture of boc ciprofloxacin (**9**) 680 mg (1.58 mmol), N,N,N',N'-tetramethyl-O-(1*H*-benzotriazol-1-yl)uronium hexafluorophosphate (HBTU) 1.71 g (4.5 mmol) and N,N-

diisopropylethylamine 1.58 mL (9 mmol) in 13 mL NMP was stirred at room temperature for 15 minutes. Then, N,N-dimethylpyridin-4-amine (DMAP) 183 mg (1.5 mmol) was added followed by SMA-Val-Cit-PABOH (**8**) 888 mg (1.5 mmol) and the stirring was continued for 48 h at room temperature. The reaction mixture was diluted with 200 mL 10 % 2-propanol/$CHCl_3$, washed with water (100 mL) and brine (100 mL). The organic phase was dried over anhydrous sodium sulfate and the solvent was concentrated under reduced pressure. Crude product was purified by silica gel column chromatography using 11 % methanol in CH_2Cl_2 containing 0.2 % triethylamine. The product obtained after column chromatography was dissolved in 1:4 methanol/$CHCl_3$ (20 mL) and triturated into ether. Yield = 737 mg (53.03 %). ^{1}H NMR (300 MHz, DMSO-d_6) δ 0.85 (t, J = 7.7 Hz, 6H), 1.10 (m, 2H), 1.26 (m, 2H), 1.32 – 1.50 (1s, 1m, 11H), 1.53 – 1.78 (m, 2H), 1.87 (s, 3H), 1.98 (m, 1H), 2.40 – 2.60 (m, 4H, merged with solvent peak), 2.98 (m, 2H), 3.21 (s, 4H), 3.54 (s, 4H), 3.64 (s, 1H), 4.15 – 4.30 (m, 5H), 4.37 (q, J = 5.1, 1H), 5.20 (s, 2H), 5.41 (s, 2H), 5.69 (s, 1H), 5.98 (t, J = 5.6 Hz, 1H), 6.02 (s, 1H), 7.41 (d, J = 8.6, 2H), 7.46 (d, J = 7.4, 1H), 7.62 (d, J = 8.6, 2H), 7.79 (d, J = 13.3, 1H), 7.96 (d, J = 8.5, 1H), 8.09 (d, J = 7.5, 1H), 8.46 (s, 1H), 9.96 (s, 1H). MS (ESI, m/z): calculated for $C_{50}H_{65}FN_8O_{13}$ (M): 1005.1, found: 1006.3 $[M+H]^+$ and 1028.0 $[M+Na]^+$.

SMA-Val-Cit-PAB-ciprofloxacin (11):

SMA-VC-PAB-Boc ciprofloxacin (**10**) 550 mg (0.55 mmol) in 20 % trifluoroacetic acid in CH_2Cl_2 (10 mL) was stirred at room temperature for 25 minutes. The reaction mixture was triturated into ether and the solid obtained was washed with ether. Yield = 527 mg (94.02 %). ^{1}H NMR (300 MHz, DMSO-d_6) δ 0.84 (t, J = 7.5 Hz, 6H), 1.10 (m, 2H), 1.26 (m, 2H), 1.42 (m, 2H), 1.52 – 1.80 (m, 2H), 1.86 (s, 3H), 1.99 (m, 1H), 2.40 – 2.58 (m, 4H, merged with solvent peak), 2.96 (m, 2H), 3.20– 3.61 (2s, merged with H_2O peak, 8H), 3.65 (s, 1H), 4.15 – 4.30 (m, 5H), 4.36 (m, 1H), 5.20 (s, 2H), 5.40 (bs, 2H), 5.68 (s, 1H), 5.98 (t, J = 5.8 Hz, 1H), 6.02 (s, 1H), 7.41 (d, J = 8.6, 2H), 7.48 (d, J = 7.4, 1H), 7.62 (d, J = 8.6, 2H), 7.82 (d, J = 13.2, 1H), 7.95 (d, J = 8.5, 1H), 8.08 (d, J = 7.4, 1H), 8.47 (s, 1H), 8.89 (s, 2H), 9.95 (s, 1H). MS (ESI, m/z): ESI-MS calculated for $C_{47}H_{58}F_4N_8O_{13}$ (M): 1019 and $C_{45}H_{57}FN_8O_{11}$ (M-CF_3COOH): 905.0, found: 905.7 $[M\text{-}CF_3COOH+H]^+$ and 453.6 $[M\text{-}CF_3COOH+2H]^{2+}$.

2. Synthesis of ciprofloxacin methacrylate monomer with phenyl ester linker (CTM monomer)

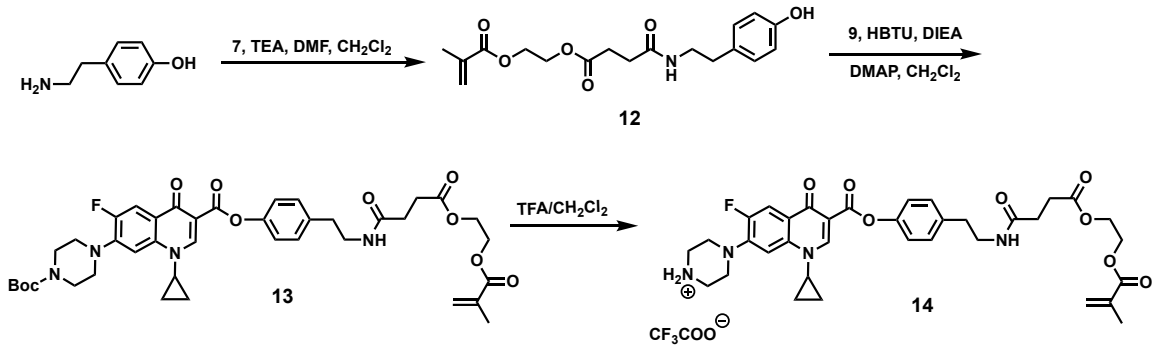

Scheme S2. Synthesis of ciprofloxacin methacrylate monomer with phenyl ester linker (CTM monomer, 14).

Butanoic acid, 4-[(4-hydroxyphenyl)ethylamino]-4-oxo, 1-(2 methacryloyloxy)ethyl ester (12):

SMA-OSu (**7**) 16.35 g (50 mmol) in 20 mL CH_2Cl_2 was added to 4-(aminoethyl)phenol 8.22 g (60 mmol) pre-dissolved in 40 mL *N*,*N*-dimethylformamide at 4 °C, followed by 16.73 mL (0.12 mol) triethylamine. After stirring for 4 h at room temperature, the reaction mixture was diluted with 200 mL CH_2Cl_2, and washed with water (2 X 100 mL). The organic layer was dried over anhydrous sodium sulfate and concentrated under reduced pressure. The oily residue obtained was triturated with 1:1 ether/hexane and then further purified by silica gel column chromatography using 5 % methanol in chloroform. Yield: 14.61 g (83.6 %). ^{1}H NMR (300 MHz, $CDCl_3$) δ 1.93 (s, 3H), 2.43 (t, J = 6.9 Hz, 2H), 2.69 (m, 4H), 3.46 (q, J = 6.9 Hz, 2H), 4.31 (s, 4H), 5.59 (s, 1H), 5.87 (t, J = 5.4 Hz, 1H), 6.12 (s, 1H), 6.71 (s, 1H), 6.77 (d, J = 8.4 Hz, 2H), 7.00 (d, J = 8.4 Hz, 2H). MS (ESI, m/z): calculated for $C_{18}H_{23}NO_6$ (M): 349.4, found: 373.0 $[M+Na]^+$.

Boc-CTM (13):

Boc ciprofloxacin (**9**) 4.3 g (10 mmol) and N,N-dimethylpyridin-4-amine (DMAP) 1.22 g (10 mmol) were taken in 350 mL CH_2Cl_2 and cooled to 4 °C. To this solution, N,N,N',N'-tetramethyl-O-(1*H*-benzotriazol-1-yl)uronium hexafluorophosphate (HBTU) 9.48 g (25 mmol) was added, followed by N,N-diisopropylethylamine 7.0 mL (40 mmol). After 10 min at 4 °C, the reaction mixture was stirred at room temperature for 30 min, and then cooled back to 4 °C. Phenolic monomer **(12)** 3.49 g (10 mmol) was introduced and the reaction was continuously stirred at 4 °C for 20 min, and then at room temperature for 16 h. The reaction mixture was filtered and the filtrate was washed with water (150 mL) and brine (150 mL). The organic phase

was dried over anhydrous sodium sulfate and the solvent was evaporated under reduced pressure. The residue was precipitated in diethyl ether, and then purified by silica gel column chromatography using 30 % tetrahydrofuran in chloroform. Yield = 5.76 g (75.5 %). ^{1}H NMR (300 MHz, $CDCl_3$) δ 1.18 (m, 2H), 1.35 (q, J = 6.7 Hz, 2H), 1.5 (s, 9H), 1.94 (s, 3H), 2.43 (t, J = 6.9 Hz, 2H), 2.68 (t, J = 6.9 Hz, 2H), 2.82 (t, J = 6.9 Hz, 2H), 3.23 (t, J = 4.8 Hz, 4H), 3.49 (m, 3H), 3.66 (t, J = 4.8 Hz, 4H), 4.33 (s, 4H), 5.58 (s, 1H), 5.78 (t, J = 5.7 Hz, 1H), 6.12 (s, 1H), 7.15 (d, J = 8.4, 2H), 7.21 (d, J = 8.4, 2H), 7.30 (d, J = 7.2, 1H), 8.07 (d, J = 13.2 Hz, 1H), 8.65 (s, 1H). MS (ESI, m/z): calculated for $C_{40}H_{47}FN_4O_{10}$ (M): 762.8, found: 763.9 $[M+H]^+$ and 785.7 $[M+Na]^+$.

CTM (14):

BocCTM (**13**) 2.29 g (3 mmol) was treated with 25 % trifluoroacetic acid in CH_2Cl_2 (60mL) at 4 °C, and the resulting solution was stirred at 4 °C for 5 min, and then at room temperature for 2 h. The reaction solution was concentrated to 10 mL under reduced pressure and then precipitated into ether. Yield = 2.31 g (99.1%). ^{1}H NMR (300 MHz, DMSO-d_6) δ 1.15 (m, 2H), 1.26 (m, 2H), 1.85 (s, 3H), 2.33 (t, J = 6.9 Hz, 2H), 2.50 (t, merged with solvent peak, 2H), 2.70 (t, J = 7.4 Hz, 2H), 3.25 (q, J = 6.9 Hz, 2H), 3.33 (s, 4H), 3.45 (s, 4H), 3.71 (m, 1H), 4.26 (s, 4H), 5.67 (s, 1H), 6.02 (s, 1H), 7.09 (d, J = 8.4, 2H), 7.25 (d, J = 8.4, 2H), 7.51 (d, J = 7.5, 1H), 7.82 (d, J = 13.2 Hz, 1H), 7.99 (t, J = 5.6 Hz, 1H), 8.64 (s, 1H), 9.02 (bs, 2H). MS (ESI, m/z): calculated for $C_{37}H_{40}F_4N_4O_{10}$ (M): 776.7 and $C_{35}H_{39}FN_4O_8$ (M-CF_3COOH): 662.7, found: 663.5 $[M-CF_3COOH+1]^+$ and 685.7 $[M-CF_3COOH+Na]^+$

3. Synthesis of mannose methacrylate monomer

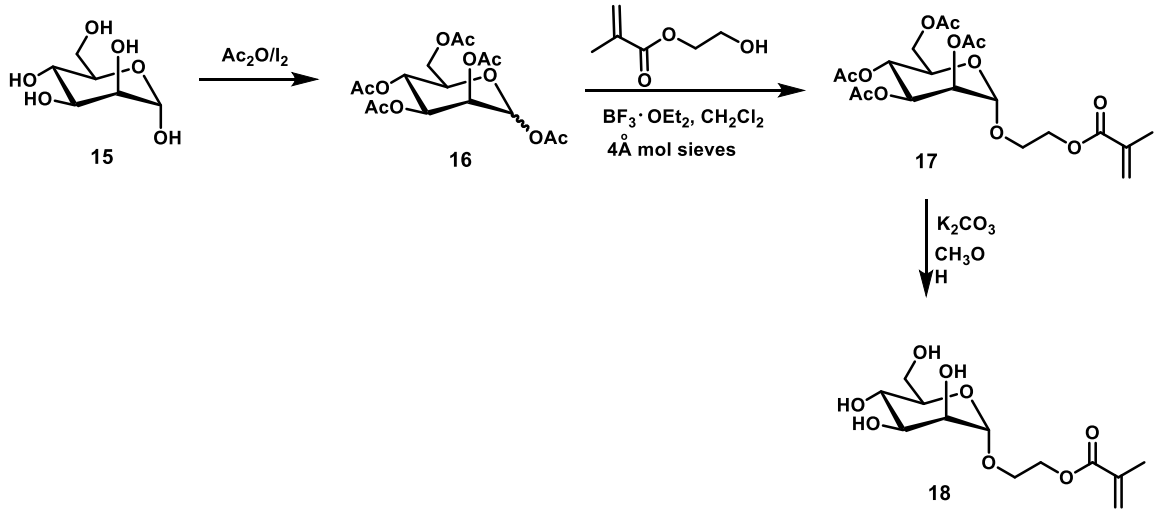

Scheme S3. Synthesis of mannose methacrylate monomer (18).

Synthesis of 2-(α-D-mannosyloxy)ethyl methacrylate (18):

α-D-mannose pentaacetate (**15**) was prepared following literature procedure[3].

To a solution of α-D-mannose pentaacetate **16** (9.0 g, 23.05 mmol) and 2-hydroxyethyl methacrylate (4.5 g, 34.58 mmol) in 40 mL anhydrous CH_2Cl_2 was added activated molecular sieves 4Å (5 g). After 30 min at room temperature, the mixture was cooled to 0 °C and $BF_3 \cdot Et_2O$ (20 mL, 0.16 mol) was added slowly. After stirring for 30 min at 0 °C and an additional 20 h at room temperature, the reaction mixture was filtered and diluted with 100 mL CH_2Cl_2. The resulting solution was washed with water (1 x 100 mL), saturated aqueous solution of $NaHCO_3$ (3 x 100 mL) and again with water (2 x 100 mL). The organic layer was dried over anhydrous sodium sulfate and concentrated under reduced pressure. This crude 2-(2',3',4',6'-tetra-*O*-acetyl-α-D-mannosyloxy)ethyl methacrylate (**17**) was dissolved in 70 mL MeOH, treated with K_2CO_3 (4.0 g, 28.94 mmol) and stirred for 10 min. The reaction solution was neutralized by filtering into a flask containing Amberlite® IR120 hydrogen form resin (18 g). The resin was filtered off and the filtrate was subsequently concentrated under reduced pressure. The resulting oily liquid was purified by silica gel column chromatography using 12 % MeOH in $CHCl_3$. The product obtained after column chromatography was further purified by precipitating into ether. Overall yield for two steps = 1.90 g (28.2 %). ^{1}H NMR (300 MHz, DMSO-d_6)) δ 1.88 (s, 3H), 3.28 – 3.49 (m, 4H, partially merged with solvent peak), 3.61 (m, 3H), 3.81 (m, 1H), 4.23 (m, 2H), 4.43 (t, J = 5.9 Hz, 1H), 4.57 (d, J = 5.5, 2H), 4.65 (s, 1H), 4.72 (s, 1H), 4.73 (s, 1H), 5.68 (s, 1H), 6.04 (s, 1H). MS (ESI, m/z): ESI-MS calculated for $C_{12}H_{20}O_8$ (M): 292.3, found: 315.3$[M+Na]^+$.

4. Drugamer characterization

The composition of drugamers was analyzed by spectroscopy (Bruker AV 300) in deuterated dimethyl sulfoxide (DMSO-d_6). To determine ciprofloxacin wt% in drugamers, Boc protected-ciprofloxacin (compound 9 in **Scheme 2**) was used an internal standard. Briefly, 5 mg drugamer was dissolved in Boc-protected ciprofloxacin solution (DMSO-d_6, 0.8 mg/mL, 0.7 mL) and analyzed using ^{1}H NMR. Molar composition of VC drugamer was determined by comparing a single proton resonance from the internal standard at δ = 8.67 ppm against a single proton resonance from ciprofloxacin containing drugamer at δ = 8.42 ppm. For CTM drugamer, molar composition was determined by comparing a single proton resonance from the internal standard at δ = 8.67 ppm against a single proton resonance from ciprofloxacin containing drugamer at δ = 7.10-7.12 ppm.

Size exclusion chromatography (SEC) was used to determine molecular weights and dispersities (M_w/M_n, Đ) of drugamers. To prepare materials for analysis, the purified drugamer was dissolved at 5 mg/mL in the running buffer (0.15 M sodium acetate buffered to pH 4.4 with acetic acid) for analysis by SEC. Samples were then applied to an OHpak SB-804 HQ column (Shodex) in line with a miniDAWN TREOS light scattering detector (Wyatt) and a OptiLab rEX refractive index detector (Wyatt). Absolute molecular weight average (M_n) was calculated based on dn/dc values calculated separately for each copolymer using ASTRA software (Wyatt). Additional synthetic details, summaries of drugamer properties, and representative NMR spectra and SEC profiles can be found in **Table 1** and **Figure S10-S12**.

5. Drugamer stability in human serum

The stability of VC drugamer in human serum was evaluated by incubating drugamers in 95% human serum and quantifying the released ciprofloxacin concentration over time. Drugamer solution (concentration ~ 3 mg/mL, equivalent to 1 mM ciprofloxacin, 20 μL) was added to human serum (180 μL, Sigma S7023) to a final ciprofloxacin concentration of 100 μM and incubated at 37 °C. At various time points, samples were diluted with acetonitrile 5 times to precipitate serum proteins and halt the reaction. The samples were centrifuged at 13,000 rpm for 4 min to collect supernatants. The supernatants were subsequently concentrated 4 times by speedvac and analyzed by LC-ESI MS (configured as described below). 100% ciprofloxacin release was defined by incubating drugamers (concentration ~ 3 mg/mL, equivalent to 1 mM ciprofloxacin, 20 μL) in 0.1 N NaOH (180 μL) for 24 hours at room temperature to hydrolyze all ester bonds between PAB and ciprofloxacin.

6. LC-ESI MS for ciprofloxacin quantification (*in vitro* samples)

Samples were analyzed with the Bruker Esquire-LC ion trap mass spectrometer (Bruker Daltonics with an 1100 liquid chromatograph system (Hewlett Packard). The liquid chromatography separation was performed on an Agilent zorbax SB-C18 column (narrow bore 2.1 × 100 mm, 3.5 μm) (Agilent Technologies) with mobile phase A (94% water + 5% acetonitrile + 1% acetic acid) and mobile phase B (99% acetonitrile + 1% acetic acid). The column was kept at 25°C and the flow rate was 0.2 mL/min. The linear gradient was as follows: 0–22 min, 10–90% B linear; 22–24 min, 90–10% B linear; 8 min post time with 90% mobile phase A to flush and equilibrate the column. The autosampler was set at 15 °C. The injection volume was 10 μL. UV detection was carried out at 280 nm. Mass spectra were acquired with positive electrospray ionization at the capillary voltage of 4,000 V and the end plate offset of -500V. The nebulizer gas was 30 psi. The dry gas flow was 10 L/min and the dry temperature was 350 ºC.

7. Tissue sample process for liquid chromatography-tandem mass spectrometry (LC-MS/MS) analysis

Organs were first mixed with 1 mL of ultrapure H_2O (0.8 mL for liver samples) and homogenized using an Omni Bead Ruptor 24 (OMNI International Inc., Kennesaw, GA, USA) shaken for 25 seconds at 24 °C (3 homogenization cycle). Homogenized tissues were then diluted 10x with ultrapure water (all except spleen and plasma) to aid ciprofloxacin extraction. 300 µL aliquots were taken out and the internal standard ciprofloxacin-d8 (10 µL of 500 ng/mL) and ultrapure water (10 µL, to compensate the volume of standard solution added in the 300 µL non-treated tissue homogenate) were added and vortexed for 1 min. The aliquot was then diluted 3 times with ACN (600 µL) to extract the released ciprofloxacin and to precipitate proteins. Samples were vortexed for another 1 minute and centrifuged at 18000xg for 20 minutes at 4ºC. The supernatant was collected and stored on ice until analyzed for ciprofloxacin via LC-MS/MS.

The bronchoalveolar lavage fluid was centrifuged to collect alveolar macrophages (4 °C, 400×g, 15 min). The collected cells were washed with PBS and centrifuged again to remove the supernatant. The cell pellet was resuspended in PBS (50 µL) and the obtained cell number was counted using crystal violet staining (0.1% in 0.1 M citric acid) to determine the total cell volume. The average mouse alveolar macrophage cell volume is 493±161 x 10^{-9} L^4. The cell suspension was then mixed with an internal standard solution, ciprofloxacin-d8 (5 µL of 500 ng/mL in H_2O), diluted 3x in ACN and incubated on ice for 1 hour to lyse the cells. Cell lysates were lyophilized by evaporation under N_2 (TurboVap; Biotage), reconstituted in 150 µL of 66% ACN, and centrifuged at 18000xg for 20 minutes at 4 ºC. The collected supernatants were stored on ice until analyzed via LC-MS/MS.

Plasma was collected from blood by centrifuging the BD PST plasma tubes (BD Biosciences) for 10 minutes at 600xg at room temperature. To a 40 µL aliquot of plasma sample, the internal standard ciprofloxacin-d8 (5 µL of 500 ng/mL) and ultrapure water (5 µL, to compensate the volume of standard solution added in 40 µL blank plasma) were added. Those samples were vortexed for 1 minute, diluted 3 times with ACN (100 µL). Samples were subsequently vortexed for another 1 minute and centrifuged at 18000xg for 20 minutes at 4ºC. The supernatant was collected and stored on ice until analyzed via LC-MS/MS.

8. Determination of ciprofloxacin concentrations in tissues using LC-MS/MS

Ciprofloxacin concentrations in tissue samples were analyzed with an Agilent 1290 Infinity LC system (Agilent Technologies) under gradient elution using a Hypersil GOLD PFP column (100 mm x 2.1 mm internal diameter, 1.9 µm particle size) (Thermo Scientific). The column was maintained at room temperature. The mobile phase was a mixture of (A) H_2O containing 10 mM

formic acid and (B) acetonitrile containing 10 mM formic acid at a flow rate of 0.3 mL/min. The linear gradient was as follows: a gradient of 10%–100% B over 4 minutes followed by 1 min 100% B, then 0.1 minute to 10% B to re-equilibrate the column for 1.9 min. The autosampler was set at 5 °C; the injection volume was 10 μL.

The 6460 Triple Quad mass spectrometer (Agilent Technologies) was operated in a positive ion multiple reaction-monitoring (MRM) mode. The ciprofloxacin precursor (Q1) ion monitored was 332.0 m/z and the product (Q3) ion monitored was 314.1 m/z. Internal standard ciprofloxacin-d8 precursor (Q1) ion monitored was 340.0 m/z and the product (Q3) ion monitored was 322.1 m/z. The MS/MS setting parameters were as follows: collision energy 13 eV, nozzle voltage 500 V, capillary voltage 4500 V, nebulizer gas 45 psi, gas temperature 350 ºC, dwell time 150 ms.

For ciprofloxacin concentration determinations in plasma, linear calibration curves were obtained for 9.77–5000 ng/mL concentration range by spiking ciprofloxacin into non-treated plasma that were treated similarly to samples. The concentration ranges of calibration curves for organs and alveolar macrophage cell lysate were 0.61–312.5 ng/mL and 19.53–10,000 ng/mL, respectively, in the corresponding non-treated tissues or macrophages.

B. Supplementary data

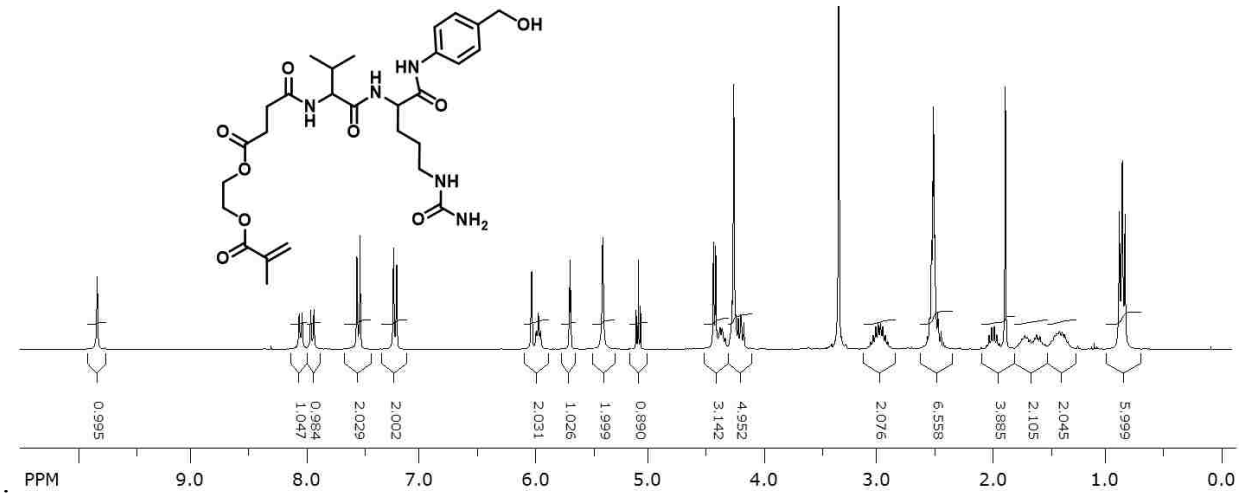

Figure S1. [1]H-NMR spectrum of SMA-Val-Cit-PABOH (**8**)

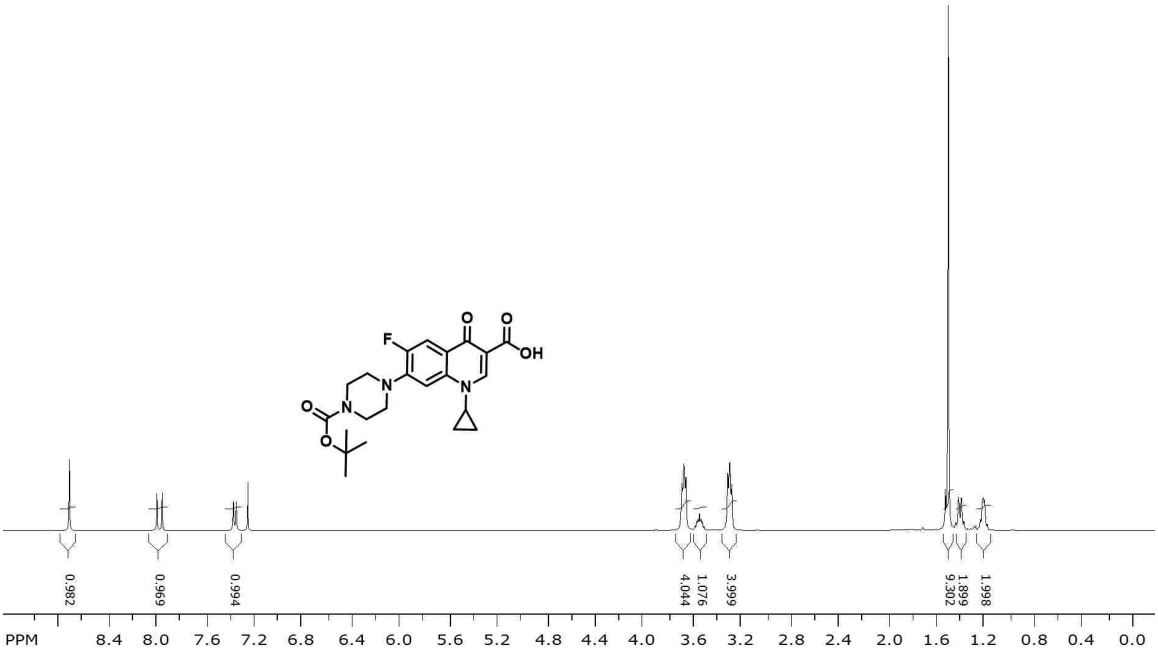

Figure S2. [1]H-NMR spectrum of Boc ciprofloxacin (**9**)

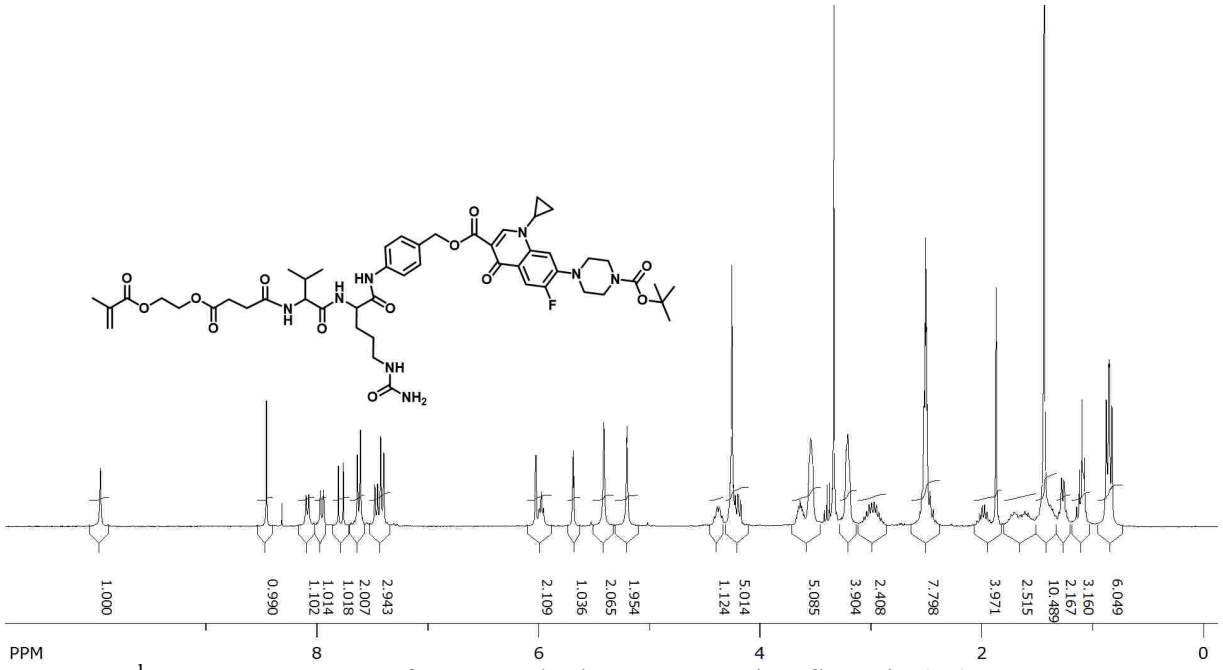

Figure S3. [1]H-NMR spectrum of SMA-Val-Cit-PAB-Boc ciprofloxacin (**10**)

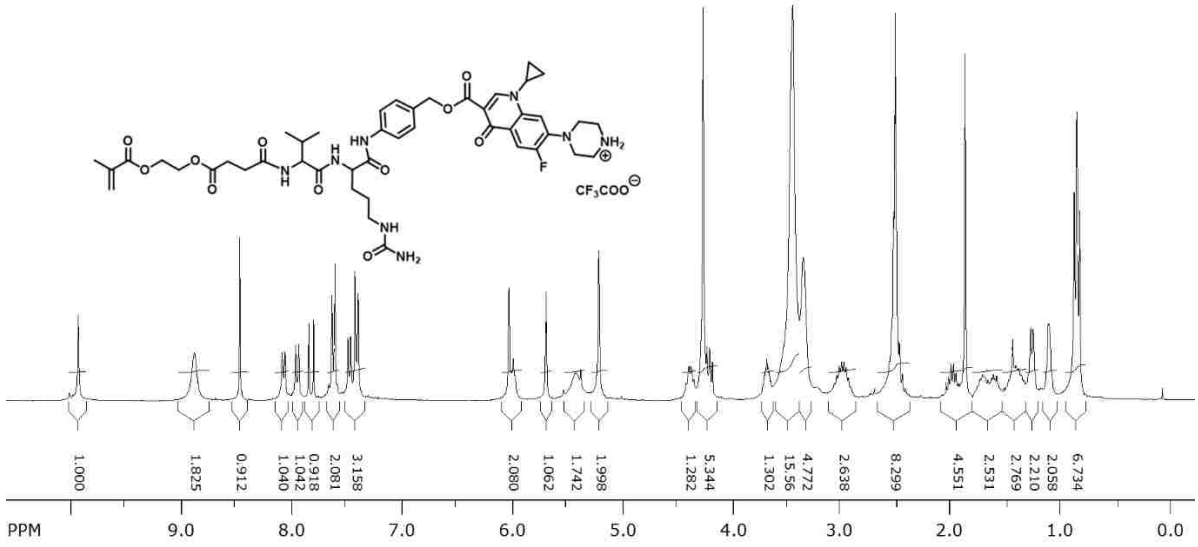

Figure S4. [1]H-NMR spectrum of cathepsin B cleavable monomer SMA-Val-Cit-PAB-ciprofloxacin (**11**)

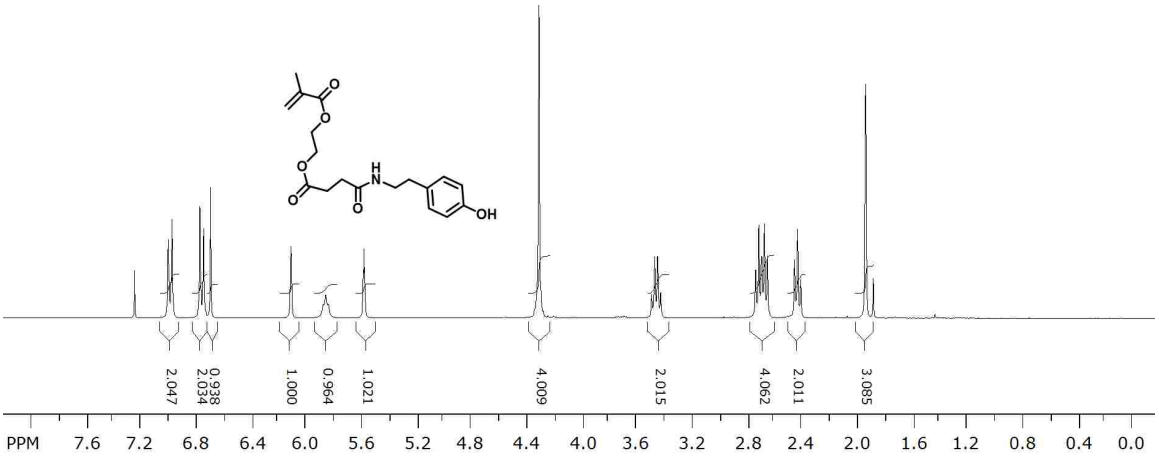

Figure S5. [1]H-NMR spectrum of butanoic acid, 4-[(4-hydroxyphenyl)ethylamino]-4-oxo, 1-(2-methacryloyloxy)ethyl ester (**12**)

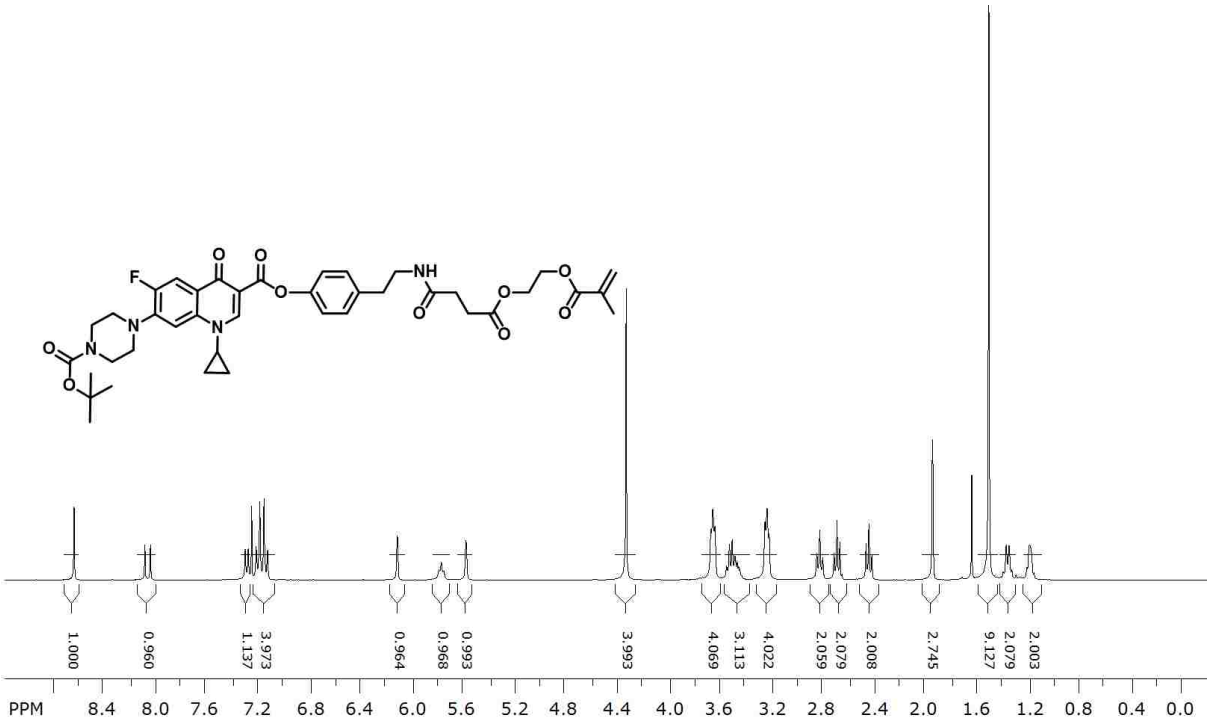

Figure S6. [1]H-NMR spectrum of BocCTM (**13**)

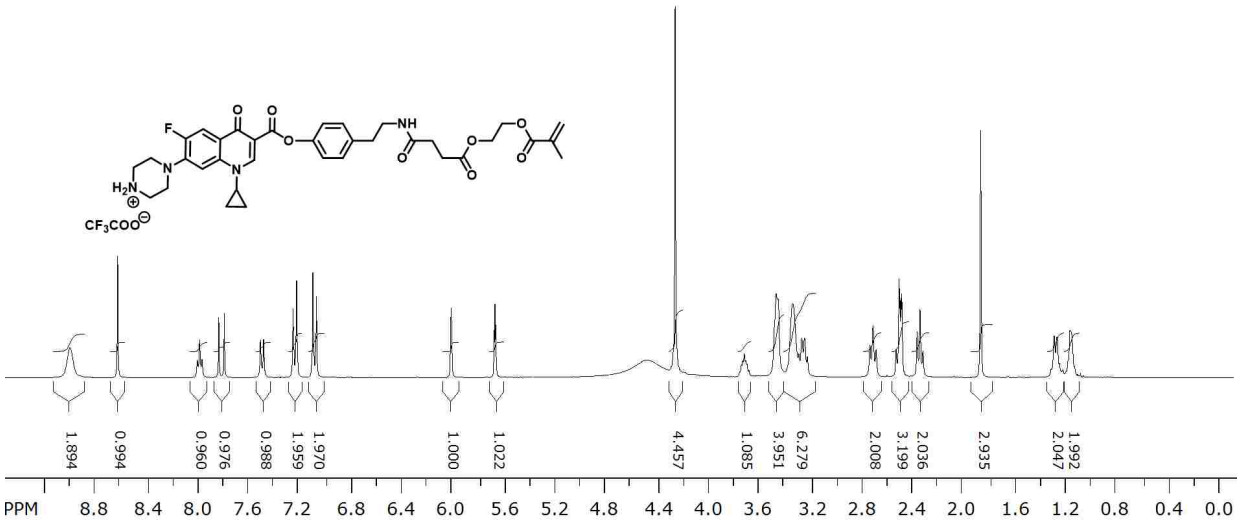

Figure S7. [1]H-NMR spectrum of CTM (**14**)

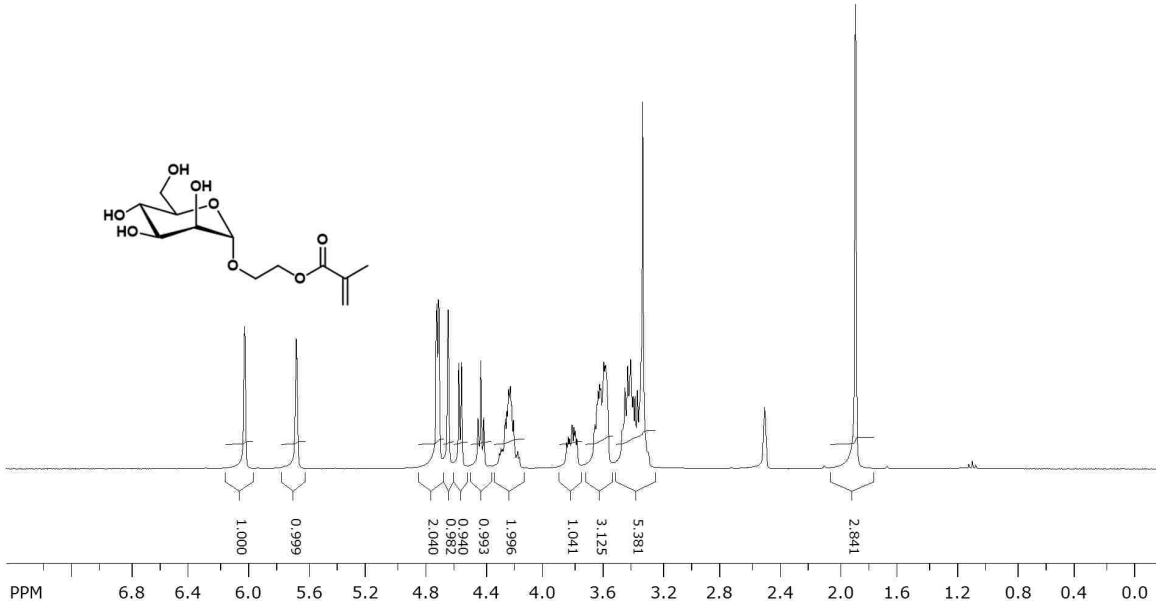

Figure S8. [1]H-NMR spectrum of 2-(α-D-mannosyloxy)ethyl methacrylate (mannose monomer)

Cathepsin B-mediated ciprofloxacin release form prodrug monomers

To investigate if the VC dipeptide linker in the prodrug monomer construct is accessible for lysosomal protease, ciprofloxacin monomers were incubated with lysosomal protease cathepsin B for various durations, and the released ciprofloxacin was identified and quantified using LC-ESI MS (**Figure S9**). In contrast to the control assay lacking the enzyme, the presence of cathepsin B rapidly induced ciprofloxacin release from VC monomer in its active form (~75% in 30 min, **Figure S9A, C, D**). By contrast, no detectable ciprofloxacin was released from CTM monomer after 24 h incubation with cathepsin B (**Figure S9B**).

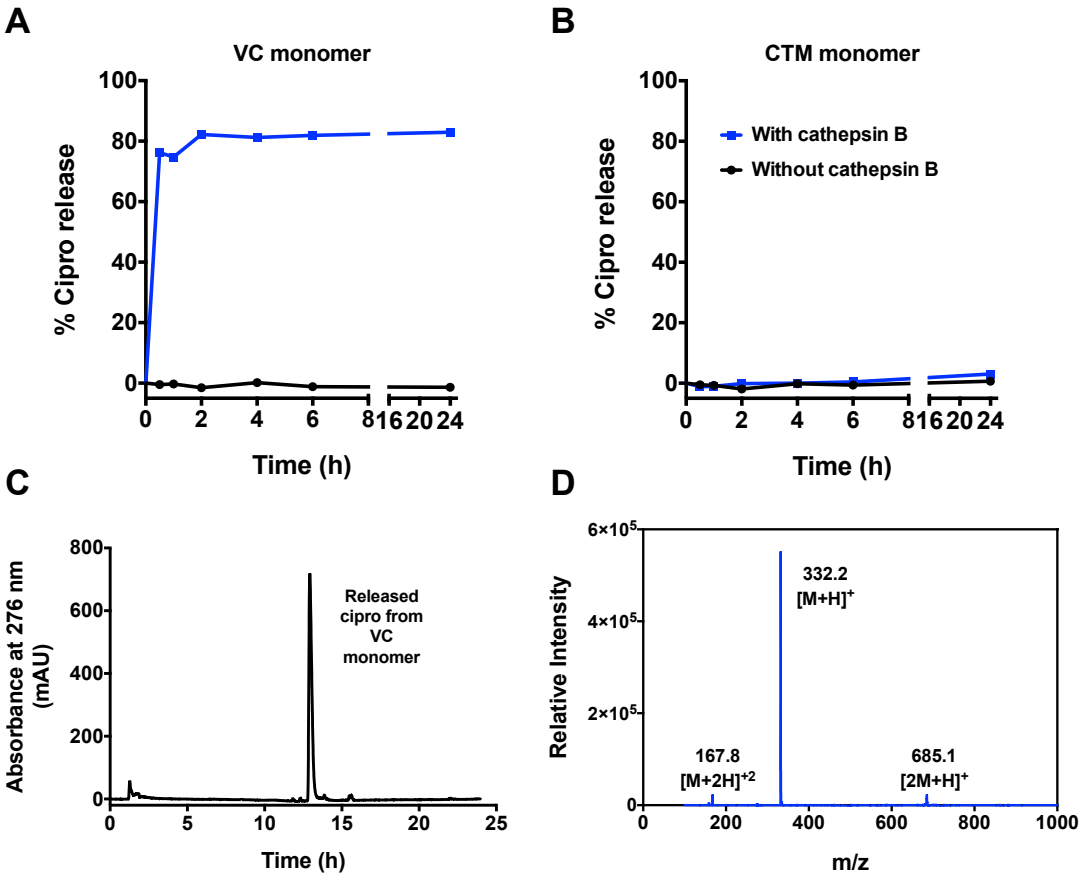

Figure S9. Lysosomal protease (cathepsin B)-mediated ciprofloxacin release from prodrug monomers with either protease cleavable Val-Cit dipeptide linker (VC monomer) or hydrolytic ester linker (CTM monomer). Monomers were incubated with human cathepsin B and the released ciprofloxacin was quantified using LC-ESI MS. ciprofloxacin release kinetics of VC monomer (A) and CTM monomer (B). (C) Liquid chromatogram showing the released ciprofloxacin from VC monomer after 4 h incubation with cathepsin B. (D) ESI-MS identified the released ciprofloxacin peak shown in (C). Cipro: ciprofloxacin.

Feed molar ratio		Monomer conversion[a] (%)	Ciprofloxacin wt%[b]	Solubility in PBS[c]
Mannose	VC			
5.5	1	78	9.70	✓
3	1	72	11.24	✗
2.5	1	70	14.47	✗
2	1	52	14.52	✗
1	1	37	17.40	✗

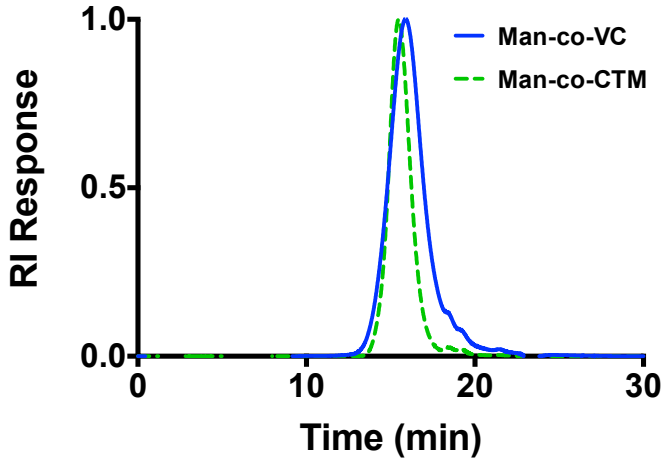

Figure S10. Representative size exclusion chromatography (SEC) of polymeric ciprofloxacin prodrugs with Val-Cit dipeptide linker (Man-*co*-VC) or ester linker (Man-*co*-CTM). Man: mannose monomer. VC: ciprofloxacin monomer with Val-Cit dipeptide linker. CTM: ciprofloxacin monomer with phenol ester linker. RI: refractive index.

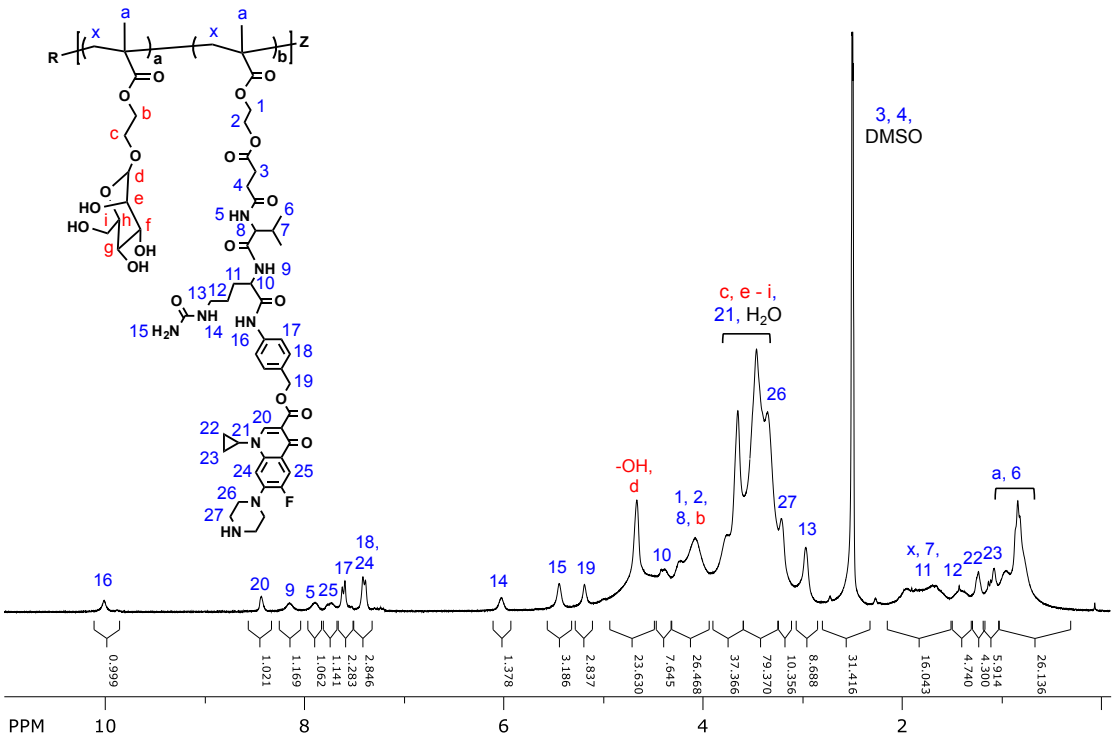

[redacted]

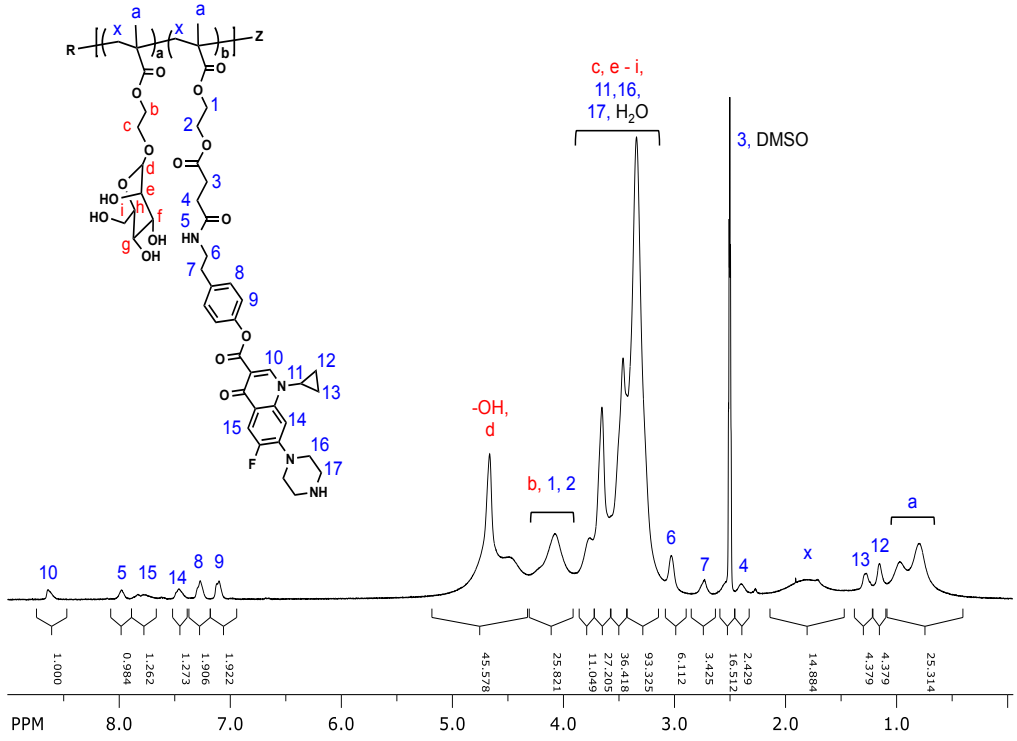

[redacted]

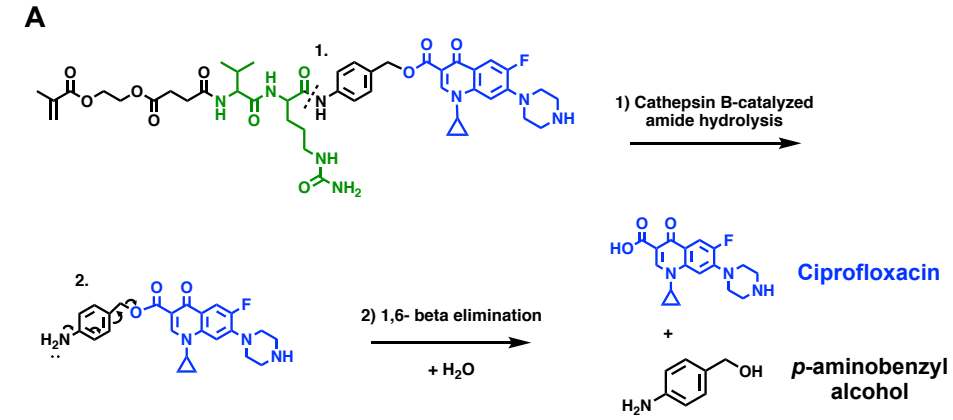

[redacted]

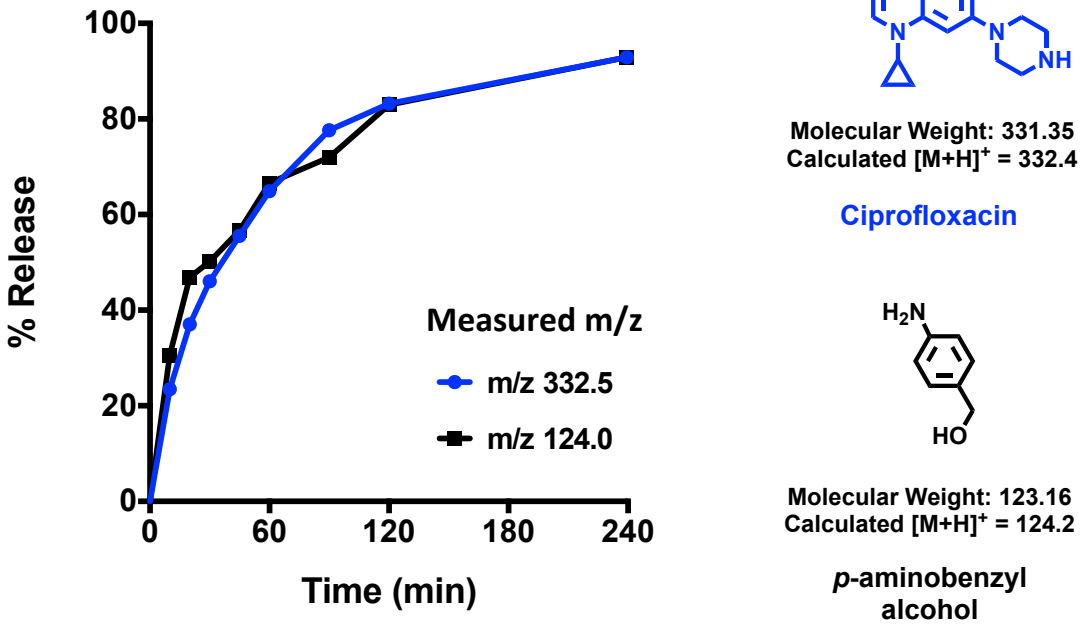

[redacted]

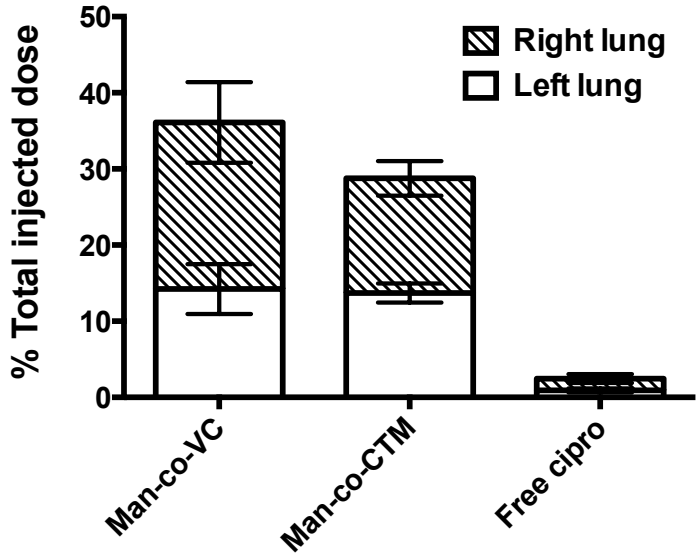

Figure S14. Actual deposited dose of polymeric ciprofloxacin prodrugs or free ciprofloxacin in mouse lungs. Intratracheal aerosolization of polymeric ciprofloxacin prodrugs or free ciprofloxacin (20 mg/kg) was delivered to mice using a MicroSprayer®. Lung tissues were harvested about 10 min after dosing. The harvested lungs were homogenized and treated with 20 v/v% H_2SO_4 to release all ciprofloxacin from polymer backbones. The released ciprofloxacin were quantified using LC-MS/MS to calculate the deposited dose. The relatively lower deposited dose of free ciprofloxacin was postulated to result from the rapid lung clearance of free ciprofloxacin[5]. Each value represents the mean ± SEM (n=4). Man-co-VC: polymeric ciprofloxacin prodrug with Val-Cit dipeptide linker. Man-co-CTM: polymeric ciprofloxacin prodrug with ester linker.

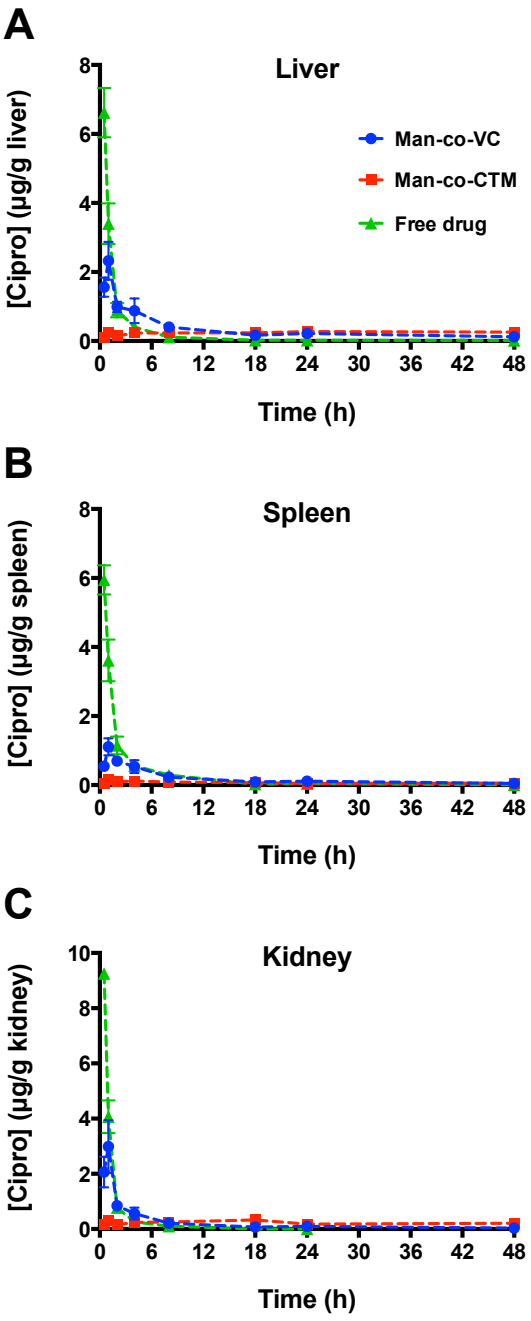
A
Liver
[Cipro] (µg/g liver)
Man-co-VC
Man-co-CTM
Free drug
Time (h)
B
Spleen
[Cipro] (µg/g spleen)
Time (h)
C
Kidney
[Cipro] (µg/g kidney)
Time (h)

[redacted]

Pharmacokinetic parameters of ciprofloxacin in liver, spleen, and kidney after intratracheal administration of polymeric prodrugs to mice. Parameters were obtained from data shown in **Figure S15**.

Treatment	Tissue	t_{max} [a] (h)	C_{max} [b] (μg/g)	AUC_{0-24} [c] (μg*h/g)	C_{max}/MIC [d]	AUC_{0-24}/MIC [d] (h)
VC		1	2.32 ± 0.55	11.50	35.77	176.99
CTM	Liver	24	0.28 ± 0.08	5.56	4.24	85.53
Free		0.5	6.62 ± 0.72	9.46	101.83	145.56
VC		1	1.10 ± 0.25	6.44	17.02	99.03
CTM	Spleen	1	0.15 ± 0.04	1.93	2.33	29.62
Free		0.5	5.95 ± 0.43	11.43	91.5	175.89
VC		1	2.99 ± 0.95	8.59	45.95	132.14
CTM	Kidney	18	0.33 ± 0.15	6.17	5.03	95.00
Free		0.5	9.25 ± 0.18	10.37	142.38	159.47

[a] The time to reach maximum concentration (C_{max}) after administration.

[b] C_{max} are represented as mean ± SEM. Values were normalized to retrieved organ mass (g).

[c] Area under the curve are presented as mean value from 0 to 24 h (AUC_{0-24}) and determined by GraphPad Prisim 5.

[d] MIC: 0.03 μg/mL; 0.065 μg/g. The volume distribution of ciprofloxacin (2.16 L/kg, for mice treated with 20 mg/kg ciprofloxacin) was used to convert MIC to a more tissue-relatable value (0.065 μg/g)[6,7].

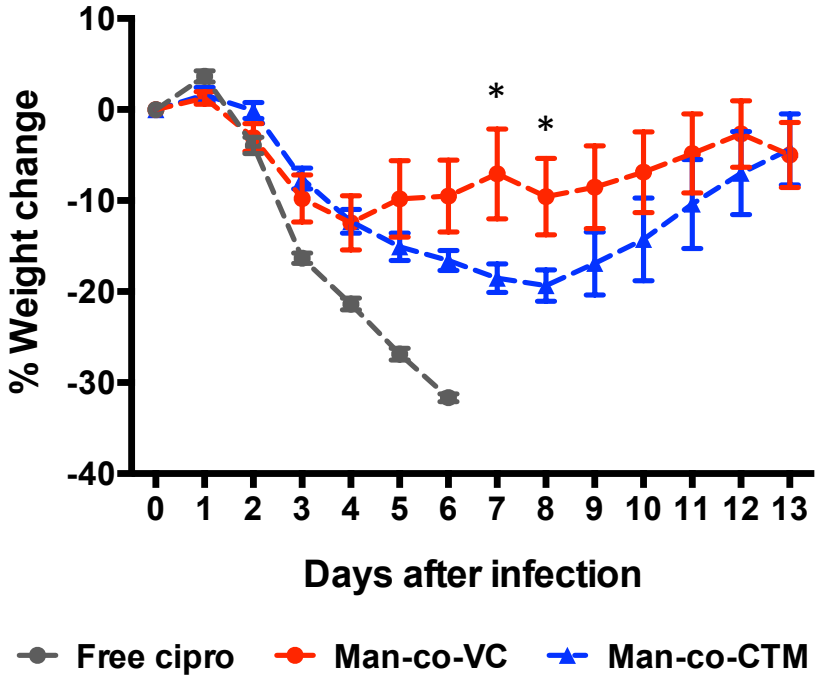
10
0
-10
-20
-30
-40
% Weight change
0 1 2 3 4 5 6 7 8 9 10 11 12 13
Days after infection
*
*
Free cipro
Man-co-VC
Man-co-CTM

[redacted]

Reference

1. G.M. Dubowchik, R.A. Firestone, L. Padilla, D. Willner, S.J. Hofstead, K. Mosure, et al., Cathepsin B-labile dipeptide linkers for lysosomal release of doxorubicin from internalizing immunoconjugates: Model studies of enzymatic drug release and antigen-specific in vitro anticancer activity, Bioconjug. Chem. 13 (2002) 855–869.
2. D. Das, S. Srinivasan, A.M. Kelly, D.Y. Chiu, B.K. Daugherty, D.M. Ratner, et al., RAFT polymerization of ciprofloxacin prodrug monomers for the controlled intracellular delivery of antibiotics, Polym. Chem. 7 (2016) 826–837.
3. J. Beignet, J. Tiernan, C.H. Woo, B.M. Kariuki, L.R. Cox, Stereoselective synthesis of allyl-C-mannosyl compounds: Use of a temporary silicon connection in intramolecular allylation strategies with allylsilanes, J. Org. Chem. 69 (2004) 6341–6356.
4. K.C. Stone, R.R. Mercer, P. Gehr, B. Stockstill, J.D. Crapo, Allometric relationships of cell numbers and size in the mammalian lung, Am. J. Respir. Cell. Mol. Biol. 6 (1992) 235–243.
5. D. Cipolla, J. Blanchard, I. Gonda, Development of liposomal ciprofloxacin to treat lung infections, Pharmaceutics. 8 (2016) 1–31.
6. L.C. Kingry, J.M. Petersen, Comparative review of Francisella tularensis and Francisella novicida, Front. Cell Infect. Microbiol. 4 (2014) 35.
7. F. Scaglione, J.W. Mouton, R. Mattina, F. Fraschini, Pharmacodynamics of levofloxacin and ciprofloxacin in a murine pneumonia model: Peak concentration/MIC versus area under the curve/MIC ratios, Antimicrob. Agents Chemother. 47 (2003) 2749–2755.

Chapter 5. Drugamers with enzyme-cleavable linkers effectively treat pulmonary Burkholderia infection

Abstract

Melioidosis, caused by *Burkholderia pseudomallei*, is a highly infectious disease of public health importance in Southeast Asia and Australia. Inhalation of *B. pseudomallei* is one of the most common and infectious exposure routes. Treatment of pulmonary melioidosis is lengthy and treatment failure is common, mainly because systemically delivered antibiotics fail to retain in the lungs and alveolar macrophages (AMs), an important host cell for *B. pseudomallei*. Herein we evaluated the activity of a polymeric antibiotic prodrug therapeutic, termed drugamer, against pulmonary melioidosis. This macrophage-targeted, enzyme cleavable drugamer was previously shown to not only improve released drug pharmacokinetic (PK) properties (maximum drug concentration and total drug exposure) in the lungs and AMs, but also led to full survival rate in a lethal mice model of pulmonary tularemia. Evaluated using a representative mouse challenge model of pulmonary melioidosis, the drugamer provided full protection against the completely lethal infection, where PBS and free drug led to 0 and 25% survival rate, respectively. As an extension of our previous PK studies, this study further evaluated the drugamer distribution and accumulation in the lungs *in vivo*. By using rhodamine-labeled drugamer and confocal microscopy, preferential accumulation of drugamer was observed in lung macrophages even at 48 h after dosing. Collectively, this study provides further evidence that the macrophage-targeted, enzyme cleavable drugamer effectively targeted concentrated drug depots to lung macrophages and could potentially be an effective therapeutic for the treatment of pulmonary intracellular infections.

Keywords: Prodrug, ciprofloxacin, drug conjugate, melioidosis, alveolar macrophage targeting

5.1 INTRODUCTION

Burkholderia pseudomallei, the causative agent of melioidosis, exhibits a great public health toll in Southeast Asia and northern Australia[1]. A recent report estimated that annually, *B. pseudomallei* causes 165,000 human infections and 89,000 deaths worldwide[1]. Inhalation or transcutaneous inoculation is the most likely routes of infection, and pneumonia is the most common manifestation[2]. The current antibiotic regimen regularly fails, leading to high fatality rate (50% in Thailand and 20% in Australia)[3]. Furthermore, *B. pseudomallei* is a Tier 1 select agent, due to the potential risk of exposure as an aerosolized bioterrorism agent[4]. Melioidosis therapy is biphasic and lengthy[5]. Depending on the clinical manifestations of the disease, treatment for *B. pseudomallei* usually starts with 10–14 days of intravenous therapy (acute phase, 3 doses/day), followed by weeks to months of oral eradication therapy (eradication phase, 2-3 doses/day)[5]. This prolonged systemic antibiotic therapy may not only lead to side effects, but potentially facilitate colonization with antibiotic-resistant bacteria, which could cause recurrent infections[6].

Management of melioidosis remains a challenge due to the intrinsically antibiotic resistance and intracellular inhabitation of *B. pseudomallei*[7,8]. *B. pseudomallei* is resistant to a wide range of antibiotics, including β-lactams, aminoglycosides and macrolides[9]. Although some *B. pseudomallei* isolates are susceptible to fluoroquinolones by *in vitro* testing[10], clinical evidence indicates that fluoroquinolones (e.g., ciprofloxacin) are not effective[11,12]. Acquired resistance to the current drug of choice for melioidosis, ceftazidime, has been reported in clinical isolates as a result of ceftazidime therapy[13,14]. Another challenge is that *B. pseudomallei* can sequester within macrophages and other non-phagocytic cells, where they are protected from antibiotics and adaptive immune responses[8]. For example, alveolar macrophage (AM) is an important host cell for Burkholderia infection in the lungs[15,16]. This intracellular localization limits the efficacy of antibiotics delivered through IV or oral route, due to their limited lung distribution and poor intracellular accumulation[17]. Considering the clinical significance of meiloidosis, there is an imperative need to design a new approach that can effectively deliver antibiotics to the lungs, especially to the cytosol of AMs, while avoiding the emergence of antibiotic resistance.

Inhaled antibiotics are a promising avenue to pursue for pulmonary diseases, including melioidosis, since this mode of delivery mimics the likely exposure route and can provide high drug doses directly to the infected tissue[18]. A recent report revealed that aerosolized ceftazidime provided comparable treatment outcomes to ceftazidime delivered intraperitoneally, suggesting the potential aerosolized antibiotics in improving the treatment regimen[19]. Inhaled free drugs, however, are usually subject to rapid absorption from the lung and require frequent, high-dose administration[20]. Our group has recently developed a series of inhalable polymeric antibiotic prodrugs, termed drugamers, to improve pulmonary intracellular infections, such as respiratory tularemia[21,22]. The drugamers incorporates (1) hydrophilic mannose residues to target and enhance AM uptake and intracellular delivery, and (2) enzyme-cleavable Valine-Citrulline (VC) dipeptide linker to provide high and sustained intracellular AM drug dosing. Notably, inhalation of the mannose-targeted, enzyme-cleavable drugamer (VC drugamer) sustained ciprofloxacin dosing in lungs and AMs above the minimum inhibitory concentration (MIC) over at least a 48 h period, and maintained significantly improve PK properties (maximum concentration and total drug exposure) of ciprofloxacin in the lungs and AMs as well. Additionally, the targeted drugamers achieved full survival (100%) in a highly lethal mouse model of pneumonic tularemia, contrasted with 0% survival using free ciprofloxacin[21]. Our findings suggest the strong therapeutic potential of drugamers in treating pulmonary intracellular infections.

Building upon our previous findings, the goal of this work was to evaluate the ciprofloxacin VC drugamer as a potential new therapeutic for respiratory melioidosis. Although ciprofloxacin has been proved to show poor clinical efficacy, we hypothesized that the superior PK properties afforded by the VC drugamer could potentiate the efficacy of ciprofloxacin in treating melioidosis. To test this hypothesis, we used a murine pneumonic infection with aerosolized *B. thailandensis* as a lab surrogate model for *B. pseudomallei*[23]. Delivered using intratracheal administration, a three-day once-daily treatment of VC drugamer resulted in an unexpected full protection (100% survival), whereas free ciprofloxacin and PBS led to 25 and 0% survival rate, respectively. Together with our previous success with respiratory Francisella infection, the VC drugamer may represent an efficacious therapeutic against other aerosolized intracellular pathogens.

5.2 EXPERIMENTAL SECTION

5.2.1 *Bacterial strains and growth conditions.*

B. thailandensis E264 was kindly provided by Dr. Donald Woods at the University of Calgary, Alberta, Canada. Bacteria were grown from frozen glycerol stock in LB broth shaking at 37°C for 18 h, isolated by centrifugation, washed twice, and suspended in Dulbecco's PBS to the desired concentration. An optical density of 0.20 at 600nm yielded approximately 1×10^8 colony-forming units (CFU)/ml.

5.2.2 *Animals.*

Specific-pathogen-free C57BL/6 mice (female, 8 weeks) were obtained from Jackson Laboratories (Bar Harbor, ME, USA). All animals were housed in laminar flow cages and were permitted *ad-lib* access to sterile food and water. Euthanasia was accomplished with intraperitoneal injection of pentobarbital followed by exsanguination from cardiac puncture. All animal procedures and handling were conducted under protocols (4047-02 and 2671-10) approved by the Institutional Animal Care and Use Committee at the University of Washington.

5.2.3 *Drugamer synthesis and characterization.*

Enzyme-cleavable drugamer was synthesized and fully characterized as described previously[21].

5.2.4 *Drugamer uptake by alveolar microphages and immunofluorescence*

Eight-week old female C57BL/6 mice were anesthetized with isoflurane and intratracheally dosed with 50µl of rhodamine labeled drugamers (ca. 80 mg/ml, equivalent to 20 m/kg ciprofloxacin dose). Mice were sacrificed using CO_2 and cardiac puncture at time points of 1, 4, 24, and 48 h. Lungs were immediately harvested, fixed in neutral-buffered formalin for 24-48 h, washed with PBS, cryo-protected in sucrose solution (30% (w/v) in PBS) overnight, and processed through OCT embedding. Five µm sections were cut for the following

immunofluorescence staining. Slides were treated with proteinase K at 37°C for 15 min, followed by normal goat serum (10% in tris-buffered saline) at RT for 20 min. The primary antibody for immunofluorescence was rat monoclonal anti-mouse F4/80 (MF48000, Invitrogen). The antibody was incubated at dilutions 1:200 at RT for 60 min, the sections were washed with PBS-T and incubated with secondary antibodies (Anti-rat Cy5) diluted 1:100 in PBS containing 5% NGS for 1 h at RT. Sections were then washed with PBS-T, counterstained with DAPI for 5 min at RT, washed with PBS, mounted using mounting media (VectaMount or VectaShield, Vector laboratories) and examined using a confocal microscope (Leica SP8X).

5.2.5 *Antibacterial efficacy against pulmonary Burkholderia infection.*

The antibiotic activity of drugamers was tested in C57Bl/6 mice (female, 8 weeks old, n = 8) challenged with aerosolized *B. thailandensis* E264. Mice were given three consecutive doses of free ciprofloxacin or VC drugamers using MicroSprayer®, with 24 h interval between each dose. The challenge study was conducted with ciprofloxacin dosing at 20 mg/kg. Mice were exposed to aerosolized bacteria using a Biaera whole-body exposure chamber (Biaera Technologies, Maryland, USA), with total airflow through the chamber maintained at 19.5 L/min during a 20 min exposure. Aerosols were generated from a MiniHEART hi-flo nebulizer (Westmed, Tucson, AZ, USA) driven at 40 psi. Airflow through the system was maintained for 10min at 24l/min followed by 5min purge with air. Bacterial deposition in each experiment was determined from quantitative culture of lung tissue from sentinel mice sacrificed immediately after infection. Animals were examined daily for illness or death and abdominal surface temperatures were measured using a Ranger MX4P digital infrared thermometer (Raytek, Santa Cruz, CA, USA). Animals with temperatures <25°C or weight loss of >20%, ruffled fur, eye crusting, hunched posture and lack of resistance to handling were deemed terminal and euthanized.

The infected animals were monitored daily for mobility and for deaths from the infection. At day 14 after infection, the number of mice that survived the otherwise lethal infection was recorded. The left lung, median hepatic lobe, and spleen were harvested from mice that survived 14 days after infection and plated to determine viable bacteria surviving after treatment. Organs were homogenized in 1 ml sterile Dulbecco's PBS and serial dilutions plated on LB agar. Colonies

were counted after 2–4d of incubation at 37°C in humid air with 5% CO_2. Verification of *B. thailandensis* growth was confirmed by plating on Ashdown's agar, a selective medium that contains crystal violet and gentamicin to inhibit growth of other bacteria. Plates were counted after 4d of incubation at 37°C in humid air with 5% CO_2. Typical *Burkholderia* colonies on Ashdown's appear purple and wrinkled.

5.2.6 *Statistical Analysis.*

Student's two-tailed t-tests were performed to compare two groups and analysis of variance (ANOVA) was performed for comparisons of multiple groups, through GraphPad Prism (version 5.0, GraphPad Software Inc.). Unless otherwise stated, data reported denote the means ± SD. Survival analyses were performed using a log-rank test in GraphPad Prism. No specific methods of randomization were applied to group or animal allocation. Investigators were not blinded to group allocation. $p < 0.05$ was considered statistically significant.

5.3 RESULTS

5.3.1 *Targeted in vivo delivery of VC drugamer to macrophages*

To determine whether the mannose residues enhance the drugamer uptake by macrophages, we intratracheally delivered mice with rhodamine-labeled VC drugamer and harvested lung at pre-determined time points for immunofluorescence staining using anti-F4/80 antibody to identify lung macrophages. We found that VC drugamer preferentially accumulated in $F4/80^+$ cells in the lung tissue sections. This preferential accumulation was observed even 48 h post-administration (**Figure 5.1**). It is noted that F4/80 staining cannot differentiate alveolar macrophages and interstitial macrophages, which are about 63% and 37% of total macrophages in murine lungs[24].

5.3.2 *Activity of VC drugamer in protecting from lethal B. thailandensis infection*

B. thailandensis is biochemically and genetically closely related to *B. pseudomallei*, but is relatively avirulent to human and require less stringent facilities than *B. pseudomallei*[25]. Prior

study has shown that deposition of 10^5 CFU of *B. thailandensis* per lung is predictably fatal in C57BL/6 mice[23]. The actual bacterial inoculation in the current study was 4.53 x 10^5 CFU/lung, which was therefore considered as a lethal infection. Mice were intratreacheally administrated with PBS, ciprofloxacin (20 mg/kg), or VC drugamer (20 mg/kg ciprofloxacin) at 0 (1 h prior to infection), +1, and +2 days. Animal survival was monitored until mice qualified for euthanasia or reached the experimental end-point (14 days postbacterial exposure). As expected, mice treated with PBS show limited survival extension with all treated animals succumbing to the bacterial infection (n = 8/8) within three days (**Figure 5.2**). In contrast, free ciprofloxacin provided limited improvement in survival rate (25%). Impressively, VC drugamer led to full protection with all mice survived until the end point of this study (14 days).

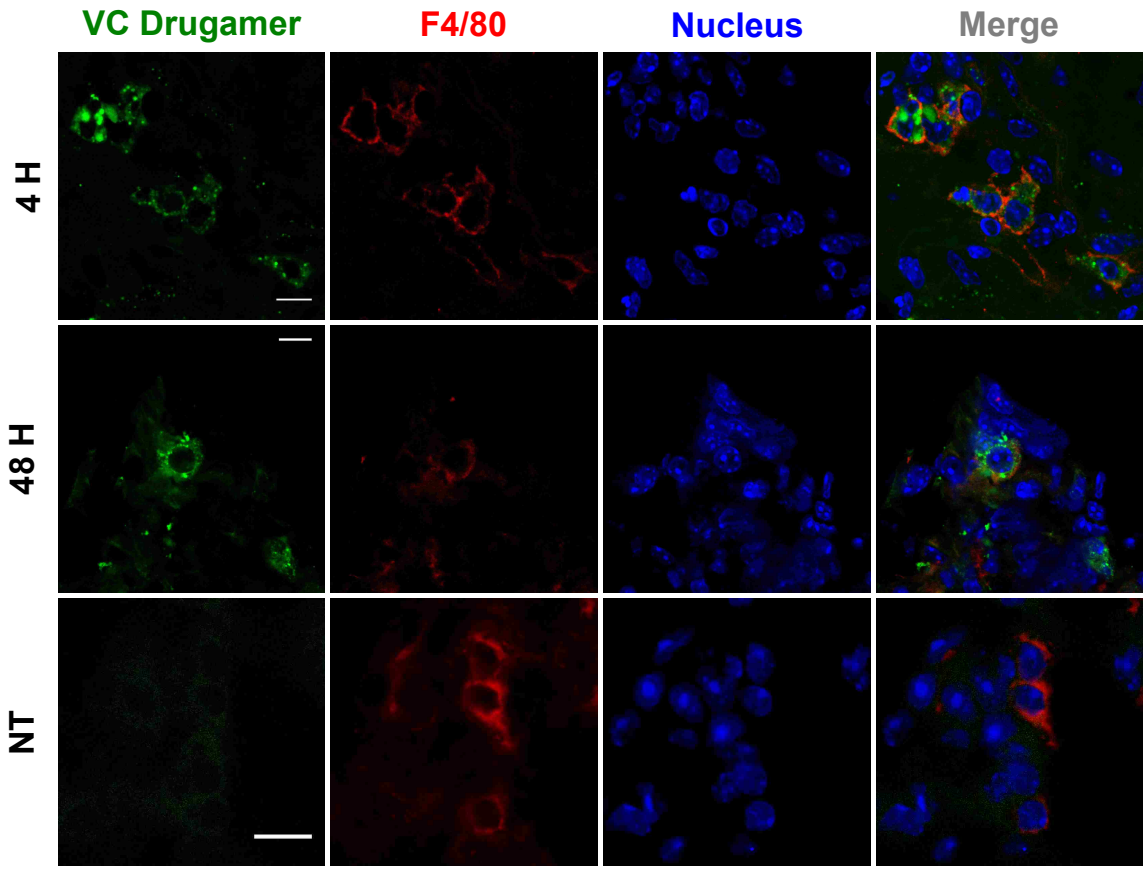

Figure 5.1. Lung sections stained for VC drugamer (green), F4/80 (red), and nuclei (blue). The VC drugamer highly accumulated within F4/80-expressing lung macrophages. Scale bar, 10 µm. Lungs were harvested from mice treated with rhodamine-labeled VC drugamer after 4 or 48 h or mice without any treatment (NT).

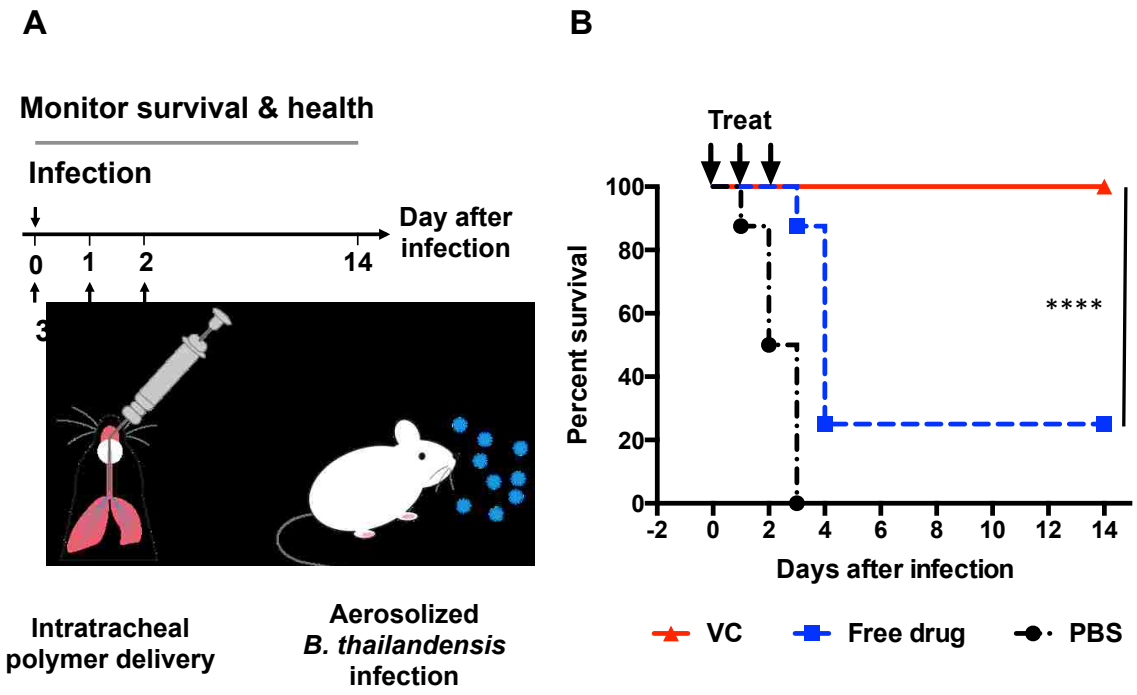

Figure 5.2. Comparison of antibacterial efficacies of ciprofloxacin durgamer with enzyme-cleavable linker (VC drugamer) with free ciprofloxacin in mouse Burkholderia lung infection model. (a) Workflow schematic. Free ciprofloxacin or polymeric ciprofloxacin prodrugs with protease-cleavable linker (VC drugamer) was intratracheally administered (50 µL aerosolization) at 0, 1, and 2 days using a MicroSprayer® (n = 8 for each treatment group). All bacterial inoculation occurred 1 h after treatment on day 0. Survival rate and health condition of mice were monitored for 14 days. (b) Survival of lung-infected mice treated with 20 mg/kg ciprofloxacin dose. Data analysis was performed using the statistical software GraphPad Prism (**** $p < 0.0001$).

5.3.3 *Clinical observations*

The average weight of mice prior to exposure was 19.04 ± 1.02 g with no significant difference among the three treatment groups (PBS, free ciprofloxacin, and VC drugamer). Following challenge, mice were observed daily for changes in weight, temperature, and morbidity (**Figure 5.3**). Mice in the PBS groups succumbed to infection within 72 h. Prior to euthanasia, the PBS-treated mice exhibited severe weight loss along with a significant temperature decrease, hunched posture, and subdued activity. Mice treated with free ciprofloxacin became symptomatic (i.e., decrease in body weight, surface temperature, and morbility) about 24 hrs after infection; however, survival rate was improved. Both free ciprofloxacin and VC drugamer treatment

regimens displayed weight loss one day after the infection, but the drugamer-treated mice began to gain weight at day 2 and regained their baseline weight around 5 days post-infection.

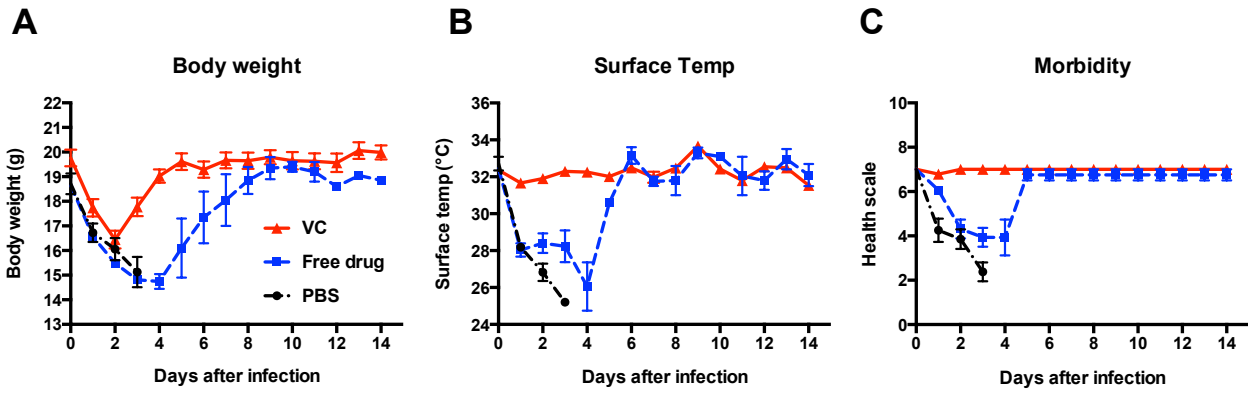

Figure 5.3. Measurements of health were recorded by monitoring changes in mice after therapeutic treatment with polymeric prodrugs of ciprofloxacin. (A) body weight, (B) surface temperature, and (C) morbidity. The challenge end-point was marked at 14 days post-bacterial exposure at which point any surviving mice were euthanized. Representative changes in health-metrics for mice administered with polymeric prodrugs (n = 8) at 20 mg/kg ciprofloxacin for the therapeutic treatment cycle (0, 1, and 2 days). The health of the mice after bacterial inoculation was evaluated by monitoring the appearance of each mice using an appearance chart a pre-determined scoring rubric. Mice with high health scores display high general activity, cleanliness, regular breathing, normal posture, and clear and open eyes. Lethargic, sickly mice have low scores associated to poor responsiveness during interaction and stimulation. Data is presented as mean ± SEM.

Measurements of abdominal surface temperature correlated well with morbidity and clinical outcome. The surface temperature and morbidity of mice treated with free drug began to drop 24 h after the infection, but recovered to the baseline at around day 5. In contrast, all drugamer-treated mice maintained temperatures higher than 27^{o}C and the morbidity did not seem to be affected by the Burkholderia infection. Notably, drugamer-treated mice recovered slower from anesthesia after the second and third dose, compared with mice treated with either PBS or free drug. Clearly, VC drugamer-treated mice demonstrated better health conditions in contrast to the other two control groups.

5.3.4 *Bacteria burden in major organs*

We also quantified bacterial burdens in the lung, liver and spleen of surviving mice at endpoint of the study to assess the degree of bacterial replication and dissemination. In addition to lung, visceral organs such as the spleen and liver are commonly affected by melioidosis[26]. Consistent with prior studies, no bacteria were detectable in lung, liver or spleen of the surviving mice (**Figure. 5.4**)[23].

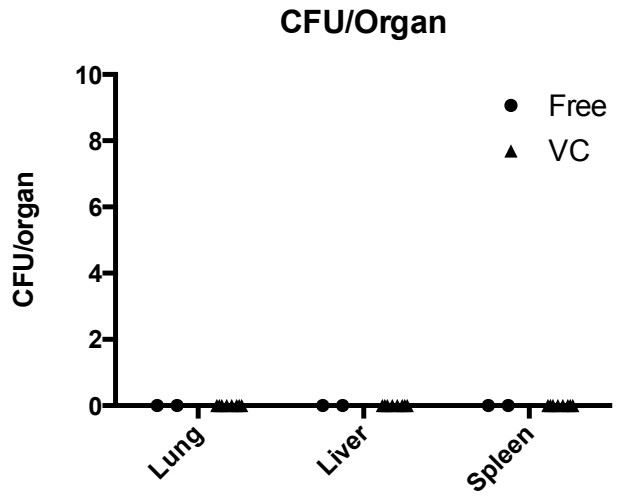

Figure 5.4. Bacteria burden in mice that survived to the endpoint of Burkholderia challenge study. Lung, liver and spleen were harvested and quantitatively cultured at 14 d after infection (endpoint). VC drugamer group (VC) comprises eight mice, whereas there are two in the free ciprofloxacin treatment group (Free).

5.4 DISCUSSION & CONCLUSION

Although there are established antimicrobial treatment regimens currently available for treatment of pulmonary Burkholderia infections, problems such as the prolonged length of treatment, frequent treatment failures, and limited options of active antibiotics highlight the need for new anti-melioidosis therapeutics. The prolong treatment regimens mainly result from the poor antibiotic distribution and accumulation in the lungs and AMs, due to systemic delivery routes (IV or oral). Although drug carriers have been widely used as PK modifiers and for targeted drug delivery, little has been done to develop antibiotic carriers for the treatment of melioidosis. The goal of this report is to investigate whether using drug carriers to improve antibiotic PK

properties (retention and maximum concentration) in the lungs and AMs would improve the antibiotic treatment outcome for pulmonary melioidosis. Improving antibiotic PK properties may reduce dosing frequency and treatment duration, thus potentially avoiding side effects and emergence of antibiotic resistance[27].

This study used a reported polymeric ciprofloxacin prodrug, termed VC drugamer, with AM-targeting mannose residues and enzyme-cleavable linkers to improve the antibiotic PK properties[21]. The antibacterial efficacy of VC drugamer was compared with free ciprofloxacin via a representative mouse model of melioidosis using airborne *B. thailandensis* as an avirulent surrogate for *B. pseudomallei*[23]. Consistent with previous reports, none of the mice treated with PBS survived for more than 4 days[23] and free ciprofloxacin only led to 25% survival rate. In contrast, VC ciprofloxacin drugamer, 20 mg/kg, one daily dose for 3 days, provided full protection and all mice were cured without any bacteria left in the major organs at the endpoint of the study (14 days). This observation was unexpected, as free ciprofloxacin is known to be ineffective against melioidosis in mice and human[11,12,28]. For example, free ciprofloxacin (100 mg/kg) given orally at 12 hourly intervals for 14 days starting at 6 h post-challenge led to 90% survival at 14 days and 75% survival rate at 42 days[28]. The superior survival rate of VC drugamer than free ciprofloxacin could be attributed to the better released drug PK properties of VC drugamer.

As an extension of our prior drugamer PK study in AMs, this study used confocal microscopy to visualize the distribution of drugamer depots in the lungs and AMs. Identified using anti-mouse F4/80 immunofluorescence staining, macrophages (include AMs and interstitial macrophages) in the lung sections appeared to be heavily loaded with rhodamine-labeled VC drugamer 4 h after dosing and even at 48 h post-treatment. This observation is consistent with our PK data in AMs, in which we demonstrated that drugamer kept concentrated intracellular depots with drug concentrations more than three orders of magnitude higher than MIC[21]. Additionally, the preferential accumulation of mannose-targeted VC drugamer in macrophages corresponding well to prior data published by our group and others showing the macrophage-specific uptake of mannose-functionalized polymers or liposomes[29-32]. Collectively, those confocal images provide

further evidence to prove drugamer activity in preferential and prolonged accumulation in macrophages.

Despite of those promising results described above, there are two major limitations of this study that require further exploration in the future studies. First, the dosing scheme is "concurrent" with the infection, meaning that bacterial infection was induced about 2 h after the first dosing. This dosing scheme may not represent the actual prophylactic or post-exposure prophylactic conditions. Therefore, future studies are necessary to test the antibacterial efficacy of drugamers using more clinical relevant dosing schemes, such as 24 h before or after the infection. Second, the mouse challenge model in this study was established using *B. thailandensis* as a lab surrogate. Although *B. thailandensis* has high degree of genetic similarities with *B. pseudomallei* and has similar disease manifestation as *B. pseudomallei* infections, *B. thailandensis* may not completely mimic the virulence of *B. pseudomallei.* Hence, future studies will include mice challenge studies with aerosolized *B. pseudomallei.*

Overall, this study demonstrates that mannose-targeted, enzyme-cleavable VC drugamer is highly active against pulmonary infections of *B. thailandensis*. We demonstrated for the first time that improved PK properties (e.g., C_{max} and AUC) could enhance anti-melioidosis activity of ciprofloxacin, which has been proven to be ineffective *in vivo*. Demonstration of full protection against *B. thailandensis* infection is promising for future mice challenge studies with *B. pseudomallei*, the actual lethal pathogen for humans. In conjunction with our previous study showing VC drugamer provided full protection against highly lethal pulmonary Francisella infection, this study provide further evidence for the strong therapeutic activity of VC drugamer in treating pulmonary intracellular infections.

5.5 ACKNOWLEDGEMENTS

This work was supported by the Defense Threat Reduction Agency (Grant #HDTRA1-13-1-0047) and by the NIH (R01AI134729). We would like to thank Megan Larmore and Brian Johnson from the University of Washington Histology and Imaging Core for their assistance in

IHC method development". F.Y.S. is an international student research fellow of the Howard Hughes Medical Institute.

5.6 REFERENCE

1. Limmathurotsakul, D. *et al.* Predicted global distribution of Burkholderia pseudomallei and burden of melioidosis. *Nat Microbiol* **1,** (2016).
2. White, N. J. Melioidosis. *The Lancet* **361,** 1715–1722 (2003).
3. Cheng, A. C. & Currie, B. J. Melioidosis: epidemiology, pathophysiology, and management. *Clin Microbiol Rev* **18,** 383–416 (2005).
4. Wiersinga, W. J. *et al.* Melioidosis. *Nature Reviews Disease Primers* **4,** 17107 EP –
5. Dance, D. Treatment and prophylaxis of melioidosis. *Int. J. Antimicrob. Agents* **43,** 310–318 (2014).
6. Ventola, C. L. The antibiotic resistance crisis: part 2: management strategies and new agents. *P T* **40,** 344–352 (2015).
7. Jones, A. L., Beveridge, T. J. & Woods, D. E. Intracellular survival of Burkholderia pseudomallei. *Infect Immun* **64,** 782–790 (1996).
8. Wiersinga, W. J., van der Poll, T., White, N. J., Day, N. P. & Peacock, S. J. Melioidosis: insights into the pathogenicity of Burkholderia pseudomallei. *Nat. Rev. Microbiol.* **4,** 272–282 (2006).
9. Thibault, F. M., Hernandez, E., Vidal, D. R., Girardet, M. & Cavallo, J. D. Antibiotic susceptibility of 65 isolates of Burkholderia pseudomallei and Burkholderia mallei to 35 antimicrobial agents. *Journal of Antimicrobial Chemotherapy* **54,** 1134–1138 (2004).
10. Dance, D. A., Wuthiekanun, V., Chaowagul, W. & White, N. J. The antimicrobial susceptibility of Pseudomonas pseudomallei. Emergence of resistance in vitro and during treatment. *J Antimicrob Chemother* **24,** 295–309 (1989).
11. Chaowagul, W., Suputtamongkul, Y., Smith, M. D. & White, N. J. Oral fluoroquinolones for maintenance treatment of melioidosis. *Transactions of the Royal Society of Tropical Medicine and Hygiene* **91,** 599–601 (1997).
12. Chetchotisakd, P., Chaowagul, W., Mootsikapun, P., Budhsarawong, D. & Thinkamrop, B. Maintenance therapy of melioidosis with ciprofloxacin plus azithromycin compared with cotrimoxazole plus doxycycline. *Am J Trop Med Hyg* **64,** 24–27 (2001).
13. Sarovich, D. S. *et al.* Characterization of ceftazidime resistance mechanisms in clinical isolates of Burkholderia pseudomallei from Australia. *PLoS ONE* **7,** e30789 (2012).
14. Behera, B., Prasad Babu, T. L. V. D., Kamalesh, A. & Reddy, G. Ceftazidime resistance in Burkholderia pseudomallei: first report from India. *Asian Pac J Trop Med* **5,** 329–330 (2012).
15. Goodyear, A. *et al.* Protection from pneumonic infection with burkholderia species by inhalational immunotherapy. *Infect Immun* **77,** 1579–1588 (2009).
16. Lu, R., Popov, V., Patel, J. & Eaves-Pyles, T. Burkholderia mallei and Burkholderia pseudomallei stimulate differential inflammatory responses from human alveolar type II cells (ATII) and macrophages. *Front Cell Infect Microbiol* **2,** (2012).
17. Wise, R. & Honeybourne, D. Pharmacokinetics and pharmacodynamics of fluoroquinolones

in the respiratory tract. *Eur Respir J* **14,** 221–229 (1999).
18. Quon, B. S., Goss, C. H. & Ramsey, B. W. Inhaled Antibiotics for Lower Airway Infections. *Annals of the American Thoracic Society* **11,** 425–434 (2014).
19. Ruiz, S. I., Bowen, L. E., Bailey, M. M. & Berkland, C. Pulmonary Delivery of Ceftazidime for the Treatment of Melioidosis in a Murine Model. *Mol. Pharmaceutics* **15,** 1371–1376 (2018).
20. Strong, P., Ito, K., Murray, J. & Rapeport, G. Current approaches to the discovery of novel inhaled medicines. *Drug Discovery Today* (2018).
21. Su, F.-Y. *et al.* Macrophage-targeted drugamers with enzyme-cleavable linkers deliver high intracellular drug dosing and sustained drug pharmacokinetics against alveolar pulmonary infections. *J Control Release* **287,** 1–11 (2018).
22. Das, D. *et al.* Synthetic Macromolecular Antibiotic Platform for Inhalable Therapy against Aerosolized Intracellular Alveolar Infections. *Mol. Pharmaceutics* **14,** 1988–1997 (2017).
23. West, T. E., Frevert, C. W., Liggitt, H. D. & Skerrett, S. J. Inhalation of Burkholderia thailandensis results in lethal necrotizing pneumonia in mice: a surrogate model for pneumonic melioidosis. *Transactions of the Royal Society of Tropical Medicine and Hygiene* **102,** S119–S126 (2008).
24. Crowell, R. E., Heaphy, E., Valdez, Y. E., Mold, C. & Lehnert, B. E. Alveolar and interstitial macrophage populations in the murine lung. *Exp Lung Res* **18,** 435–446 (1992).
25. Yu, Y. *et al.* Genomic patterns of pathogen evolution revealed by comparison of Burkholderia pseudomallei, the causative agent of melioidosis, to avirulent Burkholderia thailandensis. *BMC Microbiol.* **6,** 46 (2006).
26. Warawa, J. M. Evaluation of surrogate animal models of melioidosis. *Front Microbiol* **1,** 141 (2010).
27. Lee, C.-R., Cho, I. H., Jeong, B. C. & Lee, S. H. Strategies to Minimize Antibiotic Resistance. *International Journal of Environmental Research and Public Health* **10,** 4274–4305 (2013).
28. Steward, J. *et al.* Comparison of gatifloxacin, moxifloxacin and ciprofloxacin for treatment of experimental Burkholderia pseudomallei infection. *J Antimicrob Chemother* **55,** 523–527 (2005).
29. Chen, J. *et al.* Nanostructured glycopolymer augmented liposomes to elucidate carbohydrate-mediated targeting. *Nanomedicine* **12,** 2031–2041 (2016).
30. Su, F.-Y. *et al.* Polymer-augmented liposomes enhancing antibiotic delivery against intracellular infections. *Biomater Sci* **6,** 1976–1985 (2018).
31. Song, E.-H. *et al.* In vivo targeting of alveolar macrophages via RAFT-based glycopolymers. *Biomaterials* **33,** 6889–6897 (2012).
32. Wijagkanalan, W. *et al.* Efficient targeting to alveolar macrophages by intratracheal administration of mannosylated liposomes in rats. *J Control Release* **125,** 121–130 (2008).

Chapter 6. Summary & future directions for antimicrobial drugamer therapeutics

6.1 SUMMARY OF KEY FINDINGS IN THIS THESIS

This thesis focused on improving antibiotic therapy for the treatment of pulmonary intracellular infections, including tularemia and melioidosis. A key approach to achieve this goal is engineering pharmacokinetics (PK) properties of free antibiotics in the lungs and alveolar macrophages, an important host cell for inhaled intracellular bacteria. Based on the disease settings and pharmacological properties of antibiotics, this thesis developed two polymer-based therapeutics: polymer-augmented liposome (PAL) and enzyme-cleavable polymeric antibiotic prodrug (VC drugamer). Their efficacy against intracellular infection was tested using an *in vitro* macrophage-bacteria co-culture model and representative murine challenge models of pulmonary tularemia and melioidosis. The released drug PK profiles were analyzed using a well-established tandem LC-MS method.

In chapter 2, we demonstrate the design rationale and efficacy of PALs in enhancing cytosolic delivery of antibiotics with poor membrane permeability, such as streptomycin. A multifunctional diblock copolymer was engineered to functionalize PALs with carbohydrate-mediated targeting, pH-responsive drug release, and endosomal release activity with a single functional polymer that replaces the PEGylated lipid component to simplify the liposome formulation. PALs displayed 2.5 times higher internalization by RAW macrophages and significantly improved *in vitro* intracellular antibacterial efficacy compared to control PEGylated liposomes. Although those data suggest the activity of PALs in enhancing cytosolic delivery of membrane-impermeable antibiotics, PALs was found to show typical burst release profiles and some drug leakage (16% in 6 h) in PBS, which were not ideal for sustained drug release in the lungs and AMs under the actual physiological conditions.

To have better control over drug release kinetics, in chapter 3, we synthesized and optimized macrophage-targeted ciprofloxacin drugamers with ciprofloxacin antibiotic covalently linking to the drugamer matrix through enzyme-cleavable dipeptide linkers or hydrolytic ester linkages.

Using RAFT polymerization, the synthesized drugamers had well-defined compositions and similar drug wt%. The drugamers with covalent linkages displayed minimal drug leakage at physiological and lysosomal pH; active ciprofloxacin released from the enzyme-cleavable drugamer (VC drugamer) was found to be rapid and cathepsin B-dependent, especially in lysosomal pH. The compositions of VC drugamer were further optimized to achieve desirable *in vivo* lung compatibility.

In chapter 4, we found that a single dose of the drugamers sustained ciprofloxacin dosing in lungs and AMs above the minimum inhibitory concentration (MIC) over at least a 48 h period. Additionally, VC drugamer achieved a greater than 10-fold increase in sustained ciprofloxacin in AM, and maintained a significantly higher whole lung PK as well. In contrast, ciprofloxacin dosed in identical fashion displayed rapid clearance with a half-life of approximately 30 min. Notably, inhalation of the mannose-targeted ciprofloxacin drugamers achieved full survival (100%) in a highly lethal mouse model of pneumonic tularemia, contrasted with 0% survival using free ciprofloxacin. In chapter 5, the therapeutic efficacy of VC drugamer was further demonstrated in a lethal murine model of pulmonary melioidosis. VC drugamer led to 100% survival rate, whereas free ciprofloxacin only achieved 25% survival rate. As ciprofloxacin has been known to re ineffective against melioidosis, our results suggest that improving the PK properties of free drug in targeting tissues and cell populations can be an effective approach to enhance the activity of antibiotics. Collectively, the VC drugamer developed in this thesis was proven to be a highly effective therapeutic for the treatment of pulmonary tularemia and melioidosis in murine models. Its clinical utility and other potential applications are discussed below.

6.2 PROPOSED FUTURE DIRECTIONS

6.2.1 *Evaluating released drug PK profiles in infected animal models*

Translatability of pre-clinical animal model PK to patients usually includes both healthy and infected animals, as infection process can have marked effects on the PK of a drug[1]. Infections can cause changes in antibiotic penetration in the physiologic tissues due to the inflammatory

process initiated by the host or a change in drug clearance. Infections in lung, bone, and central nervous system have been found to alter tissue penetration, while infections of the bloodstream have been shown to expand the volume of distribution (V_d) and enhance drug clearance[2]. For instance, animals with meningitis showed a fourfold increase in cerebrospinal fluid vancomycin levels compared with healthy controls[3]. Additionally, lung infection was found to produce large discordance between the blood and pulmonary profiles of tedizolid and linezolid[4]. On the other hand, Genentech revealed that *Staphylococcus aureus* infection had minimal effect on the PK profiles of an antibody antibiotic conjugate (THIOMAB™)[5]. To better understand the effects of lung infections on drugamer released drug PK, evaluating the PK properties of the drugamer system in infected mice or non-human primates would be a critical next step toward future clinical application.

6.2.2 *Employing clinically relevant inhalers for clinical translation*

Another critical step for translating the drugamer system for clinical application is to deliver the drugamer therapeutics using clinically relevant devices, such as nebulizers and dry powder inhalers. In this thesis, the antibiotic drugamer system was delivered using Microsprayer® for direct intratracheal delivery. Although intratracheal instillation/aerosolization is widely used as an alternative method for studying inhalation exposure, lung distribution of delivered materials has been shown to differ between actual inhalation and intratracheal instillation[6,7]. For example, inhaled materials deposited thinly and uniformly throughout the entire lungs, whereas intratracheal instillation showed uneven distribution. In addition to nebulizer, delivering using dry powder inhaler would be a more portable and user-friendly option[8]. Therefore, delivery of drugamer system using nebulizer and eventually dry powder inhaler would be important for future clinical application.

To ensure the efficient drugamer delivery of using nebulizers, care must betaken for factors that affecting drug output (**Table 6.1)**[9]. For example, the droplet size was found to be proportional to the viscosity of the nebulizer fluid, and the more viscous fluids had the lower outputs[10]. As described in chapter 1, the aerosol droplet size would affect the location where droplets deposit in the lungs. When using ultrasonic nebulizer, one must pay attention to the characteristics of

drug solution/suspension. Highly viscid solutions do not form standing waves as easily and are nebulized poorly. Suspensions are also nebulized poorly, perhaps because drug particles in suspension are vibrated away from the area of droplet generation[9]. Based on those prior studies, parameters of drugamer solutions require further optimization for effective delivery using nebulizers.

Table 6.1. Factors affecting output of drug solutions from jet nebulizers

Factor	*Positive effect*	*Negative effect*
Increase driving gas flow/ compressor rating	Smaller particle size, shorter nebulisation time	More expensive compressor
Increase volume fill	Greater proportion of drug nebulised	Longer nebulisation time
Decrease residual volume	Greater proportion of drug nebulised	Longer nebulisation time
Increase baffles	Smaller particle size	Longer nebulisation time
Decrease solution viscosity (e.g. warm solution)	Smaller particle size	Minor effect
Use an "open vent" nebuliser	Shorter nebulisation time	Nebuliser cost
Use nebuliser with manual interrupter/ assisted "open vent"	No drug wasted in expiration. Increased dose to patient	Coordination required. Longer treatment time
Use "breath assisted open vent" nebuliser	Greater (twice or more) drug delivery to patient	Effectiveness has only been shown in adults using bronchodilator solutions

6.2.3 *Evaluating scalability with Current Good Manufacturing Practices (cGMP) procedures*

Manufacturing therapeutic products under cGMP-compatible conditions is important to ensure that a manufacturer can consistently control and produce products to meet the identity, strength, purity and quality appropriate to their intended use. Furthermore, scalable synthesis using cGMP procedures are important to prepare for future dose escalation studies in large animal models and phase I clinical trials. Currently, we are evaluating the feasibility to outsource the drugamer manufacture to a contract manufacturing organization with cGMP facilities.

6.2.4 *Host-directed therapy*

The emergence of resistance to multiple antimicrobial agents in pathogenic bacteria has become a significant global public health threat. Although the drugamer system can potentiate the activity of antibiotics, it may not be effective against infections caused by drug-resistant bacteria, such as extensive/totally drug resistant melioidosis and tuberculosis. Host-directed therapeutics have been reported as promising adjuvant therapeutic strategy to antibiotics for treating infections caused by drug resistant bacteria[11,12]. Combination therapy with antibiotics and host-

directed therapy may lead to shorter therapies, reduced lung tissue damage and better outcome for the patients[13].

Host-directed therapeutics act via host-mediated responses to pathogens rather than acting directly on the pathogen, like traditional antibiotics[11]. Promising host targets include various biological processes that modify host cell function, modulate the inflammatory response, or affect bacterial replication and virulence[11]. For example, sirolimus, an mTOR inhibitor, has found to significantly decrease intracellular survival of *B. pseudomallei*, by boosting autophagy activity[14]. In a murine model of *B. pseudomallei* infection, intraperitoneal delivery of glyburide, a small molecule that regulates pattern recognition receptor (PRR) signaling pathway, significantly reduces bacterial dissemination into both liver and spleen[15].

Using drugamers to deliver host-directed therapeutics holds two potential advantages. First, drugamers can co-deliver antibiotics and host-directed therapeutics that have synergistic effects. For instance, AR-12, a celecoxib derivative, has been show to sensitize intracellular *Salmonella Typhimurium* to aminoglycosides and prolonged the survival rate of the infected mice[16]. Host-directed therapeutics that stimulate the immune system are associated with risks of excessive inflammation leading to cytokine storm or systemic inflammatory response syndrome[11]. Another potential advantage is that drugamers can help avoid side effects by enhancing the delivery of host-directed therapeutics to specific cells populations. Therefore, drugamers could potentially be a useful platform to deliver the combination therapy of antibiotics and host-directed therapeutics.

6.2.5 *Applying VC drugamer to different disease settings*

This thesis has demonstrated the modularity of VC drugamer in sustaining the released drug retention in the lungs and AMs. This drugamer system holds the promise to treat different disease settings by delivering various drugs to specific cell populations. In addition to treat other lung infections (e.g., tuberculosis, *Pseudomonas* infections in Cystic Fibrosis patients), a logical next step is applying VC drugamer to cancer treatment, as our group has extensive experience with lung delivery and anticancer drugamer development. For example, VC drugamer may be re-

engineered to treat lung cancers by carrying anticancer drugs. In this case, mannose residues on the drugamer need to be replaced by other solubilizing agents, such as PEG or ligands that can target cancer cells, because engagement of mannose receptors on tumor-associated macrophages (TAMs) has been shown to modulate cytokine production by TAMs toward an immune-suppressive profile[17]. Another possibility is to deliver molecules that can induce macrophage repolarization to a tumoricidal state (M1 phenotype) that leads to potent anti-tumor activity[18]. It would be interesting to see if drugamers could not only transform TAMs into M1 phenotype, but also turn alveolar macrophages into tumoricidal.

6.3 CONCLUSION

Overall, this thesis demonstrates the modularity of drugamer prodrugs in spatial and temporal control of the drug release profiles in the lung and alveolar macrophages. By engineering linker chemistry, release mechanism of drguamer with Valine-Citeulline dipeptide linker (VC drugamer) was enzyme-dependent and avoided the burst release profiles that are commonly observed with drugs physically encapsulated in nanoparticle formulations. Using mannose as targeting ligands, a single dose of the enzyme cleavable VC drugamer extended the released drug concentrations in the lungs and alveolar macrophages for at least 48 hours. This superior PK property can potentially be used for prophylactic dosing and reducing dosing frequency (from three doses/day to one dose every other day). Additionally, VC drugamer provided full protection in highly lethal murine surrogate models of tularemia and melioidosis, where free drug was not active. Collectively, the VC drugamer developed in this thesis is a promising new therapeutic for pulmonary tularemia and melioidosis, and can potentially be used for other lung infections and disease setting that required improved intracellular PK properties in specific cell populations (e.g., cancer, malaria).

6.4 EPILOGUE

Overall, those future directions suggest the translational potential and versatility of VC drugamer and the drugamer platform as a whole. I hope that VC drugamer would one day become a useful therapeutic that benefit patients who are suffered from lung infections. I hope my thesis

dissertation and my efforts in the past five years have moved the filed of drug delivery forward a small step. This is the end of my thesis dissertation, but another exciting beginning of my adventure in scientific discovery!

6.5 REFERENCE

1. Zhao, M., Lepak, A. J. & Andes, D. R. Animal models in the pharmacokinetic/pharmacodynamic evaluation of antimicrobial agents. *Bioorg. Med. Chem.* **24,** 6390–6400 (2016).
2. Onufrak, N. J., Forrest, A. & Gonzalez, D. Pharmacokinetic and Pharmacodynamic Principles of Anti-infective Dosing. *Clin Ther* **38,** 1930–1947 (2016).
3. Krontz, D. P. & Strausbaugh, L. J. Effect of meningitis and probenecid on the penetration of vancomycin into cerebrospinal fluid in rabbits. *Antimicrob. Agents Chemother.* **18,** 882–886 (1980).
4. Keel, R. A., Crandon, J. L. & Nicolau, D. P. Pharmacokinetics and pulmonary disposition of tedizolid and linezolid in a murine pneumonia model under variable conditions. *Antimicrob. Agents Chemother.* **56,** 3420–3422 (2012).
5. Zhou, C. *et al.* Pharmacokinetics and pharmacodynamics of DSTA4637A: A novel THIOMAB antibody antibiotic conjugate against Staphylococcus aureus in mice. *MAbs* **8,** 1612–1619 (2016).
6. Brain, J. D., Knudson, D. E., Sorokin, S. P. & Davis, M. A. Pulmonary distribution of particles given by intratracheal instillation or by aerosol inhalation. *Environ. Res.* **11,** 13–33 (1976).
7. Leong, B. K., Coombs, J. K., Sabaitis, C. P., Rop, D. A. & Aaron, C. S. Quantitative morphometric analysis of pulmonary deposition of aerosol particles inhaled via intratracheal nebulization, intratracheal instillation or nose-only inhalation in rats. *J Appl Toxicol* **18,** 149–160 (1998).
8. Ibrahim, M., Verma, R. & Garcia-Contreras, L. Inhalation drug delivery devices: technology update. *Medical Devices (Auckland, N.Z.)* **8,** 131–139 (2015).
9. O'Callaghan, C. & Barry, P. W. The science of nebulised drug delivery. *Thorax* **52,** S31–S44 (1997).
10. MCCALLION, O. N. M., TAYLOR, K. M. G., THOMAS, M. & TAYLOR, A. J. Ultrasonic Nebulisation of Fluids with Different Viscosities and Surface Tensions. *Journal of Aerosol Medicine* **8,** 281–284 (1995).
11. Chiang, C.-Y. *et al.* Mitigating the Impact of Antibacterial Drug Resistance through Host-Directed Therapies: Current Progress, Outlook, and Challenges. *MBio* **9,** (2018).
12. Kaufmann, S. H. E., Dorhoi, A., Hotchkiss, R. S. & Bartenschlager, R. Host-directed therapies for bacterial and viral infections. *Nat Rev Drug Discov* **17,** 35–56 (2018).
13. Dallenga, T. *et al.* Targeting neutrophils for host-directed therapy to treat tuberculosis. *Int J Med Microbiol* (2017). doi:10.1016/j.ijmm.2017.10.001
14. Cullinane, M. *et al.* Stimulation of autophagy suppresses the intracellular survival of Burkholderia pseudomallei in mammalian cell lines. *Autophagy* **4,** 744–753 (2008).
15. Koh, G. C. K. W. *et al.* Glyburide Reduces Bacterial Dissemination in a Mouse Model of

Melioidosis. *PLoS Negl Trop Dis* **7,** (2013).
16. Lo, J.-H., Kulp, S. K., Chen, C.-S. & Chiu, H.-C. Sensitization of Intracellular Salmonella enterica Serovar Typhimurium to Aminoglycosides In Vitro and In Vivo by a Host-Targeted Antimicrobial Agent. *Antimicrob. Agents Chemother.* **58,** 7375–7382 (2014).
17. Allavena, P. *et al.* Engagement of the mannose receptor by tumoral mucins activates an immune suppressive phenotype in human tumor-associated macrophages. *Clin. Dev. Immunol.* **2010,** 547179 (2010).
18. Gustafson, H. H. & Pun, S. H. Instructing macrophages to fight cancer. *Nature Biomedical Engineering* **2,** 559–561 (2018).

APPENDIX A: Ciprofloxacin LC-MS/MS method development

1. Reagents and tissues

Formic acid and ciprofloxacin (cipro) hydrochloride were obtained from Alfa Aesar (Ward Hill, MA, USA) and cipro-d8 hydrochloride internal standard was purchased from Sigma-Aldrich (St Louis, MO, USA). HPLC-grade acetonitrile (ACN) and ultra pure water were purchased from Thermo Fisher Scientific (Waltham, MA, USA). Blank tissues (lung, liver, spleen, and kidney) alveolar macrophages, and plasma were harvested from non-treated C57BL/6 mice (female, 6-8 weeks) to prepare matrix-matched calibration standards and fortified samples. Blank organs or organs obtained from the PK studies were first mixed with 1 ml of ultrapure H_2O (0.8 ml for liver samples) and homogenized using an Omni Bead Ruptor 24 (OMNI International Inc., Kennesaw, GA, USA) shaken for 25 seconds at 24 °C (3 homogenization cycle). The blank tissue homogenates were diluted 10 times with ultrapure water before use.

2. Instrumentation

The liquid chromatography system was composed of an Agilent 1290 Infinity UPLC system (Agilent Technologies, Palo Alto, CA, USA) with flow injection analysis and temperature-controlled autosampler maintained at 5°C. Samples were separated on a Hypersil GOLD PFP column (100 mm x 2.1 mm internal diameter, 1.9 µm particle size) (Thermo Fisher Scientific) at ambient conditions. The chromatographic system was coupled to a 6460 Triple Quad mass spectrometer (Agilent Technologies) with electrospray ionization (ESI) source. The LC–MS/MS system and data analysis was carried out using MassHunter Data Acquisition and Processing (version B.05.00) (Agilent Technologies).

3. Calibration standard, internal standard and quality control (QCs) solutions

Stock solutions of cipro and cipro-d8 (**Fig. 1**) were prepared at a concentration of 1 mg mL^{-1} in ultrapure water, and then were diluted with ultrapure water to make calibration standards with a working concentration range from 20–10000 ng mL^{-1}. Internal standards were diluted with ultrapure water into 500 ng mL^{-1}. Three separate quality control stock were weighed and prepared separately from the calibration standards. QCs were prepared at working concentrations of 50 ng mL−1(low), 500 ng mL−1(medium) and 5000 ng mL−1(high). To a 300 µl aliquot of blank tissue homogenates, the calibration/QC standard (10 µl) and the internal standard cipro-d8 (10 µl of 500 ng ml-1) were added and vortexed thoroughly for 1 min. The aliquot was then diluted 3 times with ACN (600 µl) to extract cipro and to precipitate proteins. Samples were vortexed for another 1 minute and centrifuged at 18000xg for 20 minutes at 4ºC. The supernatant was collected and stored on ice until analyzed via LC-MS/MS. Calibration standards were prepared fresh for each analysis. The cipro concentration range before and after dilution with ACN was shown in **Table 1**.

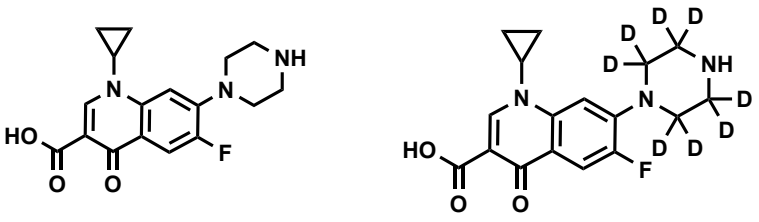

Ciprofloxacin
m/z 332.0

Ciprofloxacin-d8
m/z 340.0

Table 1 Concentration of stock solutions, working solutions, calibration range and quality controls (QC).

Tissue	Stock solution solvent	Stock solution concentration (mg mL−1)	Working solution range[a] (ng mL^{-1})	Calibration range[b] (ng mL−1)	QC[c] (ng mL−1)
Organ	H_2O	1	20–10000	0.2–100	52, 5.21, 0.52
Alveolar macrophage/plasma	H_2O	1	20–10000	0.65–333	166.7, 16.67, 1.67

[redacted]

To create calibration curve for alveolar macrophages (AMs) or plasma, 5 µl of the calibration/QC standard and the internal standard cipro-d8 (5 µl of 500 ng ml-1) were added to 40 µl of blank cell suspension (ca. 10^5 cells) or plasma. Samples were vortexed for 1 minute, diluted 3 times with ACN (100 µl) and processed using the same procedures as described above. The cipro concentration range before and after dilution with ACN was shown in Table 1.

4. LC-MS/MS conditions

Mobile phase A was composed of 10 mM formic acid in ultra pure water and mobile phase B was composed of 10 mM formic acid in ACN. Solvents were prepared before each set of analysis. The linear gradient was as follows: a gradient of 10%-100% B over 4 minutes followed by 1 min 100% B, then 0.1 minute to 10% B to re-equilibrate the column for 1.9 min. The flow rate was 0.3 mL min^{-1} with an injection volume of 10 µL.

The mass spectrometer was operated in positive ion mode. The selected m/z transitions and typical retention time for each analyte are reported in Table 2. The MS/MS setting parameters were as follows: nozzle voltage 0.5 kV, capillary voltage 4.5 kV, collision energy 13 V, nebulizer gas 45 psi, and gas temperature 350 ºC. The spectrometer was engaged during minutes 3-4.5 of each run. Data acquisition was performed in the multiple-reaction monitoring (MRM) mode with a dwell time of 0.15 s per channel.

Table 2 Instrument method for the LC-MS/MS analysis for ciprofloxacin (cipro) with cipro-d8 as an internal standard.

Drug/Internal Standard	Precursor Ion (m/z)	Fragmentation Ion (m/z)	Type	Dwell Time (s)	Nozzle Voltage (kV)	Collision Energy (V)	Retention Time (min)
Cipro	332.0	314.1	Quantification	0.15	0.5	13	3.79
		288.1	Confirmation				
Cipro-d8	340.0	322.1	Quantification	0.15	0.5	13	3.78
		296.2	Confirmation				

5. PK sample preparation

5.1 Organs

Homogenized tissues were diluted 10x with ultrapure water (all except spleen and plasma) to aid cipro extraction. 300 µl aliquots were taken out and the internal standard cipro-d8 (10 µl of 500 ng ml-1) and ultrapure water (10 µl, to compensate the volume of standard solution added in 300 µl non-treated tissue homogenate) were added and vortexed for 1 min. The aliquot was then diluted 3 times with ACN (600 µl) to extract the released cipro and to precipitate proteins. Samples were vortexed for another 1 minute and centrifuged at 18000xg for 20 minutes at 4ºC. The supernatant was collected and stored on ice until analyzed for ciprofloxacin via LC-MS/MS.

5.2 Alveolar macrophages (AMs)

The bronchoalveolar lavage fluid was centrifuged to collect AMs (4 °C, 400×g, 15 min). The collected cells were washed with PBS and centrifuged again to remove the supernatant. The cell pellet was resuspended in PBS (50 µL) and the obtained cell number was counted using crystal violet staining (0.1% in 0.1 M citric acid) to determine the total cell volume. The average mouse alveolar macrophage cell volume is 493±161 x 10^{-9} L^{1}. The cell suspension was then mixed with an internal standard solution, cipro-d8 (5 µL of 500 ng mL-1 in H2O), diluted 3x in ACN and incubated on ice for 1 hour to lyse the cells. Cell lysates were lyophilized by evaporation under N2 (TurboVap; Biotage), reconstituted in 150 µl of 66% ACN, and centrifuged at 18000xg for 20 minutes at 4ºC. The collected supernatants were stored on ice until analyzed via LC-MS/MS.

5.3 Plasma

Plasma was collected from blood by centrifuging the BD PST plasma tubes (BD Biosciences) for 10 minutes at 600xg at room temperature. To a 40 µL aliquot of plasma sample, the internal standard cipro-d8 (5 µl of 500 ng mL-1) and ultrapure water (5 µL, to compensate the volume of standard solution added in 40 µl blank plasma) were added. Those samples were vortexed for 1 minute, diluted 3 times with ACN (100 µL). Samples were subsequently vortexed for another 1 minute and centrifuged at 18000xg for 20 minutes at 4ºC. The supernatant was collected and stored on ice until analyzed via LC-MS/MS.

6. Quantification

To compensate variability in MS detection and ion suppression/enhancement due to matrix effects, stable isotopically labeled analogues have been widely used in LC-MS/MS analysis due to their nearly identical chemical and physical properties of the target analytes[2]. Quantitative analysis of cipro in this study was performed with a deuterated internal standard, cipro-d8. Each level of the calibration curve was analyzed at the beginning of the run, and one standard was analyzed at the end of each run. A ten-point calibration curve was calculated and fit using linear regression of peak area ratios (drug peak area/internal standard peak area) versus concentration. Representative LC traces, peak integrations and mass spectra of cipro and cipro-d8 were shown in **Fig. 2.** The calibration was established over the range of 0.2–100 ng mL−1 (after ACN dilution) in organ tissue homogenate and of 0.65–333 ng mL−1 in alveolar macs/plasma so as to cover the released cipro concentrations in the pharmacokinetics samples. LC trace overlay of cipro standards was shown in **Fig. 3.** Chromatographic data acquisition, peak integration and quantification were performed in MassHunter Data Acquisition and Processing (version B.05.00) (Agilent Technologies).

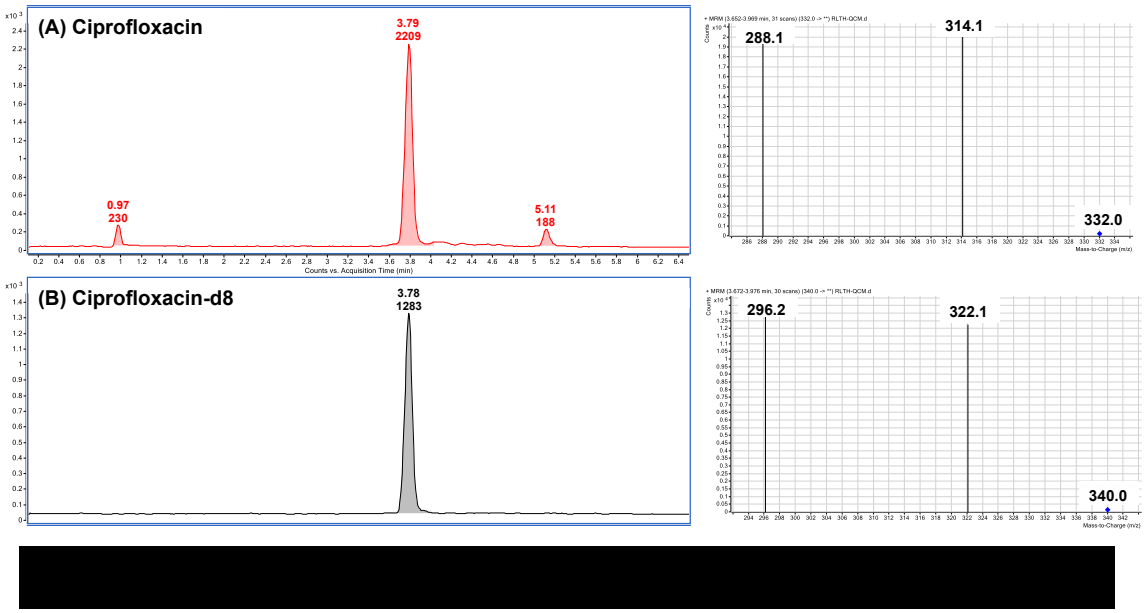

[redacted]

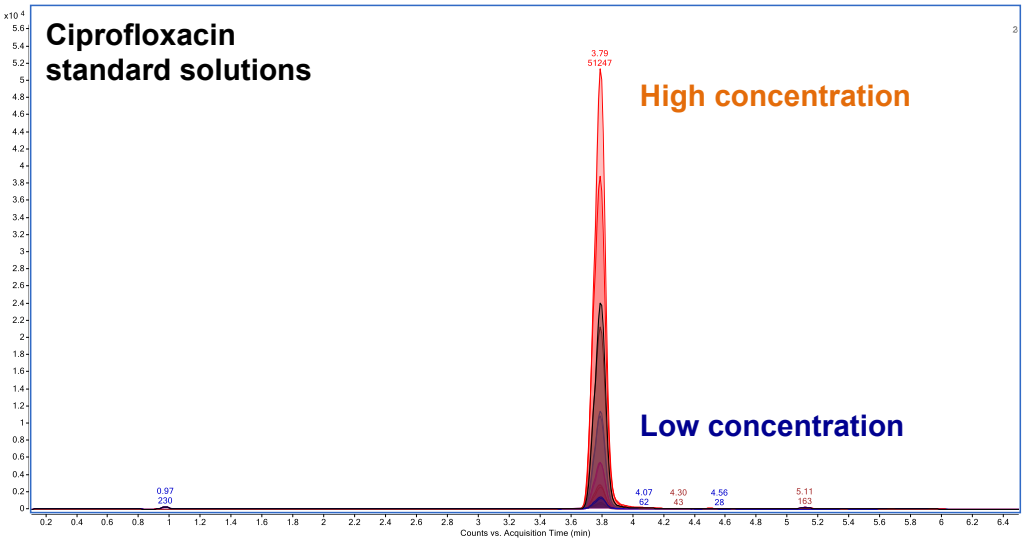

[redacted]

7. Limit of quantification and limit of detection

The limit of quantification (LOQ) for each drug analyzed was defined as the lowest calibration standard for which the standard curve returned accurate and precise results within the given limits. The limit of detection (LOD) was defined as the lowest calibration level for which a drug peak above the noise level was visible on the chromatogram, with a signal to noise of 3:1.

8. Matrix effect and recovery

The matrix effect on chromatography for tissue samples and plasma was first examined by observing whether blank matrix samples had any visible peaks at the expected retention times, and whether matrix eluates spiked with analytes affected the retention time. Subsequently, the matrix effect for cipro in each matrix was assessed. Three series of QC samples at low, medium and high concentrations in triplicate were prepared as follows:

A. Neat standards of cipro subjected to the same extraction process;
B. Non-treated tissue samples and plasma spiked with cipro and cipro-d8 after extraction;
C. Non-treated tissue samples and plasma spiked with cipro and cipro-d8 before precipitation.

Matrix effect, extraction yield and overall recovery were assessed by comparing the absolute peak areas of analytes either solubilized in extraction buffer (A), or added after (B) or before(C) the extraction process[2, 3]. Mean peak area ratios (B2, C2) were calculated as the ratio of cipro to cipro-d8 within the same sample. The matrix effect was defined as the ratio of peak areas of the analytes added to blank matrix after extraction to the neat standard (B/A). The extraction yield was defined as the ratio of peak areas of blank matrix samples spiked before and after extraction (C/B). The overall recovery was defined as the ratio of mean peak area ratios for cipro for samples spiked before extraction to those spiked after extraction (C2/B2). The process efficiency was defined as the ratio of the peak area of analytes spiked before extraction to the peak area of analytes spiked into neat extraction buffer.

Reference

1 K.C. Stone, R.R. Mercer, P. Gehr, B. Stockstill, and J.D. Crapo, "Allometric relationships of cell numbers and size in the mammalian lung.," *Am J Respir Cell Mol Biol*, **6** [2] 235–243 (1992).

2 B.K. Matuszewski, M.L. Constanzer, and C.M. Chavez-Eng, "Strategies for the Assessment of Matrix Effect in Quantitative Bioanalytical Methods Based on HPLC−MS/MS," *Anal. Chem.*, **75** [13] 3019–3030 (2003).

3 A.K. Blakney, Y. Jiang, D. Whittington, and K.A. Woodrow, "Simultaneous measurement of etravirine, maraviroc and raltegravir in pigtail macaque plasma, vaginal secretions and vaginal tissue using a LC–MS/MS assay," *J Chromatogr B Analyt Technol Biomed Life Sci*, **1025** 110–118 (2016).